

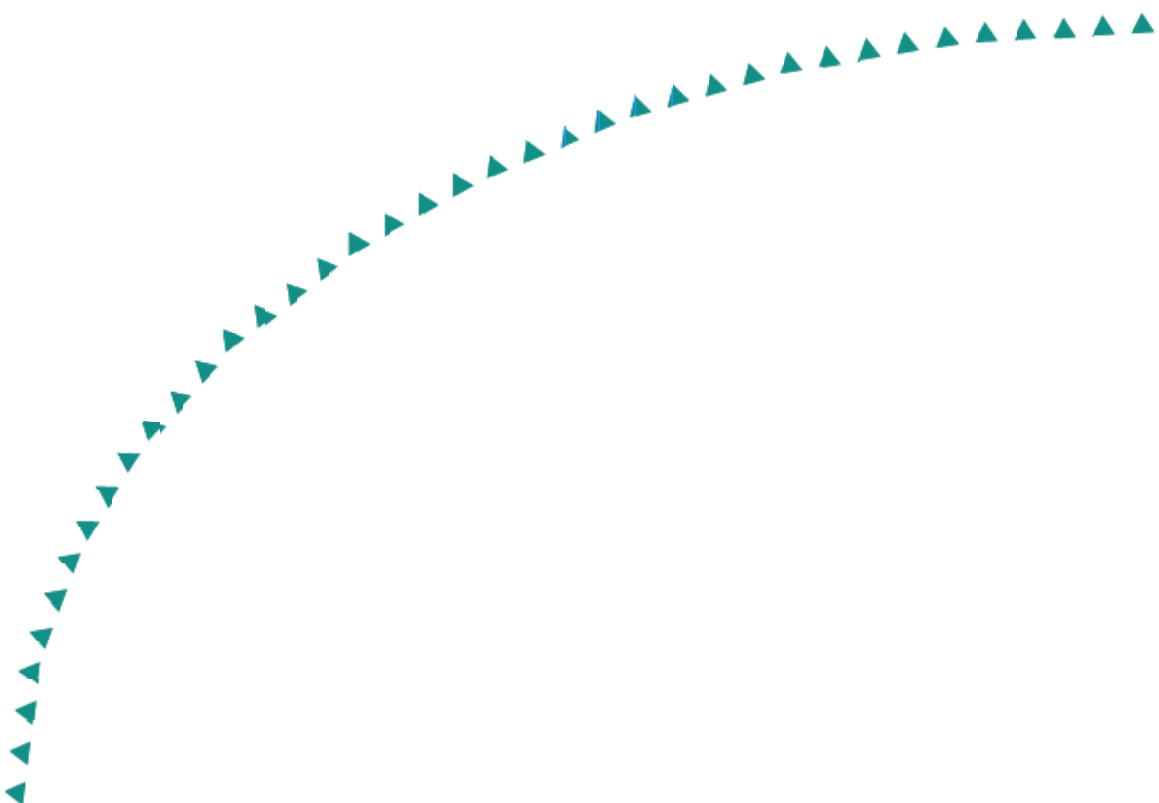
2006-04

Final Report

Use of Adhesives to Retrofit  
Out-of-Plane Distortion Induced  
Fatigue Cracks



Research



## Technical Report Documentation Page

1. Report No. <b>MN/RC-2006-04</b>	2.	3. Recipients Accession No.	
4. Title and Subtitle <b>Use of Adhesives to Retrofit Out-of-Plane Distortion Induced Fatigue Cracks</b>		5. Report Date <b>February 2006</b>	
		6.	
7. Author(s) <b>Yuying Hu, Carol K. Shield, Robert J. Dexter</b>		8. Performing Organization Report No.	
9. Performing Organization Name and Address <b>Department of Civil Engineering University of Minnesota 500 Pillsbury Dr. S.E. Minneapolis, Minnesota 55455</b>		10. Project/Task/Work Unit No.	
		11. Contract (C) or Grant (G) No. <b>(c) 74708 (wo) 133</b>	
12. Sponsoring Organization Name and Address <b>Minnesota Department of Transportation 395 John Ireland Boulevard Mail Stop 330 St. Paul, Minnesota 55155</b>		13. Type of Report and Period Covered <b>Final Report</b>	
		14. Sponsoring Agency Code	
15. Supplementary Notes <a href="http://www.lrrb.org/PDF/200604.pdf">http://www.lrrb.org/PDF/200604.pdf</a>			
16. Abstract (Limit: 200 words)  <p>Prior to 1985, it was common practice to avoid welding the connection plates to the tension flange of the girders of steel bridges. However, extensive fatigue cracking has developed in the unstiffened web gaps because of out-of-plane distortion. A new retrofit option was investigated that uses a room-temperature-cured two-part epoxy (3M Adhesive DP460-NS) to join a small length of 3/4-inch thick steel angle to the tension flange and the connection plate. A field test on two skewed bridges showed that the adhesive-angle retrofit system decreased the out-of-plane strain range by 40 to 50% when the original strain range was more than 50 microstrains. The ten adhesive-angle retrofits remained in place and were in good condition after three and a half years, suggesting that the chosen adhesive had good environmental durability. A laboratory large-scale specimen test with 8 web gaps showed that the retrofit system stopped or retarded most cracks even without stop holes when the measured out-of-plane strains were approximately 600 microstrains. Coupon tests conducted to investigate the environmental durability of the chosen adhesive showed that the chosen adhesive is suitable for applications at room or low temperature, even with high relative humidity.</p>			
17. Document Analysis/Descriptors <b>distortional fatigue, web gap, plate girder bridges</b>		18. Availability Statement <b>No restrictions. Document available from: National Technical Information Services, Springfield, Virginia 22161</b>	
19. Security Class (this report) <b>Unclassified</b>	20. Security Class (this page) <b>Unclassified</b>	21. No. of Pages <b>260</b>	22. Price

# **Use of Adhesives to Retrofit Out-of-Plane Distortion Induced Fatigue Cracks**

## **Final Report**

*Prepared by:*  
Yuying Hu  
Carol K. Shield  
Robert J. Dexter

Department of Civil Engineering  
University of Minnesota

**February 2006**

*Published by:*  
Minnesota Department of Transportation  
Research Services Section  
395 John Ireland Boulevard, MS 330  
St. Paul, Minnesota 55155-1899

This report represents the results of research conducted by the authors and does not necessarily represent the views or policies of the Minnesota Department of Transportation and/or the Center for Transportation Studies. This report does not contain a standard or specified technique.

The authors and the Minnesota Department of Transportation and/or Center for Transportation Studies do not endorse products or manufacturers. Trade or manufacturers' names appear herein solely because they are considered essential to this report

## **Acknowledgements**

Funding for this research was provided by the Minnesota Department of Transportation (Mn/DOT) and the University of Minnesota. We would like to thank both for the financial support given. In addition, we would like to thank 3M and Hilti for technical support.

We would like to thank the many people from Mn/DOT who have helped with this research including Gary Peterson and Erik Wolhowe of the bridge office, Mark Pribula, and the Metro maintenance crews. We would also like to thank all the people from the University of Minnesota that helped in this project, especially Paul Bergson for his continuous help throughout all the experiment work. We thank Clifford Youngberg, Katusuyoshi Nozaka, Eric Corwin, and Scott Nesvold for their help with the field tests. We also thank Brian Tri, Brian Siljenberg, and Gil Huie for their help with the laboratory large-scale test. We thank Timothy Clyne for his help in the laboratory coupon test.

## Table of Contents

<b>CHAPTER 1 INTRODUCTION.....</b>	<b>1</b>
1.1 Background.....	1
1.2 Retrofit methods used by other researchers.....	1
1.3 Advantages of the proposed retrofit method.....	4
1.4 Objective.....	5
1.5 Outline.....	5
<b>CHAPTER 2 LITERATURE REVIEW.....</b>	<b>6</b>
2.1 Research on distortion-induced fatigue.....	6
2.2 Research on adhesives.....	8
2.2.1 Outline.....	8
2.2.2 Research on adhesive application on steel structures.....	11
<b>CHAPTER 3 FIELD TEST.....</b>	<b>14</b>
3.1 Bridge selection.....	14
3.2 Adhesive selection.....	15
3.3 Bridge instrumentation and retrofit location.....	16
3.3.1 Bridge instrumentation.....	16
3.3.2 Retrofit plan.....	17
3.4 Test trucks and test setups.....	18
3.5 Comparison of typical strain gage readings.....	19
3.5.1 Bent-plate-diaphragm bridge (Bridge #27763).....	19
3.5.1.1 Comparison of out-of-plane strains.....	19
3.5.1.2 Comparison of in-plane strains.....	19
3.5.1.3 Comparison of out-of-plane strains and in-plane strains.....	20
3.5.1.4 Comparison of bent-plate diaphragm strains.....	20
3.5.1.5 Comparison of connection plate strains.....	20
3.5.1.6 Effect of differential deflection and rotation on out-of-plane strains.....	20
3.5.2 Cross-frame-diaphragm bridge (Bridge #27984).....	21
3.5.2.1 Comparison of out-of-plane strains.....	21
3.5.2.2 Comparison of in-plane strains.....	22
3.5.2.3 Comparison of out-of-plane strains and in-plane strains.....	22
3.5.2.4 Comparison of the cross-frame diaphragm strains.....	22
3.5.2.5 Comparison of connection plate strains.....	23
3.5.2.6 Effect of differential deflection and rotation on out-of-plane strains.....	23
3.6 Field inspection of the adhesive-angle retrofit system.....	23
3.7 Conclusions of the field test.....	24
3.7.1 Controlling contributions to the out-of-plane distortion.....	24
3.7.2 Conclusions of the retrofit method.....	24
<b>CHAPTER 4 LARGE-SCALE TEST.....</b>	<b>26</b>
4.1 Large-scale specimen configuration.....	26
4.2 Finite element analysis of the large-scale specimen.....	27
4.3 Testing scheme of the large-scale specimen.....	28
4.3.1 Instrumentation.....	28
4.3.2 Test Procedure.....	29

4.4 Test results and discussion.....	31
4.4.1 Static test before cyclic loading.....	31
4.4.1.1 Out-of-plane strains.....	32
4.4.1.2 Out-of-plane distortion.....	33
4.4.1.3 In-plane stresses.....	33
4.4.1.4 In-plane deflection.....	33
4.4.1.5 Stresses in the diaphragm end channel support.....	34
4.4.1.6 Summary of static test results before cyclic loading.....	34
4.4.2 Static test before retrofit and after retrofit (when the longest crack reached approximately 4 in.).....	35
4.4.2.1 Strains at the crack tip.....	35
4.4.2.1.1 Strain at the crack tip at web gap SW-1/2.....	35
4.4.2.1.2 Strain at the crack tip at web gap NE-C.....	36
4.4.2.1.3 Strain at the crack tip at web gap SE-C.....	36
4.4.2.1.4 Strain at the crack tip at other web gaps.....	37
4.4.2.1.5 Summary of strain at the crack tip.....	37
4.4.2.2 In-plane stresses.....	37
4.4.2.3 In-plane deflection.....	37
4.4.2.4 Stresses in the diaphragm end channel support.....	37
4.4.3 Cyclic test.....	38
4.4.3.1 Web gap at SW-1/2.....	38
4.4.3.2 Web gap at NE-C.....	39
4.4.3.3 Web gap at SE-C.....	40
4.4.3.4 Summary of crack growth under cyclic loading.....	41
4.5 Conclusions.....	42
<b>CHAPTER 5 COUPON TEST.....</b>	<b>44</b>
5.1 The coupon specimen and the testing machine.....	44
5.2 The performance of the baseline specimens.....	46
5.2.1 The ultimate strength and the stiffness of the baseline specimen.....	46
5.2.2 Failure mode of the baseline specimen.....	49
5.3 The performance of the environmentally exposed specimens.....	50
5.3.1 Specimens without GPS pretreatment.....	51
5.3.1.1 Air at 65°F.....	51
5.3.1.2 Immersion in tap water at 65°F.....	52
5.3.1.3 Immersion in tap water at 111°F.....	53
5.3.1.4 Air at -4°F.....	54
5.3.1.5 Freeze and thaw chamber.....	54
5.3.1.6 Temperature cycles between -4°F and 122°F (unloaded).....	55
5.3.1.7 Temperature cycles between -4°F and 122°F (loaded at 0.95 k).....	56
5.3.1.8 Outdoors.....	57
5.3.1.9 Outdoors and fire.....	58
5.3.1.10 Summary of performance of specimens without GPS pretreatment in different environments.....	60
5.3.2 Comparison of specimens with GPS pretreatment, with specimens without GPS pretreatment.....	61
5.3.2.1 Effect of GPS pretreatment on environments other than fire.....	61

5.3.2.2 Effect of GPS pretreatment on environment of fire after outdoor exposure .....	61
5.3.2.3 Summary of the effect of GPS pretreatment .....	62
5.4 The influence of the stiffness on the effectiveness of the retrofit system .....	62
5.5 Conclusion .....	64
<b>CHAPTER 6 CONCLUSION .....</b>	<b>66</b>
6.1 Findings from the field test.....	66
6.2 Findings from the large-scale test .....	67
6.3 Findings from the small-scale coupon test .....	68
6.4 Conclusion remarks and recommended future work.....	68
<b>REFERENCES .....</b>	<b>71</b>
<b>TABLES .....</b>	<b>77</b>
<b>FIGURES .....</b>	<b>101</b>
Appendix A	Gage labeling of the bridges for the field test
Appendix B	The procedure of applying the retrofitting angles in the field test
Appendix C	Strain ranges at web gap before/after retrofit in the field test
Appendix D	In-Plane strain ranges before/after retrofit in the field test
Appendix E	Strain ranges measured by single weldable gages on the diaphragm before/after retrofit in the field test
Appendix F	Strain ranges measured by rosettes on the connection plate and diaphragm before/after retrofit in the field test
Appendix G	Linear Variable Differential Transformer (LVDT) labeling for the large-scale test
Appendix H	Gage labeling for the large-scale test
Appendix I	The procedure of applying the retrofitting angles in the large-scale test
Appendix J	Measured out-of-plane strains for the large-scale specimen
Appendix K	Coupon specimen fabrication procedure
Appendix L	Strength and stiffness of the baseline coupon specimens and environmentally exposed coupon specimens
Appendix M	The recommended procedure of applying the retrofitting angles in the field

## List of Tables

Table 3.1	Retrofitting angle application situation.....	77
Table 3.2	Web gap strain ranges on B5 of the BPD bridge.....	78
Table 3.3	Web gap strain ranges on B4 of the BPD bridge.....	79
Table 3.4	In-plane strain ranges on B5 of the BPD bridge.....	80
Table 3.5	Strain ranges on the diaphragm of the BPD bridge .....	81
Table 3.6	Web gap strain ranges on B4 of the CFD bridge.....	82
Table 3.7	Web gap strain ranges on B3 of the CFD bridge.....	83
Table 3.8	In-plane strain ranges on B4 of the CFD bridge.....	84
Table 3.9	Strain ranges on the diaphragm of the CFD bridge .....	85
Table 4.1	Measured active web gap length .....	86
Table 4.2	Out-of-plane strains before cyclic loading.....	87
Table 4.3	Out-of-plane distortion before cyclic loading .....	88
Table 4.4	In-plane stresses before cyclic loading .....	88
Table 4.5	In-plane deflection before cyclic loading.....	89
Table 4.6	Diaphragm end channel support stresses before cyclic loading.....	89
Table 4.7	Crack tip strains before and immediately after retrofit.....	90
Table 4.8	In-plane stresses before and immediately after retrofit.....	91
Table 4.9	In-plane deflection before and immediately after retrofit.....	92
Table 4.10	Diaphragm end channel support stresses before and immediately after retrofit ...	92
Table 5.1	Baseline specimen testing matrix .....	93
Table 5.2	Baseline specimen testing results .....	93
Table 5.3(a)	Effects of different parameters on the ultimate strength and the stiffness of baseline specimens (comparison of average values).....	94
Table 5.3(b)	Effects of different parameters on the ultimate strength and the stiffness of baseline specimens (statistic analysis).....	95
Table 5.4	Environment specimen testing matrix .....	96
Table 5.5	Environment specimen testing results .....	97
Table 5.6(a)	Effects of environment exposure on the ultimate strength and the stiffness of specimens, No GPS (comparison of average values).....	98
Table 5.6(b)	Effects of environment exposure on the ultimate strength and the stiffness of specimens, No GPS (statistic analysis) .....	99
Table 5.7(a)	Effects of environment exposure on the ultimate strength and the stiffness of specimens, GPS vs. No GPS (comparison of average values) .....	100
Table 5.7(b)	Effects of environment exposure on the ultimate strength and the stiffness of specimens, GPS vs. No GPS (statistic analysis) .....	100

## List of Figures

Figure 1.1 Girder differential deflection and web gap detail .....	101
Figure 1.2 Proposed retrofit scheme with adhesives.....	101
Figure 2.1 Test specimens by Albrecht (1987).....	102
Figure 2.2 Specimens of Gasparini et al. (1990) to investigate durability of adhesives.....	102
Figure 2.3 Large-scale specimens used by Hashim et al. (1990) .....	103
Figure 2.4 Specimens with bonded transverse intermediate stiffeners used by Martin (1992) ..	103
Figure 3.1 Pictures of the field bridges .....	104
Figure 3.2 Plan view of the field bridges .....	106
Figure 3.3 Application of DP-460 NS.....	107
Figure 3.4 Instrumentation and retrofit plans for the field bridges.....	108
Figure 3.5 Instrument location detail for the field bridges.....	109
Figure 3.6 Strain gage application .....	111
Figure 3.7 Retrofitting angle configuration.....	111
Figure 3.8 Picture of retrofitting angle.....	112
Figure 3.9 Bondline thickness of retrofitting angle .....	112
Figure 3.10 Field test truck.....	113
Figure 3.11 Field test truck position cross section view .....	114
Figure 3.12 Field test truck position plan view .....	115
Figure 3.13 Web gap strains before and after retrofit for the BPD bridge.....	116
Figure 3.14 Strain range reduction vs. original strain range for the BPD bridge.....	117
Figure 3.15 Effects of differential deflection, diaphragm rotation, and deck rotation on the BPD bridge .....	118
Figure 3.16 Web gap strains for the CFD bridge before and after retrofit.....	119
Figure 3.17 Strain range reduction vs. original strain range for the CFD bridge.....	120
Figure 3.18 Effects of differential deflection and deck rotation on the CFD bridge.....	121
Figure 3.19 Pictures of the field inspection of the adhesive-angle retrofit system 3.5 years after it was applied.....	122
Figure 4.1 Large-scale specimen configuration.....	123
Figure 4.2 Spring support details.....	124
Figure 4.3 Global model of the large-scale specimen.....	124
Figure 4.4 Submodel of the web gap region for the large-scale specimen .....	125
Figure 4.5 Out-of-plane stresses predicted by the FEA at web gaps .....	126
Figure 4.6 Out-of-plane stresses predicted by the FEA at web gap where in-plane stress was 6 ksi .....	127
Figure 4.7 LVDT locations.....	128
Figure 4.8 LVDTs that measure in-plane deflections and strain gages that measure diaphragm end support strains.....	129
Figure 4.9 LVDTs that measure out-of-plane deflections.....	130
Figure 4.10 Strain gage locations.....	131
Figure 4.11 Strain gages that measure in-plane strains.....	131
Figure 4.12 Strain gages that measure out-of-plane strains .....	132
Figure 4.13 Strain gages that measure strains at the tip of the crack for web gaps .....	133
Figure 4.14 Measured out-of-plane strains at SW-1/2 web gap before cyclic loading.....	134

Figure 4.15 Comparison of measured out-of-plane strains with FEA predicted out-of-plane strains at SW-1/2 web gap .....	134
Figure 4.16 In-plane deflection for LVDT locations before cyclic loading.....	135
Figure 4.17 Actuator load vs. time before cyclic loading .....	136
Figure 4.18 Picture of cracks at web gap SW-1/2 at 1,101,000 cycles.....	137
Figure 4.19 Measured strains at the crack tips at web gap SW-1/2.....	138
Figure 4.20 Picture of cracks at web gap NE-C at 1,101,000 cycles.....	139
Figure 4.21 Measured strains at the crack tips at web gap NE-C.....	140
Figure 4.22 Picture of cracks at web gap SE-C at 1,101,000 cycles .....	141
Figure 4.23 Measured strains at the crack tips at web gap SE-C .....	142
Figure 4.24 Picture of cracks at web gap NW-1/2 at 1,101,000 cycles .....	143
Figure 4.25 Measured strains at the crack tips at web gap NW-1/2 .....	144
Figure 4.26 Picture of cracks at web gap NW-C at 1,101,000 cycles .....	145
Figure 4.27 Measured strains at the crack tips at web gap NW-C.....	146
Figure 4.28 Picture of cracks at web gap SW-C at 1,101,000 cycles.....	147
Figure 4.29 Measured strains at the crack tips at web gap SW-C .....	148
Figure 4.30 Picture of cracks at web gap NE-1/2 at 1,101,000 cycles .....	149
Figure 4.31 Measured strains at the crack tips at web gap NE-1/2 .....	150
Figure 4.32 Picture of cracks at web gap SE-1/2 at 1,101,000 cycles .....	151
Figure 4.33 Measured strains at the crack tips at web gap SE-1/2 .....	152
Figure 4.34 Crack tip strain reduction vs. original crack tip strain.....	153
Figure 4.35 Crack tip strain reduction vs. crack length .....	153
Figure 4.36 Crack growth at web gap SW-1/2 .....	154
Figure 4.37 Cracks at web gap SW-1/2 at 3,101,000 cycles.....	155
Figure 4.38 Detached angle at web gap SW-1/2 .....	156
Figure 4.39 Crack growth at web gap NE-C .....	156
Figure 4.40 Detached angle at web gap NE-C .....	157
Figure 4.41 Crack growth at web gap SE-C.....	157
Figure 4.42 New crack at web gap SE-C at 3,101,000 cycles.....	158
Figure 4.43 Crack growth at web gap NW-1/2.....	158
Figure 4.44 Detached angle at web gap NW-1/2.....	159
Figure 4.45 Crack growth at web gap NW-C.....	159
Figure 4.46 Detached angle at web gap NW-C .....	160
Figure 4.47 Crack growth at web gap SW-C.....	160
Figure 4.48 Detached angle at web gap SW-C.....	161
Figure 4.49 Crack growth at web gap NE-1/2.....	161
Figure 4.50 Detached angle at web gap NE-1/2 .....	162
Figure 4.51 Crack growth at web gap SE-1/2 .....	162
Figure 4.52 Detached angle at web gap SE-1/2.....	163
Figure 4.53 Crack propagation through the thickness of the web .....	164
Figure 5.1 Coupon specimen dimension .....	165
Figure 5.2 Coupon specimen fabrication .....	165
Figure 5.3 Test set up.....	166
Figure 5.4 Load vs. displacement curve for a baseline specimen with bondline thickness $t_a=$ 0.020 in. ....	167

Figure 5.5 Least squares regression of load vs. displacement curve for a baseline specimen with bondline thickness $t_a= 0.020$ in. ....	167
Figure 5.6 Histogram and normal quantile plot for the standard baseline specimens .....	168
Figure 5.7 Normal quantile plot for the baseline specimens with GPS .....	169
Figure 5.8 Ultimate strength vs. testing temperature for baseline specimens .....	170
Figure 5.9 Ultimate strength of lab-ambient-air(73°F)-cured specimens and cold-air(50°F)-cured specimens.....	171
Figure 5.10 Failure mode of a standard baseline specimen.....	172
Figure 5.11 Failure mode of a specimen pretreated by GPS .....	172
Figure 5.12 Failure mode of a specimen tested at 122°F .....	173
Figure 5.13 Failure mode of a specimen tested at -40°F.....	173
Figure 5.14 Failure mode of a cold temperature(50°F) cured baseline specimen .....	174
Figure 5.15 Failure mode of specimen kept in lab air at 65°F for 180 days and 447 days .....	174
Figure 5.16 Failure mode of specimen immersed in tap water at 65°F for 92 days and 201 days .....	175
Figure 5.17 Failure mode of specimen immersed in tap water at 111°F for 92 days and 210 days .....	175
Figure 5.18 Failure mode of specimen kept in cold air at -4°F for 196 days and 382 days.....	176
Figure 5.19 Failure mode of specimen kept in freeze and thaw chamber for 92 days and 193 days .....	176
Figure 5.20 Specimens stored in the cold chamber .....	177
Figure 5.21 Failure mode of unloaded specimen subjected to temperature cycles between -4°F and 122°F for 197 days and 380 days .....	177
Figure 5.22 Self-equilibrium loading device.....	178
Figure 5.23 Failure mode of loaded(0.95 k) specimen subjected to temperature cycles between -4°F and 122°F for 211 days and 370 days.....	178
Figure 5.24 Failure mode of loaded(0.95 k) specimen subjected to temperature cycles between -4°F and 122°F .....	179
Figure 5.25 Coupon specimens kept outdoors.....	180
Figure 5.26 Failure mode of specimen kept outdoors for 184 days and 271 days .....	180
Figure 5.27 Ultimate strength and stiffness of specimens exposed to the outdoor environment and an unexpected fire .....	181
Figure 5.28 Failure mode of specimen that failed during the fire after 371 days of outdoor exposure .....	182
Figure 5.29 Failure mode of specimen that underwent fire after 371 days of outdoor exposure	182
Figure 5.30 Failure mode of specimen that underwent fire after 374 days of outdoor exposure	183
Figure 5.31 A 20-node solid element (brick element) was used to model both the adhesive and the angle for the large-scale specimen.....	183
Figure 5.32 Out-of-plane stresses predicted by the FEA at web gap in the constant moment region where in-plane stress was 12 ksi .....	184

## Executive Summary

In this research, adhering a small length of  $\frac{3}{4}$ -inch thick steel angle shape to the connection plate and the tension flange was shown to be an effective retrofit for out-of-plane fatigue cracks in the web gap region. The comprehensive study of the retrofit consisted of a field test and a large-scale laboratory test. Furthermore, since environmental durability is vital for long-term performance, small-scale coupon tests were conducted to investigate the durability of the chosen adhesive, DP-460 NS, a product of 3M. Major findings from this research project are presented as follows.

The field test represented the real environment and loading under which the adhesive will be applied and exposed. Therefore, two representative multi-girder steel bridges were chosen to conduct the field test. Both bridges were three-span continuous bridges. One had staggered bent-plate diaphragms and one had continuous cross-frame diaphragms. Both bridges were designed in 1981 with web gap details and large skew angles. This led them to be susceptible to web-gap out-of-plane distortion problems, particularly in the negative moment region. Two three-axle Mn/DOT sand trucks were used for the test. Each truck weighed approximately 50 kips. Truck tests were conducted before and after the retrofit was applied.

It was found that the retrofit was effective at places where the original strain range was larger than 50 microstrains. This retrofit method achieved at least 38% strain range reduction for the bent-plate-diaphragm (BPD) bridge and at least 50% strain range reduction for the cross-frame-diaphragm (CFD) bridge when the original strain range was more than 50 microstrains. If such reduction percentage can be obtained for strain ranges large enough to initiate a crack, the fatigue life of the connection can be extended at least 4.6 times by this retrofit method. Or, if the strain range was reduced below the threshold level, then no fatigue cracks would initiate. The 50 microstrain value corresponded to a 1.45 ksi stress range in the field bridges. The detail under investigation was considered Category C, therefore, stress ranges below 10ksi should not initiate cracks. The largest strain ranges measured on the field bridges were 200 microstrains, and as expected for these ranges, no cracking was identified in the field test bridges.

Because normal traffic flow was not interrupted when the retrofit was conducted, it could be concluded that the vibration caused by the traffic would not influence the effectiveness of the adhesive performance, provided that the manufacturer's requirements are met.

Because the adhesive application represented the worst situation of field application (applied at 50°F instead of the manufacture recommended 70°F), the obtained results should provide the lower bound performance of the 3M adhesive, DP460-NS.

The ten adhesive-angle retrofits remained in place and were in good condition after three and a half years, suggesting that the chosen adhesive had good environmental durability.

The maximum out-of-plane strain range was only approximately 200 microstrains in the BPD bridge and 100 microstrains in the CFD bridge for the field test, therefore, a large-scale test was conducted in the lab under controlled conditions, so that the effectiveness of the adhesive attachment under larger stresses could be studied. The large-scale specimen consisted of two 32

ft. long side-by-side plate girders tied together by two intermediate diaphragms and four 3/4-in.-thick-plate-and-W-shape combinations. The 3/4-in.-thick-plate-and-W-shape combinations were clamped to the bottom flange that was in tension in the primary stress field. These elements served the purpose of simulating the concrete deck in the field. In other words, the whole test set-up was an upside-down replica of the field configuration in the negative moment region. The girders were tested in four-point bending with a 5-ft. constant moment region at the center of the span.

First, a static test was performed. The measured out-of-plane strain ranges before retrofit were approximately 600 microstrains when the in-plane stress range was 12 ksi in the constant moment region.

Then, cracks were initiated and propagated in the 8 web gaps. 27 strain gages were applied at the tip of web gap cracks to measure strains before and immediately after retrofit. It was found that crack tip strain ranges were decreased to approximately 20% of the original values on average after retrofit. Strain range readings from two crack tip gages that were located on each side of the web for a through-thickness crack were treated as outliers because this crack had already propagated away from the web gap and grown perpendicular to the in-plane stress on the web.

Cycling under the same load range resumed for 2 million cycles after retrofit. At places where the angles became loose on the tension flange side, due to the unrealistically large stress ranges used in the large-scale lab specimen (in-plane stress of 12 ksi), powder actuated fasteners were used to reconnect the angle with the tension flange. Even without stop holes, most cracks were stopped, or retarded, by the adhesive-angle retrofit system. Had stop holes been drilled at all crack tips, as would be the case for any field retrofit application, some of the retarded cracks might have been stopped completely. Cracks were stopped completely when the load range was reduced to one third of the original load range.

The retrofit method had little effect on the crack growth rate for two cracks which had grown out of the web gap region and become perpendicular to the in-plane stress. This was expected because the adhesive-angle retrofit system, though effective at decreasing out-of-plane stress, did not affect the in-plane stress. This retrofit method is not recommended for cracks which are longer than 2 in. and have grown perpendicular to the in-plane stresses.

Since environmental durability was one of the most important parameters in the choice of adhesives, and it was not directly correlated to the initial strength, thus it was desirable to understand the performance of the chosen adhesive under different environmental exposure schemes. Coupon tests were conducted for this purpose. Because the retrofit method of adhesive-angle combination relied more on the stiffness of the system than on the strength of the system, the stiffness of the adhesive was studied.

The relative aggressiveness of the environment with respect to stiffness is ranked from least to most detrimental environments: air at 65°F; air at -4°F; immersion in tap water at 65°F; outdoor environment, freeze and thaw cycling, temperature cycles (unloaded); temperature cycles (loaded at 10% of the initial strength), immersion in tap water at 111°F; and fire after outdoor exposure.

Even though the stiffness of the coupon specimens decreased under various environments, it was postulated from the results of the FEA of the large-scale specimen that environments which introduced less than a 50% decrease in the coupon specimen stiffness would not have significant influence on the effectiveness of the adhesive-angle retrofit system. In other words, except for the cases with a constant stress of 10 % of the strength, simultaneously subjected to temperature cycles, immersion in tap water at 111°F, and fire after outdoor exposure, all other tested environments were not likely to deteriorate the effectiveness of the adhesive-angle retrofit system. None of these three exposures are likely to occur in the perceived retrofit environment. Because the retrofit only sees live load, it will not be subjected to a constant stress, the location of the retrofit basically protects it from immersion in water, and all angles should be replaced, as well as the bridge inspected, in the unlikely event of a fire.

Based on the above observations, it was concluded that the chosen adhesive (3M DP460-NS) is suitable for applications at room or low temperature, even with high relative humidity. In other words, it is applicable to the steel bridges in Minnesota. The adhesive is not suitable for places where temperature is higher than or close to its glass transition temperature (122.5°F).

If the effectiveness of the retrofit is found to decrease overtime because of long periods of environmental exposure, or because of a disastrous event, such as fire, the old adhesive-angle combination can be disassembled with torching and be replaced by a new adhesive-angle combination, without deleterious effect to the bridge.

This research found that the adhesive-angle retrofit system was effective. However, there are several recommendations for future studies on the use of adhesives to retrofit out-of-plane fatigue cracks:

1. Bondline thickness of 0.020 in. was used for both the field test and the large-scale test. It is recommended that smaller bondline thickness be investigated. In particular, cases without spacers such as glass beads to maintain bondline thickness, and thus expediting the retrofit process, can be investigated. It is possible that the irregularities of the flange surface, connection plate, and the angle provide “spacers” for the bondline.
2. The adhesive retrofit should be investigated further to see if it is effective, together with stop hole drilling, when the detail has already exhibited a small web-gap crack in a field test.
3. A database of in-service durability performance does not exist due to the scarcity of adhesives used in steel-to-steel bonding in civil structures. However, results from this study and other future studies can be built into such a database.
4. Even though the ten adhesive-angle retrofits remained in place and were in good condition after three and a half years, it is suggested that more coupon specimens be fabricated and stored outdoors for prolonged and quantitative durability study. Outdoor exposure for 5, 10, 15, and 20 years can be investigated.

5. Powder actuated fasteners were used in combination with adhesives to attach the angle to the tension flange in this research. The testing results were consistent with the S-N curve provided by Niessner and Seeger (1999), which shows that the base metal with powder actuated fasteners has an infinite life if the stress range is smaller than 100 Mpa, which is equivalent to 14.5 ksi. Due to the simplicity of the application, a new retrofit method with powder actuated fasteners connecting the angle and the tension flange, and high strength bolts connecting the angle and the connection plate, should be investigated.
6. The effect of girder, diaphragm, connection plate, and retrofit angle dimensions on the effectiveness of the retrofit can be studied to determine a rationale detail design for the retrofit system.

# Chapter 1 Introduction

## 1.1 Background

Multigirder steel bridges are in wide use in the U.S. state and interstate highway systems. These bridges are composed of steel girder members tied together with a concrete slab and transverse steel diaphragms. The diaphragms help to brace the longitudinal girder members during construction before the concrete slab is poured and hardened. They also help distribute lateral load (such as wind or earthquake load) among girders. To a much lesser degree, diaphragms also distribute live load among girders. The diaphragms are connected to the girders by connection plates, or stiffeners, which are welded to the girders. Diaphragms have been required by the American Association of State Highway and Transportation Officials (AASHTO) specification since 1949 in multigirder steel bridges.

Prior to 1985, it was common practice to avoid welding the connection plates to the tension flange of the girders to evade a possible fatigue-sensitive detail. However, this led to a small unstiffened segment of the web which is commonly referred to as the “web gap” as illustrated in Figure 1.1. Fatigue cracking has developed in the web gap regions of some bridges because of unexpected out-of-plane distortion. Skewed bridges tend to be more prone to this problem due to the relatively larger differential deflections between adjacent girders under live load. Since the diaphragm has relatively high stiffness, the differential deflections are accommodated by the concentrated deformation at the small web gap region (Figure 1.1), resulting in high levels of stresses in the girder web. This situation is exacerbated in negative moment regions where the tension flange is restrained from rotation about the longitudinal axis by the concrete slab. Demers and Fisher (1990) summarized multigirder bridges with cracking at the diaphragm connection plate and found that among 15 bridges that had cracks in web gaps, 14 had cracks at web gaps at top flange and only 5 had cracks at web gaps at bottom flange. Since 1985, the American Association of State Highway and Transportation Organization (AASHTO) has required a positive attachment between the connection plate and both flanges of the girder, as well as a cope length of at least 2 in. or four times the web plate thickness in the connection plate, whichever is larger. This requirement has eliminated distortion-induced fatigue problems in bridges designed subsequently.

Unfortunately, according to Altay et al. (2003), 85% of the steel bridges in the State of Minnesota were built prior to 1986. Many of these bridges have details that are prone to out-of-plane fatigue cracking. Distortion-induced fatigue cracks have already been discovered in Minnesota (Dexter and Bergson, 1998) and elsewhere (Fisher, 1978, 1984; Lee, 1989; Demers and Fisher, 1990; Akesson et al., 1997; Khalil et al., 1998; Fraser et al., 2000; Zhao and Roddis, 2003), and more are expected to occur in the years to come if retrofit measures are not performed.

## 1.2 Retrofit methods used by other researchers

Retrofit methods for distortion-induced fatigue details fall into two philosophies. The first involves decreasing the stiffness of the system so as to decrease the stress concentration at the

web gap. Such methods include drilling stop holes, cutting back the connection plate, and reducing the driving force by removing the diaphragm or loosening the diaphragm bolts. The second retrofit method involves increasing the stiffness of the system so that a new load transfer route is provided, thus decreasing the stress at the web gap. Such methods are referred to as positive attachment. They include welding the connection plate to the tension flange of the girder, and bolting the connection plate and the tension flange with heavy angle or tee sections.

Drilling stop holes at the crack tip causes a reduction of the stress intensity at the crack tip. Fisher et al. (1980) claimed that the stop holes were effective in stopping crack growth in a plane perpendicular to the in-plane bending when the relationship

$$\frac{\Delta K}{\sqrt{\rho}} < 4\sqrt{\sigma_y} \text{ (for } \sigma_y \text{ in ksi)} \quad (1-1)$$

was satisfied, where,  $\Delta K$  is the stress intensity range for the in-plane stress range at the hole with radius,  $\rho$ , and  $\sigma_y$  is the yield stress of the girder web. Lai (1997) suggested that Equation (1-1) is not valid for fatigue cracks caused by out-of-plane distortion because the equation only takes Mode I into consideration, while out-of-plane distortion also involves Mode III. Fisher et al. (1990) later added that stop holes were effective in arresting web gap cracks only when the distortion-induced cyclic stress was less than 15 ksi and the in-plane bending stress was less than 6 ksi. In a laboratory test, Fraser et al. (2000) found that for an in-plane stress range of 5.1 ksi and principal stress range of 9.6 ksi, cracks began to propagate past drilled holes whose radii were calculated by Equation (1-1). Keating (1994), on the other hand, found that the hole size needed to be related to the length of the crack. He found that for bridge steels with a yield stress of 36 ksi and a maximum stress range of 6 ksi near the hole, crack reinitiation from the hole was avoided if the hole diameter was at least 1/5 of the total length of the crack. It was also found that drilling holes alone would not solve the problem for many cases and may only serve as a temporary retrofit. Nevertheless, it has been universally recognized that stop holes should always be drilled when cracks are detected. Whether additional repair methods are needed varies from case to case.

Dexter and Bergson (1998) and Fisher et al. (1990) both retrofitted bridges by cutting back the connection plate, and thus increasing the web gap length. Cracks were successfully stopped or retarded using this method. One of the disadvantages of this retrofit was that the increased web gap must be at least 12 in. (Fisher and Keating, 1989) or 20 times of the web thickness (Fisher et al., 1990) to be effective. In some cases, the diaphragms were connected in a way that made cutting back so much of the connection plate impossible. Another disadvantage is that the stub of the connection plate should be completely removed and ground smooth for the repair to be successful. A third disadvantage is that the increased web gap flexibility may result in larger out-of-plane distortion, which in turn may have a vicious effect on the out-of-plane bending stress at the web gap. For example, Fisher et al. (1979) found that in one skewed girder structure, increasing the web gap from 2 in. to 4 in. resulted in an increase in the out-of-plane web bending stress. Thus careful calculation must be performed to ensure the effectiveness of this method from case to case. A fourth disadvantage is that if the connection plate also serves as a transverse stiffener, then web crippling may be a problem and must be checked. A fifth problem with this type of repair is that once performed, positive attachment repair options are no longer possible or difficult to achieve.

Stallings et al. (1996, 1999) evaluated removing diaphragms as a retrofit method on a simple span bridge and a three span bridge. Once the diaphragms are removed, there is no driving force transferred from the diaphragm to the web gap, thus eliminating the source of out-of-plane distortion fatigue. However, the effect of removing the diaphragms on the whole structure has to be studied. Research conducted by Stallings et al. focused on the contribution of the diaphragm to the live load distribution among girders and found that removing the diaphragms increased the maximum bottom flange stresses at the most heavily loaded girder up to 15%. Stallings et al. decided from comparisons of measured and calculated stresses that the conservatism of design practice was not significantly affected by removal of the diaphragms. However, since diaphragms provide lateral support for the girders in the negative moment region, and they help to distribute lateral load such as wind or collision; extreme care must be exercised before this retrofit method is conducted. Additional expense for temporary bracing during deck replacement should also be considered. Removing the interior diaphragms may affect the service life of the deck as a result of increasing the bending moment in the deck.

Tarries et al. (2001, 2003) proposed loosening bolts to prevent out-of-plane distortional fatigue cracking in multiple steel girder bridges. By loosening the bolts in diaphragm connections, but leaving them in place, the connection allowed for slight rotation of the diaphragms, thus reducing diaphragm forces and web gap stresses. Retaining the loose connection allowed the bolts in the connections to move into bearing if the girders experienced significant lateral displacement, caused by lateral load such as wind or collision, thus the diaphragms would engage to provide stability to the bridge. The field test on an I-beam diaphragm bridge, a channel diaphragm bridge, and an X-type diaphragm bridge all showed approximately 80% reduction in out-of-plane strains after this retrofit. However, Tarries et al. also mentioned that for each bridge, calculations should be performed to ensure stability. Lateral load distribution should also be addressed, and a system must be devised to ensure that the loose bolts remain in place and do not fall out because of vibration caused by traffic.

Providing positive attachment is considered to be the most effective retrofit method for distortion-induced fatigue (Fisher and Menzemer, 1990). Indeed, as mentioned above, positive attachment is required in the current AASHTO specifications. If the method of positive attachment is chosen, bolting or welding can be used. When a bolted connection is used, a relatively rigid splice angle or Tee sections should be incorporated. It was found from field experience (Fisher and Keating, 1989) and laboratory study (Fisher et al., 1990) that for this type of retrofit to be successful, the components should be at least  $\frac{3}{4}$  in. thick and connected with four or more pre-loaded high strength bolts per shear plane. Research by D'Andrea et al. (2001) seemed to have supported the above statement. In a laboratory study conducted by D'Andrea et al. on dismantled girders of a multigirder skewed bridge with staggered diaphragms, a  $\frac{1}{2}$  in. thick repair angle was connected to the connection plate and to the tension flange with two  $\frac{7}{8}$  in. A325 bolts per shear plane. This laboratory study gave mixed results. Each of the three girders where this repair was performed shared one of the possible outcomes: the web gap crack growth stopped, or retarded, or showed no signs of slowing down.

Bolting the connection plate to the tension flange of the girder with an angle or a Tee section is a good retrofit for the positive moment region. However, bolting to the top flange requires partial removal of the concrete slab in the negative moment region, which in turn, requires partial closure to traffic. While welding may be more convenient, its use should be

minimized due to several potential problems. The quality of the weld might be affected because it would be performed under field conditions in the overhead position. The corrosion and dirt buildup during service life may contaminate the weld metal during application. Also, the preheat requirements may be hard to meet with the large concrete mass above the top flange of the girder. Furthermore, the bridge is still required to be closed during the welding operation to limit structure vibration. Fisher et al. (1982) used field welding to attach a shear tab to the stiffener and the tension flange, thus providing positive attachment, to repair displacement-induced fatigue cracking of a box girder bridge in 1982. It was later reported (Demers and Fisher, 1990) that cracking was observed in the welds in the negative moment regions during a site inspection in 1984. Undersized and poor quality welds were found to be the cause of the cracking. The shear tabs were partially replaced and retrofit holes were drilled at the crack tips in 1986. No cracks were reported afterwards. Since the field weld quality can not be guaranteed, Departments of Transportation are generally reluctant to conduct field welding for repair of distortion-induced fatigue in fear of introducing another fatigue sensitive detail in the primary load carrying member.

The above disadvantages of bolting and welding led to the exploration of a third alternative, attaching an angle to the tension flange and the connection plate with adhesives. In the current study, the feasibility of using adhesives will be investigated. The proposed detail is shown in Figure 1.2. The diaphragm force that induces out-of-plane displacement can be transferred through the adhesive to the angle, and then through the adhesive to the tension flange. Note that a stainless steel bolt is used and its function will be described in the following section.

### **1.3 Advantages of the proposed retrofit method**

One of the main advantages of this type of retrofit is that it can be applied from under the bridge and therefore does not need to disrupt traffic. The vibration caused by the passing traffic does not seem to affect the quality of the performance of adhesives (Nozaka, 2002). Also, provided that the requirements demanded by the manufacturer are met, the application of adhesives is relatively easy compared with field welding. Furthermore, with the availability of two-part thermoset adhesives, or room-temperature-cured adhesives, the application of adhesives can be conducted without specialized equipment in the field. In addition, the stainless steel bolt that connects the angle to the stiffener serves two purposes: to hold the angle in place before the adhesive has cured, and to keep the angle from dropping down if some disastrous event, such as fire, occurs to the bridge and damages the adhesive. This adhesively bonded retrofit does not introduce other fatigue sensitive details that are introduced by other retrofit methods (bolts or welds).

It is also worth mentioning that adhesives may not be suitable for many joining applications on steel bridges, particularly because they generally creep under sustained load. However, the retrofit of web-gap details with adhesives avoids this disadvantage because the out-of-plane loading is dynamically applied and returns to zero between passages of heavy trucks.

## 1.4 Objective

The objectives of the report are:

1. To find an appropriate adhesive for the proposed joint configuration and location.
2. To conduct a field test to develop retrofit procedures, study the effectiveness of the retrofit method under field conditions, and examine the long-term durability under outdoor exposure.
3. To conduct a large-scale lab test to study the effectiveness of the retrofit method by adhesives under controlled conditions. Variables such as in-plane stress and out-of-plane stress can be set so that this research is not limited to one or two specific bridges, but is applicable to a wide range of field conditions.
4. To conduct a set of coupon tests to study the environmental resistance of the chosen adhesive.

## 1.5 Outline

Chapter 2 presents a literature review of the problems associated with web gap out-of-plane distortion and research that has been conducted to understand and correct the problem. Chapter 2 also includes a literature review of adhesives, and their application in civil engineering, especially in steel structures. Parameters that are most important for such applications are also reviewed.

Chapter 3 discusses the field test to investigate the effectiveness of the adhesive-angle system retrofit method. The choice of the bridges, the instrumentation, the retrofit procedure, truck passes, and strain gage readings obtained before and after the proposed retrofit are addressed.

Chapter 4 describes the large-scale laboratory specimen test that adopts the adhesive-angle system retrofit method. The large-scale laboratory specimen design philosophy, finite element analysis, instrumentation and crack growth before and after the retrofit are discussed.

Chapter 5 documents small-scale laboratory coupon tests, conducted to investigate the durability of the adhesive. Coupon specimen configuration choice is described. Parameters such as bondline thickness, testing temperature, surface pretreatment, exposure temperature, exposure relative humidity, and exposure time are studied.

Chapter 6 reviews the findings of this study as well as the conclusions and importance of this research. Proposed future study is also included.

## Chapter 2 Literature Review

This chapter presents a literature review of the problems associated with web gap out-of-plane bending and research that has been conducted to understand the problem. This chapter also includes a literature review of adhesives and their application in civil engineering, especially in steel structures. Parameters that are most important for such applications are also reviewed.

### 2.1 Research on distortion-induced fatigue

According to Fisher (1978), there were no reported problems with steel bridges that could be associated with out-of-plane distortion-induced fatigue cracking until the early 1970's. However, distortion-induced fatigue cracking has now developed in many types of bridges, such as multigirder bridges, floorbeam bridges, and box girder bridges, and has plagued many of the U.S. state and interstate highway bridges and railroad bridges. In fact, web-gap cracking is the most common type of fatigue cracking in U.S. bridges (Fisher and Mertz, 1985; Keating, 1994). Unfortunately, most distortion-induced out-of-plane stresses that lead to fatigue cracks are difficult to predict, because they occur at very local regions which are not necessarily accounted for by an idealized design process. This section will discuss experimental studies and finite element studies conducted to understand, predict, and retrofit distortion-induced fatigue.

Goerg (1963), and Mueller and Yen (1968) have done tests with small T-shaped specimens designed to simulate the flange-web boundary. Fisher (1978) found that these test results demonstrated that Category C is a reasonable lower bound estimate of the fatigue resistance from the web gaps. However, since the transferability of fatigue data from small specimens to full-scale structures is still unsolved (Cui, 2002), Category C can only be treated as an approximate estimate before large-scale test data are available.

Fisher et al. (1990) conducted a laboratory experiment on 12 girders with each girder having 2 web gaps produced by connection plates welded only to the web and compression flange. It was found that the weld at the end of the transverse connection plate had a higher stress concentration than the flange-web weld, because most of the fatigue cracks initiated at the end of the connection plates, even though the stress range was greater at the flange-web weld. Fisher et al. contributed such an observation to the smoother configuration of the flange-web weld than the stiffener-web weld.

Strain measurements taken in the field by Fisher (1978) suggested that the web gap is subjected to double curvature. This was confirmed by Fisher and Keating (1989), and Fraser et al. (2000). Thus, the deformed shape of the web gap can be idealized as a fixed-fixed beam with out-of-plane displacement, and thus the out-of-plane bending moment can be expressed as

$$M = \left( \frac{6EI_g \delta}{g^2} \right)$$
, where  $E$  is modulus of elasticity,  $I_g$  is moment of inertia of the web gap,  $\delta$  is out-of-plane displacement at the web gap, and  $g$  is length of the web gap. This leads to the following equation for the calculation of out-of-plane stress

$$\sigma_{wg} = \left( \frac{3Et_w}{g^2} \right) \left( \frac{h\Delta}{S} \right) \quad (2-1)$$

Where  $\sigma_{wg}$  is the maximum out-of-plane bending stress,  $t_w$  is the thickness of the web,  $h$  is depth of the diaphragm,  $\Delta$  is differential deflection of the girders, and  $S$  is girder spacing.

However, in a finite element study conducted by Jajich and Schultz (2003), it was found that for the specific staggered bent-plate diaphragm bridge geometry modeled, rotation of the connection plate,  $\theta$ , caused by the differential deflection of the adjacent girders, was the primary deformation mechanism. In other words, the out-of-plane bending moment can be expressed as

$$M = \left( \frac{4EI_g}{g} \theta \right).$$

It should be pointed out that the concrete deck was not included in this finite element research. Instead, rotational fixity of girder top flanges was assumed. Jajich and Schultz believed that the differences between this rotational fixity and the restraint imposed by the deck had little effect on the local behavior of the web-gap region. They proposed the following equation to determine out-of-plane stress

$$\sigma_{wg} = \left( \frac{2Et_w}{g} \right) \left( \frac{\Delta}{S} \right) \quad (2-2)$$

Because differential deflection,  $\Delta$ , was the only unknown parameter in both Equation (2-1) and (2-2) for the prediction of out-of-plane bending stress, Berglund and Schultz (2003) performed a parametric study on a finite element model of the entire bridge studied in the research of Jajich and Schultz (2003). Shell elements were used to model the concrete deck and rigid elements were used to connect the deck to the upper flange of the steel girder. It was found that differential deflection increased with larger skew angle and larger girder spacing. Differential deflection decreases with larger bridge span length (when the main span length is larger than 140 ft.), and the inverse is true for the shortest span length. Furthermore, it was found that every 1 in. of increase in deck thickness resulted in an approximately 15% decrease in differential deflection. On the other hand, differential deflection was found to be relatively insensitive to the length of adjacent spans and diaphragm depth. Berglund and Schultz (2002) proposed the following equation to evaluate the ratio of differential deflection to girder spacing,  $\Delta/S$

$$\frac{\Delta}{S} = \frac{A \cdot L^2 + B \cdot L + C}{L} \quad (2-3)$$

Where  $L$  was the main span length, and constants  $A$ ,  $B$ , and  $C$  depended on the skew angle of the bridge and were determined by curve fitting the results of a parametric study.

In follow-up research by Severtson et al. (2004) on a staggered X-braced diaphragm bridge, it was found that Equation (2-3) was only valid for the staggered bent-plate-diaphragm bridge. The differential deflection of a staggered X-braced diaphragm bridge was found to be smaller than that of the staggered bent-plate-diaphragm bridge, and modifications were

suggested to Equation (2-3). Berglund and Schultz used single frame line elements to model bent plate diaphragms, while Severtson et al. used four frame line elements to model cross frame diaphragms. Also, Severtson et al. found that, for the specific bridge studied, the web gap stress was primarily generated by the rotation of the top flange and the connection plate. This was in contrast to the findings that the web gap stress was mainly due to the out-of-plane displacement (Fisher, 1978; Fisher and Keating, 1989; and Fraser et al., 2000), or, as Jijach and Schultz (2003) discovered that the web gap stress was mainly caused by the rotation of the connection plate.

It was found that out-of-plane bending stress at the web gap was most severe in the negative moment region because of the restraint provided by the concrete deck (Fisher and Mertz, 1984; Keating, 1994; Khalil, et al., 1998; Jajich and Schultz, 2003; Zhao and Roddis, 2005). However, some research projects seemed to have found otherwise. For example, in a finite element analysis on a five-span skewed bridge with staggered diaphragms, Zhao and Roddis (2003) found that out-of-plane stresses were most severe in the positive moment region because of the larger differential deflection at the midspan. In this research, 8-node brick elements were used to model the concrete deck and 4-node shell elements were used to model the girder, diaphragm, and connection plates.

The above literature review on the out-of-plane bending stresses at web gaps demonstrates that out-of-plane bending stresses are difficult, if not impossible to predict, without a detailed finite element analysis. Even with finite element analysis, different simplification methods applied to the model may also change the predicted stresses. Thus, even though the retrofit philosophy of decreasing the stiffness of the system so as to decrease the stress concentration at the web gap was used successfully in several cases before, there is no guarantee that such methods will be effective on all bridges. Furthermore, if finite element analysis has to be conducted for each particular case to ensure the effectiveness of reducing the stiffness in the web gap region, then the cost of the retrofit will be increased. Therefore, providing positive attachment may be the best retrofit method for out-of-plane fatigue problems.

To date, positive attachment has been achieved by welding and bolting. However, as described in Chapter 1, both welding and bolting have disadvantages. Thus the feasibility of using adhesives will be investigated in the current study. Since there are many types of adhesives, it is evident that a literature review on adhesives and their application to steel-to-steel bonding should be conducted before choosing the adhesive for the proposed retrofit method.

## **2.2 Research on adhesives**

### **2.2.1 Outline**

Adhesives have been widely used in the aerospace and automobile industries, and they have also found many applications in civil engineering structures, both nonstructural and structural (Mays, 1985; Vardy and Hutchinson, 1986). However, adhesives have only been used previously for steel structures in limited research (Albrecht, 1987; Gasparini et al., 1990; Hashim et al., 1990; Martin, 1992; Nozaka, et al., 2001; Nozaka, 2002; Schnerch et al., 2004; Shaat et al., 2004). The main reason is that the specialized processes used in the fabrication of airplanes or automobiles are either not applicable or not economical for building or retrofitting steel structures. Also, compared with airplanes or automobiles, most steel structures are expected to be

in service for a longer period of time. Thus there is more rigorous demand for the durability of the adhesive.

Gasparini et al. (1990) listed several properties that engineers should consider in their choice of adhesives for civil engineering applications, these included:

- viscosity
- toxicity
- shelf life
- pot life
- curing temperature and pressure
- polymerization shrinkage
- glass transition temperature ( $T_g$ )
- coefficient of thermal expansion
- stress-strain relationship below  $T_g$
- uniaxial tensile creep rupture data
- fatigue life
- diffusion coefficient
- resistance to agents in design environment

Of course, due to the different formulations of different adhesives, one adhesive may outperform another in one respect, yet be inferior in another respect, thus it is very important for the engineer to decide which properties are more important for a particular engineering application.

As mentioned earlier, durability of the adhesives is a major concern for application in civil engineering structures. It has been found that joint strength of fresh specimens, or unaged specimens, gives no indication of the joint strength of aged specimens (Fay and Maddison, 1990; Bistac et al., 1998; Ashcroft et al., 2001). Gasparini et al. (1990) listed three possible approaches to the durability issue. The first one was to predict durability theoretically, however, theories of adhesion are not sufficiently developed at present to use this approach.

The second approach to the durability issue was to perform “accelerated aging” tests by exposing the specimens to high/low temperature, high relative humidity, salt bath or other more hostile environments so that the adhesives deteriorated at a faster speed than they would normally do under service conditions. The results of the “accelerated aging” test could then be used to predict the durability of in-service adhesives.

The third approach to the durability issue was to use a database of in-service durability performance, however, this database does not exist due to the scarcity of adhesives used in steel-to-steel bonding in civil structures. As a result, the second approach has been used extensively. Though there are no widely accepted theories to infer service life from accelerated test data, accelerated tests are still valuable comparative tools (Gasparini et al., 1990; Hashim, 1999; Knox and Cowling, 2000a). Accelerated durability testing should be conducted in an environment physically similar to that of the service condition and great caution must be exercised in the interpretation of the results (Gledhill and Kinloch, 1974; Brewis, 1983; Mays and Vardy, 1983; Arrowsmith, 1987; Kinloch, 1987; Bowditch, 1996; Chang et al., 1997; Knox. and Cowling, 2000a).

Kinloch (1983) listed some of the main parameters that influence the durability of structural adhesive joints, these were:

- environment
- concentration of water
- temperature
- adhesive and adherend type
- adherend surface preparation
- applied stress
- joint design

One of the most important factors in determining the permanence of adhesively bonded joints in most weathering service environments is water, be it in liquid or vapor form. Thus water has become the focus of many research projects.

Summarized by Comyn (1983) and Bowditch (1996), water can enter a joint by: (1) diffusion through the adhesive, which is regarded by many as the primary access route; (2) diffusion through the adherend, which is only possible with organic adherends; (3) transporting or wicking along the interface, which occurs where wetting of the substrate is incomplete; and (4) capillary action, which is found mainly in elderly joints.

According to Comyn (1983), water may cause weakening by one or a combination of the following actions after it has entered a joint: (1) altering the properties of the adhesive in a reversible manner, such as plasticizing and swelling; (2) altering the properties of the adhesive in an irreversible manner, such as hydrolysis, cracking, or crazing; and (3) attacking the adhesive/substrate interface either by displacing the adhesive or by hydrating the metal or metal oxide surface of the adherend. Indeed, Bowditch (1996) has found through experiments that some, and not all of the lost strength of the adhesively bonded joints due to water invasion, was recovered after drying, confirming that water attack could be divided into reversible and irreversible parts.

Whereas exposure of adhesive joints to high relative humidity usually causes weakening, it has been frequently observed that adhesive joints can withstand exposure to low relative humidity (RH 45~55%) under room temperature for long periods of time without any weakening. This prompted Gledhill et al. (1980) to propose that there must be a critical water concentration below which water attack does not have negative effects on the adhesively bonded joint. Bowditch et al. (1992) suggested that two mechanisms, a plasticizing process which may reduce stress concentration at the joint end and thus enhance joint strength on one hand, and interfacial attack which will cause a degradation of the joint on the other, might in certain circumstances be in a state of balance over a limited range of water contents.

Nevertheless, it is generally accepted that because of the high surface energy of metals, the stability of the interfacial layer between the adhesive and the adherend is the controlling feature for the durability in aqueous environments for all polymer/metal bonds.

This finding was first demonstrated by research conducted by Gledhill et al. (1974), where steel butt joints bonded by an epoxy adhesive were immersed in distilled water at various temperatures. In this research, cohesive failure, i.e., failure within the adhesive layer, was found

at the center of the butt joint. Adhesive failure (sometimes referred to as interfacial failure), i.e., failure between the adhesive and the substrate, was found at the edge of the same joint.

The same phenomenon has been observed by Butt and Cotter (1976), and Brewer et al. (1990). As a result, researchers have been looking for methods that improve the durability of the interfacial layer with a view to improving the durability of the whole joint. It is widely accepted that chemical etching, which is commonly used for pretreating aluminum and titanium substrates, is not suitable for steel substrates because of the corrosive residues left on the etched surface (Kozman and Olefjord, 1987). Mechanical abrasion, such as grinding, brushing or sandblasting, followed by solvent (such as acetone) wiping, provided the baseline surface preparation for steel substrates (Brockmann, 1983; Adams and Wake, 1984; Knox and Cowling, 2000b). Furthermore, Gettings and Kinloch (1977) found that a primer named  $\gamma$ -glycidoxypropyltrimethoxy silane (GPS) significantly improved durability for steel joints. Kozma and Olefjord (1987), Fay and Maddison (1990), Tod et al. (1992), and Abdel Wahab (2002) also had similar findings in their research. As discussed in Chapter 5, GPS will be investigated in this research to find its influence on the durability of adhesively bonded steel joints.

### **2.2.2 Research on adhesive application on steel structures**

Though metal to metal bonding is common in other branches of engineering, it may be surprising that it is almost non-existent in civil engineering and only very limited research has been conducted in this respect. The following literature review is focused on steel to steel bonding, though glass fiber reinforced polymers (GFRP) and carbon fiber reinforced polymers (CFRP) to steel bonding has been investigated by a number of researchers (Nozaka et al., 2001; Nozaka, 2002; Schnerch et al., 2004; Shaat et al., 2004).

Albrecht (1987) investigated the fatigue resistance of bonding two ½ in. thick cover plates to the tension flange of 17 steel girders. The W14X30 girders were loaded in four-point bending (Figure 2.1). The two cover plates were symmetrically bonded to the lower side of the bottom flange outside of the constant moment region. An acrylic structural adhesive which became handleable after 8 to 16 minutes of curing at 75°F and developed full strength after 24 hours, was used to bond the cover plates. All the cover plates showed gradual debonding at the end closest to the midspan for the first three girders. Then the cover plate ends on the fourth girder closest to midspan were clamped to the flange with two ¾ in. diameter ASTM A325 high-strength bolts. However, it was found that the cover plate then began to debond from the support end. Indeed, as mentioned by Kinloch (1987), from the aspect of joint design, attempts should be made not only to keep stress concentrations to a minimum, but also to distribute the imposed loads within the adhesive layer as a combination of compressive and shear stress, avoiding tensile, cleavage and peeling stresses as much as possible. Since cleavage stresses were introduced to the adhesive layer at the ends of the cover plates, it was not surprising that debonding occurred in the first four steel girders.

Albrecht (1987) then bolted both ends of the bonded cover plates prior to stress cycling on the remaining 13 steel girders. Therefore, there were altogether 28 bonded and bolted midspan ends of cover plates. Four stress ranges at 21 ksi, 23 ksi, 27.4 ksi and 30 ksi resulted in 9 failures from cracks that initiated at the bolt holes in the flange, 2 failures from fretting cracks

in the flange, and no failures in the remaining 16 cover plates ends. The data indicated that the fatigue strength of bonded cover plates with bolted ends exceeded that of Category B details, which was a large improvement over the Category E detail provided by the welded cover plates.

In an attempt to generate in-service durability data for adhesively bonded steel to steel connections, Gasparini et al. (1990) bonded attachments to the webs of girders of a bridge in Ohio. Two adhesives, a modified acrylic and an epoxy, were used. Bondline thickness was 0.01 in. and surface preparation consisted of grinding and wiping with Toluene. Steel tee sections with 3 in. by 3 in. bonding area were bonded and stressed in tension and in flexure (Figure 2.2). Hollow cylindrical sections were bonded and stressed in shear (Figure 2.2). Four nominal constant stress values at 1.5 ksi, 1.0 ksi, 0.5 ksi and 0.25 ksi were applied. There were three specimens for each parameter combination. It was found that most of the connections made with the modified acrylic adhesive were still carrying the applied stress after 5 years, though the epoxy adhesive used in this research was not as durable. However, the authors commented that other epoxies might be more durable.

Hashim et al. (1990) investigated bonding two I-shapes to a steel plate to make a large-scale composite bending beam (Figure 2.3). A single part hot cured toughened epoxy adhesive was used. Surface preparation consisted of gritblasting and wiping with acetone. Four point loading tests were used. The adhesive shear stress at the maximum design load level was estimated, using composite beam theory, to be approximately 20% of the maximum average strength value. The specimens showed noticeable plastic deformation of the I-shapes, which suggested the effectiveness of the adhesive bonding for this connection and the fact that adhesive bonding did not need to be as strong as the components being joined to be effective.

Martin (1992) investigated the application of bonded transverse intermediate stiffeners to the webs of steel girders (Figure 2.4). The three adhesives investigated were a two-part cold curing toughened epoxy resin and two single-part toughened epoxy resins. A large number of bonded double lap joint tests, under both static and fatigue loading, indicated that one of the single-part toughened epoxies had the highest elastic modulus and the greatest shear capacity, and this adhesive was used to bond the stiffeners. The surface preparation for the web plate and the stiffener consisted of degreasing and gritblasting. The stiffeners were produced by cutting and grinding from 2-in. x 2-in. x 1/4-in. T-bar sections (Figure 2.4). The fatigue test results obtained for the bonded unstressed transverse stiffeners indicated that the joints remained undamaged even when subjected to main plate stress ranges of 29 ksi for 20 million cycles. Similar welded details could not be expected to survive more than 1 million cycles at such high stress ranges. Also, when tested under ultimate load conditions, the theoretical to experimental failure load ratios of the three girders with bonded stiffeners were in complete agreement with the theoretical to experimental failure load ratios of three other girders with fully welded stiffeners. Furthermore, the three girders with bonded stiffeners all developed tension field action and shear collapse mechanisms, indicating the effectiveness of the adhesive bond. Nevertheless, the author also mentioned that durability of the adhesively bonded steel joints should be investigated and fire protection of such joints was of particular importance for building structures.

To summarize, adhesives have been successfully used for steel-to-steel bonding on civil engineering applications, however, more experimental work is needed to gain more confidence

in their performance. Aspects such as environmental durability and fire resistance are of particular interest. Structural engineers should work closely with adhesive manufacturers to find the most suitable adhesives for the proposed application.

## Chapter 3 Field Test

The field test was an indispensable part of this project used to determine the effectiveness of the proposed retrofit method, because it represented the real environment and loading under which the adhesive will be applied and exposed. Therefore, representative multi-girder steel bridges were to be chosen from available bridges to conduct the field test. The major considerations for the choice of the multi-girder steel bridges were that they should be susceptible to web-gap out-of-plane distortion problems and preferably, be accessible with minimum interference to traffic.

Two representative bridges were chosen for the truck test (Bridge #27763 and Bridge #27984). Both bridges were three-span continuous bridges. Bridge #27763 had staggered bent-plate diaphragms and Bridge #27984 had continuous cross-frame diaphragms. Both bridges were designed in 1981 with web gap details and large skew angles. This led them to be susceptible to web-gap out-of-plane distortion problems, particularly in the negative moment region.

Out-of-plane stress ranges were measured at the web gap in the negative moment region for controlled truck tests conducted both before and after the retrofit. Out-of-plane stress ranges from both truck tests were compared for the bent-plate-diaphragm bridge (Bridge #27763) and for the cross-frame-diaphragm bridge (Bridge #27984).

In this chapter, bridge selection criteria and the selected bridge description are discussed in Section 3.1. Adhesive selection criteria and the chosen adhesive are provided in Section 3.2. Bridge instrumentation and application of the angles are described in Section 3.3. Test trucks and test setups are shown in Section 3.4. Comparison of typical strain gage readings for truck tests both before and after retrofit is provided in Section 3.5. Field inspection of the adhesive-angle retrofit system is described in Section 3.6. Conclusions of the field test are shown in Section 3.7.

### 3.1 Bridge selection

The major considerations for the choice of the multi-girder steel bridges for the field test were that they should be prone to web-gap out-of-plane distortion problems and be accessible with minimum interference to traffic. The overviews of the two bridges chosen for the project are shown in Figures 3.1(a)~(c). The plan views of these two bridges are shown in Figures 3.2(a)~(b). Both the bent-plate-diaphragm bridge and the cross-frame-diaphragm bridge were located 1.9 miles east of the junction of Trunk Highway 36 and Trunk Highway 494.

The following reasons made the two selected bridges likely to be susceptible to out-of-plane distortion problems:

1. Both the bent-plate-diaphragm bridge (BPD bridge, Bridge #27763) and the cross-frame-diaphragm bridge (CFD bridge, Bridge #27984) were designed in 1981, when positive attachment between the connection plate and the girder tension flange was not required in the AASHTO specifications. As a result, small web gaps on the order of 2 to 2 ½ in. existed between the connection plate and the tension flange of the girder in both bridges.

2. Both bridges had large skew angles (approximately 50°).

The BPD bridge was a three-span (151 ft. - 156 ft. - 117 ft.) six-girder continuous bridge with deep staggered diaphragms rigidly connected to the connection plates. The skew angles of this bridge varied from 46° to 58°, from the north abutment to the south abutment.

The CFD bridge was a three-span (197 ft. - 177 ft. - 134 ft.) five-girder continuous bridge with continuous diaphragms. The skew angles of this bridge varied from 50° to 63°, from the north abutment to the south abutment.

### **3.2 Adhesive selection**

Several factors listed by Gasparini et al. (1990) and others (Adams and Wake, 1984; Nara et al., 1985; Nozaka, 2002) were studied before the final choice of the adhesives was made. Among them, field applicability, substrate compatibility and environmental durability constituted the major parameters that led to the choice of the adhesive named DP-460NS, which is a product of 3M.

DP-460NS is a two-part room-temperature-cured epoxy in a viscous liquid form. Firstly, room-temperature-cured adhesives do not require heat blankets, which is particularly advantageous for field application. Moreover, since DP-460NS is cured at room temperature, or service temperature, no internal shrinkage stress will be induced from a difference of coefficient of thermal expansion between the substrate and the adhesive because there is no cooling process. Though polymerization and crosslinking may also induce contraction of the adhesive, and thus introducing shrinkage stress within the adhesive, it is usually of secondary importance (Kinloch, 1987).

Secondly, the viscous liquid form is favorable in the field. If the viscosity is too high, like paste, wetting of adherend, which is of prime importance for strong and durable bonding (Minford, 1983), will be difficult. Also, since bondline thickness must be compatible with the surface irregularities of thick steel plate in the field, the adhesives must have gap-filling properties, which cannot be achieved by a paste form. On the other hand, if the viscosity is too low, the adhesive can drain from the relatively large joint, leaving insufficient amount to form a continuous film, thus creating a 'starved joint', which is then a weak joint. Figure 1.2 shows that both an overhead position and a vertical position are involved in the proposed retrofit method, a 'starved joint' may form if the adhesive has too low viscosity.

Thirdly, unlike most other two-part adhesives, this adhesive is packaged in a twin pack cartridge system so that the exact amount of both parts can be squeezed into a static mixing nozzle and dispensed directly onto the adherends, thus achieving better quality with less labor (Figure 3.3). Furthermore, based on the recommendation of the manufacturer, DP-460 NS is expected to provide very good environmental durability, which is vital for long-term performance. Small-scale coupon tests to investigate the durability of this adhesive will be discussed in Chapter 5.

### 3.3 Bridge instrumentation and retrofit location

#### 3.3.1 Bridge instrumentation

The objective of the instrumentation was to accurately obtain the stress ranges at designated places under known loads. As a result, comparisons could be made between stress ranges in the web gap regions before and after retrofit.

For accessibility reasons, only the second span, i.e., the center span, was instrumented for each bridge. The total number of strain gages used on each bridge was limited by time constraints associated with the need for bridge maintenance crew assistance, as well as the availability of channels on the data acquisition system. Thus, not all girders in the second span were instrumented.

There were two lanes of traffic going in the northeast direction on each bridge. There were shoulders of varying width along the length of both bridges. For logistical reasons, static and low speed loads could only be applied to the right lane and shoulder, the majority of instrumentation was placed on the girders associated with the right lanes. Only negative moment regions of both bridges were instrumented as it was assumed that the out-of-plane distortion fatigue problems would be more severe in the negative moment region than in the positive moment region (Fisher, 1978; Demers and Fisher, 1990; Khalil et al., 1998). Also, the easiest access to the underside of the bridge was located in the negative moment region.

Although the main objective was to investigate the difference in stress ranges at web gaps before and after retrofit, it was still desirable to obtain the stress range in the primary stress field. Firstly, the primary stress range could be used to compare the consistency of loading before and after retrofit. Secondly, it was instrumental to know the difference of the primary stress range and the secondary stress range. Single element weldable 350-ohm gages were used at places where primary or secondary stress fields were of interest.

It was postulated that if the alternate load path provided by the adhesive-angle combination was effective, then the shear stress field on the connection plate at places close to the web gap would change after the retrofit was provided. Adhesively bonded 350-ohm rosettes were applied to locations where the shear stress field was of interest.

Figure 3.4 shows the locations of instrumentation on the bridge plan view. The circled areas denote the places where instrumentation was applied. The short bold lines denote the places that were chosen to receive retrofit angles.

Figure 3.5 shows the typical locations of each gage on the steel girder, connection plate, and the diaphragm. In this figure, each single weldable gage is denoted by one short bold line, and each rosette is denoted by three short bold lines. The direction of the short bold line denotes the direction of strains the gage measured.

Figure 3.6 shows the application of a weldable strain gage. The vertical strain gages were applied as close to the flange-web fillet weld toe as possible, in order to capture the maximum out-of-plane distortion strains.

Surface preparation for both the weldable gages and the adhesively bonded rosettes consisted of grinding the layers of paint off the steel until a smooth shiny surface of steel was exposed. Then the surface was cleaned with a degreaser. Afterwards, the weldable gages were welded onto the steel with a portable welding/soldering unit and the adhesively bonded rosettes were adhered to the cleaned surface with a fast setting adhesive. The installed strain gages were then covered with caulking to protect the gages from humidity, temperature changes, and other environmental effects. Duct tape was used on top of the caulking.

The gage labeling, corresponding location, and gage types can be found in Appendix A.

### **3.3.2 Retrofit plan**

In Figure 3.4, the short bold lines denote the places where retrofitting angles were applied. The retrofitting angles are denoted such that the first capital letter “A” referred to “Angle”, the first number referred to the bridge (“1” for BPD bridge and “2” for CFD bridge), and the second number referred to the number of the angle on each bridge. The second number in the labeling changed from “1” to “8”, as the angle location moved from the north to the south. It should be mentioned that the numbering was not continuous. There were five retrofitting angles on each bridge and the location of retrofitting angles coincides with the location of the instrumentation in most cases.

The retrofitting angle configuration is shown in Figure 3.7. The bolt hole was not located at the center of the leg and the hole size was considerably larger than the stainless steel bolt size. This was because the hole pattern of the retrofitting angle needed to be compatible with the hole pattern of the connection plate, and the 7/8 in. diameter hole size on the angle was chosen to be large enough to accommodate the hole pattern inaccuracies of the field drilled connection plates. The thickness of the angle was chosen to be  $\frac{3}{4}$  in. because previous research (Fisher, 1990; D’Andrea et al., 2001) implied that a thinner dimension might not provide enough stiffness for the retrofit method to be effective. The lengths of the angle were chosen so that the angle was not too heavy for easy application, yet it still had enough adhering surface to resist out-of-plane forces.

A picture of the on-site application of the retrofitting angle is shown in Figure 3.8. Note that the excess adhesive was squeezed out. Also, the stainless steel bolt that connected the angle to the stiffener served two purposes: to hold the angle in place before the adhesive had cured, and to keep the angle from dropping down if some disastrous event, such as fire, occurred to the bridge and damaged the adhesive. Glass beads were used as spacers to maintain a bondline thickness of 0.020 in. Such thickness was believed to be compatible with the irregularities of thick steel plates. The procedure of applying the retrofitting angles can be found in Appendix B.

The temperature recommended for the use of this adhesive is around 70°F. The angles were bonded to the bridges in November, 2001. The daytime temperature was approximately 50°F and the adhesive became so thick that the two parts could not be squeezed out through the manufacture supplied static mixing nozzle (Figure 3.3). As a result, the two parts were squeezed out directly from the cartridge to the angle surface, and then they were mixed with a spatula. Though efforts were made to mix them as thoroughly as possible, there were likely areas of incomplete mix. This application represented the worst situation of field application and should

provide the lower bound performance of the adhesive. In some cases, a heat gun was used to facilitate squeezing the adhesives out and mixing them. Sometimes, a heat gun was also used to heat the angle for five minutes after the angle was put on to facilitate curing of the adhesive. Table 3.1 describes the individual application situation for each angle.

Since only one stainless bolt was used to connect the retrofitting angle to the connection plate, the bondline thickness was not constant due to the 14 pounds of self weight of the angle as is shown in Figure 3.9. The bondline was maintained at 0.020 in. at the angle stem and was larger than 0.020 in. at the angle tip. Angles “A2-5”, “A2-6” and “A2-7” had very small gaps in the bondline at the angle tips. In other words, there were some areas on the flange face where the adhesive was not thick enough to fill in the volume. These areas were small (about 5~10% of total area) and could be reasonably accepted for field application. However, in one particular case, a gap of approximately 1/8 in. at the tip occurred for Angle “A2-4”. Angle “A2-8” did not have any glass beads to control the bondline thickness.

Normal traffic was not interrupted when the retrofit was conducted. Vibration caused by the driving vehicles could be felt when the angles were adhered to the girders, however, this did not introduce any inconvenience for the retrofit process. If the retrofit was found to be effective, conclusions could be drawn that vibration caused by the traffic would not influence the effectiveness of the adhesive performance.

### **3.4 Test trucks and test setups**

Two three-axle Mn/DOT sand trucks were used for the test. Each truck weighed approximately 50 kips. The front axle carried approximately 26% of the total weight while the second and third axle both carried approximately 37% of the total weight. Spacings and axle loads are shown in Figure 3.10.

Eight loading passes were made with the trucks. Among them, the first three passes were static ones, i.e., once the truck reached the designated position, it stayed there for approximately 30 seconds and then changed to another location. The static passes had the advantage of ensuring that the loading positions before and after retrofit were the same. The latter five passes involved at least one moving truck. The dynamic passes had the advantage of showing less drift effects of the strain gages because the values obtained from them were strain ranges over short periods of time. The dynamic passes also represented a more realistic loading situation on the bridge.

The truck positions are shown in Figures 3.11 and 3.12. Figure 3.11 shows that the left wheels of the trucks were positioned above a particular girder so as to create the largest possible differential deflections between adjacent girders. Figure 3.12 shows the positions of the truck for the static passes. For Pass 4, the static truck stayed at the same position as in Pass 2 and the dynamic truck moved at 10 mph. For Pass 7, two trucks were traveling side by side. Pink paint was used to draw lines on the roadway to guide the trucks in passes up to 10 mph. For other passes, the truck drivers were simply told to drive close to the left or right lane marker. Therefore the positions of the trucks were less accurate for faster passes than for slower passes. Thus, the following analysis is based on three static passes (Passes 1~3) and three 10 mph dynamic passes (Passes 4, 5, and 8) unless otherwise noted.

## 3.5 Comparison of typical strain gage readings

### 3.5.1 Bent-plate-diaphragm bridge (Bridge #27763)

#### 3.5.1.1 Comparison of out-of-plane strains

Figure 3.13 shows the out-of-plane strains before and after retrofit for the instrumented web gap on B5 for slow moving passes along the same positions as Passes 1~3 at 10 mph. As can be seen from the figure, the strain readings on the same side of the web were approximately the same, and the strain readings on the opposite side of the web had opposite signs and comparable absolute values. Thus the four web gap gages gave consistent readings.

Comparison of Figure 3.13(a) and (b) shows that the out-of-plane strains at the web gap on B5 were reduced to 40~60% of the original strains by the proposed retrofit method. Tables 3.2 and 3.3 show the web gap strain ranges on B5 and B4 before and after retrofit for the BPD bridge (Bridge #27763). Note that only three static passes and three 10 mph dynamic passes are included because it is believed that static passes and slow moving dynamic passes provided more repeatable results. Web gap strain ranges for other passes and on other girders can be found in tables in Appendix C.

Figure 3.14 shows the relationship between out-of-plane strain range reduction and the original out-of-plane strain range for the bent-plate-diaphragm bridge. Note that web gaps at B5, B4, and B3 were retrofitted. This retrofit method achieved at least 38% strain range reduction when the original strain range was more than 50 microstrains. The web gap at B4W was not retrofitted. Strain range reduction was approximately zero for the untreated web gap. There was  $\pm 10\%$  variation for the web gap at B4W, which could be explained by small variation in size, weight and position of the truck, and data acquisition before and after retrofit. It also demonstrated that the 38% strain range reduction at web gaps at B5, B4, and B3 was achieved by the retrofit method, and was not due to the variation of the test. Moreover, it can be concluded that the retrofit at one location does not increase the potential for cracking at nearby unretrofitted connections.

#### 3.5.1.2 Comparison of in-plane strains

Table 3.4 shows that the in-plane strains on B5 before and after retrofit were very close, indicating that the truck followed the same path in both truck tests. Except for one point, there was  $\pm 21\%$  variation for the in-plane strains on B5, which could be explained by variation in size, weight, and position of the truck before and after retrofit. The extreme point occurred at gage 1-B5-5-B for Pass 3. The strain was  $-4 \mu\epsilon$  before retrofit and  $-3 \mu\epsilon$  after retrofit. The magnitude of both values was very small and a small noise could introduce a large strain variation. The close values of in-plane strains before and after retrofit suggested that the reduction in out-of-plane strain observed in the previous section was due to the retrofit method, and was not because of the change of the truck traveling path. In-plane strain ranges for other passes and on other beams can be found in tables in Appendix D.

### ***3.5.1.3 Comparison of out-of-plane strains and in-plane strains***

Comparison of Table 3.2 and Table 3.4 shows that the out-of-plane strain range at the web gap before retrofit was approximately five times larger than the largest in-plane strain range at similar locations in B5 for Passes 1~3. For Passes 4, 5, and 8, the ratio mentioned above was approximately three to four. Thus it is not surprising that web gap cracking is the most common type of fatigue cracking in bridges in the United States (Fisher and Mertz, 1985; Keating, 1994).

### ***3.5.1.4 Comparison of bent-plate diaphragm strains***

As shown in Table 3.5, the strain values measured by the three horizontal single gages on the bent-plate diaphragm showed little difference before and after retrofit. This was expected because the web gap effect was a local effect which mostly focused on a small area on the web. Also, the strain values suggested that, as predicted, the diaphragm was subjected to end moment. Only results from the static passes were analyzed for this comparison. The bent-plate diaphragm strains measured by single gages are provided in Appendix E. The bent-plate diaphragm strains measured by rosettes are provided in Appendix F.

### ***3.5.1.5 Comparison of connection plate strains***

Two rosettes were used on the connection plates, one on B5 and the other on B4. No conclusive observations could be drawn from the strain readings of the rosettes. The strains measured by rosettes are provided in Appendix F.

### ***3.5.1.6 Effect of differential deflection and rotation on out-of-plane strains***

As can be observed from Table 3.2 and Table 3.3, for Passes 1~5 and Pass 8, the original strain range was greater for B5 than for B4. The following analysis on the contribution of differential deflection and rotation on out-of-plane strain can explain this observation for Passes 1~3 and Pass 8, when only one truck was involved.

Figure 3.15 shows three concurrent movements (displacements) of the girders for the static passes, i.e., differential deflection of adjacent girders B5 and B4, rotation of the diaphragm that connects girders B5 and B4, and rotation of the concrete slab. In this figure, “+” denotes tension and “-“ denotes compression. It can be seen that, differential deflection, diaphragm rotation and deck rotation all produced positive strain on the northwest (NW) side of the web gap for B5. Differential deflection and diaphragm rotation produced negative strain on the southeast (SE) side of the web gap for B4; deck rotation produced positive strain at the same location.

It can be concluded that the combined effect of differential deflection and diaphragm rotation was more dominant than deck rotation, because the out-of-plane strain readings of B4 had the sign predicted by differential deflection and diaphragm rotation (Table 3.3). Figure 3.15 could also explain why larger out-of-plane strains were measured for web gap at B5 than for web gap at B4. Since differential deflection and diaphragm rotation produced the same sign, it was difficult to differentiate between these two effects without finite element analysis.

Other passes were analyzed in the same fashion and it was found that for most cases, differential deflection and diaphragm rotation were more dominant than deck rotation. However, if a girder was two girder spacings away from the truck, the analysis described above was no longer valid because of the complicated interaction effects of girders, diaphragms and concrete slabs.

### **3.5.2 Cross-frame-diaphragm bridge (Bridge #27984)**

#### ***3.5.2.1 Comparison of out-of-plane strains***

Figure 3.16 shows the out-of-plane strains before and after retrofit for the instrumented web gap on B4 for slow moving passes along the same positions as Passes 1~3 at 10 mph. As can be seen from the figures, the four web gap gages gave consistent readings. Also, the original out-of-plane strains on the CFD bridge were much smaller than the original out-of-plane strains on the BPD bridge (Tables 3.6 and 3.7 vs. Tables 3.2 and 3.3).

One possible reason for the smaller initial strain ranges was that the CFD bridge had back-to-back diaphragms, while the BPD bridge had staggered diaphragms. Back-to-back diaphragms may be able to share the out-of-plane force among several diaphragms in the line of force so that the out-of-plane force exerted on one web gap was smaller than the case for the staggered diaphragm system. Another possible reason was that the cross-frame-diaphragm was less stiff than the bent-plate-diaphragm, thus smaller out-of-plane force was applied at the web gap for the CFD bridge than for the BPD bridge. A third possible reason was that the CFD bridge had deeper girders and longer spans and therefore the relatively stiffer system in the negative moment region near the piers resulted in smaller differential deflection between adjacent girders, leading to smaller initial out-of-plane strains. In fact, with a finite element model refined to match the field data, Berglund and Schultz (2002) conducted a parametric study and found that main span length, angle of skew, girder spacing and concrete deck thickness all have a significant impact on the amount of differential deflection.

One interesting observation was that the out-of-plane strains changed signs for Pass 3 and Pass 8 before retrofit (Table 3.6 and Figure 3.16(a)). The fact that all four web gap gages showed the same phenomenon for both passes ruled out possible noise or gage malfunction. The fact that this phenomenon was observed in both Pass 3 and Pass 8 ruled out possible wrong truck position. Factors such as dynamic effect, interaction of the slab, girders, and diaphragms, and variation of truck position were considered, however, none of these could explain the out-of-plane strain sign change observed before retrofit. One conclusion was that the out-of-plane strains were very sensitive to small changes in the location of the truck. No sign changes were observed in either Pass 3 or Pass 8 after retrofit (Table 3.6 and Figure 3.16(b)). No sign changes were observed for all other passes before or after retrofit. Web gap strain ranges for other passes and on other beams can be found in tables in Appendix C.

Figure 3.17 shows the relationship between out-of-plane strain range reduction and the original out-of-plane strain range for the CFD bridge. Note that web gaps at B4, B3, and B3W were retrofitted. This retrofit method achieved at least 50% reduction in strain range when the original strain range was more than 50 microstrains. The web gap at B2 was not retrofitted. Strain range reduction was approximately zero for the untreated web gap. There was less than

$\pm 20\%$  variation for the web gap at B2, which could be explained by small variation in size, weight and position of the truck, and data acquisition before and after retrofit.

### ***3.5.2.2 Comparison of in-plane strains***

Table 3.8 shows that the in-plane strains on B4 before and after retrofit for the static passes (Passes 1~3) were reasonably close, indicating that the truck followed the same path in both truck tests. There was  $\pm 20\%$  variation for the in-plane strains on B5, which could be explained by small variation in size, weight, and position of the truck before and after retrofit. The close values of in-plane strains before and after retrofit suggested that the reduction in out-of-plane strain observed in the previous section was due to the retrofit method, and was not because of the change of the truck traveling path.

Table 3.7 also shows that the in-plane strains on B4 before and after retrofit for the slow moving dynamic passes (Passes 4, 5, and 8) were not as close as the in-plane strains for the static passes. However, there was approximately 80% reduction in the out-of-plane strain range for Pass 4 though the in-plane strain range reduction was only approximately 30%. For Pass 5, the out-of-plane strain range was reduced by approximately 80% while the in-plane strain range remained the same. For Pass 8, the out-of-plane strain range was reduced by approximately 50% while the in-plane strain range was only reduced by 20%. Therefore, even though Passes 4, 5, and 8 before and after retrofit for the CFD bridge might have not followed the same route, the fact that reduction in the out-of-plane strains was considerably larger than reduction in the in-plane strains indicated that part of the reduction in out-of-plane strain was due to the retrofit method.

In-plane strain ranges for other passes and on other beams can be found in tables in Appendix D.

### ***3.5.2.3 Comparison of out-of-plane strains and in-plane strains***

Comparison of Table 3.6 and Table 3.8 shows that the out-of-plane strain range at the web gap before retrofit was approximately the same as the largest in-plane strain range at similar locations in the girder for Passes 1~3. For Passes 4, 5, and 8, the ratio mentioned above was approximately two to four. It seemed that dynamic effect was more pronounced for the out-of-plane strain range than for the in-plane strain range for the CFD bridge.

### ***3.5.2.4 Comparison of the cross-frame diaphragm strains***

As shown in Table 3.9, the strain values measured by three pairs of single gages on the cross-frame diaphragm showed little difference before and after retrofit. The strain values measured by six pairs of single gages on the CFD bridge showed little difference before and after retrofit. This was expected because the web gap effect was a local effect which mostly focused on a small area on the web. Also, of the two diagonal braces that connected two adjacent girders, the strain values were positive for one and were negative for the other, indicating that differential deflection did occur as expected. Only results from static passes were analyzed for this comparison. The cross-frame diaphragm strains are provided in Appendix E.

### **3.5.2.5 Comparison of connection plate strains**

Two rosettes were used on the connection plates, one on B4 and the other on B3. No conclusive observations could be drawn from the strain readings of the rosettes. The strains measured by rosettes are provided in Appendix F.

### **3.5.2.6 Effect of differential deflection and rotation on out-of-plane strains**

As can be observed from Table 3.6 and Table 3.7, for Passes 1~5 and Pass 8, the original strain range was greater for B4 than for B3. The following analysis on the contribution of differential deflection and rotation on out-of-plane strain can explain this observation for Passes 1~3 and Pass 8, when only one truck was involved.

Figure 3.18 shows two concurrent movements (displacements) of the girders for the static passes, i.e., differential deflection of adjacent girders B4 and B3, and rotation of the concrete slab. In this figure, “+” denotes tension and “-“ denotes compression. It can be seen that, the two effects were additive for B4 and subtractive for B3. This was one of the reasons why larger out-of-plane strains were measured for the web gap at B4 than for the web gap at B3. It can also be concluded that differential deflection was more dominant than deck rotation, because the out-of-plane strain readings had the sign predicted by differential deflection.

Other passes were analyzed in the same fashion and it was found that differential deflection was dominant in some cases, and deck rotation was dominant in other cases. In some cases, differential deflection and deck rotation were equally important. This observation was different from that of the BPD bridge where differential deflection was decisively dominant in most cases. Transverse deck stiffness was discussed in an attempt to explain such phenomenon. However, though the concrete deck was 9 in. for the CFD bridge and 10 in. for the BPD bridge, the girder spacing was 9.5 ft. for the CFD bridge and approximately 12 ft. for the BPD bridge, thus the transverse deck stiffness in the CFD bridge may not be necessarily smaller than the transverse deck stiffness in the BPD bridge. In other words, transverse deck stiffness could not explain why deck rotation played a more important role in the CFD bridge than in the BPD bridge. However, it is possible that differential deflection was smaller for the CFD bridge because the continuous diaphragm offers larger stiffness to the system in the direction perpendicular to the primary structure members. As is the case for the BPD bridge, if a girder was two girder spacings away from the truck, the analysis described above is no longer valid because of the complicated interaction effects of girders, diaphragms and concrete slabs.

## **3.6 Field inspection of the adhesive-angle retrofit system**

As described in Chapter 2, environmental durability is one of the major considerations for steel-to-steel bonding in civil engineering applications. Section 3.2 mentions that environmental durability was one of the major parameters that led to the choice of DP-460NS, which is a product of 3M, for this research project. Chapter 5 also describes coupon specimens that were tested to investigate the environmental durability of the chosen adhesive. However, investigation of the conditions of the in-service adhesive-angle retrofit system provides the most valuable information on how well the adhesive performed in an outdoor environment with intermittent

stresses. Thus field inspection of the adhesive-angle retrofit system was conducted in May, 2005, three and a half years after the adhesive-angle retrofit system was put on the bridges.

The temperature was 32°F to 38°F during the inspection. The non-destructive inspection was conducted with the following procedures. First, visual inspection was made to determine whether visible cracks had formed in the adhesive or between the adhesive and the adherend. Then, the angle was struck with a steel hammer to see if the angle was loose. It was found that of the 10 inspected angles, not a single angle was loose. In other words, these ten adhesive retrofits remained in place and in good condition after three and a half years.

Pictures of the field inspection are shown in Figure 3.19.

### **3.7 Conclusions of the field test**

#### **3.7.1 Controlling contributions to the out-of-plane distortion**

Differential deflection between adjacent girders and diaphragm rotation were more dominant than concrete deck rotation in the contribution to out-of-plane distortion for the BPD bridge studied in the field test. For the CFD bridge studied in the field test, however, though differential deflection was still dominant for some cases, concrete deck rotation also played an important role, and sometimes, a dominant role, in the out-of-plane distortion.

#### **3.7.2 Conclusions of the retrofit method**

The following conclusions can be drawn for the retrofit method applied in the field:

1. The retrofit of adhering an angle to the connection plate and the tension flange of the girder was effective at places where the original strain range was greater than 50 microstrains. At these locations, this retrofit method achieved at least 38% strain range reduction for the BPD bridge and at least 50% strain range reduction for the CFD bridge. If such reduction percentage can be obtained for strain ranges large enough to initiate a crack, the fatigue life of the connection can be extended at least 4.6 times by this retrofit method. Or, if the strain range was reduced below the threshold level, then no fatigue cracks would initiate.
2. The thickness of the angle was chosen to be  $\frac{3}{4}$  in. This was based on previous research that suggested  $\frac{3}{4}$  in. was the minimum thickness to provide enough stiffness for the retrofit method to be effective. The leg lengths of the angle were chosen so that the angle was not too heavy for easy application, yet it still had enough adhering surface to resist out-of-plane forces.
3. The  $\frac{1}{4}$  in. diameter stainless steel bolt that connected the angle to the stiffener served two purposes: to hold the angle in place before the adhesive had cured, and to keep the angle from dropping down if some disastrous event, such as fire, occurred to the bridge and damaged the adhesive.

4. Because normal traffic flow was not interrupted when the retrofit was conducted, it could be concluded that the vibration caused by the traffic would not influence the effectiveness of the adhesive performance, provided that the manufacturer's requirements are met.
5. Because the adhesive application represented the worst situation of field application (applied at 50°F instead of 70°F), the obtained results should provide the lower bound performance of the 3M adhesive, DP460-NS.
6. These ten adhesive-angle retrofits remained in place and in good condition after three and a half years, suggesting that the chosen adhesive had good environmental durability.
7. The adhesive retrofit is recommended for implementation as a retrofit technique for details that have the potential for cracking but have not yet exhibited any detectable cracks. In this case, no additional stop-hole drilling is required. The retrofits should be inspected from the ground during the biannual inspections.

## Chapter 4 Large-Scale Test

As described in Chapter 3, the retrofit of adhering an angle to the connection plate and the tension flange of the girder was found to be effective in the field test. However, the maximum out-of-plane strain range in the bent-plate-diaphragm bridge was only approximately 200 microstrains and the maximum out-of-plane strain range in the cross-frame-diaphragm bridge was less than 100 microstrains in the field test. Thus, it was not known whether the adhesive-angle system would be effective for bridges with original out-of-plane strains at web gaps larger than 200 microstrains. Therefore, a large-scale test was conducted in the laboratory under controlled conditions, so that the effectiveness of the adhesive attachment under maximum possible stress conditions could be studied. Also, close monitoring of the load and fatigue crack growth in the large-scale specimen offered information that was not available in the field test. Since the field test results indicated that staggered bent-plate-diaphragm bridges experience larger out-of-plane stress ranges than the continuous cross-frame-diaphragm bridges under the same load, the large-scale lab test specimen was chosen to represent a bent-plate-diaphragm bridge. This configuration was also chosen by Fisher et al. (1990) and D'Andrea et al. (2001) for large-scale lab tests.

In this chapter, the configuration of the large-scale specimen is described in Section 4.1. Finite element analysis for the specimen is discussed in Section 4.2. Testing schemes such as instrumentation and testing procedures are shown in Section 4.3. Testing results and discussion are provided in Section 4.4. Conclusions of the large-scale test are presented in Section 4.5.

### 4.1 Large-scale specimen configuration

Figure 4.1 shows the large-scale specimen configuration. The two side-by-side plate girders were 32 ft. long and 32 in. deep. Both the web plate and the connection plate were  $\frac{3}{8}$  in. thick. The girders were connected by two intermediate diaphragms and four  $\frac{3}{4}$ -in.-thick-plate-and-W-shape combinations. The intermediate diaphragms served two purposes: to control the overall torsion of the two girders and to simulate the staggered bent-plate diaphragm configuration. The  $\frac{3}{4}$ -in.-thick-plate-and-W-shape combinations (Section D-D in Figure 4.1) were clamped to the bottom flange that was in tension in the primary stress field. These elements served the purpose of simulating the concrete deck in the field. In other words, the whole test set-up was an upside-down replica of the field configuration in the negative moment region. The original plan was to clamp the W-shape to the bottom flange directly. However, in order to have enough room for handling instrumentation, the W-shape was welded to a  $\frac{3}{4}$  in. thick plate and the plate was clamped to the bottom flange.

The girders were tested in four-point bending (Figure 4.1). Two 110-kip actuators were used to apply the static and cyclic loads on the girders with a 5-ft. constant moment region at the center of the span. A spreader beam (W14X145) oriented in the east-west direction was used for both the north and the south actuators to create two loading points for each girder. Rollers were used at both the end supports and the loading points of the girders.

The connection plates for the intermediate diaphragms were welded to the web and both flanges. The connection plates for the side diaphragms were welded to the web and the top

flange, but were not welded to the bottom flange, thus creating 2 in. long web gaps at each of the eight side diaphragm connection plates. Among the eight web gaps, four (denoted as NW-C, NE-C, SW-C and SE-C) were located in the constant moment region, and the other four (denoted as NW-1/2, NE-1/2, SW-1/2 and SE-1/2) were located at positions where the in-plane stresses were half of those in the constant moment region.

Springs with adjustable stiffness supported the ends of the side diaphragms, thus simulating the inflection points shown in Figure 1.1. The springs were simulated by simply supported beams made of 1-in. by 6-in. plates as shown in Figure 4.2. The spring stiffness could be adjusted by moving the spring supports to change the spring span length  $L$ . As described in Section 4.2, different diaphragm support stiffness was required to obtain the same out-of-plane stresses for web gaps in the constant moment region and web gaps where the in-plane stresses were half of those in the constant moment region.

#### 4.2 Finite element analysis of the large-scale specimen

In order to predict the out-of-plane stresses as well as the in-plane stresses, finite element analysis was conducted using the structural analysis program ABAQUS (ABAQUS, 1994). Two types of finite element models were developed: a global model that predicted the global behavior of the specimen, and a submodel that predicted the local behavior of the specimen at the web gap region. The global model represented the whole specimen, including flange, web, connection plate, and bent-plate diaphragm. The submodel represented the web gap region with a much finer mesh, using the results from the global model as boundary conditions. The submodeling feature allowed proper modeling of the local web gap out-of-plane behavior, and at the same time minimized computing time as well.

Figure 4.3 shows the mesh of the global model. Because the specimen was doubly symmetric, only a quarter of the structure was modeled. Because of symmetry, the girder's centerline can only undergo vertical and transverse (out-of-plane) deflections, and rotation about the longitudinal axis. Symmetric boundary restraint conditions were applied on the nodes on the symmetric axis, i.e., three degrees of freedom,  $u_3$ ,  $\phi_1$ , and  $\phi_2$ , were restrained. Vertical restraint was applied on the bottom flange nodes at the girder roller support. The mesh size for the global model was 1.5 in. x 1.5 in. for the flange, connection plate and the bent-plate diaphragm; 1.5 in. x 0.75 in. for the web at regions close to the web gap; 1.0 in. x 0.75 in. for the web gap area; and 1.5 in. x 1.5 in. for other locations on the web.

An 8-node three-dimensional thick shell element, S8R, which takes into account transverse shear flexibility and second-order interpolation, was used to model the flange, web, connection plate, and the bent-plate diaphragm. A two-noded Timoshenko beam element, B31, which allows for transverse shear deformation, was used to model the W-shape which simulated the restraint of the concrete slab. To model the effect of the heavy clamp, a 2-node rigid element was used to connect the nodes on the beam element for the W-shape to the corresponding nodes on the shell element for the bottom flange. Each node in the 8-node shell element, 2-node beam element, and the rigid element, had 6 degrees of freedom — three displacement degrees of freedom and three rotational degrees of freedom.

Spring elements, which act in the vertical direction, were used to simulate the spring supports at the ends of the side diaphragms. The stiffness of the spring was adjusted during the analysis so that the out-of-plane stresses had approximately the same values for web gaps in the constant moment region and for web gaps at other locations. The spring stiffness was taken to be  $48EI/L^3$ , where  $E$  was the modulus of elasticity for steel,  $I$  was the moment of inertia for the 1 in. x 6 in. plate, and  $L$  was the span of the simply supported spring. It was found that in order to obtain the same magnitude of out-of-plane stresses at all of the web gaps,  $L$  needed to be larger for the diaphragms in the constant moment region than for the other diaphragms.

Figure 4.4 shows the mesh of the submodel. The submodel represented 18 in. in the longitudinal direction of the girder (direction “3” in Figure 4.3), 12 in. in the vertical direction of the girder (direction “2” in Figure 4.3), and 4 in. in the diaphragm direction (direction “1” in Figure 4.3). The mesh size was 1/8 in. x 1/8 in. for the 8 in. (horizontal) x 5 in. (vertical) web gap region and 1/4 in. x 1/4 in. for other places. A 2-node truss element was used to model the fillet weld. The modulus of elasticity of the weld was taken to be the same as that of the steel, i.e., 29,000 ksi.

Figure 4.5 shows the out-of-plane stresses predicted by the finite element analysis (FEA) for the web gaps where the in-plane stress was 12 ksi (in the constant moment region) and the web gaps where the in-plane stress was 6 ksi. The same magnitude of out-of-plane stresses at all web gaps was achieved by adjusting the diaphragm end support spring stiffness. The spring stiffness was 11 kip/in. for the diaphragms in the constant moment region, corresponding to a simply supported spring span of 40 in. (Figure 4.2). The spring stiffness was 22 kip/in. for the other diaphragms, corresponding to a simply supported spring span of 32 in. (Figure 4.2).

From Figure 4.5, it can be observed that double curvature occurred in the 2 in. web gap region. Also zero out-of-plane stress occurred approximately one third up the web gap from the stiffener end. Zero out-of-plane stress was also found to occur one third up the web gap from the stiffener end by finite element analysis conducted by Zhao and Roddis on one four-girder skewed bridge (2003) and one two-girder bridge (2005) in Kansas.

Figure 4.6 shows the out-of-plane stresses predicted by the FEA at the web gap where the in-plane stress was 6 ksi. The upper graph shows stresses along the flange-web fillet weld toe, and the lower graph shows stresses along the horizontal line at the stiffener end. Both graphs were drawn for stresses on the web side that faced towards the diaphragm. It can be seen that the magnitude of the out-of-plane stresses decreased at a much faster rate at the stiffener end than at the flange-web fillet weld toe. This is because the change in the out-of-plane stiffness is more abrupt for the stiffener end.

### **4.3 Testing scheme of the large-scale specimen**

Testing schemes such as instrumentation and testing procedures are shown in this section.

#### **4.3.1 Instrumentation**

Figure 4.7 shows the location of the linear variable differential transformers (LVDTs) that measured in-plane deflection and out-of-plane deflection in the plan view. Figures 4.8 and

4.9 are pictures of the LVDTs that measure in-plane deflection and out-of-plane deflection. LVDTs with “BB” labeling measured in-plane deflection close to the girder. LVDTs with “BD” labeling measured in-plane deflection close to the diaphragm support. The range of the LVDTs that measured in-plane deflection was  $\pm 0.5$  in. LVDTs with “G” labeling measured out-of-plane distortion at the web gap region. The range of the web gap LVDTs was  $\pm 0.05$  in. The LVDT labeling, corresponding location, and LVDT types can be found in Appendix G.

Figure 4.10 shows the location of the strain gages that measured in-plane strains and out-of-plane strains in the plan view. Six 120 ohm single strain gages were mounted on the girders to monitor the strain distribution over the depth of the girder at four sections as shown in Figure 4.11. Two 120 ohm strip gages and one 120 ohm single strain gage were mounted at each web gap to monitor the out-of-plane strain distribution as shown in Figure 4.12. The strip gage was 1 11/16 in. long and 7/16 in. wide, with each grid 9/64 in. long and 6/64 in. wide. Only four out of the ten available gages in each strip gage were utilized. The single gage was 23/64 in. long and 1/8 in. wide, with an active area of grid of 9/64 in. long and 5/64 in. wide. All web gaps were instrumented with out-of-plane strain gages. The gage labeling, corresponding location, and gage types can be found in Appendix H.

In order to determine the reaction force applied at the diaphragm end, two single strain gages were mounted vertically on the vertical channel support, one on the north side of the channel and one on the south side of the channel as shown in Figure 4.8. Only the channel supports on the north girder were instrumented with strain gages.

After cracks had initiated and propagated to the point where the longest crack was approximately 4 in., the cyclic loading was stopped and the adhesive-angle retrofit system was applied. Single strain gages were mounted at the crack tip before the retrofit was conducted. The strain readings of these gages before retrofit and immediately after retrofit were recorded. Figure 4.13(a) shows the crack tip gages at the “smiley face” crack and the horizontal crack. Figure 4.13(b) shows the crack tip gage at the horizontal crack formed along the flange-web fillet weld toe.

### 4.3.2 Test Procedure

The in-plane stress range at the bottom flange of the girders was chosen to be 12 ksi for the constant moment region, and 6 ksi at the other web gap locations. These stress ranges were much larger than the realistic values obtained in the field studies with typical maximum measurements of between 1 and 3 ksi. The major reason was to present an environment that would be much more severe than anything found in the field and to search for the retrofit upper limit. As mentioned earlier, the field test had established that the retrofit was effective when the out-of-plane stress was larger than 1.45 ksi (corresponding to 50 microstrains) and in-plane stress was smaller than 1 ksi (corresponding to 34 microstrains). The in-plane stress of 12 ksi in the constant moment region and 6 ksi at the other web gap locations were used to investigate the upper limit where the retrofit system remained effective. A second reason for using a stress range larger than reality was to facilitate crack growth.

This 12 ksi in-plane stress range was produced by a 76 k load range for each actuator. Static tests were carried out prior to cyclic loading and at periodic intervals during the fatigue

tests. The static tests provided data for: (1) in-plane and out-of-plane deflection; (2) in-plane and out-of-plane strains; (3) reaction force provided by the spring support; and (4) for studying whether the in-plane and out-of-plane behavior of the girder was in the elastic region.

The procedures used for testing were as follows:

1. One girder was placed into the load frame. Two intermediate diaphragms were installed. Then the second girder was positioned in place.
2. Side diaphragms were attached to the girders. Spring supports were provided at the free end of the side diaphragms.
3. A static test was performed to determine whether the actuator load and spring member span lengths produced the desired in-plane and out-of-plane stress ranges. The actuator load was set to be 90 k, corresponding to 14 ksi in-plane stress in the constant moment region.
4. In order to initiate the out-of-plane cracks faster, cyclic loading started with an 84 k load range on the actuator (corresponding to 13 ksi in-plane stress range in the constant moment region) for the first 117,000 cycles. After cracks had initiated at several places, the cyclic loading was set to a 76 k load range on the actuator (corresponding to the target 12 ksi in-plane stress range in the constant moment region). Unless otherwise specified, all the following cyclic loading was set to the 76 k load range with the mean load of 48 k.
5. At 227,000 cycles, when cracks had initiated at all other web gaps except NE-C and NW-C, the side diaphragm spring support span at these two locations was adjusted to 35 in. (from 40 in.), so as to introduce larger out-of-plane stresses.
6. At 497,000 cycles, the side diaphragm spring support span at NE-C was adjusted to 30 in., in order to initiate cracks at this location.
7. It was predetermined that the retrofit would be provided at all web gaps when the longest crack was 4 in. in the web, or the shortest crack was 2 in. The longest crack occurred at SE-C and reached approximately 4 in. before the shortest crack reached 2 in. at other web gap locations. The cyclic loading was stopped at 1,101,000 cycles.
8. Single strain gages were mounted at the crack tips (Figure 4.13). A static test was performed to determine the stress at the crack tips before retrofit.
9. The adhesive-angle retrofit system was applied at all 8 web gap locations. When the retrofit system was applied, the actuator load was set at 48 k, the mean load for the cyclic loading. In other words, the adhesive-angle retrofit system would undergo a stress ratio of  $-1$  in the following cyclic loading. The dimension of the angle and application procedures can be found in Appendix I.
10. A static test was performed 8 days after the last angle was applied to determine the stress at the crack tips after retrofit. (The recommended cure time for the 3M DP460-NS adhesive by the manufacture is 7 days in room temperature.)

11. Cyclic loading continued for another 2 million cycles after retrofit. In other words, the cyclic loading was stopped at 3,101,000 cycles.
12. A static test was performed to determine the in-plane stresses and deflection of the girders.
13. During the aforementioned process, if a crack initiated and grew toward the bottom flange, a  $\frac{3}{4}$  in. diameter hole was drilled at the crack tip. Otherwise, the crack was allowed to grow to a point when it was clear that the retrofit did not work effectively for that particular crack and the crack was considered to be detrimental to the performance of the whole girder. Then a hole was drilled at the crack tip. The diameter of the hole was  $\frac{3}{4}$  in. unless otherwise mentioned. At locations NE-C and SE-C, cracks propagated at the flange-web fillet weld toe, where drilling holes at the crack tips was difficult. Instead of drilling a hole, other procedures were taken and will be discussed in Section 4.4.
14. Approximately 2 million cycles after retrofit, all the angles were taken off except those at locations NE-C and SE-C. During this process, the adhesive that attached the angle to the stiffener and the tension flange was heated using a propane torch, and then a prying bar was used to detach the angles.
15. The adhesive-angle retrofit system was reapplied at all 6 web gap locations where the original angles were detached. The application procedures were the same as before.
16. A static test was performed to determine the in-plane stresses and deflection of the girders 7 days after the last angle was applied.
17. The cyclic loading was set to 25.3 k load range on the actuator (corresponding to a target 4 ksi in-plane stress range in the constant moment region, a third of the original stress range).
18. Cyclic loading continued for another 2 million cycles after the second retrofit. In other words, the cyclic loading was stopped at 5,101,000 cycles.
19. A static test was performed to determine the in-plane stresses and deflection of the girders.

#### **4.4 Test results and discussion**

Large-scale specimen test results are discussed in this section. The results of the static test before cyclic loading are described in Section 4.4.1. The results of the static test before retrofit and after retrofit are discussed in Section 4.4.2. The crack growth rates during the cyclic loading, with an emphasis on the difference of growth rates before and after retrofit, are presented in Section 4.4.3.

##### **4.4.1 Static test before cyclic loading**

A static test was performed to determine whether the actuator load and spring member span lengths produced the desired in-plane and out-of-plane stress ranges. Section 4.4.1.1

describes the out-of-plane stresses from the static test and compares those values with FEA predicted values. Section 4.4.1.2 shows the out-of-plane distortion. Section 4.4.1.3 gives the in-plane stresses from the static test and compares those values with FEA predicted values. Section 4.4.1.4 presents the in-plane deflection. Section 4.4.1.5 describes stresses in the diaphragm end channel support. Section 4.4.1.6 provides a summary of the static test before cyclic loading.

#### **4.4.1.1 Out-of-plane strains**

Figure 4.14 shows the out-of-plane strains for the web gap location SW-1/2 for four consecutive static tests with the maximum actuator load set at 90 k (14 ksi in-plane stress). It can be seen that when the in-plane stress in the constant moment region was 14 ksi, the measured out-of-plane strains were still in the elastic region, when  $\epsilon_{yield}$  was assumed to be 1,700 microstrains (i.e.,  $F_y / E_s = 50 \text{ ksi} / 29000 \text{ ksi}$ ). This suggests that the out-of-plane strains were still in the elastic region when the in-plane stress range in the constant moment region was 12 ksi in the cyclic loading.

Figure 4.15 compares the measured out-of-plane strains with FEA predicted out-of-plane strains at the SW-1/2 web gap. The FEA predicted out-of-plane strains were drawn for the location where the strain gages were instrumented so that comparison of measured strains and FEA predicted strains could be made. It can be seen that both the measured values and FEA predicted values shared the same signs in curvature and showed that double curvature occurred in the 2 in. web gap region. Similar test observations can be obtained for web gaps at other locations and are provided in Appendix J. In a similar experiment conducted by Fisher et al. (1990), single curvature was obtained for 1½ -in. web gap and double curvature was obtained for 3 in. web gap. The web gap length used in the current research and the research by Fisher et al. (1990) was nominal web gap length, i.e., the distance from the end of the stiffener plate to the top of the bottom flange. When the wrap-around fillet weld at the stiffener and the flange-web weld were considered, the real web gaps were smaller than the nominal web gap (Figure 4.12).

However, Figure 4.15 also showed that the measured values were much smaller than the predicted values. This can be explained by the following considerations. Because the stress field in the web gap region changes very rapidly, even a small deviation in strain gage placement can yield a large variation in strain reading, as shown in Figures 4.5 and 4.6. It was possible that the strain gages were not placed as close to the stiffener as assumed because of the irregularities of the stiffener-web fillet weld. Another possible reason was that the flexibility of the connections, such as the bolted stiffener-diaphragm connections and the clamped tension-flange-W-shape connections, which was inherent in the large-scale specimen, was not well modeled in the finite-element analysis. In a study conducted by Jajich and Schultz (2003), a finite element analysis and field test were conducted for a Mn/DOT Bridge (#27734). The finite element analysis predicted an out-of-plane stress of 12 ksi, while strain gages in the field test measured only 4 ksi. The aforementioned reasons were also considered to be the cause of the inconsistency of the predicted and measured out-of-plane stresses.

Another important reason for the inconsistency of the measured out-of-plane strains and the predicted values was the difference between the real active web gap length (nominal web gap length minus the fillet weld size) and the assumed active web gap length. The assumed active

web gap length was taken as 1 3/8 in. (2 in. – 5/16 in. × 2), however, as shown in Table 4.1, the measured active web gap lengths were smaller than the assumed ones at all locations.

Table 4.2 lists out-of-plane strains measured by strain gages, the maximum absolute value of measured strains, and the maximum absolute value of the FEA predicted strains. The measured out-of-plane strains were 29~60% of the predicted out-of-plane strains. The average ratio of measured strain and predicted strain was 42%.

#### ***4.4.1.2 Out-of-plane distortion***

Table 4.3 gives out-of-plane distortion measured by the LVDTs and predicted by FEA. There was significant scatter in the measured out-of-plane distortion. The measured out-of-plane distortion was much smaller than that predicted by FEA at all web gap locations. The average ratio of measured distortion and predicted distortion was 17%. One possible reason is that a small misalignment of the LVDT in the web gap region might have led to a large decrease of measured distortion.

#### ***4.4.1.3 In-plane stresses***

Table 4.4 gives in-plane stresses calculated from the measured strains by the strain gages and in-plane stresses predicted by FEA. Since the in-plane stresses were in the elastic region, the measured stresses were calculated by multiplying measured strains by 29,000 ksi, which was the assumed modulus of elasticity for steel. As expected, the agreement between measured and predicted values for the in-plane stresses was much better than that for the out-of-plane stresses. The measured in-plane stresses were 70~124% of the predicted in-plane stresses. The average ratio of measured stress and predicted stress was 91%.

It can be inferred from the predicted in-plane stresses that overall torsion would occur in the girders. For example, strain gage locations N-1/4-1-B and N-1/4-2-B were symmetrically placed on the girder (Figure 4.11), had there been no overall torsion in the girder, the same in-plane stresses would have been predicted by the FEA at these two locations. However, different in-plane stresses were predicted for strain gage positions N-1/4-5-B and N-1/4-6-B, suggesting that overall torsion occurred in the girders and introduced warping stresses (Figure 4.11). Also, different stress values were predicted for strain gage positions at S-1/4-5-B and S-1/4-6-B, at N-C-1-B and N-C-2-B, and at S-C-1-B and S-C-2-B. Furthermore, since the bending stress and the warping stress at gage locations 1 and 5 were additive, and the bending stress and the warping stress at gage locations 2 and 4 were subtractive, larger absolute values of stress were predicted for gage locations 1 and 5. However, because the W-shapes were clamped to the tension flange symmetrically to simulate the concrete slab, little torsion could occur at the tension flange in the mid point of the girders, resulting in the similar predicted stress values at N-C-5-B and N-C-6-B, and at S-C-5-B and S-C-6-B.

#### ***4.4.1.4 In-plane deflection***

Figures 4.16(a) and (b) show the in-plane deflections for LVDT locations at NW-C and SW-C, and at NE-C and SE-C, for four consecutive static tests with the maximum actuator load set at 90 k (14 ksi in-plane stress). Because the measured deflections were all linear with respect

to time (Figure 4.16), and the actuator loads were set to be linear with respect to time in the static test (Figure 4.17), it could be postulated that the measured deflections were all linear with respect to the loads. This suggested that the simply supported beam for the diaphragm end support (Figure 4.2) was still in the linear elastic region, thus the stiffness of the spring support was justified to be taken as  $48EI/L^3$  in the FEA.

Table 4.5 gives in-plane deflection measured by the LVDTs and predicted by the FEA. The agreement between measured and predicted values for in-plane deflection was much better than that for out-of-plane distortion. The measured in-plane deflection was 83~126% of the predicted in-plane deflection. The average ratio of measured deflection and predicted deflection was 104%. However, there was much scatter in the differential deflection between the girder and the diaphragm support end. Since the differential deflection was on the order of 0.05 in., the relative effect of experimental error was more prominent than if the differential deflection was larger. The average ratio of measured differential deflection and predicted differential deflection was 86%.

Table 4.5 also shows that the measured differential deflections at NW-C and NE-C were much smaller than those at other locations and were only 10 to 20% of those predicted by FEA. This observation is consistent with the fact that out-of-plane cracks could not be initiated for web gaps at NW-C and NE-C in the first 227,000 cycles, when out-of-plane cracks had been initiated at all other web gaps. One possible reason was that bolts slipped in the diaphragm end channel support for NW-C and NE-C.

#### ***4.4.1.5 Stresses in the diaphragm end channel support***

Table 4.6 gives stresses calculated from the measured strains by the strain gages on the diaphragm end channel support (Figure 4.8) and predicted by the FEA. Since stresses on the diaphragm end channel support were in the elastic region, the measured stresses were calculated by multiplying measured strains by an assumed modulus of 29,000 ksi. As can be seen from the stresses, some moment was introduced in the vertical channel because of the clamped connection at the bottom (Figure 4.8). For example, had there been no moment, stresses at strain gages positions NW-1/2-N-D and NW-1/2-S-D should have been very close and had the same sign, because strain gages NW-1/2-N-D and NW-1/2-S-D were applied symmetrically with respect to the strong axis of the channel. However, different stress values with opposite signs were observed, thus it was inferred that some moment was introduced in the vertical channel. It is believed that the average value of the stresses calculated from the measured strains by two strain gages (one on the north side of the channel and one on the south side of the channel) on the same vertical channel were reasonable estimates of the axial stress for that channel.

The predicted stress was calculated by dividing the FEA computed diaphragm spring force by the channel area. The measured stresses were 68~120% of the predicted stress. The average ratio of measured stresses and predicted stresses was 104%.

#### ***4.4.1.6 Summary of static test results before cyclic loading***

The measured in-plane stresses, in-plane deflections, and diaphragm end support stresses were consistent with the FEA predicted values (the ratio of measured values and predicted values

was between 86% and 104%). However, the measured out-of-plane stresses were only 42% of the FEA predicted values and the measured out-of-plane distortion was only 17% of the FEA predicted values. Apart from the reasons discussed above, the sensitivity of the out-of-plane behavior to the detail may be another cause for such inconsistency. In other words, the exact geometry of the weld is difficult to model while the out-of-plane behavior is highly dependent on the exact geometry of the weld.

#### **4.4.2 Static test before retrofit and after retrofit (when the longest crack reached approximately 4 in.)**

As mentioned in Section 4.3.2, cyclic loading was stopped when the longest crack reached approximately 4 in. at the web. Then single strain gages were mounted at the crack tips. A static test was conducted before the retrofit and after the retrofit. Comparison of the measured strains before and after retrofit was used to evaluate the effectiveness of the retrofit system immediately after it was applied and cured. The measured strains at the crack tip are discussed in Section 4.4.2.1. The in-plane stresses, in-plane deflection, and stresses in the diaphragm end channel support are provided in Section 4.4.2.2 to Section 4.4.2.4.

##### ***4.4.2.1 Strains at the crack tip***

The crack tip gage labeling and corresponding location can be found in Appendix H. The pictures of the web gap cracks and the strains at crack tips are provided in Figures 4.18 to 4.33. Cracks are labeled in the same way as the crack tip gages. “-g” denotes that a strain gage was mounted at the crack tip. “-h” denotes that a hole was drilled at the tip of the crack at some point of the cyclic loading. In this section, the strains at web gaps SW-1/2, NE-C, and SE-C are discussed. A summary of strains at all web gaps is provided at the end of this section.

##### ***4.4.2.1.1 Strain at the crack tip at web gap SW-1/2***

Single strain gages were mounted on three crack tips at web gap SW-1/2. The crack lengths for SW-1/2-nw-g, SW-1/2-ne(1)-g, and SW-1/2-se-g were 1 5/32 in., 9/16 in., and 1 13/16 in. respectively. Figure 4.18 shows the picture of these three cracks before strain gages were mounted. Figure 4.19 shows measured strains before and after retrofit at each of the crack tips at web gap SW-1/2. Crack tip strains were decreased to approximately 40% of the original values on average, indicating that the retrofit was effective. The less than smooth strain changes measured by strain gage SW-1/2-ne(1)-g prior to retrofit might have been caused by the friction between the materials on either side of the crack as the web gap distorted.

All three crack tip strain gages at web gap SW-1/2 were located above the end of the stiffener, i.e., the position similar to the upper photo in Figure 4.13(a). According to the FEA results for the uncracked web as shown in Figure 4.15, positive strain values were predicted for the north side of the web and negative strain values were predicted for the south side of the web. However, measured strains, as shown in Figure 4.19, gave the opposite signs. One possible reason for the inconsistency is that once cracks formed in the web gap region, the strain field changed dramatically, especially at the crack tips, where the strain gages were mounted.

Even though the cracks were predicted to grow in a certain pattern, such as the “smiley face” pattern as shown in Figure 4.13(a), they did not necessarily follow the pattern predicted by the FEA. In other words, the presence of local strain raisers and local flaws, which were not included in the FEA, played an important role in the fatigue crack initiation and growth. This could be the second possible reason for the inconsistency of measured values and predicted values mentioned above.

#### 4.4.2.1.2 Strain at the crack tip at web gap NE-C

Single strain gages were mounted on four crack tips at web gap NE-C. The crack lengths for NE-C-nw-g, NE-C-ne(1)-g, NE-C-sw(3)-g, and NE-C-se-flangeweb-g were 2 13/16 in., 1 27/32 in., 1 3/4 in. and 1/2 in. respectively. Figure 4.20 shows the picture of these four cracks before strain gages were mounted. Figure 4.21 shows measured strains before and after retrofit at each of the crack tips at web gap NE-C. Crack tip strains were decreased to approximately 10% of the original values on average, indicating that the retrofit was very effective.

Strain gage NE-C-se-flangeweb-g was positioned at the tip of a crack that formed along the flange-web fillet weld toe (as shown in Figure 4.13(b)). It measured a strain level of 3,900 microstrain before retrofit, which was well beyond the yielding strain of the material when  $\epsilon_{yield}$  was assumed to be 1,700 microstrains (i.e.,  $F_y / E_s = 50 \text{ ksi} / 29000 \text{ ksi}$ ). It was possible that the strain gage measured the strains due to the plastic deformation in front of the crack tip.

Except for strain gage NE-C-nw-g, measured strains at web gap NE-C changed signs after retrofit. Because the adhesive-angle retrofit system altered the complicated stress field in the web, the signs of measured strains after retrofit did not necessarily match the signs of measured strains before retrofit.

#### 4.4.2.1.3 Strain at the crack tip at web gap SE-C

Single strain gages were mounted on four crack tips at web gap SE-C. The crack lengths for SE-C-nw(1)-g, SE-C-ne-g, SE-C-sw-g, and SE-C-se-g were 3 1/4 in., 1 1/4 in., 4 5/16 in. and 1/2 in. respectively. Figure 4.22 shows the picture of these four cracks before strain gages were mounted. Figure 4.23 shows measured strains before and after retrofit at each of the crack tips at web gap SE-C. Crack tip strains were decreased at most locations, except where strain gage SE-C-nw-g was positioned (as shown in upper photo in Figure 4.13(a)). In fact, this was the only one out of 27 crack tip strain gages that measured larger strain after retrofit than before retrofit.

Figure 4.23 shows that, before retrofit, there were two strain cycles for strain gage SE-C-nw(1)-g for each load cycle. It was possible that some internal stress relief system was involved so that the strain was zero when the largest load was reached (i.e., 90 k). After retrofit, however, there was only one strain cycle for the same strain gage for each load cycle, suggesting that the stress relief system had diminished. Also, since the crack had already propagated away from the web gap and grew perpendicular to the in-plane stress on the web, the proposed retrofit system, which targeted decreasing the out-of-plane stress, might not be very effective for this crack. As discussed in Section 4.4.3, the retrofit system did not stop or retard the crack growth at this location. It should be mentioned that the measured strains at the tip of crack SE-C-sw-g (on the south side of the through-thickness crack SE-C-nw(1)-g) were smaller after retrofit.

#### *4.4.2.1.4 Strain at the crack tip at other web gaps*

Other web gaps at NW-1/2, NW-C, SW-C, NE-1/2, and SE-1/2 experienced similar cracking and reduction in crack tip strains after retrofit, as shown in Figures 4.24 to 4.33.

#### *4.4.2.1.5 Summary of strain at the crack tip*

Table 4.7 summarizes the measured strains before and immediately after retrofit. Of the 27 crack tip locations, strains at 7 crack tip locations changed signs after retrofit. As mentioned above, only one crack tip strain gage (SE-C-nw(1)-g) measured larger strain after retrofit than before retrofit. Since cracks SE-C-nw(1)-g and SE-C-sw-g had already propagated away from the web gap and grown perpendicular to the in-plane stress on the web, these two data points could be treated as outliers because of the type of crack formed. If these two data points are not included, crack tip strains were decreased to approximately 20% of the original values on average. Figure 4.34 shows there was little correlation between crack tip strain reduction and the original crack tip strain. Figure 4.35 shows there was little correlation between crack tip strain reduction and crack length. A possible reason for the little correlation is that the strain gradients were large at the crack tips. Measuring in a slightly different place relative to the crack tip could give a significantly different answer. Data points from cracks SE-C-nw(1)-g and SE-C-sw-g are not included in Figures 4.34 and 4.35.

#### *4.4.2.2 In-plane stresses*

Table 4.8 gives in-plane stresses for the static test before and after retrofit. Since in-plane stresses were in the elastic region, the measured stresses were calculated by multiplying measured strains by an assumed modulus of 29,000 ksi. Just as expected, the adhesive-angle retrofit system did not influence the in-plane stresses of the large-scale specimen. The ratio of in-plane stresses after retrofit and in-plane stresses before retrofit was between 90% and 105%.

#### *4.4.2.3 In-plane deflection*

Table 4.9 gives in-plane deflection measured by the LVDTs before and after retrofit. There was a clear trend that differential deflection, i.e., deflection of the side diaphragm end subtracted from deflection at the girder, decreased after retrofit. The differential deflection after retrofit was decreased to approximately 60% of the differential deflection before retrofit. The decrease in differential deflection was expected because the adhesive-angle retrofit increased the stiffness of the out-of-plane system. In fact, reduced differential deflection resulted in reduced out-of-plane stresses in the web gap, which was the purpose of the retrofit.

#### *4.4.2.4 Stresses in the diaphragm end channel support*

Table 4.10 gives stresses on the diaphragm end channel support (Figure 4.8) before and after retrofit. As observed from the table, the reaction force on the diaphragm end support increased by approximately 10% after retrofit. Such an increase was a direct result of a stiffer out-of-plane system and was consistent with the decrease in differential deflection described above.

#### 4.4.3 Cyclic test

As discussed in Section 4.3.2, various methods were used to initiate a crack at a faster speed before 497,000 cycles. There was no change in the diaphragm end support spring stiffness after 497,000 cycles. At 1,101,000 cycles, the adhesive-angle retrofit system was applied. Cyclic loading was continued under the same load range for 2 million cycles and was stopped at 3,101,000 cycles. Then angles were detached and the adhesive-angle retrofit system was reapplied. Cyclic loading was continued under a third of the original load range for another 2 million cycles and was stopped at 5,101,000 cycles. In other words, the load range was 76 k from 497,000 to 3,101,000 cycles and 25.3 k from 3,101,000 to 5,101,000 cycles. It was found that, even without stop holes, all cracks were retarded or stopped if the retrofit angles did not become loose after retrofit from 1,101,000 cycles to 3,101,000 cycles. Had stop holes been drilled at all crack tips, the retarded cracks likely would have been stopped completely. All cracks were stopped and no retrofit angles became loose after retrofit from 3,101,000 cycles to 5,101,000 cycles.

The load range of 76 k corresponded to an in-plane stress range of 12 ksi at web gaps in the constant moment region and 6 ksi at other web gaps, which was larger than typical in-plane stress ranges for bridges in service. The load range of 25.3 k corresponded to an in-plane stress range of 4 ksi at web gaps in the constant moment region and 2 ksi at other web gaps, which was more representative of in-plane stress ranges for bridges in service. In fact, the largest measured in-plane stress range (based on the assumed modulus of 29,000 ksi) in the field test of this project was less than 1.5 ksi.

The crack growth rates at all web gaps and pictures of adhesives from detached angles are shown in Figures 4.36 to 4.52. The legend in these figures labeled the cracks in the same way as the crack tip gages were labeled. When there was more than one crack at one location, numbers such as “(1)” and “(2)” were used, just as shown in Figure 4.13. Also, as shown in Figure 4.53, cracks on the north surface of the web did not necessarily grow in the same pattern as cracks on the south surface of the web. In other words, crack propagation through the thickness of the web was not necessarily perpendicular to the surface of the web. Thus, all cracks on both the north and the south surface of the web were listed in the figures. “-g” denotes that a strain gage was mounted at the crack tip. “-h” denotes that a hole was drilled at the tip of the crack. Unless otherwise specified, the diameter of the hole was  $\frac{3}{4}$  in. In order to separate the effect of the adhesive-angle retrofit system from the effect of the stop hole on the crack growth rate, stop holes were not drilled at the crack tip unless the crack was growing toward the tension flange, or, had grown perpendicular to the in-plane stress and was long enough to be considered detrimental to the overall performance of the girder.

The crack growth rates at web gaps SW-1/2, NE-C, and SE-C are discussed in detail in this section. A summary of crack growth rate at all web gaps is provided at the end of this section.

##### 4.4.3.1 Web gap at SW-1/2

Figure 4.36 shows the crack growth rate for the cracks at web gap SW-1/2. It illustrates that all the existing cracks were stopped, or retarded, by the retrofit method at the 76 k load range. However, one new crack, SW-1/2-ne(4), was found to have initiated and propagated after

retrofit. Crack SW-1/2-ne(4) was formed at the end of crack SW-1/2-ne(3), but propagated in a different direction. The growth rates of this new crack and Crack SW-1/2-se seemed to indicate that Crack SW-1/2-se became a through-thickness crack after retrofit, and the crack growth seemed to be concentrated on one surface at a time. Figures 4.18 and 4.37 show the cracks at web gap SW-1/2 at 1,101,000 cycles and 3,101,000 cycles respectively.

The adhesive that attached the angle with the connection plate and the tension flange was intact after 2 million cycles at the 76 k load range. In other words, there were no visual signs that the adhesive had deteriorated. When the angle was detached after 2 million cycles, it was found that penetrant had penetrated a small area at the boundary of the angle on the side of the tension flange as shown in Figure 4.38. This suggested that the adhesive had cracked at the boundary, yet the crack was too thin to be observed visually before the angle was detached.

Figure 4.36 also shows that all cracks were stopped by the retrofit method at the 25.3 k load range, corresponding to an in-plane stress range of 2 ksi at SW-1/2. As expected, the adhesive that attached the angle with the connection plate and the tension flange was intact after 2 million cycles at 25.3 k load range.

#### **4.4.3.2 Web gap at NE-C**

Figure 4.39 shows the crack growth rate at the web gap NE-C (refer to Figure 4.20 for pictures of the cracks). At 1,101,000 cycles, the adhesive-angle retrofit system was applied. At 2,350,000 cycles, it was found that the retrofit angle was loose. At the same time, three cracks, NE-C-sw(2), NE-C-sw(3)-g, and NE-C-se-flangeweb-g had grown noticeably (Figure 4.39). It was obvious that there was a correlation between the crack growth rate and the performance of the adhesive.

The angle at NE-C was then taken off. Figure 4.40 shows that penetrant had penetrated all surface of the angle on the side of the tension flange. The surface of the angle on the side of the connection plate remained intact. The same retrofit was applied a second time at this location. However, the actuator load was set at 0 k, instead of 48 k. In other words, the cleavage stress experienced by the adhesive in this case was twice as large as that in the first retrofit.

At 2,419,000 cycles, less than 100,000 cycles after the second retrofit at NE-C, the retrofit angle was loose again. The angle was then taken off for a second time.

Previous experience showed that there was more demand on the adhesive that attached the angle to the tension flange than on the adhesive that attached the angle to the connection plate. A literature review (Niessner and Seeger, 1999) shows that base metal with powder actuated fasteners can be classified into the Eurocode 3 detail Category 90 if less than 1 million cycles are applied, and Category 100 if more than 1 million cycles are applied. The slope of the fatigue S-N curve is suggested to be 3 for Category 90 and 5 for Category 100. The fatigue strength values used in the Eurocode 3 are related to the probability of survival of 95%.

Since more than 1 million cycles are expected for the bridge application, Category 100 is applicable to the current research. The S-N curve provided by Niessner and Seeger (1999) showed that the base metal with powder actuated fasteners has an infinite life if the stress range

is smaller than 100 MPa, which is equivalent to 14.5 ksi. This value falls in between Category B (threshold fatigue stress range is 16 ksi) and Category C (threshold fatigue stress range is 10 ksi) specified by AISC. Thus, the base metal with powder actuated fasteners is better than a Category C detail. According to AISC, base metal at a transverse stiffener end connections using a pair of fillet welds is a Category C detail. Therefore, base metal with powder actuated fasteners should not be the governing detail for fatigue.

Moreover, unlike bolts, powder actuated fasteners do not require partial removal of the concrete slab in the negative moment region. They can be shot beneath the top flange with a semi-automatic fastening tool. Thus, powder actuated fasteners were chosen in the current research to attach the angle to the tension flange in the large-scale test.

The third retrofit at web gap NE-C involved application of adhesives and powder actuated fasteners at 2,418,000 cycles. The application procedures can be found in Appendix I.

At 2,945,000 cycles, the longest crack at this web gap (NE-C-nw-g) grew perpendicular to the in-plane stress. A 2 3/8 in. diameter hole was drilled at the crack tip. At the same time, penetrant was observed to be pumping out at the edge of the angle, both on the bottom flange side and on the connection plate side, when the girders were cyclic loaded. This suggested that adhesive at the edge of the angle had fractured. Thus one heavy clamp was used to clamp the angle with the bottom flange and another heavy clamp was used to clamp the angle with the connection plate.

Figure 4.39 shows all the cracks were stopped, or retarded, by the retrofit method before the angle became loose. Also, no cracks were found on the tension flange 682,000 cycles after nailing of the retrofit angle under 12 ksi stress range, indicating the powder actuated fasteners had a satisfactory fatigue resistance.

Figure 4.39 also shows that without the use of stop holes, all cracks were stopped by the adhesive-angle retrofit method at 25.3 k load range, corresponding to an in-plane stress range of 4 ksi. No cracks were found on the tension flange 2 million cycles after nailing of the retrofit angle under 4 ksi stress range.

#### **4.4.3.3 Web gap at SE-C**

Figure 4.41 shows the crack growth rate at the web gap SE-C (refer to Figure 4.22 for pictures of the cracks). At 1,101,000 cycles, the retrofit was applied. It can be seen that the retrofit had little effect on the crack growth rate for cracks SE-C-nw(1)-g and SE-C-sw-g. This was because these two cracks had grown out of the web gap region and become perpendicular to the in-plane stress (Figure 4.22). The adhesive-angle retrofit system, though effective at decreasing out-of-plane stress, did not affect the in-plane stress. That explained why the growth of these two cracks was not retarded. A 2 3/8 in. diameter hole was drilled at the tip of the two cracks when it was evident that the crack growth rate did not change after the retrofit was applied.

At 2,488,000 cycles, it was found that the retrofit angle was loose. At the same time, a new crack, SE-C-ne-flangeweb, had initiated and grown noticeably at the flange-web fillet weld

toe. Thus, a correlation between the crack growth rate and the performance of the adhesive existed for web gap SE-C, just as the case for web gap NE-C. The new crack at the toe of the flange-web fillet weld is shown in Figure 4.42.

The angle at SE-C was then taken off. Just as the angle at NE-C, penetrant had penetrated all surface of the angle on the side of the tension flange. The surface of the angle on the side of the connection plate was intact.

The second retrofit at web gap SE-C involved application of adhesives and powder actuated fasteners. The application procedures can be found in Appendix I.

At 2,650,000 cycles, penetrant was observed to be pumping out at the edge of the angle, both on the bottom flange side and on the connection plate side when the girders were cyclic loaded. This suggested that adhesive at the edge of the angle had fractured. Thus one heavy clamp was used to clamp the angle with the bottom flange and another heavy clamp was used to clamp the angle with the connection plate. Also, no cracks were found on the tension flange after 451,000 cycles under 12 ksi stress range, indicating the powder actuated fasteners had a satisfactory fatigue resistance.

Figure 4.41 also shows that all cracks were stopped by the adhesive-angle retrofit method at the 25.3 k load range without the use of stop holes. The adhesive that attached the angle with the connection plate and the tension flange was intact after 2 million cycles at the 25.3 k load range. No cracks were found on the tension flange 2 million cycles after nailing of the retrofit angle under the 4 ksi stress range.

#### ***4.4.3.4 Summary of crack growth under cyclic loading***

Section 4.4.3.1 to Section 4.4.3.3 discussed crack growth rates at web gaps SW-1/2, NE-C, and SE-C. This section summarizes the observation of crack growth rates at all of the web gaps.

As can be seen from Figures 4.36, 4.39, 4.41, 4.43, 4.45, 4.47, 4.49, and 4.51, the adhesive-angle retrofit system stopped, or retarded, most cracks. If stop holes had been drilled at all crack tips, as would be the case for any field retrofit application, some of the retarded cracks might have been stopped completely.

However, the retrofit method had little effect on the crack growth rate for two cracks at web gap SE-C (i.e., Crack SE-C-nw(1)-g and Crack SE-C-sw-g, which were on either side of the web for a through-thickness crack). This was because these two cracks had grown out of the web gap region and become perpendicular to the in-plane stress (Figure 4.22). The adhesive-angle retrofit system, though effective at decreasing out-of-plane stress, did not influence the in-plane stress. A 2 3/8 in. diameter hole was drilled at the tip of the two cracks and they did not reinitiate after 1,467,000 cycles.

Also, it was evident that there was a correlation between the crack growth rate and the performance of the adhesive. Crack growth rates at SW-C, NE-C and SE-C showed that the cracks grew at a much faster speed shortly after the retrofit angle became loose. Thus, inspection

of the adhesive condition could, qualitatively though not quantitatively, determine whether the retrofit remains effective. The retrofit angle remained intact for all of the other web gaps.

#### 4.5 Conclusions

The following conclusions are made from the large-scale test.

1. The measured in-plane stresses, in-plane deflections, and diaphragm end support stresses were consistent with the FEA predicted values (the ratio of measured values and predicted values was between 68% and 126%).
2. The measured out-of-plane stresses were only 42% of the FEA predicted values on average and the measured out-of-plane distortion was only 17% of the FEA predicted values on average. One reason was because the strain gages were been applied as close to the flange-web weld as planned. Another possible reason was that flexibility of the connections (such as the clamped connections between the W-shape and the tension flange, and the bolted stiffener-diaphragm connections), which was inherent in the large-scale specimen, was not modeled in the finite-element analysis. The sensitivity of the out-of-plane behavior to the detail may be a third cause for such inconsistency.
3. Of 27 crack tip locations, only one crack tip strain gage measured larger strain range after retrofit (1432 microstrains) than before retrofit (302 microstrains). It was possible that some internal stress relief system was involved before retrofit and the stress relief system had diminished after retrofit. Also, this crack tip strain gage was located at the tip of a through-thickness crack which had already propagated away from the web gap and grown perpendicular to the in-plane stress on the web. Thus strain range readings from two crack tip gages that were located on each side of the web for this through-thickness crack could be treated as outliers because of the type of crack formed. If these two data points are treated as outliers and are not included, crack tip strain ranges were decreased to approximately 20% of the original values on average.
4. Even without stop holes, the adhesive-angle retrofit system had successfully stopped or retarded most cracks under the same in-plane stress range, i.e., 12 ksi in the constant moment region. The corresponding measured out-of-plane strain ranges were approximately 600 microstrains when the in-plane stress range was 12 ksi in the constant moment region. Working in combination with the stop holes, the proposed retrofit system might have stopped some of the retarded cracks completely. When a third of the original in-plane stress range (i.e., 4 ksi in the constant moment region) was used afterwards, all cracks were stopped completely.
5. It was obvious that there was a correlation between the crack growth rate and the performance of the adhesive. If the angle was not loose, the crack growth rate was slow or zero. It was postulated that field inspection of angles and adhesives could provide qualitative information as to whether the retrofit system remained effective.
6. The retrofit method had little effect on the crack growth rate for two cracks which had grown out of the web gap region and become perpendicular to the in-plane stress. This

was expected because the adhesive-angle retrofit system, though effective at decreasing out-of-plane stress, did not affect the in-plane stress. Thus, such retrofit method is not recommended for cracks which are longer than 2 in. and have grown perpendicular to the in-plane stresses.

7. No cracks were found on the tension flange after 682,000 cycles at NE-C and 451,000 cycles at SE-C under 12 ksi stress range when powder actuated fasteners were used in combination with adhesives to attach the angle to the tension flange. No cracks were found on the tension flange at NE-C and SE-C after an additional 2 million cycles under 4 ksi stress range. This was consistent with the S-N curve provided by Niessner and Seeger (1999), which shows that the base metal with powder-actuated fasteners has an infinite life if the stress range is smaller than 14.5 ksi (between Category B and C). Powder-actuated fasteners in combination with adhesives is recommended to retrofit web gap cracks when the out-of-plane force is significant.
8. Although three out of eight angles became detached when cycling at the 12 ksi in-plane stress range, none of the angles showed any distress after 2 million cycles at the lower stress range which better approximated the demand on the adhesive in the field.

## Chapter 5 Coupon Test

The results of the field test and large scale test showed that the retrofit method of adhesive-angle combination was effective for the out-of-plane fatigue problem. Because the testing after retrofit was done shortly after the application of the adhesive, however, it was not known how the outdoor environment was going to influence the performance of the adhesive. As mentioned earlier, durability was one of the most important parameters in the choice of adhesives, and it was not directly correlated to the initial strength, thus it was desirable to understand the performance of the chosen adhesive (3M DP460-NS) under different environmental exposure schemes. Coupon tests were conducted for this purpose.

It is generally accepted that because of the high surface energy of metals, the stability of the interfacial layer between the adhesive and the adherend is the controlling feature for the durability in aqueous environments for all polymer/metal bonds. Thus, researchers have been looking for methods that improve the durability of the interfacial layer with a view to improving the durability of the whole joint. Previous research (Gettings and Kinloch, 1977; Kozma and Olefjord, 1987; Fay and Maddison 1990; and Tod et al., 1992) has found that a primer named  $\gamma$ -glycidoxypropyltrimethoxy silane (GPS) significantly improved durability for steel joints. Therefore, the effect of GPS on durability was studied in this research.

In this chapter, the design of the coupon specimen and the choice of the testing machine are described in Section 5.1. The performance of the baseline specimens, or fresh specimens without exposure to different environments, tested under different testing temperatures, is provided in Section 5.2. The performance of the environmentally exposed specimens, tested in the lab ambient air, is shown in Section 5.3. The influence of the retrofit system stiffness on the effectiveness of the retrofit system is discussed in Section 5.4. Conclusions of the coupon test are given in Section 5.5.

### 5.1 The coupon specimen and the testing machine

Though single lap shear adhesive joints are most widely used for simplicity, double lap shear adhesive joints were chosen in this project to eliminate global bending. It is worth mentioning that the dimensions shown in Figure 5.1 were specifically designed for this project, following the rules described in American Standard Test Method (ASTM) D 3528-96. The ASTM recommended thicknesses are 0.063 in. for the side adherend and 0.126 in. for the center adherend. These thicknesses are more representative of the sheet metal used in the aerospace or automobile industry. In civil engineering applications, however, the adherends tend to be much thicker (In this project, for example, the retrofitting angle was  $\frac{3}{4}$ -in. thick, the top flange was 1~1.125 in. thick and the connection plate was  $\frac{3}{8}$  ~  $\frac{3}{4}$  in. thick). Because it is well known (Adams and Wake, 1984; Hart-Smith, 1981; Knox and Cowling, 2000-b) that the thickness of the adherend influences the performance of the adhesive, the thicknesses were chosen to be  $\frac{3}{16}$  in. for the side adherend and  $\frac{3}{8}$  in. for the center adherend, so as to better represent the field application in the realm of civil engineering.

Another modification to the ASTM guidelines was that wedge grips were not used. A hole was drilled in the center adherend. A rod inserted into the hole of the center adherend was used to align the test specimen as soon as the load was applied. This modification was done so that the available MTS testing machine in the laboratory could be used to conduct the test. As described later, the hole also enabled the specimens to be stressed by means of a spring-loaded device for environmental loading.

The adherends were made with A36 steel. They were manufactured by a local company with high pressure water cutting. The as-received steel pieces were coated with mill oil. Glass beads of different diameters were used as spacers to maintain the desired bondline thickness. Though chemical etching is widely used as a surface preparation method for aluminum adherends, it has not been widely accepted for low-carbon mild steels. The best results are usually obtained by using mechanical roughening techniques and solvent cleaning (Brockmann, 1983; Kozma, 1987; Knox, 2002). Thus 220-grit emery sand paper abrasion and acetone cleaning was chosen to be the surface preparation method for the coupon specimens. The coupon specimen fabrication procedure can be found in Appendix K. A picture of the coupon specimen sitting in the jig is shown in Figure 5.2. Note that after being cured, the excess adhesive, or fillet, was ground away by a grinder, to aid reproducibility since different sizes of fillets may introduce large coefficients of variation, and the fillet-free configuration is potentially more controllable.

The length of the overlap was designed according to the formula given by ASTM (D 3528). The width of the specimen was designed so that there was enough clearance for the hole on the center adherend, and the breaking load of the specimens fell between 15~85% of the full-scale capacity of the MTS testing machine.

Figure 5.3 shows the test set-up in the testing machine. The door of the thermal chamber could be closed and the chamber temperature could be controlled during testing. The crosshead testing speed was set to be 0.0172 in./min to achieve loading rates close to those recommended by ASTM.

Because the retrofit method of adhesive-angle combination relied more on the stiffness of the system than on the strength of the system, the stiffness of the adhesive was also studied. Two Linear Variable Differential Transformers (LVDTs) with  $\pm 0.1$  in. range were used to measure the relative displacement between the two center adherends. The crosshead displacement was 10~14 times the displacement measured by the LVDTs before the coupon specimen reached its ultimate strength, and was 1~3 times the displacement measured by the LVDTs after the specimen had reached its ultimate strength. Thus it was impossible to obtain the relative displacement between the center adherends by the crosshead displacement.

There were 5 specimens in each batch. Each batch of specimens were made with the same batch of adhesive at the same time. To investigate the influence of GPS on the durability of the DP460-NS adhesively bonded steel joints, a companion batch (without GPS) was made at the same time as a batch with GPS in most cases, with the same batch of adhesives. Though ASTM D3528-96 requires a minimum of 5 test specimens for the double lap shear test and ASTM D2919-95 requires a minimum of 6 test specimens for each test environment, the number “five” was chosen due to project constraints. The number of specimens in a batch is commonly chosen to be two to ten by other researchers (Two by Su et al., 1992; Knox and Cowling, 2000a, 2000b.

Three by Brewis et al., 1980; Mays and Tilly, 1982; Zewi et al., 1984; Mays, 1985; Fay and Maddison, 1990; Davis and Fay, 1993; Hshim, 1999. Four by Gledhill and Kinloch, 1974; Brewer et al., 1990. Five by Hylands and Sidwell, 1980; Gosselin, 1985; Arrowsmith et al., 1987; Fay and Maddison, 1990. Six by Brewis et al., 1980; Comyn et al., 1987; Konat, 1994; Abdel Wahab, 2002; Gordon and Fakley, 2003. Ten by Allen et al., 1984.) It was regarded that the choice of five specimens in a batch represented the mainstream of testing schemes adopted by researchers in this field.

The following notation will be used throughout the rest of this report, specimens without pretreatment of GPS primer (No GPS), specimens with pretreatment of GPS primer (GPS), and bondline thickness ( $t_a$ ).

## **5.2 The performance of the baseline specimens**

The performance of the baseline specimens, or fresh specimens without exposure to different environments, tested under different testing temperatures, is provided in this section. The strength and stiffness of the baseline specimens are described in Section 5.2.1. The failure modes are presented in Section 5.2.2.

### **5.2.1 The ultimate strength and the stiffness of the baseline specimen**

The typical load versus displacement (measured by LVDTs) curve for a baseline specimen with bondline thickness  $t_a = 0.020$  in. is shown in Figure 5.4. The load-displacement curve was linear up to very close to the ultimate strength. It was believed that the section of curve between zero load and load at 50% of the ultimate strength was linear enough to be used to obtain the value of the stiffness. As demonstrated in Figure 5.5, further analysis showed that the square of the correlation coefficient,  $R^2$ , was greater than 0.990. The same phenomenon was observed for the four other batches of baseline specimens for which displacements were measured by LVDTs. Therefore, it was believed that the criterion described above was appropriate for obtaining the stiffness of the specimens.

The baseline specimen testing matrix is shown in Table 5.1. For some cases, more than one batch of specimens were made, thus the number of data points may be larger than five. In order to simulate the unfavorable field application environment in November, 2001, one batch of specimens was made outdoors, when the temperature was approximately 50°F during the daytime, left outdoors for the night and then kept in the environmental chamber at 50°F for 16 days. Just as in the field application for this project, the adhesive became so thick that the two parts could not be squeezed out through the manufacture supplied static mixing nozzle. As a result, the two parts were squeezed out directly from the cartridge to the adherend, and then they were mixed with a spatula. It was believed that the above batch of specimens represented the field application of this project, and thus the results should shed some light on the performance of the adhesive used in the field.

For testing temperatures other than room temperature, the specimens were kept in the testing chamber for at least one hour before the test was conducted. This ensured that the temperature of the specimen was the same as that of the testing chamber.

Table 5.2 lists the average strength, coefficient of variation for strength, the average stiffness, and coefficient of variation for stiffness for the baseline specimens. The strength and stiffness for individual specimens are provided in Appendix L. There are two ways in analyzing the results. One is to evaluate the effects of GPS pretreatment, bondline thickness, testing temperature, curing temperature, and 1 million cycles of loading (15.7 Hz) between 0.2~2 kips by comparing the changes in the average ultimate strength and average stiffness, so that the percentage of change can be observed. The results from the above comparison are listed in Table 5.3(a). Another method to analyze the results is to use Student's *t*-test to find whether an increase or a decrease in the mean ultimate strength and stiffness occurred at a particular confidence interval for different batches of the baseline specimens. Statistic software R 1.5.1 was used to conduct Student's *t*-test. The results are shown in Table 5.3(b). The notation of "57% ↑" denotes that one is 57% confident of an increase, and the notation of "62% ↓" denotes that one is 62% confident of a decrease. Each notation listed in the table is strictly limited to a comparison between the groups noted, and thus does not apply when more than one parameter is changed at a time.

Two-sample *t*-tests require that one simple random sample is drawn from a normal population and the other independent simple random sample is drawn from another normal population. However, since there were only five specimens in one sample(batch), it was hard to decide whether the population distribution was normal. Fortunately, there were 24 data points for the standard baseline specimens ( $t_a= 0.020$  in., No GPS, room temperature cured, room temperature tested), and both histogram and normal quantile plot (frequently referred to as QQ plot) of this sample were drawn in Figure 5.6. The shape of the histogram was reasonably normal and the normal quantile plot did not deviate substantially from a straight line. Both graphs suggested that the population distribution for the standard baseline specimens was normal. Thus it was reasonable to postulate that the population distribution for other batches of specimens was also close to normal.

In addition, it has been shown that the two-sample *t*-test was robust. In other words, when the sizes of the two samples were equal and the distributions of the two populations being compared had similar shapes, probability values from the *t* table were quite accurate when the sample sizes were as small as  $n_1=n_2=5$  (Posten, 1978). As a result, it was believed that the two-sample *t*-test was an appropriate method to be used in this research.

There were 20 data points for specimens with GPS ( $t_a= 0.020$  in., room temperature cured, room temperature tested). The normal quantile plot of this sample is shown in Figure 5.7(a). The 5 data points from the first batch deviated from the normal quantile plot. One possible reason was that this was the first batch made with GPS. Though careful attention was given to make every batch in the same fashion, it was still possible that lack of experience for the first batch may have affected the performance of the adhesive. Figure 5.7(b) gives normal quantile plot of this sample with 15 data points, eliminating these 5 data points from the first batch. It can be seen that the normal quantile plot did not deviate substantially from a straight line. However, since this phenomenon was observed after the data were analyzed, it would lead to biased results if data points obtained from the first batch were discarded. Thus, all the following discussion uses all the 20 data points for specimens with GPS ( $t_a= 0.020$  in., room temperature cured, room temperature tested), including the 5 data points obtained from the first

batch. The tables, on the other hand, list analyses with both 20 data points and 15 data points, so that readers can make judgment at their own discretion.

Table 5.3(a) shows that GPS pretreatment did not influence the average ultimate strength and stiffness for more than 10% except for bondline thickness of 0.059 in. Also, the percentage of decrease in average ultimate strength for bondline thickness of 0.039 in. and 0.059 in. compared to bondline thickness of 0.020 in. was less than 10%, while the percentage of decrease in average stiffness for bondline thickness of 0.039 in. and 0.059 in. compared to bondline thickness of 0.020 in. was approximately 30%. Table 5.3(b) shows that, when the bondline thickness increased from 0.020 in. to 0.039 in., the ultimate strength of the specimens decreased at a 62% confidence level, while the stiffness of the specimens decreased at a 99% confidence level. When the bondline thickness changed from 0.020 in. to 0.059 in., the ultimate strength and stiffness of the specimens decreased at a 99% confidence level. Thus, as expected, the two different methods yield similar trends for the prediction of changes in ultimate strength and stiffness. Both methods tend to indicate that the stiffness was more sensitive than the ultimate strength to surface treatment and changes in bondline thickness.

The fact that the stiffness decreased when the bondline thickness increased from 0.020 in. to 0.039 in. or 0.059 in. suggested that the choice of bondline thickness of 0.020 in. for the field application was appropriate. Also, as shown in Figure 3.9, the bondline thickness was not constant in the adhesive-angle combination retrofit. The bondline was maintained at 0.020 in. at the angle stem and was larger than 0.020 in. at the angle tip. This may have decreased the stiffness of the retrofit system. The effect of stiffness decrease on the retrofit will be discussed in Section 5.4.

Tables 5.3(a) and (b) also show that, as expected, the ultimate strength of the baseline specimens was smaller when tested at an elevated temperature (122°F) and was greater when tested at a low temperature (-40°F). Figures 5.8(a) and (b) give the relationship between the ultimate strength and the testing temperature for bondline thicknesses of 0.020 in. and 0.059 in. respectively. A nonlinear relationship existed between the ultimate strength and the testing temperature in the range of -40°F~122°F. Since the glass transition temperature ( $T_g$ ) of the 3M DP460-NS adhesive was 144.5°F, it was reasonable to postulate that the ultimate strength would decrease at a much faster rate as temperature continued to increase after it had reached 122°F. It should be mentioned that the nitrogen was used up after the testing of the first two specimens with  $t_a=0.020$  in. Therefore only the data points for the first two specimens were used in the analysis (Figure 5.8(a)).

Table 5.3 also illustrates that, as expected, the ultimate strength of the cold temperature (50°F) cured specimens was smaller than that of the room temperature cured specimens. More information can be obtained using the boxplots shown in Figure 5.9. A boxplot is a graph of the five-number summary, where the central box spans the first quartile and the third quartile, the line in the box marks the median, lines extend from the box out to the smallest and largest observations that are not suspected outliers, and the individual dots are suspected outliers. An observation is called a suspected outlier if it falls more than 1.5 times the interquartile range (IQR) above the third quartile or below the first quartile, where IQR is defined as the distance between the first and third quartiles.

It can be seen from Figure 5.9 that the ultimate strength decreased from approximately 9 kips for the room temperature cured specimens to roughly 5 kips for the cold temperature cured specimens. It is reasonable to believe that the field application at 50°F represented the worst situation of field application and should provide the lower-bound performance of the adhesive.

Table 5.3(b) also demonstrates that, at a 99.9% confidence level, the strength of the baseline specimens decreased after 1 million cycles of loading between 0.2~2 kips with a sinusoidal wave form. On the other hand, the strength of the GPS pretreated specimens increased after 1 million cycles of loading at an 88% confidence level when 20 data points were used for the baseline specimens, and the effect reversed when 15 data points were used for the baseline specimens.

### 5.2.2 Failure mode of the baseline specimen

Figure 5.10 shows a picture of the failure mode for a standard baseline specimen ( $t_a=0.020$  in., No GPS, room temperature cured) tested at lab ambient air. The major area of failure was cohesive, i.e., failure within the adhesive layer. A small part area of failure was adhesive, i.e., interfacial failure between the adherend and the adhesive. This suggested that surface treatment for the specimens had been adequately conducted. In other words, the cohesive failure mode suggested the weakest link was within the adhesive, and was not between the adherend and the adhesive. More elaborate surface treatment may not increase the strength and stiffness of the specimens.

Figure 5.11 shows a picture of the failure mode for a GPS pretreated specimen. It can be seen that all of the failure was cohesive. This suggested GPS pretreatment affected the failure mode for fresh specimens.

Figure 5.12 is a picture of the failure mode for a specimen tested at 122°F ( $t_a=0.020$  in., No GPS, room temperature cured). The failure mode was similar to that of a standard baseline specimen. However, the area of adhesive failure was larger and some parts of adhesive were detached from both adherends.

Figure 5.13 shows a picture of the failure mode for a specimen tested at -40°F ( $t_a=0.020$  in., No GPS, room temperature cured). It was more difficult to define cohesive failure and adhesive failure for this case. Though it looked like adhesive failure in some areas, a very thin visible layer of adhesive existed on the adherend surface. Also, the texture of the adhesive tested at -40°F was completely different. Visible cracks were introduced within the adhesive, suggesting a very brittle failure mode. The fact that a snap sound was heard when the ultimate strength was reached reinforced the point.

Figure 5.14 is a picture of the failure mode for a cold temperature (50°F) cured specimen ( $t_a=0.020$  in., No GPS, room temperature tested). As mentioned earlier, it was believed that this batch of specimens represented the field application of this project, when the adhesive was cured at cold temperature instead of at the manufacture recommended room temperature. A large part of the adhesive had not cured even after 16 days. Thus it was not surprising that the ultimate strength of this batch of specimens was very low compared with room temperature cured specimens (4.6 kips vs. 8.9 kips).

The lack of cure could be explained by two possible reasons. One possible reason was that mixing of the two parts of the adhesive was not complete. Since the adhesive became so thick that the two parts could not be squeezed out through the manufacture supplied static mixing nozzle, the two parts were squeezed out directly from the cartridge to the adherend, and then they were mixed with a spatula. Therefore, it was reasonable to believe that the mixing was not complete and the uncured adhesive was just one part of the two-part adhesive. If this was the reason, then curing would not occur even if temperature rose to room temperature afterwards.

The second possible reason was that because the temperature was well below the recommended curing temperature (50°F vs. 70°F), polymerization and crosslinking could not occur efficiently. In other words, the adhesive was not cured efficiently. If this was the reason, then postcure might occur if temperature rose to room temperature afterwards.

### 5.3 The performance of the environmentally exposed specimens

The environment specimen testing matrix is shown in Table 5.4. Nine different environments were investigated. These were air at 65°F, immersion in tap water at 65°F, immersion in tap water at 111°F, air at -40°F, freeze and thaw chamber, temperature cycles (specimens were either unloaded or loaded at 0.95 k), outdoors, and fire. It is worth mentioning that the environment of fire was not originally designed. Fire broke out unexpectedly at the location where the outdoor specimens were stored.

Unlike the baseline specimens, parameters such as bondline thickness and testing temperature were not studied for the performance of the environmentally exposed specimens. Bondline thickness  $t_a$  was 0.020 in. for all batches of specimens, because the results for the baseline specimens suggested that it provided greater stiffness than other bondline thicknesses. Also, this was the bondline thickness used in the field application. Testing temperature was room temperature for all batches of specimens.

The load versus displacement curve for the environmentally exposed specimens resembled that of the standard baseline specimen as shown in Figure 5.4. As for the baseline specimens, the load-displacement curve between zero load and load at 50% of the ultimate strength was used to obtain the value of the stiffness. The square of the correlation coefficient,  $R^2$ , was greater than 0.950 for all the specimens under all the environments except for fire. For the environment with the fire,  $R^2$  was at least 0.880 for all the specimens.

Table 5.5 lists the average strength, coefficient of variation for strength, the average stiffness, and coefficient of variation for stiffness for the specimens subjected to different environments. The strength and stiffness for individual specimens are provided in Appendix L. For batch E3-5, which was immersed in tap water at 111°F for 210 days and then mechanically cycled for 1 million cycles, the average strength was only 3.61 kips and the coefficient of variation for strength was as high as 0.94. The reason was because two specimens failed during the cyclic loading before the static test was conducted. In other words, two zero data points were used. The same reason accounted for the high coefficient of variation for batches E7-1 and E7-3, which underwent temperature cycles and were loaded at 0.95 k. Both E7-1 and E7-3 had one zero data point because one specimen failed in the hot chamber during the temperature cycles for each batch. The reason for the high coefficient of variation for batch E7-4 was a little different.

No specimens failed during the temperature cycles. However, one specimen had a final strength of 2.6 k, well below the strengths of other four specimens. That explained why the coefficient of variation for batch E7-4 was high, yet was not as high as that for batches E7-1 and E7-3.

The physical reason that lay behind the high coefficient of variation for batches E3-5, E7-1, E7-3, and E7-4 was the same. Immersion in tap water at 111°F for 210 days followed by mechanical cyclic loading, or temperature cycles with 0.95 kips mechanical loading for 211 or 370 days, were the most hostile environments for the specimens except for fire. The coefficient of variation for the batches that were subjected to the fire was also very high (batches E9-1 and E9-2). It is generally accepted that the more hostile the environment, the more scattered the results will be. In research conducted by Fay and Maddison (1990), some stressed specimens also failed while other stressed specimens survived during the environment exposure.

As described in Section 5.2.1, there are two ways to analyze the results. One is to evaluate the effects of different environments, different exposure time and GPS pretreatment on the ultimate strength and the stiffness of the environmental specimens by comparing the changes in the average ultimate strength and average stiffness, so that the percentage of change can be observed. The results from the above comparison are listed in Tables 5.6(a) and 5.7(a).

Another method to analyze the results is to use Student's *t*-test to find whether an increase or a decrease in ultimate strength and stiffness occurred at a particular confidence interval for different environments, different exposure time, and GPS pretreatment. Statistic software R 1.5.1 was used to conduct Student's *t*-test. The effect of 1 million cycles loading that took place after the environment exposure and before the static test was also studied. The results are shown in Tables 5.6(b) and 5.7(b).

Tables 5.6(a) and (b) give the trend of change for specimens without GPS pretreatment. Tables 5.7(a) and (b) give the comparison between specimens with and without GPS pretreatment. As before, each notation listed in the table is strictly limited to one comparison, and thus does not apply to the whole table.

### **5.3.1 Specimens without GPS pretreatment**

Because GPS pretreatment was not used in the field application, results of coupon specimens without GPS pretreatment were more applicable to the field application. Tables 5.6(a) and 5.6(b) list the trend of change in the ultimate strength and stiffness of GPS unpretreated specimens for nine environments.

Sections 5.3.1.1 through 5.3.1.9 describe the performance of the specimens under each environment. Section 5.3.1.10 gives a summary of the observations.

#### **5.3.1.1 Air at 65°F**

Specimens exposed to room temperature air are often used as control specimens, which could be compared with specimens exposed to other environments (Gosselin, 1985). They also serve to investigate the phenomenon of postcure, i.e., polymerization and crosslinking over time,

after the adhesive has already cured. Lees and Hutchinson (1992) proposed the concept of postcure in their research on room-temperature cured structural adhesives.

As can be seen from Tables 5.6(a) and (b), holding the specimens in air at 65°F for 180 days did not change the ultimate strength or the stiffness of the specimens. However, this environment increased the ultimate strength and the stiffness of the specimens after 447 days. After exposure of 180 days followed by cyclic loading, the specimens showed improved ultimate strength and stiffness when compared with the fresh baseline specimens. This suggested that postcure did occur for this adhesive under such a favorable environment.

Figure 5.15 shows a picture of the failure mode of a specimen kept in the lab air at 65°F for 447 days. Comparison of Figure 5.15 with Figure 5.10 revealed that more adhesive failure occurred for the 15 months old specimens than for the fresh baseline specimens. A possible explanation was that postcure increased the crosslinking within the adhesive, however, it did not increase the adhering strength between the adhesive and the adherend as much. Since the failure always occurred at the weakest link, more adhesive failure was observed for the postcured specimens, though their ultimate strength and stiffness increased.

### ***5.3.1.2 Immersion in tap water at 65°F***

Immersion in room-temperature water is frequently used as an accelerated environment test for adhesives (Minford, 1973; Gledhill and Kinloch, 1974; Lark and Mays, 1984; Zewi et al., 1984; Gosselin, 1985; Brewer et al., 1990; Shaat et al., 2004). It is believed that this environment will accelerate the deterioration of the adhesive by introducing 100% relative humidity. At the same time, since the temperature of the water is approximately the average temperature at which the adhesive will experience in the normal application, it will not introduce a failure mode that is not representative of the field application.

Table 5.6(a) shows that the decrease in average ultimate strength and average stiffness subjected to tap water immersion at 65°F was less than 10%, suggesting that the effectiveness of the retrofit was unlikely to be influenced by this environment. Table 5.6(b) shows that, after the specimens had been immersed in tap water at 65°F for 92 and 201 days, there was a decrease in both the ultimate strength and the stiffness of the specimens. The less than 10% decrease in stiffness indicates that even if the angle-adhesive combination in the field was immersed in cold water for three months (92 days), which was unlikely, the stiffness of such a combination would not decrease. In other words, if snow was splashed onto the retrofit by the vehicles traveling below the bridge and melted afterwards, it would not deteriorate the effectiveness of the retrofit.

Figure 5.16 shows the failure mode of the specimen immersed in tap water at 65°F for 207 days. This picture was taken shortly after the specimen was pulled apart. It can be seen that water had infiltrated into the adhesive at the boundary. The failure mode at the boundary was completely adhesive and the greenish watermarks were clearly visible. The center of the bonding area was still intact. The greenish watermarks changed into off-white color after several days of exposure in the lab air, suggesting that water was evaporating.

### 5.3.1.3 Immersion in tap water at 111°F

Immersion in warm water is also frequently used for an accelerated test environment for adhesives (Minford, 1973; Wegman, 1977; Brewis et al., 1980; Zewi et al., 1984; Gosselin, 1985; Brewer et al., 1990; Tod et al., 1992; Harris and Beevers, 1999; Abdel Wahab et al., 2002; Shaat et al., 2004). It is more hostile than immersion in cold water because the elevated temperature will accelerate the deterioration of the adhesive by increasing the diffusion rate of the water. However, since the temperature is higher than the temperature the adhesive will experience in normal use, extreme care must be taken to avoid introducing a failure mode that is not representative of the field application. Otherwise there will be little correlation between the accelerated testing and the field application. Brewis(1983) suggested that only moderate increases above the likely maximum temperature should be used and a shift above the glass transition temperature of the adhesive should be avoided.

Based on the knowledge obtained in the baseline test, a nonlinear relationship existed between the ultimate strength and the testing temperature in the range of -40°F to 122°F. Since the glass transition temperature ( $T_g$ ) of the 3M DP460-NS adhesive was given as 144.5°F by the manufacturer, it was reasonable to postulate that 111°F was low enough not to introduce a different failure mode, yet also high enough to accelerate the adhesive aging.

As shown in Tables 5.6(a) and (b), after the specimens had been immersed in tap water at 111°F for 92 days and 210 days, there was a decrease in both the ultimate strength and the stiffness of the specimens. This was predicted because immersion in the warm water was more hostile than immersion in the cold water. Among the five cyclic loaded specimens, one specimen failed at 16,445 cycles and another specimen failed at 428,980 cycles. The remaining three specimens were statically tested. All five data points, including the two zeroes, were used in the analysis for Tables 5.6(a) and (b).

Figure 5.17 shows the failure mode of a specimen immersed in tap water at 111°F for 92 days and 210 days. The major failure mode was adhesive. Greenish watermarks could be observed for both cases. Comparison of Figure 5.17 and Figure 5.16 shows, as expected, that the area of greenish watermarks was larger for specimens immersed in warm water than for those immersed in cold water. Figure 5.17 also shows that corrosion occurred at the boundary of the bonding area. Since the watermarks occupied a much larger area than the corrosion, it was reasonable to believe that corrosion was a result of adhesive failure mode, and was not the reason for the adhesive failure mode. This observation supported the assertion of Gledhill and Kinloch (1974), and Brewis et al. (1980), that corrosion was a post-failure phenomenon. Thus it was postulated that corrosion inhibitors would not enhance the durability of the chosen adhesive (3M DP460-NS) and steel combination. It should be mentioned, however, that Davis and Fay (1993) observed a different phenomenon in their research. They studied the durability of epoxy bonded steel joints under tropical conditions. They found that the durability of mild steel joints was worse than that of coated steel joints. They observed corrosion within the bond area for the mild steel joints. For coated steel joints, on the other hand, this corrosion was virtually eliminated, improving retained strength values. The above discussion suggests that the failure mechanism differs for different adherend-adhesive combinations.

#### **5.3.1.4 Air at -4°F**

The accelerated testing with specimens exposed to air below freezing temperature, without alternating to air at elevated temperature, is not often used in the adhesive industry. However, due to the fact that the adhesive retrofit was proposed for use on the bridges of the State of Minnesota, one of the coldest states in the United States, it was worth investigating the influence of cold air on the adhesive. Also, since there was an environment which alternated the specimens between the hot chamber and the cold chamber on a weekly basis, comparison of these two environments could somewhat isolate the effect of the influence of hot air on the adhesive.

Table 5.6(a) gives less than 15% of increase in average ultimate strength and less than 10% of change in average stiffness of specimens subjected to air at -4°F. According to Table 5.6(b), conditioning the specimens in air at -4°F for 196 and 382 days increased the ultimate strength of the specimens at a 99.9% confidence level. However, this environment seemed to have mixed influence on the stiffness of the specimens after 196 days of exposure. After exposure for 197 days, cyclic loading resulted in an increase of the ultimate strength at a 99.9% confidence level and a decrease in the stiffness at a 76% confidence level. Since the angle-adhesive retrofit system relied more on the stiffness than on the ultimate strength, the less than 10% of change in average stiffness indicates that cold air had little effect on the effectiveness of the retrofit system.

Figure 5.18 shows the failure mode of the specimen kept in cold air at -4°F for 196 days and 382 days. It can be seen that the failure mode of cold air exposed specimens was similar to that of the standard baseline specimens.

#### **5.3.1.5 Freeze and thaw chamber**

It is well known that freeze and thaw is an important factor that affects the durability of concrete. Since the structure of the cured adhesive was somewhat similar to that of the cured concrete, it was postulated that freeze and thaw might also influence the performance of the adhesive. Thus, though not frequently investigated by other researchers, the effects of freeze and thaw was studied in this project.

The freeze and thaw chamber in this project was run at three hour cycles. The temperature started at 40°F, then it went down to 0°F in 2 hours, and then went up to 40°F in 1 hour. The temperature of the specimens was below 32°F for approximately 2 hours out of each 3 hour cycle. The specimens had been immersed in tap water at 111°F for 65 hours before they were put into the freeze and thaw chamber. This immersion was used to simulate the water that might have been absorbed in the joint. It was postulated that if joints were allowed to absorb water prior to freezing, ice crystals might develop in the adhesive upon freezing. The work of Brewis et al. (1980) indicated that with 10 cycles of freeze and thaw, the ice crystals did not affect the bond strength. However, with 500 to 1000 cycles of freeze and thaw, the ice crystals might influence the performance of the adhesive. Nevertheless, it should be noted that 65 hours of immersion in warm water prior to freeze and thaw was part of accelerated aging test. The water absorbed in this test may not represent the water absorbed in field application.

Table 5.6(a) shows the percentage of decrease in average stiffness was 10 to 15%, more than the percentage of decrease in average ultimate strength of the specimens. Table 5.6(b) also shows that freeze and thaw cycles did not have significant influence on the ultimate strength of the specimens. However, it did decrease the stiffness of specimens at a 95% confidence level for exposure time of 193 days. Since the angle-adhesive retrofit system relied more on the stiffness than on the ultimate strength, one could draw the conclusion that freeze and thaw cycles may slightly decrease the effectiveness of the retrofit system. The effect of stiffness change on the performance of the retrofit will be discussed in Section 5.4.

Figure 5.19 shows the failure mode of specimen kept in the freeze and thaw chamber for 92 days and 193 days. The greenish watermarks could be seen in both pictures. There were a few cracks within the adhesives, indicating that the adhesive had become brittle.

#### ***5.3.1.6 Temperature cycles between -4°F and 122°F (unloaded)***

Conditioning specimens with temperature cycles is often used to evaluate the durability of the adhesive (Mays and Vardy, 1983; Konate, 1994). In this research, the specimens were hung on a rod in the environment chamber. Each temperature cycle lasted 2 weeks and the specimens were moved manually from one chamber to the other. The average relative humidity was 42% in the cold chamber and 47% in the hot chamber. Figure 5.20 shows a picture of how the specimens were stored in the environmental chamber.

As can be seen from Table 5.6(a), temperature cycles between -4°F and 122°F increased the ultimate strength of the specimens by less than 10%. However, there was a decrease of 10 to 20% in average stiffness of the specimens subjected to such an exposure. Table 5.6(b) also shows that such an exposure did not have significant influence on the ultimate strength of the specimens after 197 days. However, this environment increased the ultimate strength of the specimens after 380 days at a 95% confidence level. After exposure for 207 days, cyclic loading resulted in a decrease in the ultimate strength at a 75% confidence level. Unfortunately, the stiffness of the specimens in the above three cases all decreased at a confidence level larger than 90%.

Because the angle-adhesive retrofit system relied more on stiffness than on ultimate strength, one could draw the conclusion that temperature cycles between -4°F and 122°F, which resembled the change of temperature in the winter and the summer, may decrease the effectiveness of the retrofit system. It should be noted that this is accelerated aging and the normal field application is not expected to be detrimental enough to decrease the stiffness of the retrofit by 10 to 20% in one year. The effect of stiffness on the retrofit will be discussed in Section 5.4.

Though the increase in the ultimate strength after 380 days was a little unexpected, the results were not surprising. Since cold air increased the strength of the specimens, as described in section 5.3.1.4, and hot air decreased the strength of the specimens, as generally believed, it was not surprising that the combined effect of cold air and hot air yielded the above results. However, from the 100% adhesive failure mode described below, it was reasonable to believe that the strength of the specimens would have decreased with a longer exposure time. Nevertheless, as

discussed in Section 5.3.1.1, even if postcure occurred at 122°F, it only increased the crosslinking within the adhesive.

Figure 5.21 shows the failure mode of unloaded specimen conditioned with temperature cycles between -4°F and 122°F for 197 days and 380 days. It can be seen that the failure mode was 100% adhesive. Cracks within the adhesive could be seen in both pictures, indicating the adhesive had become brittle in this environment exposure. A loud snap sound was heard when the load reached the ultimate strength during the static testing. Corrosion occurred at the boundary of the bonding area for the specimen exposed for 380 days.

### ***5.3.1.7 Temperature cycles between -4°F and 122°F (loaded at 0.95 k)***

Static loading during temperature cycling is often used to evaluate the durability of the adhesive (Davis and Fay, 1993). In the field, the adhesive-angle retrofit system was expected to experience intermittent load, which was not as detrimental as the static loading. However, it was beneficial to understand the performance of the adhesive under more hostile environments. The 0.95 kips of static load was approximately 10% of the average ultimate strength of the GPS-nontreated fresh specimens tested under room temperature. The value of 10% was chosen in accordance with literature review that working stress of adhesives was to be limited to 10 to 20% of their ultimate strength (Hart-Smith, 1981; Adams and Wake, 1984; Gasparini et al. 1990).

A self equilibrium loading device was designed to apply the 0.95 kips static load. As shown in Figure 5.22, when the nuts were tightened, the springs were compressed. Since the whole system was self equilibrating, a tension load was applied to the specimens. Two 120-ohm strain gages were installed on both sides of the center adherend to monitor the tightening process. After the specimens were loaded at room temperature, they were put into the environment chamber. Similar to the unloaded specimens with temperature cycles, these specimens were moved manually from one chamber to the other between the two-week cycles.

Since the loading device was self equilibrating and the adhesive crept under static load, the load applied on the specimens decreased overtime. In order to maintain a more constant load on the specimens, the device was unloaded and reloaded on a regular basis. For the first two weeks, the specimens were reloaded every week. For the following month, the specimens were reloaded every two weeks. It was found that 90 to 96% of the initial 0.95 kips was maintained. As a result, it was believed that creep was not significant over short periods of time. The next reloading occurred seven weeks later, when 95% of the initial 0.95 kips was maintained. No reloading was conducted afterwards.

As can be seen from Table 5.6(a), temperature cycling between -4°F and 122°F, combined with 0.95 kips of loading, decreased the average strength by 15 to 30%. This environment decreased the average stiffness of the specimens by 30 to 40%, more than the 10 to 15% of decrease for the unloaded cases. This result was expected because permanent loading during temperature cycling was a more hostile environment than temperature cycling alone. The effect of reduced stiffness on the retrofit system will be discussed in Section 5.4. Table 5.6(b) shows that this environmental exposure did not have significant influence on the ultimate strength of the specimens after 211 days. However, this conditioning decreased the ultimate

strength of the specimens after 370 days at an 84% confidence level. Unfortunately, the stiffness of the specimens in the above two cases was decreased at a confidence level larger than 85%.

It should be mentioned that one specimen in each of the 211-day-exposure batch and 370-day-exposure batch failed in the hot chamber before the final static test was conducted. Since the chambers were monitored on a weekly basis, it was not known when exactly the specimens failed. The failure day was thus postulated to be the 4<sup>th</sup> day during the week that the specimens were kept in the hot chamber. It was believed that such a postulation was close enough because the specimens failed after 122 days of environment exposure. All five data points, including one zero, were used in the analysis for Tables 5.6(a) and (b). This explains why the decrease in the stiffness in the loaded specimens had a smaller confidence level than the decrease in the stiffness in the unloaded specimens.

Figure 5.23 shows the failure mode of a loaded specimen subjected to temperature cycles between -4°F and 122°F for 211 days and 370 days. It can be seen that the failure mode resembled that of the unloaded specimen in temperature cycles. The failure mode was 100% adhesive and cracks within the adhesive could be observed, suggesting the adhesive had become brittle in the environment exposure. A loud snap sound was heard when the load reached the ultimate strength. Corrosion was more widespread for the loaded specimens than for the unloaded specimens.

Figure 5.24 shows the failure mode of the two loaded specimens that were subjected to temperature cycles and failed in the hot chamber before the static test was conducted. The failure mode was 100% adhesive. Corrosion occurred over the majority of bonding area. Thus, it was not surprising that these two specimens failed prematurely. Since the same surface pretreatment procedure was practiced strictly on all the specimens, it was not known why these two specimens had been more severely damaged by the environment than others. One explanation was that the more hostile environment tended to produce more scattered results. In research conducted by Fay and Maddison (1990), some stressed specimens failed while other stressed specimens survived during the environmental exposure. The survived stressed specimens were found to have retained a greater percentage of their initial strength than the unstressed specimens.

### **5.3.1.8 Outdoors**

To simulate the uncontrollable environment of the field application, 50 specimens were placed outside of the Civil Engineering Building.

Figure 5.25 shows a picture of how the specimens were kept outdoors. The specimens were hung on a rod which was supported by a wooden rack. The rack was stored below a protruding roof so that snow and rain would not fall on the specimens directly, thus resembling the environment of the adhesive in the field application.

Originally, the testing matrix was designed so that one batch of specimens would be tested statically after 6 months, 12 months, 24 months and 48 months of outdoor exposure. Another two batches would be tested cyclicly after 9 months and 24 months of outdoor exposure. The effect of GPS pretreatment on the performance of adhesive subjected to outdoor exposure

would also be investigated. Unfortunately, only two batches of specimens were statically tested and one batch was cyclicly tested before the breakout of the unexpected fire on April 12<sup>th</sup>, 2003.

Table 5.6(a) shows that there was less than 5% change in the ultimate strength of the specimens after 184 days of outdoor exposure between February, 2002 and August, 2002. The same observation could be made for the specimens cyclicly loaded after 271 days of outdoor exposure between April, 2002 and January, 2003. The decrease in average stiffness for both cases was less than 10%.

Table 5.6(b) shows that the ultimate strength of the specimens for both batches of specimens exposed outdoors increased at a 65% confidence level. However, the stiffness decreased at a 90% confidence level for both cases. The results of the outdoor environment resembled that of lab temperature cycles without loading.

Figure 5.26 shows the failure mode of specimens kept outdoors for 184 days and 271 days. As can be seen from the pictures, the major failure mode was adhesive. Corrosion could be seen on the specimen that had been exposed for 271 days. Though similar ultimate strengths and stiffnesses were measured for specimens conditioned outdoors and those subjected to temperature cycling without loading, the failure modes were different (Compare Figure 5.26 with Figure 5.21). The percentage of cohesive failure mode was larger for outdoor specimens than for unloaded temperature cycled specimens, when the specimens were exposed to the above environments for approximately the same amount of time.

### ***5.3.1.9 Outdoors and fire***

Fire has never been used as an environment to study the durability of the adhesive in previous research, though it is known that fire has a devastating effect on adhesives. Since fire broke out unexpectedly on the evening of April 12<sup>th</sup>, 2002, at the location where the outdoor specimens were stored, data became available for the uncontrolled environment of fire.

As can be seen from Table 5.6(a), there was an approximately 90% decrease in the average strength and 80% decrease in the average stiffness of specimens because of the fire after an average of 371 days of outdoor exposure. The specimens had been stored outdoors for a period of time between 347 days and 416 days. However, since the fire was much more hostile than the outdoor exposure, it was believed that averaging the days of exposure time would not have an impact on the interpretation of the effect of the environment. Table 5.6(b) also shows that both the ultimate strength and the stiffness decreased at a 99.99% confidence level after being exposed to this environment. As mentioned before, one of the major disadvantages of adhesives was their poor performance in fire, thus, it was not surprising that fire after outdoor exposure was the most devastating environment of all the tested environments.

As described in Chapter 3, in the field application of the adhesive-angle combination, a stainless steel bolt will hold the angle in place if a fire strikes, preventing the angle from dropping down if the adhesive has lost all the strength. If the bridge is found to be usable after the fire, then a similar new retrofit can be conducted after the steel bolt is unscrewed and the damaged adhesive-angle combination is dissembled. If the damaged adhesive still maintained some strength, torching can be used to help dissemble the damaged adhesive-angle combination

and a new adhesive-angle combination can be applied. In other words, such retrofit can be conducted many times if necessary. Furthermore, if the effectiveness of the retrofit is found to decrease overtime because of long periods of environmental exposure, the old adhesive-angle combination can also be disassembled with torching and be replaced by a new adhesive-angle combination, without a deleterious effect on the bridge. Torching was used to dismantle the adhesive-angle combination in the large-scale test described in Chapter 4.

Figure 5.27 shows the trend and scatter of data in both the ultimate strength and the stiffness of the specimens. As can be seen from the figures, though 10 out of 20 specimens failed in the fire, some of the remaining specimens still maintained some strength and stiffness. All 20 data points, including 10 zeroes, were used in the analysis for Tables 5.6(a) and (b). Furthermore, Figure 5.27 shows, as expected, the scatter was tremendous in the ultimate strength, and particularly in the stiffness. Because the fire was not monitored, it was not known what temperature it reached and how long it lasted. Since the fire was started by paper and all the wooden racks were completely consumed, it was reasonable to believe that the fire had reached 400°F~450°F. Also, since all the wooden racks had been burned out, it was postulated that all the specimens had been exposed to the fire, though probably for different lengths of time. Postmortem analysis found that specimens stored closest to the side plates of the wooden box had all failed during the fire (except one specimen with GPS pretreatment which retained 0.17 kips out of the average strength of 8.91 kips of fresh specimens), while some other specimens hung in the center of the box still maintained some strength.

Figure 5.28 shows the failure mode of specimen that failed in the fire after 371 days of outdoor exposure. It can be seen that the failure mode was 100% adhesive. Corrosion and scorch marks could be seen in both pictures. Corrosion marks were brown or dark brown while scorch marks were black. Corrosion combined with scorching could only be observed in the left picture, suggesting that a variety of reasons may have contributed to the failure of the left specimen, while scorching seemed to be the major reason for the failure of the right specimen.

Figure 5.29 shows the failure mode of specimens that were statically tested after they underwent fire after 371 days of outdoor exposure. The specimen on the left had an ultimate strength of 0.7 kips and a stiffness of 400 k/in., while the specimen on the right had an ultimate strength of 5.4 kips and a stiffness of 3000 k/in. As can be seen from Figure 5.29, failure mode for the specimen on the left was 100% adhesive and corrosion had taken place over the entire bonding area. The failure mode for the specimen on the right, on the other hand, was partly cohesive and corrosion had only occurred at the boundary of the bonding area. Thus it was not surprising that the specimen on the right had much greater ultimate strength and stiffness. Scorching marks were not visible on either specimens, suggesting that the specimens had not been consumed by fire for a long period of time. Even so, it was difficult to know the effect of fire and to separate it from the effect of outdoor exposure. However, one can still draw the conclusion that improved surface pretreatment would improve the performance of adhesively bonded steel joints.

### ***5.3.1.10 Summary of performance of specimens without GPS pretreatment in different environments***

As mentioned earlier, each result listed in Table 5.6(b) is strictly limited to one comparison, and thus does not apply to the whole table. However, some useful trends can be concluded from the overview of the whole table, though at a smaller confidence level. Such observed trends from Tables 5.6(a) and (b) would facilitate in the appraisal of the hostility of different environments, and thus would shed light on the estimate of the performance of the adhesive applied in the field in this project.

The exposures of air at 65°F and air at -4°F seemed to be the most benign environments. They did not decrease the strength and the stiffness of the specimens. In some cases, they even increased the strength and the stiffness of the specimens by 10 to 15%. This leads to the conclusion that room temperature and cold temperature would not degrade the performance of the chosen adhesive (3M DP460-NS).

Immersion in tap water at 65°F, decreased the strength and stiffness of the specimens by less than 10% in 201 days. Exposure to freeze and thaw cycling, temperature cycles (unloaded), and outdoor environment (exposure time less than 12 months), on the other hand, had small effect (less than 10%) on the strength of the specimens, yet decreased the stiffness of the specimens by 10 to 20%. The stiffness of the specimens was decreased at a 90% confidence level for the last three environments. Because the adhesive-angle combination retrofit system relies on the stiffness more than on the strength in its effectiveness, it can be concluded that the last three environments mentioned above might be more detrimental to the proposed retrofit system. The effect of adhesive stiffness on retrofit performance will be discussed in Section 5.4.

Temperature cycles with specimens loaded at 0.95 kips (approximately 10% of the ultimate strength of the fresh specimens), decreased the average strength of the specimens by 15 to 30% and the average stiffness of the specimens by 30 to 40%. The stiffness of the specimens was decreased at an 85% confidence level.

Immersion in tap water at 111°F, generally believed to be one of the most hostile environments for adhesives (except fire), proved to be so for the chosen adhesive (3M DP460-NS). It decreased both the strength and the stiffness of the specimens in a relatively short period of time. The decrease in the stiffness was 20 to 60% in this environment for 3 months to 7 months.

Fire, or extreme high temperature, though not typically used as an environment to study the durability of the adhesive in previous research, is known to have the most devastating effect on adhesives (Martine, 1992). It proved to be so in this research. If such a disastrous event did occur on the bridge where the retrofit was applied, the stainless steel bolt that connected the angle to the stiffener would keep the angle from dropping down after the adhesive had been damaged.

### **5.3.2 Comparison of specimens with GPS pretreatment, with specimens without GPS pretreatment**

As mentioned earlier, previous research has found that GPS significantly improved the durability of adhesively bonded steel joints (Gettings and Kinloch, 1977; Kozma and Olefjord, 1987; Fay and Maddison 1990; and Tod et al., 1992). The chemical components of the adhesive may influence the effectiveness of such a pretreatment, and since the adhesive (3M DP460-NS) used in this research had never been investigated with the pretreatment of GPS before, GPS was investigated in this research to find its influence on the durability of the DP460-NS adhesively bonded steel joints.

Tables 5.7(a) and (b) list the comparison of the ultimate strength and the stiffness of the specimens with/without GPS pretreatment. Seven different environments were investigated. These were air at 65°F, immersion in tap water at 111°F, air at -40°F, temperature cycling (specimens were unloaded and loaded at 0.95 k, respectively), outdoors, and fire. Just as in Table 5.6(b), notations in Table 5.7(b) are strictly limited to one comparison, and thus do not apply to the whole table. Nevertheless, some useful trends could still be concluded from the overview of the whole table, though at a smaller confidence level.

#### ***5.3.2.1 Effect of GPS pretreatment on environments other than fire***

Since the adhesive-angle combination retrofit scheme depends on the stiffness of the system to work efficiently, the stiffness of the coupon specimens was more of an interest. Table 5.7(a) shows GPS pretreatment resulted in a 5 to 10% increase in average stiffness of specimens for unloaded temperature cycles and a 10 to 25% increase in average stiffness of specimens for 0.95 kips loaded temperature cycles. The coefficient of variation was large for these two environments, so the results for the stiffness of specimens are not statistically significant.

As Table 5.7(b) shows, GPS pretreatment increased the ultimate strength of the specimens in some environments (immersion in tap water at 111°F and temperature cycling unloaded); however, it did not significantly increase the stiffness of any specimens that were not exposed to fire.

Both Tables 5.7(a) and (b) suggest that GPS pretreatment did not affect the stiffness of the specimens, and thus did not influence the effectiveness of the retrofit system significantly.

#### ***5.3.2.2 Effect of GPS pretreatment on environment of fire after outdoor exposure***

In the environment of fire after outdoor exposure, GPS pretreatment increased both the strength and the stiffness of the coupon specimens. Though postmortem analysis of the fire yielded the conclusion that all the coupon specimens had been exposed to the fire, it was not known how long each specimen was in the fire and which part of the fire each specimen was in (temperature varies in different parts of the fire). Thus, a direct comparison without any analysis, was somewhat ambiguous.

Figure 5.30 shows the failure mode of the GPS pretreated specimens that underwent fire after 374 days of outdoor exposure. Just as the failure mode of the specimens unpretreated with

GPS shown in Figure 5.29, there was much scatter. The specimen on the left had an ultimate strength of 1.2 kips and stiffness of 1800 k/in., while the specimen on the right had an ultimate strength of 7.5 kips and stiffness of 2800 k/in.

As can be seen from Figure 5.30, the failure mode of the specimen on the left was 100% adhesive and corrosion had taken place throughout the entire bonding area. The failure mode of the specimen on the right, on the other hand, was approximately 20% cohesive and corrosion had only occurred at the very boundary of the bonding area. Thus it was not surprising that the specimen on the right had greater ultimate strength and stiffness. Scorching marks were not visible on either specimen, suggesting that the specimens had not been consumed by fire for a long period of time. Even so, it was difficult to know the effect of fire and to separate it from the effect of outdoor exposure.

### ***5.3.2.3 Summary of the effect of GPS pretreatment***

GPS pretreatment did not seem to increase the effectiveness of the adhesive-angle retrofit system in the following environments: air at 65°F, immersion in tap water at 111°F, air at -40°F, temperature cycling (specimens were unloaded and loaded at 0.95 k, respectively), and outdoors exposure less than 12 months.

Based on the information obtained from the coupon test, it was concluded that GPS did not affect the effectiveness of the adhesive-angle retrofit system significantly. Thus GPS pretreatment is not recommended unless further research on outdoor exposure reveals otherwise.

## **5.4 The influence of the stiffness on the effectiveness of the retrofit system**

As mentioned in Section 5.2, large bondline thickness decreased the stiffness of the specimens. It is difficult to maintain the same bondline thickness during field application (as shown in Figure 3.9), and this may result in decreased stiffness of the retrofit system. Section 5.3 also shows that the stiffness of the specimens decreased under various environments. Exposure to freeze and thaw cycling, temperature cycles (unloaded), and outdoor environment (exposure time less than 12 months), decreased the stiffness of the specimens by 10 to 20%. Temperature cycles with specimens loaded at 0.95 kips (approximately 10% of the ultimate strength of the fresh specimens), decreased the stiffness of the specimens by 30 to 40% in 12 months. Immersion in tap water at 111°F decreased the stiffness of the specimens by 20 to 60% in 3 to 7 months.

The above findings lead to the question of how much the stiffness of the adhesive influences the effectiveness of the retrofit system. Thus, the FEA model used in Chapter 4 for the large-scale specimen was modified to study the influence of the stiffness of the adhesive on the effectiveness of the retrofit system.

A global model of a quarter of the large-scale specimen (the specimen was doubly symmetric) that predicted the global behavior of the specimen, and a submodel that predicted the local behavior of the specimen at the web gap region, were already developed in Chapter 4. In order to model the effect of the adhesive-angle retrofit system, a 20-node solid element (brick element), C3D20R, was used to model both the adhesive and the angle (Figure 5.31). The

thickness of the adhesive was set to be 0.020 in. and the thickness of the angle was set to be  $\frac{3}{4}$  in. There was one layer of solid elements for the adhesive and one layer of solid elements for the angle. The solid elements for the adhesive had dimension of 0.020 x 1.5 x 1.0 in. (for the adhesive that connected the angle with the tension flange) or 0.020 x 1.5 x 0.75 in. (for the adhesive that connected the angle with the stiffener). The solid elements for the angle had dimension of  $\frac{3}{4}$  x 1.5 x 1.0 in. (for the leg that was connected to the tension flange) or  $\frac{3}{4}$  x 1.5 x 0.75 in. (for the leg that was connected to the stiffener). Although the aspect ratio for the adhesive was very high in the global model, it was believed that the inaccuracy resulting from it would not affect the out-of-plane stresses obtained from the submodel.

The analysis was materially linear except for the adhesive. The modulus of elasticity of the steel angle was set to be 29,000 ksi. An elastic-perfectly plastic stress-strain curve was specified for the adhesive. The modulus of elasticity of the adhesive was set to be 320 ksi and the Poisson's ratio was set to be 0.4 (recommended by 3M technical support).

In order to investigate the influence of the adhesive stiffness on the effectiveness of the retrofit system, the modulus of elasticity of the adhesive was set to 1%, 5%, 10%, 15%, 20%, 25%, 30%, 40%, 50%, 60%, 70%, 80%, 100%, 200%, 400%, and 9062.5% of the 320 ksi originally used for the modulus of elasticity for the adhesive. The 9062.5% of the 320 ksi was used to investigate the extreme case when the adhesive had the same modulus of elasticity as the steel. Also, another case without a web gap was investigated by connecting the nodes on the bottom of the stiffener to the tension flange. In other words, the shell elements of the stiffener bottom shared the same nodes as the tension flange at the intersection. The out-of-plane stresses predicted by the FEA at web gap in the constant moment region where in-plane stress was 12 ksi are shown in Figure 5.32. Some interesting findings are summarized below.

When there was no retrofit or the modulus of elasticity of the adhesive was smaller than 15% of  $E_a$  ( $E_a$  was the modulus of elasticity originally used for the adhesive and  $E_a = 320$  ksi), double curvature occurred in the web gap. When the modulus of elasticity of the adhesive was 20 to 200% of  $E_a$ , single curvature occurred in the web gap. However, when the modulus of elasticity of the adhesive was 400 to 9062.5% of  $E_a$ , double curvature occurred in the web gap again. When there was no web gap, single curvature occurred in the web between the flange-web fillet weld and the stiffener-web weld.

The second observation was that the out-of-plane stresses decreased by 50% when the modulus of elasticity of the adhesive was only 1% of  $E_a$ . The smallest out-of-plane stresses occurred when the modulus of elasticity of the adhesive was 30% of  $E_a$ . When the modulus of elasticity of the adhesive was 30 to 9062.5% of  $E_a$ , out-of-plane stresses even increased slightly compared with those when the modulus of elasticity of the adhesive was 30% of  $E_a$ . Of course, such an increase was very small and negligible. The change from double curvature to single curvature, and then to double curvature again might be the possible reason for the above observation. When there was no web gap, the out-of-plane stresses were closest to those when the modulus of elasticity of the adhesive was 40 to 60% of  $E_a$ . Nevertheless, out-of-plane stresses were decreased considerably (by approximately 90%) when the modulus of elasticity of the adhesive was greater than 20% of  $E_a$ .

The above observation indicated that the relationship between out-of-plane stresses and the modulus of elasticity of the adhesive was complicated and not linear. However, the fact that out-of-plane stresses was decreased by approximately 90% when the modulus of elasticity of the adhesive was greater than 20% of  $E_a$  suggested that, even though the modulus of elasticity of the adhesive had a great influence on the effectiveness of the retrofit system, the decrease in the modulus of elasticity of the adhesive did not affect the effectiveness of the retrofit system provided that 20% of the original modulus of elasticity was maintained.

It is reasonable to believe that the decrease in the stiffness of the coupon specimens shown in Section 5.3 was mainly due to the decrease in the modulus of elasticity of the adhesive, and the decrease in the adherence between the adhesive and the adherend. Since it was difficult to model the decrease in the adherence between the adhesive and the adherend, and there was geometry and mechanism difference between the coupon specimen and the adhesive-angle retrofit system in the large-scale test, a direct comparison of the coupon specimen and the adhesive-angle retrofit system was difficult. However, it was reasonable to postulate that, even though the stiffness of the coupon specimens decreased under various environments, environments that introduced less than 50% of decrease in the coupon specimen stiffness would not have significant influence on the effectiveness of the adhesive-angle retrofit system. In other words, except for temperature cycles (loaded at 0.95 k), immersion in tap water at 111°F, and fire after outdoor exposure, all other tested environments would not deteriorate the effectiveness of the adhesive-angle retrofit system significantly.

As discussed in Chapter 3, the adhesive-angle retrofit system on the bridges remained in place and was in good condition after 3.5 years (from November, 2001 to May, 2005) of exposure to outdoor environment and dynamically applied out-of-plane loading between passages of heavy trucks. This also indicates that the effectiveness of the adhesive-angle retrofit system was likely not decreased by such an environment.

## 5.5 Conclusion

Coupon tests have been conducted to investigate the effects of various exposures on the performance of the adhesive. The relative aggressiveness of the environments toward joint strength is ranked from least to most detrimental as follows: air at -4°F; air at 65°F; temperature cycles (unloaded); freeze and thaw cycling, and outdoor environment; immersion in tap water at 65°F; temperature cycles (loaded at 0.95 kips, 10% of the initial strength), and immersion in tap water at 111°F; and fire after outdoor exposure.

Since the adhesive-angle retrofit system relies more on stiffness than on strength for its effectiveness, the relative aggressiveness of the environment with respect to stiffness is also ranked. From least to most detrimental environments are: air at 65°F; air at -4°F; immersion in tap water at 65°F; outdoor environment, freeze and thaw cycling, temperature cycles (unloaded); temperature cycles (loaded at 0.95 kips, 10% of the initial strength), immersion in tap water at 111°F; and fire after outdoor exposure.

As discussed in Section 5.4, it was reasonable to postulate that, even though the stiffness of the coupon specimens decreased under various environments, environments that introduced less than 50% of decrease in the coupon specimen stiffness would not have significant influence

on the effectiveness of the adhesive-angle retrofit system. In other words, except for temperature cycles (loaded at 0.95 k, 10% of the initial strength), immersion in tap water at 111°F, and fire after outdoor exposure, all other tested environments were not likely to deteriorate the effectiveness of the adhesive-angle retrofit system.

Based on the above observations, it is concluded that the chosen adhesive (3M DP460-NS) is suitable for applications at room or low temperature, even with high relative humidity (freeze and thaw test, and immersion in tap water at 65°F). When the temperature is relatively high (111°F), it is best to apply the adhesive for an application without permanent loading and high relative humidity. If permanent loading is necessary for the application, then the mean stress of the permanent loading should be kept within 10% of its initial strength. If high relative humidity cannot be avoided, it is advised to leave the spew fillet intact, so as to lengthen the water path into the adhesive (Arrowsmith, 1987; Knox and Cowling, 2000-b). Preventive coating, such as painting, will also aid in slightly delaying the water diffusion process (Kinloch, 1984). The adhesive is not suitable for places where temperature is higher than or close to its glass transition temperature (122.5°F).

The adhesive-angle retrofit system is applicable to steel bridges in Minnesota. However, for steel bridges in warmer and more humid states, high temperature adhesive may provide better performance.

If a disastrous event, such as fire, did occur on the bridge where the retrofit was applied, the stainless steel bolt that connected the angle to the stiffener would keep the angle from dropping down after the adhesive had been damaged.

If the effectiveness of the retrofit is found to decrease overtime because of long periods of environmental exposure, or because of a disastrous event, such as fire, the old adhesive-angle combination can be disassembled with torching and be replaced by a new adhesive-angle combination, without deleterious effect to the bridge.

## Chapter 6 Conclusion

In this research, an adhesive-angle retrofit system was proposed to provide positive attachment between the connection plate and the tension flange to retrofit out-of-plane fatigue cracks in the web gap region. In order to investigate the effectiveness of such a retrofit system, a field test and large-scale test were conducted. Furthermore, since environmental durability is vital for long-term performance, small-scale coupon tests were conducted to investigate the durability of the chosen adhesive, DP-460 NS, a product of 3M. Major findings from this research project will be presented in this chapter.

### 6.1 Findings from the field test

The field test was an indispensable part of this project used to determine the effectiveness of the proposed retrofit method because it represented the real environment and loading under which the adhesive will be applied and exposed. Therefore, two representative multi-girder steel bridges were chosen to conduct the field test. The major findings from the field test are presented as follows:

1. The retrofit of adhering an angle to the connection plate and the tension flange of the girder was effective at places where the original strain range was larger than 50 microstrains. This retrofit method achieved at least 38% strain range reduction for the bent-plate-diaphragm (BPD) bridge and at least 50% strain range reduction for the cross-frame-diaphragm (CFD) bridge when the original strain range was more than 50 microstrains. If such reduction percentage can be obtained for strain ranges large enough to initiate a crack, the fatigue life of the connection can be extended at least 4.6 times by this retrofit method. Or, if the strain range was reduced below the threshold level, then no fatigue cracks would initiate.
2. The thickness of the angle was chosen to be  $\frac{3}{4}$  in. to provide enough stiffness for the retrofit method to be effective. The leg lengths of the angle were chosen so that the angle was not too heavy for easy application, yet it still had enough adhering surface to resist out-of-plane forces.
3. The  $\frac{1}{4}$  in. diameter stainless steel bolt that connected the angle to the stiffener served the following two purposes: to hold the angle in place before the adhesive had cured, and to keep the angle from dropping down if some disastrous event, such as fire, occurred to the bridge and damaged the adhesive.
4. Because normal traffic flow was not interrupted when the retrofit was conducted, it could be concluded that the vibration caused by the traffic would not influence the effectiveness of the adhesive performance, provided that the manufacturer's requirements are met.
5. Because the adhesive application represented the worst situation of field application (applied at 50°F instead of 70°F), the obtained results should provide the lower bound performance of the 3M adhesive, DP460-NS. A recommended retrofit procedure is proposed in Appendix M.

6. The ten adhesive-angle retrofits remained in place and were in good condition after three and a half years, suggesting that the chosen adhesive had good environmental durability.

## 6.2 Findings from the large-scale test

The proposed adhesive-angle retrofit system was found to be effective in the field test. However, the maximum out-of-plane strain range in the bent-plate-diaphragm bridge was only approximately 200 microstrains and the maximum out-of-plane strain range in the cross-frame-diaphragm bridge was less than 100 microstrains in the field test. Therefore, a large-scale test was conducted in the lab under controlled conditions so that the effectiveness of the adhesive attachment under maximum possible stress conditions could be studied. The major findings from the large-scale test are presented as follows:

1. Of 27 crack tip locations, only one crack tip strain gage measured a larger strain range after retrofit (1432 microstrains) than before retrofit (302 microstrains). It was possible that some internal stress relief system was involved before retrofit and the stress relief system had diminished after retrofit. Also, this crack tip strain gage was located at the tip of a through-thickness crack which had already propagated away from the web gap and grown perpendicular to the in-plane stress on the web. Thus strain range readings from two crack tip gages that were located on each side of the web for this through-thickness crack could be treated as outliers because of the type of crack formed. If these two data points are treated as outliers and are not included, crack tip strain ranges were decreased to approximately 20% of the original values on average.
2. Even without stop holes, most cracks were stopped, or retarded, by the adhesive-angle retrofit system under the same in-plane stress range, i.e., 12 ksi in the constant moment region. The corresponding measured out-of-plane strain ranges before retrofit were approximately 600 microstrains when the in-plane stress range was 12 ksi in the constant moment region. Had stop holes been drilled at all crack tips, as would be the case for any field retrofit application, some of the retarded cracks might have been stopped completely. Cracks were stopped completely when the load range was reduced to one third of the original load range (i.e., 4 ksi in the constant moment region).
3. It was obvious that there was a correlation between the crack growth rate and the performance of the adhesive. If the angle was not loose, the crack growth rate was slow or zero. It was postulated that field inspection of angles and adhesives could provide qualitative information as to whether the retrofit system remained effective.
4. The retrofit method had little effect on the crack growth rate for two cracks which had grown out of the web gap region and become perpendicular to the in-plane stress. This was expected because the adhesive-angle retrofit system, though effective at decreasing out-of-plane stress, did not affect the in-plane stress. Thus, such retrofit method is not recommended for cracks which are longer than 2 in. and have grown perpendicular to the in-plane stresses.
5. No cracks were found on the tension flange after 682,000 cycles at NE-C and 451,000 cycles at SE-C under 12 ksi stress range when powder actuated fasteners were used in

combination with adhesives to attach the angle to the tension flange. No cracks were found on the tension flange at NE-C and SE-C after an additional 2 million cycles under 4 ksi stress range. This was consistent with the S-N curve provided by Niessner and Seeger (1999), which shows that the base metal with powder actuated fasteners has an infinite life if the stress range is smaller than 14.5 ksi (between Category B and C). Powder actuated fasteners in combination with adhesives is recommended to retrofit web gap cracks when the out-of-plane force is significant.

### **6.3 Findings from the small-scale coupon test**

As mentioned earlier, environmental durability was one of the most important parameters in the choice of adhesives, and it was not directly correlated to the initial strength, thus it was desirable to understand the performance of the chosen adhesive, under different environmental exposure schemes. Coupon tests were conducted for this purpose. The major findings from the small-scale coupon test are presented as follows:

1. The relative aggressiveness of the environment with respect to stiffness is ranked from least to most detrimental environments: air at 65°F; air at -4°F; immersion in tap water at 65°F; outdoor environment, freeze and thaw cycling, temperature cycles (unloaded); temperature cycles (loaded at 10% of the initial strength), immersion in tap water at 111°F; and fire after outdoor exposure.
2. Even though the stiffness of the coupon specimens decreased under various environments, it was postulated from the results of the FEA of the large-scale specimen that environments which introduced less than a 50% decrease in the coupon specimen stiffness were not likely to influence the effectiveness of the adhesive-angle retrofit system. In other words, except for temperature cycles (loaded at 10% of the initial strength), immersion in tap water at 111°F, and fire after outdoor exposure, all other tested environments were not likely to deteriorate the effectiveness of the adhesive-angle retrofit system.
3. The chosen adhesive (3M DP460-NS) is suitable for applications at room or low temperature, even with high relative humidity. In other words, it is applicable to the steel bridges in Minnesota. If the adhesive is intended for use under relatively high temperature (111°F), then high relative humidity should be avoided. The adhesive is not suitable for places where temperature is higher than or close to its glass transition temperature (122.5°F).
4. If the effectiveness of the retrofit is found to decrease overtime because of long periods of environmental exposure, or because of a disastrous event, such as fire, the old adhesive-angle combination can be disassembled with torching and be replaced by a new adhesive-angle combination, without deleterious effect to the bridge.

### **6.4 Conclusion remarks and recommended future work**

Prior to 1985, it was common practice to avoid welding floorbeam and diaphragm connection plates to the tension flange of steel bridge girders, often resulting in “web-gap

cracking” due to out-of-plane distortion of the girder web. The most widely applicable and accepted retrofit method is to rigidly attach the connection plate to the flange. In this report, a new retrofit option was investigated that uses a room-temperature-cured two-part epoxy to join a small length of ¾-inch thick steel angle shape to the tension flange and the connection plate. Unlike bolting, this retrofit does not require access to the outer surface of the tension flange, thus partial closure to traffic due to removal of the concrete slab in the negative moment region can be avoided. Also, unlike welding, this retrofit operation is not sensitive to vibration caused by traffic and can be conducted without closing the bridge.

A field test on two skewed bridges showed that the adhesive-angle retrofit system decreased out-of-plane strain range by 40 to 50% when the original strain range was larger than 50 microstrains. The ten adhesive-angle retrofits remained in place and were in good condition after three and a half years, suggesting that the chosen adhesive had good environmental durability. Large-scale specimen test with 8 web gaps showed that the adhesive-angle retrofit system stopped or retarded most cracks even without stop holes at 12 ksi and 6 ksi in-plane stress ranges. The corresponding measured out-of-plane strain ranges for the above test were approximately 600 microstrains. The adhesive-angle retrofit system stopped all cracks at 4 ksi and 2 ksi in-plane stress ranges. There are several recommendations for future studies on the use of adhesives to retrofit out-of-plane fatigue cracks:

1. Bondline thickness smaller than 0.020 in. should be investigated in field tests. In particular, cases without spacers such as glass beads to maintain bondline thickness, and thus expediting the retrofit process, can be investigated. It is possible that the irregularities of the surface of the flange, connection plate, and the angle provide “spacers” for the bondline.
2. The adhesive retrofit should be investigated further to see if it is effective, together with stop hole drilling, when the detail has already exhibited a small web-gap crack in a field test.
3. A database of in-service durability performance does not exist due to the scarcity of adhesives used in steel-to-steel bonding in civil structures, however, results from this study, and other future studies can be built into such a database.
4. Even though the ten adhesive-angle retrofits remained in place and were in good condition after three and a half years, it is suggested that more coupon specimens be fabricated and stored in outdoor environment for prolonged and quantitative durability study. Outdoors exposure for 5, 10, 15, and 20 years can be investigated.
5. Powder actuated fasteners were used in combination with adhesives to attach the angle to the tension flange in this research. The testing results were consistent with the S-N curve provided by Niessner and Seeger (1999), which shows that the base metal with powder actuated fasteners has an infinite life if the stress range is smaller than 100 Mpa, which is equivalent to 14.5 ksi. Due to the simplicity of the application, a new retrofit method with powder actuated fasteners connecting the angle and the tension flange, and adhesives connecting the angle and the connection plate, should be investigated.

6. The effect of girder, diaphragm, connection plate, and retrofit angle dimensions on the effectiveness of the retrofit can be studied to determine a rationale detail design for the retrofit system.

## References

- Abdel Wahab, M.M., Crocombe, A.D., Beevers, A., and Ebtehaj, K. (2002). "Coupled Stress-Diffusion Analysis for Durability Study in Adhesively Bonded Joints," *International Journal of Adhesion & Adhesives*, Vol. 22, pp. 61-73.
- ABAQUS/Standard User's Manual (1994). Version 5.4.
- Adams, R.D. and Wake, W.C. (1984). **Structural Adhesive Joints in Engineering**, Elsevier Applied Science Publishers, London and New York.
- Albrecht, P. (1987). "Fatigue Strength of Adhesively Bonded Cover Plates," *Journal of Structural Engineering*, Vol. 113, No. 6, pp. 1236-1250.
- Altay, A.K., Arabbo, D.S., Corwin, E.B., Dexter, R.J., and French, C.E. (2003). "Effects of Increasing Truck Weight on Steel and Prestressed Bridges," *Report MN/RC-2003-16*, pp. 36.
- Akesson, B., Edlund, B., and Shen, D. (1997). "Fatigue Cracking in a Steel Railway Bridge," *Structural Engineering International*, IABSE Publications Committee, Vol. 2, pp. 118-120.
- Arrowsmith, D.J. and Maddison, A. (1987). "The Use of Perforated Lap Shear Specimens to Test the Durability of Adhesive-Bonded Aluminum," *International Journal of Adhesion & Adhesives*, Vol. 7, No.1, pp. 15-24.
- Ashcroft, I.A., Digby, R.P., and Shar, S.J. (2001). "A Comparison of Laboratory-Conditioned and Naturally-Weathered Bonded Joints," *Journal of Adhesion*, Vol. 75, pp. 175-201.
- Berglund, E. and Schultz, A.E. (2002). "Girder Differential Deflection and Assessing Distortional Fatigue in Skewed Steel Bridges," *Minnesota Department of Transportation, Final Report*, December 2002.
- Berglund, E. and Schultz, A.E. (2003). "Girder Differential Deflection and Distortion-Induced Fatigue in Skewed Steel Bridges," CD-ROM. *Transportation Research Board*, National Research Council, Washington, D.C.
- Bistac, S., Vallat, M.F., and Schultz, J. (1998). "Durability of Steel/Polymer Adhesion in an Aqueous Environment," *International Journal of Adhesion & Adhesives*, Vol. 18, No. 5, pp. 365-369.
- Bowditch, M.R., Hiscock, D., and Moth, D.A. (1992). "The Role of the Substrate in the Hydrolytic Stability of Adhesive Joints," *International Journal of Adhesion & Adhesives*, July, pp. 164-170.
- Bowditch, M.R. (1996). "The Durability of Adhesive Joints in the Presence of Water," *International Journal of Adhesion & Adhesives*, Vol. 16, No. 2, pp. 73-79.

- Brewer, D., Gasparini, D.A., and Andreani, J. (1990). "Diffusion of Water in Steel-to-Steel Bonds," *Journal of Structural Engineering*, Vol. 116, No. 5, pp. 1180-1198.
- Brewis, D.M., Comyn, J., and Tegg, J.L. (1980). "The Durability of Some Epoxide Adhesive-Bonded Joints on Exposure to Moist Warm Air," *International Journal of Adhesion & Adhesives*, Vol. 1, No.1, pp. 35-39.
- Brewis, D.M., Comyn, J., Cope, B.C., and Moloney, A.C. (1980). "Effect of Carriers on the Performance of Aluminum Alloy Joints Bonded with an Epoxide — Polyamide Adhesive," *Polymer*, Vol. 21, March, pp. 344-351.
- Brewis, D.M. (1983). "Chapter 5: Aluminium Adherends," **Durability of Structural Adhesives**, edited by A. J. Kinloch, Applied Science Publishers, London and New York.
- Brockmann, W. (1983). "Chapter 7: Steel Adherends," **Durability of Structural Adhesives**, edited by A. J. Kinloch, Applied Science Publishers, London and New York.
- Butt, R.I. and Cotter, J.L. (1976). "The Effect of High Humidity on the Dynamic Mechanical Properties and Thermal Transitions of an Epoxy-Polyamide Adhesive," *Journal of Adhesion*, Vol. 8, pp. 11-19.
- Chang, T., Sproat, E.A., Lai, Y.H., Shephard, N.E., and Dillard, D.A. (1997). "A Test Method for Accelerated Humidity Conditioning and Estimation of Adhesive Bond Durability," *Journal of Adhesion*, Vol. 60, pp. 153-162.
- Comyn, J. (1983). "Chapter 3: Kinetics and Mechanism of Environmental Attack," **Durability of Structural Adhesives**, Edited by Kinloch, A.J., Applied Science Publishers, London and New York.
- Cui, W. (2002). "A State-of-the-Art Review on Fatigue Life Prediction Methods for Metal Structures," *Journal of Marine Science and Technology*, Vol. 7, pp. 43-56.
- D'Andrea, M., Grondin, G.Y., and Kulak, G.L. (2001). "Behavior and Rehabilitation of Distortion-Induced Fatigue Cracks in Bridge Girders," *Structural Engineering Report No. 240*, University of Alberta, Canada.
- Davis, R.E. and Fay, P.A. (1993). "The Durability of Bonded Coated Steel Joints," *International Journal of Adhesion & Adhesives*, Vol. 13, No. 2, April, pp. 97-104.
- Demers, C.E. and Fisher, J.W. (1990). "Fatigue Cracking of Steel Bridge Structures, Volume I: A Survey of Localized Cracking in Steel Bridges — 1981 to 1988," *U.S. Department of Transportation*, Federal Highway Administration, Publication No. FHWA-RD-89-166.
- Dexter, R.J. and Bergson, P.M. (1998). "Bridge No. 9340 – Load Test Results," Letter form
- Fay, P.A. and Maddison, A. (1990). "Durability of Adhesively Bonded Steel under Salt Spray and Hydrothermal Stress Conditions," *International Journal of Adhesion & Adhesives*, Vol. 10, No. 3, pp. 179-186.

- Fisher, J.W. (1978). "Fatigue Cracking in Bridges from Out-of-Plane Displacements," *Canadian Journal of Civil Engineering*, Vol. 5, pp. 542-556.
- Fisher, J.W., Fisher, T.A., and Kostem, C.N. (1979). "Displacement Induced Fatigue Cracks," *Engineering Structures*, Vol. 1, October, pp. 252-257.
- Fisher, J.W., Barthelemy, B.M., Mertz, D.R., and Edinger, J.A. (1980). "Fatigue Behavior of Full-Scale Welded Bridge Attachments," *NCHRP Report 227, Transportation Research Board*.
- Fisher, J.W., Mertz, D.R., and Wu, K.C. (1982). "Displacement-Induced Fatigue Cracking of a Box Girder Bridge," *International Association for Bridge and Structural Engineering Symposium*, Washington, D.C., USA, pp. 71-76.
- Fisher, J.W. and Mertz, D.R. (1984). "Fatigue and Fracture in Steel Bridges," *The Conference on Bridges official proceedings, 1<sup>st</sup> International Bridge Conference*, Pittsburgh, Pa, pp. 10-21.
- Fisher, J.W. and Mertz, D.R. (1985). "Hundreds of Bridges, Thousands of Cracks," *Civil Engineering, ASCE*, Vol. 5, No. 4, pp. 64-67.
- Fisher, J.W. and Keating, P.B. (1989). "Distortion-Induced Fatigue Cracking of Bridge Details with Web Gaps," *Journal of Construction Steel Research*, Vol. 12, pp. 215-228.
- Fisher, J.W. and Menzemer, C.C. (1990). "Fatigue Cracking in Welded Steel Bridges," *Transportation Research Record*, 1282. Washington, D.C., TRB, National Research Council, pp. 111-117.
- Fisher, J.W., Jin, J., Wagner, D.C., and Yen, B.T. (1990). "Distortion-Induced Fatigue Cracking in Steel Bridges," *National Cooperative Highway Research Program (NCHRP) Report 336*.
- Fraser, R.E.K., Crondin, G.Y., and Kulak, G.L. (2000). "Behavior of Distortion-Induced Fatigue Cracks in Bridge Girders," *Structural Engineering Report, No. 235*, Department of Civil and Environmental Engineering, University of Alberta, Edmonton, Canada.
- Gasparini, D.A., Nara, H., Andreani, J., Boggs, C., Brewer, D., and Etitum, P. (1990). "Steel-to-Steel Connections with Adhesives," *Journal of Structural Engineering*, Vol. 116, No. 5, pp. 1165-1179.
- Gettings, M. and Kinloch, A.J. (1977). "Surface Analysis of Polysiloxane/Metal Oxide Interfaces," *Journal of material science*, Vol. 12, pp. 2511-2518.
- Gledhill, R.A. and Kinloch, A.J. (1974). "Environmental Failure of Structural Adhesive Joints," *Journal of Adhesion*, Vol. 6, pp. 315-330.
- Gledhill, R.A., Kinloch, A. J., and Shaw, S. J. (1980). "A Model for Predicting Joint Durability," *Journal of Adhesion*, Vol.11, 1980, pp. 3-15.
- Goerg, P. (1963). "Über die Aussagefähigkeit von Dauerversuchen mit Prüfkörpern aus Baustahl ST37 und ST52," *Der Stahlbau*, Vol. 32, No. 2, pp. 36-42.

- Gosselin, C.A. (1985). "The Durability of Lap-Shear Adhesive Bonds Following Accelerated Environmental Testing," *SAE technical paper series, International congress & exposition*, Detroit, Michigan, February 25-March 1, 1985, pp. 15-23.
- Harris, A.F. and Beevers, A. (1999). "The Effects of Grit-Blasting on Surface Properties of Adhesion," *International Journal of Adhesion & Adhesives*, Vol. 19, pp. 445-452.
- Hart-Smith, L.J. (1981). "Chapter 1: Stress Analysis: A Continuum Mechanics Approach," **Developments in adhesives-2**, edited by A.J. Kinloch. pp. 1-44, Applied Science Publishers, London
- Hashim, S.A., Cowling, M.J., and Winkle, I.E. (1990). "Design and Assessment Methodologies for Adhesively Bonded Structural Connections," *International Journal of Adhesion & Adhesives*, Vol. 10, No. 3, pp. 139-145.
- Hashim, S.A. (1999). "Adhesive Bonding of Thick Steel Adherends for Marine Structures," *Marine Structures*, Vol. 12, pp. 405-423.
- Jajich, D. and Schultz, A.E. (2003). "Measurement and Analysis of Distortion-Induced Fatigue in Multigirder Steel Bridges," *Journal of Bridge Engineering, ASCE*, pp. 84-91.
- Keating, P.B. (1994). "Focusing on Fatigue," *Civil Engineering*, November, pp. 54-57.
- Khalil, A., Wipf, T.J., Greimann, L., Wood, D.L., and Brakke, B. (1998). "Retrofit Solution for Out-of-Plane Distortion of X-Type Diaphragm Bridges," *Transportation Conference Proceedings*, pp. 99-102.
- Kinloch, A.J. (1983). "Chapter 1: Introduction," "Chapter 7: Steel Adherends," **Durability of Structural Adhesives**, edited by A. J. Kinloch, Applied Science Publishers, London.
- Kinloch, A.J. (1987). **Adhesion and Adhesives**, Chapman and Hall, London.
- Knox, E.M. and Cowling, M.J. (2000)-a. "A Rapid Durability Test Method for Adhesives," *International Journal of Adhesion & Adhesives*, Vol. 20, No. 3, pp. 201-208.
- Knox, E.M. and Cowling, M.J. (2000)-b. "Durability Aspects of Adhesively Bonded Thick Adherend Lap Shear Joints," *International Journal of Adhesion & Adhesives*, Vol. 20, pp. 323-331.
- Konate, Y. (1994). "Influence of Thermal Cycle on Resistance to Fracture under Shear Loading of Adhesive Films," *International Journal of Adhesion & Adhesives*, Vol. 14, No.3, pp. 181-184.
- Kozma, L. and Olefjord, I. (1987). "Surface Treatment of Steel for Structural Adhesive Bonding," *Material Science and Technology*, November, Vol. 3, pp. 954-962.
- Lai, L-Y. (1997). "On Drilling Holes to Arrest Fatigue Crack Growth," *Building to Last — Proceedings of the Structural Congress XV*, Vol. 1, edited by Kempner and Brown. ASCE, New York, pp. 31-35.

- Lark, R.J. and Mays, G.C. (1984). "Chapter 7: Epoxy Adhesive Formulation: Its Influence on Civil Engineering Performance," **Adhesion 9**, edited by K.W. Allen, pp. 95-110.
- Lee, J. J. (1989). "Fatigue Strength of Steel Bridge Girders with Distortion Induced Stresses," *International Journal of Fatigue*, Vol. 11, No. 3, pp. 210.
- Lees, D.E. and Hutchinson, A.R. (1992). "Mechanical Characteristics of Some Cold-Cured Structural Adhesives," *International Journal of Adhesion & Adhesives*, Vol.12, No. 3, pp. 197-205.
- Martin, D.M. (1992). "Tests on Bonded Transverse Intermediate Web Stiffeners," *The Structural Engineer*, Vol.70, No. 15/4, pp. 261-267.
- Mays, G.C. and Vardy, A.E. (1983). "Fatigue Performance and Durability of Epoxy Resin Bonded Metal Lap Joints," *Fatigue in Polymers, International Conference*, June 29<sup>th</sup> ~30<sup>th</sup>, pp. 13.1-13.10.
- Mays, G.C. (1985). "Structural Adhesive Applications for Bridges," *SAE 85, Adhesive, Sealants and Encapsulants Conference*, London, U.K., November 5-7, pp. 172-188.
- Minford, J.D. (1973). "Chapter 2: Durability of Adhesive Bonded Aluminum Joints," **Treatise on Adhesion and Adhesives**, Vol. 3, edited by Patrick, R.L., Published by Marcel Dekker, Inc., New York.
- Minford, J.D. (1983). "Chapter 4: Adhesives," **Durability of structural adhesives**, edited by A. J. Kinloch, Applied Science Publishers, London and New York.
- Mueller, J.A. and Yen, B.T. (1968). "Girder Web Boundary Stresses and Fatigue," *Welding Research Council Bulletin*, Vol. 127.
- Nara, H., Gasparini, D., Andreani, J., and Boggs, C. (1985). "Steel to Steel Bonding for Bridges," *30<sup>th</sup> National SAMPE Symposium*, March 19-21, pp. 1387-1396.
- Niessner, M and Seeger, T. (1999). "Fatigue Strength of Structural Steel with Powder Actuated Fasteners According to Eurocode 3," *Stahlbau*, Vol. 68, pp. 941-948.
- Nozaka, K., Shield, C.K., and Hajjar, J.F. (2001). "Repair of Fatigued Steel Bridge Girders with Carbon Fiber Strips," *Proceedings of the Fifth National Workshop on Bridge Research in Progress*, October, Minneapolis, Minnesota, pp. 271-276.
- Nozaka, K. (2002). "Repair of Fatigued Steel Bridge Girders with Carbon Fiber Strips," *Ph.D dissertation*, University of Minnesota.
- Posten, H.O. (1978). "The Robustness of the Two-Sample *t* Test over the Pearson System," *Journal of Statistical Computation and Simulation*, Vol. 6, pp. 295-311.
- Schnerch, D., Stanford, K., Sumner, E.A., and Rizkalla, S. (2004). "Strengthening Steel Structures and Bridges with High Modulus Carbon Fiber Reinforced Polymers: Resin Selection

and Scaled Monopole Behavior,” CD-ROM. *Transportation Research Board*, National Research Council, Washington, D.C.

Shaaf, A., Schnerch, D., Fam, A., and Rizkalla, S. (2004). “Retrofit of Steel Structures Using Fiber Reinforced Polymers (FRP): State-of-the Art,” CD-ROM. *Transportation Research Board*, National Research Council, Washington, D.C.

Stallings, J.M., Cousins, T.E., and Stafford, T.E. (1996). “Effects of Removing Diaphragms from Steel Girder Bridge,” *Transportation Research Record*, Washington D.C.: TRB, National Research Council, 1996, Vol. 1541, pp. 183-188.

Standard Specifications for Highway Bridges. (1992). 15<sup>th</sup> ed. AASHTO, Washington D.C.

Tod, D.A., Atkins, R.W., and Shaw, S.J. (1992). “Use of Primers to Enhance Adhesive Bonds,” *International Journal of Adhesion & Adhesives*, Vol. 12, No. 3, pp. 159-163.

Vardy, A.E. and Hutchinson, A.R. (1986). “Some Uses of Adhesives in Civil Engineering,” *International Conference on Structural Adhesives in Engineering*, July, 2<sup>nd</sup> ~4<sup>th</sup>, pp. 199-206.

Wegman, R.F. (1977). “Durability of Some Newer Structural Adhesives,” *Journal of Applied Polymer Science: Applied Polymer Symposia*, No. 32, pp. 1-10.

Zewi, I.G., Flashner, F., Dodiuk, H., and Drori, L. (1984). “Durability of Structural Adhesive Joints,” *International Journal of Adhesion & Adhesives*, July, pp. 137-139.

Zhao, Y. and Kim Roddis, W.M. (2003). “Finite Element Study of Distortion-Induced Fatigue in Welded Steel Bridges,” CD-ROM. *Transportation Research Board*, National Research Council, Washington, D.C.

Zhao, Y. and Kim Roddis, W.M. (2005). “Fatigue Behavior and Retrofit Investigation of Distortion-Induced Web Gap Cracking,” CD-ROM. *Transportation Research Board*, National Research Council, Washington, D.C.

## Tables

Table 3.1      Retrofitting angle application situation

Angle label	Location	Temperature*	Heat gun used for squeezing out and mixing adhesives?	Heat gun used for 5 minutes for curing adhesives?	Bondline gap at the angle tip
A1-1	B2 (BPDB)	46°F	Yes	Yes	No gap
A1-4	B3 (BPDB)	47°F	Yes	Yes	No gap
A1-6	B4 (BPDB)	49°F	Yes	Yes	No gap
A1-7	B5 (BPDB)	51°F	Yes	No	No gap
A1-8	B6 (BPDB)	55°F	Yes	No	No gap
A2-4	B3W (CFDB)	40°F	Yes	Yes	Approximately 1/8"
A2-5	B3 (CFDB)	44°F	No	No	<1/16"
A2-6	B4 (CFDB)	44°F	No	No	<1/16"
A2-7	B4 (CFDB)	46°F	No	No	<1/16"
A2-8	B4E (CFDB)	43°F	Yes	Yes	No gap
BPDB	denotes Bent-Plate-Diaphragm Bridge				
CFDB	denotes Cross-Frame-Diaphragm Bridge				
*	The temperature was taken on the steel girder with a thermal couple at the time the adhesive was applied.				

Table 3.2 Web gap strain ranges on B5 of the BPD bridge

Gage Label	Pass 1 (static)			Pass 2 (static)		
	before (µε)	after (µε)	after/before ratio	before (µε)	after (µε)	after/before ratio
1-B5-1-G(NW of web)	95	36	38%	131	64	49%
1-B5-2-G(NW of web)	93	36	39%	131	65	50%
1-B5-3-G(SE of web)	-103	-36	35%	-143	-84	59%
1-B5-4-G(SE of web)	-118	-41	35%	-157	-90	57%
Gage Label	Pass 3 (static)			Pass 4 (10 mph)		
	before (µε)	after (µε)	after/before ratio	before (µε)	after (µε)	after/before ratio
1-B5-1-G(NW of web)	137	75	55%	75	39	52%
1-B5-2-G(NW of web)	137	77	56%	74	36	49%
1-B5-3-G(SE of web)	-164	-112	68%	91	52	57%
1-B5-4-G(SE of web)	-176	-118	67%	99	55	56%
Gage Label	Pass 5 (10 mph)			Pass 8 (10 mph)		
	before (µε)	after (µε)	after/before ratio	before (µε)	after (µε)	after/before ratio
1-B5-1-G(NW of web)	70	38	54%	180	95	53%
1-B5-2-G(NW of web)	68	37	54%	183	96	52%
1-B5-3-G(SE of web)	85	55	65%	217	139	64%
1-B5-4-G(SE of web)	90	57	63%	233	149	64%
Note:						
1. All values presented here are averages if one pass was conducted more than once.						
2. Description of the passes (refer to Figures 3.11 and 3.12 for more information)						
Pass 1~3	One truck stayed with left front wheel at specific locations on B5					
Pass 4	One truck stayed at position of Pass 2, and one truck traveled at 10 mph with left wheels on B4					
Pass 5	One truck traveled at 10 mph with left wheels on B4					
Pass 8	One truck traveled at 10 mph with left wheels on B5					

Table 3.3 Web gap strain ranges on B4 of the BPD bridge

Gage Label	Pass 1 (static)			Pass 2 (static)		
	before (µε)	after (µε)	after/before ratio	before (µε)	after (µε)	after/before ratio
1-B4-1-G (SE of web)	-33	-18	55%	-25	-13	52%
1-B4-2-G (SE of web)	-33	-17	52%	-25	-12	48%
1-B4-3-G (NW of web)	38	22	58%	29	16	55%
1-B4-4-G (NW of web)	34	20	59%	26	14	54%
Gage Label	Pass 3 (static)			Pass 4 (10 mph)		
	before (µε)	after (µε)	after/before ratio	before (µε)	after (µε)	after/before ratio
1-B4-1-G (SE of web)	-18	-10	56%	33	16	48%
1-B4-2-G (SE of web)	-18	-9	50%	34	17	50%
1-B4-3-G (NW of web)	22	12	55%	40	27	68%
1-B4-4-G (NW of web)	19	11	58%	40	28	70%
Gage Label	Pass 5 (10 mph)			Pass 8 (10 mph)		
	before (µε)	after (µε)	after/before ratio	before (µε)	after (µε)	after/before ratio
1-B4-1-G (SE of web)	37	20	54%	47	24	51%
1-B4-2-G (SE of web)	36	19	53%	47	22	47%
1-B4-3-G (NW of web)	41	32	78%	50	26	52%
1-B4-4-G (NW of web)	42	31	74%	49	26	53%
Note:						
1. All values presented here are averages if one pass was conducted more than once.						
2. Description of the passes (refer to Figures 3.11 and 3.12 for more information)						
Pass 1~3	One truck stayed with left front wheel at specific locations on B5					
Pass 4	One truck stayed at position of Pass 2, and one truck traveled at 10 mph with left wheels on B4					
Pass 5	One truck traveled at 10 mph with left wheels on B4					
Pass 8	One truck traveled at 10 mph with left wheels on B5					

Table 3.4 In-plane strain ranges on B5 of the BPD bridge

Gage Label	Pass 1 (static)			Pass 2 (static)		
	before (µε)	after (µε)	after/before ratio	before (µε)	after (µε)	after/before ratio
1-B5-5-B (0.5" from top flange)	-8	-7	89%	-5	-5	89%
1-B5-6-B (1'-10" from bottom flange)	13	12	98%	14	14	98%
1-B5-7-B (bottom flange)	23	21	95%	26	25	94%
Gage Label	Pass 3 (static)			Pass 4 (10 mph)		
	before (µε)	after (µε)	after/before ratio	before (µε)	after (µε)	after/before ratio
1-B5-5-B (0.5" from top flange)	-4	-3	72%	12	14	121%
1-B5-6-B (1'-10" from bottom flange)	13	13	98%	30	26	86%
1-B5-7-B (bottom flange)	26	24	93%	37	35	93%
Gage Label	Pass 5 (10 mph)			Pass 8 (10 mph)		
	before (µε)	after (µε)	after/before ratio	before (µε)	after (µε)	after/before ratio
1-B5-5-B (0.5" from top flange)	11	10	90%	18	18	97%
1-B5-6-B (1'-10" from bottom flange)	29	27	93%	35	29	82%
1-B5-7-B (bottom flange)	37	36	98%	51	47	92%

Note:

1. All values presented here are averages if one pass was conducted more than once.
2. Description of the passes (refer to Figures 3.11 and 3.12 for more information)

Pass 1~3	One truck stayed with left front wheel at specific locations on B5
Pass 4	One truck stayed at position of Pass 2, and one truck traveled at 10 mph with left wheels on B4
Pass 5	One truck traveled at 10 mph with left wheels on B4
Pass 8	One truck traveled at 10 mph with left wheels on B5
3. For Pass 1~3, strain values are provided; for Pass 4~5 and Pass 8, strain range values are provided.

Table 3.5 Strain ranges on the diaphragm of the BPD bridge

Gage Label	Pass 1 (static)			Pass 2 (static)		
	before ( $\mu\epsilon$ )	after ( $\mu\epsilon$ )	after/before ratio	before ( $\mu\epsilon$ )	after ( $\mu\epsilon$ )	after/before ratio
1-B4-8-D (bent plate top)	21	19	90%	17	14	82%
1-B4-9-D (1'-3" from bent plate bottom)	-4	-3	75%	-4	-3	75%
1-B4-10-D (bent plate bottom)	-33	-32	97%	-31	-30	97%
Gage Label	Pass 3 (static)			Pass 4 (10 mph)		
	before ( $\mu\epsilon$ )	after ( $\mu\epsilon$ )	after/before ratio	before ( $\mu\epsilon$ )	after ( $\mu\epsilon$ )	after/before ratio
1-B4-8-D (bent plate top)	13	11	85%	27	19	70%
1-B4-9-D (1'-3" from bent plate bottom)	-3	-3	100%	17	16	94%
1-B4-10-D (bent plate bottom)	-26	-26	100%	24	17	71%
Gage Label	Pass 5 (10 mph)			Pass 8 (10 mph)		
	before ( $\mu\epsilon$ )	after ( $\mu\epsilon$ )	after/before ratio	before ( $\mu\epsilon$ )	after ( $\mu\epsilon$ )	after/before ratio
1-B4-8-D (bent plate top)	20	21	105%	34	28	82%
1-B4-9-D (1'-3" from bent plate bottom)	10	11	110%	13	17	131%
1-B4-10-D (bent plate bottom)	21	22	105%	61	51	84%
Note:						
1. All values presented here are averages if one pass was conducted more than once.						
2. Description of the passes (refer to Figures 3.11 and 3.12 for more information)						
Pass 1~3	One truck stayed with left front wheel at specific locations on B5					
Pass 4	One truck stayed at position of Pass 2, and one truck traveled at 10 mph with left wheels on B4					
Pass 5	One truck traveled at 10 mph with left wheels on B4					
Pass 8	One truck traveled at 10 mph with left wheels on B5					
3. For Pass 1~3, strain values are provided; for Pass 4~5 and Pass 8, strain range values are provided.						

Table 3.6 Web gap strain ranges on B4 of the CFD bridge

Gage Label	Pass 1 (static)			Pass 2 (static)		
	before (µε)	after (µε)	after/before ratio	before (µε)	after (µε)	after/before ratio
2-B4-1-G (NW of web)	26	16	62%	24	14	58%
2-B4-2-G (NW of web)	32	19	59%	31	17	55%
2-B4-3-G (SE of web)	-24	-10	42%	-24	-11	46%
2-B4-4-G (SE of web)	-29	-12	41%	-28	-13	46%
Gage Label	Pass 3 (static)			Pass 4 (10 mph)		
	before (µε)	after (µε)	after/before ratio	before (µε)	after (µε)	after/before ratio
2-B4-1-G (NW of web)	-37	9	-24%	99	17	17%
2-B4-2-G (NW of web)	-29	13	-45%	104	14	13%
2-B4-3-G (SE of web)	13	-9	-69%	76	18	24%
2-B4-4-G (SE of web)	8	-11	-138%	72	16	22%
Gage Label	Pass 5 (10 mph)			Pass 8 (10 mph)		
	before (µε)	after (µε)	after/before ratio	before (µε)	after (µε)	after/before ratio
2-B4-1-G (NW of web)	92	14	15%	71	28	39%
2-B4-2-G (NW of web)	90	12	13%	72	31	43%
2-B4-3-G (SE of web)	67	14	21%	47	23	49%
2-B4-4-G (SE of web)	66	13	20%	47	25	53%
Note:						
1. All values presented here are averages if one pass was conducted more than once.						
2. Description of the passes (refer to Figures 3.11 and 3.12 for more information)						
Pass 1~3	One truck stayed with left front wheel at specific locations on B4					
Pass 4	One truck stayed at position of Pass 2, and one truck traveled at 10 mph with left wheels on B3					
Pass 5	One truck traveled at 10 mph with left wheels on B3					
Pass 8	One truck traveled at 10 mph with left wheels on B4					
3. For Pass 1~3, strain values are provided; for Pass 4~5 and Pass 8, strain range values are provided.						

Table 3.7 Web gap strain ranges on B3 of the CFD bridge

Gage Label	Pass 1 (static)			Pass 2 (static)		
	before (µε)	after (µε)	after/before ratio	before (µε)	after (µε)	after/before ratio
2-B3-1-G (SE of web)	-6	-6	100%	-6	-6	100%
2-B3-2-G (SE of web)	-11	-12	109%	-11	-11	100%
2-B3-3-G (NW of web)	15	15	100%	14	13	93%
2-B3-4-G (NW of web)	17	16	94%	16	15	94%
Gage Label	Pass 3 (static)			Pass 4 (10 mph)		
	before (µε)	after (µε)	after/before ratio	before (µε)	after (µε)	after/before ratio
2-B3-1-G (SE of web)	-5	-5	100%	18	13	72%
2-B3-2-G (SE of web)	-9	-10	111%	20	18	90%
2-B3-3-G (NW of web)	13	12	92%	24	17	71%
2-B3-4-G (NW of web)	14	13	93%	26	21	81%
Gage Label	Pass 5 (10 mph)			Pass 8 (10 mph)		
	before (µε)	after (µε)	after/before ratio	before (µε)	after (µε)	after/before ratio
2-B3-1-G (SE of web)	18	14	78%	19	15	79%
2-B3-2-G (SE of web)	22	20	91%	24	21	88%
2-B3-3-G (NW of web)	26	19	73%	30	21	70%
2-B3-4-G (NW of web)	28	25	89%	28	24	86%

Note:

1. All values presented here are averages if one pass was conducted more than once.
2. Description of the passes (refer to Figures 3.11 and 3.12 for more information)

Pass 1~3	One truck stayed with left front wheel at specific locations on B4
Pass 4	One truck stayed at position of Pass 2, and one truck traveled at 10 mph with left wheels on B3
Pass 5	One truck traveled at 10 mph with left wheels on B3
Pass 8	One truck traveled at 10 mph with left wheels on B4
3. For Pass 1~3, strain values are provided; for Pass 4~5 and Pass 8, strain range values are provided.

Table 3.8 In-plane strain ranges on B4 of the CFD bridge

Gage Label	Pass 1 (static)			Pass 2 (static)		
	before (µε)	after (µε)	after/before ratio	before (µε)	after (µε)	after/before ratio
1-B4-5-B (0.5" from top flange)	-12	-10	83%	-9	-8	83%
1-B4-6-B (2'-4" from bottom flange)	11	11	100%	11	11	100%
1-B4-7-B (bottom flange)	20	19	95%	21	20	95%
Gage Label	Pass 3 (static)			Pass 4 (10 mph)		
	before (µε)	after (µε)	after/before ratio	before (µε)	after (µε)	after/before ratio
1-B4-5-B (0.5" from top flange)	-5	-4	80%	15	10	67%
1-B4-6-B (2'-4" from bottom flange)	12	12	100%	18	15	83%
1-B4-7-B (bottom flange)	21	19	90%	27	25	93%
Gage Label	Pass 5 (10 mph)			Pass 8 (10 mph)		
	before (µε)	after (µε)	after/before ratio	before (µε)	after (µε)	after/before ratio
1-B4-5-B (0.5" from top flange)	15	11	73%	19	15	79%
1-B4-6-B (2'-4" from bottom flange)	14	16	114%	24	20	83%
1-B4-7-B (bottom flange)	20	26	130%	39	35	90%
Note:						
1. All values presented here are averages if one pass was conducted more than once.						
2. Description of the passes (refer to Figures 3.11 and 3.12 for more information)						
Pass 1~3	One truck stayed with left front wheel at specific locations on B5					
Pass 4	One truck stayed at position of Pass 2, and one truck traveled at 10 mph with left wheels on B4					
Pass 5	One truck traveled at 10 mph with left wheels on B4					
Pass 8	One truck traveled at 10 mph with left wheels on B5					
3. For Pass 1~3, strain values are provided; for Pass 4~5 and Pass 8, strain range values are provided.						

Table 3.9 Strain ranges on the diaphragm of the CFD bridge

Gage Label	Pass 1 (static)			Pass 2 (static)		
	before (µε)	after (µε)	after/before ratio	before (µε)	after (µε)	after/before ratio
2-B4-8-D (cross frame diaphragm)	-62	-61	98%	-58	-56	97%
2-B4-9-D (cross frame diaphragm)	-65	-63	97%	-61	-59	97%
2-B4-10-D (cross frame diaphragm)	0	2		1	1	100%
2-B4-11-D (cross frame diaphragm)	-6	-4	67%	-5	-4	80%
2-B3-12-D (cross frame diaphragm)	57	57	100%	54	53	98%
2-B3-13-D (cross frame diaphragm)	51	50	98%	48	47	98%
Gage Label	Pass 3 (static)			Pass 4 (10 mph)		
	before (µε)	after (µε)	after/before ratio	before (µε)	after (µε)	after/before ratio
2-B4-8-D (cross frame diaphragm)	-49	-50	102%	28	24	86%
2-B4-9-D (cross frame diaphragm)	-52	-53	102%	27	26	96%
2-B4-10-D (cross frame diaphragm)	1	2	200%	21	22	105%
2-B4-11-D (cross frame diaphragm)	-4	-3	75%	28	27	96%
2-B3-12-D (cross frame diaphragm)	48	49	102%	28	25	89%
2-B3-13-D (cross frame diaphragm)	43	43	100%	26	23	88%
Gage Label	Pass 5 (10 mph)			Pass 8 (10 mph)		
	before (µε)	after (µε)	after/before ratio	before (µε)	after (µε)	after/before ratio
2-B4-8-D (cross frame diaphragm)	32	30	94%	89	90	101%
2-B4-9-D (cross frame diaphragm)	32	31	97%	91	93	102%
2-B4-10-D (cross frame diaphragm)	23	23	100%	29	25	86%
2-B4-11-D (cross frame diaphragm)	28	29	104%	38	35	92%
2-B3-12-D (cross frame diaphragm)	31	30	97%	71	72	101%
2-B3-13-D (cross frame diaphragm)	28	26	93%	62	64	103%
Note:						
1. All values presented here are averages if one pass was conducted more than once.						
2. Description of the passes (refer to Figures 3.11 and 3.12 for more information)						
Pass 1~3	One truck stayed with left front wheel at specific locations on B5					
Pass 4	One truck stayed at position of Pass 2, and one truck traveled at 10 mph with left wheels on B4					
Pass 5	One truck traveled at 10 mph with left wheels on B4					
Pass 8	One truck traveled at 10 mph with left wheels on B5					
3. For Pass 1~3, strain values are provided; for Pass 4~5 and Pass 8, strain range values are provided.						

Table 4.1 Measured active web gap length

Web gap location	Measured active web gap length on the north (in.)	Measured active web gap length on the south (in.)	Average measured active web gap length (in.)
NW-1/2	15/16	13/16	7/8
SW-1/2	1	13/16	29/32
NW-C	15/16	1	31/32
SW-C	11/16	1 1/16	7/8
NE-C	1 1/16	13/16	15/16
SE-C	1	1 3/16	1 3/32
NE-1/2	1 1/16	5/8	27/32
SE-1/2	11/16	13/16	3/4

Table 4.2 Out-of-plane strains before cyclic loading

Web gap location	Gage label	Measured strain ( $\mu\epsilon$ )*	Max absolute measured strain at a specific web gap ( $\mu\epsilon$ )	Max absolute FEM predicted strain at a specific web gap ( $\mu\epsilon$ )	Measured strain/predicted strain
NW-1/2	NW-1/2-1N-G	531	713	1715	42%
	NW-1/2-2N-G	704			
	NW-1/2-1S-G	-500			
	NW-1/2-2S-G	-713			
	NW-1/2-5S-G	426			
SW-1/2	SW-1/2-1N-G	-498	692	1715	40%
	SW-1/2-2N-G	-692			
	SW-1/2-5N-G	627			
	SW-1/2-1S-G	378			
	SW-1/2-2S-G	534			
	SW-1/2-3S-G	-263			
	SW-1/2-4S-G	-548			
NW-C	NW-C-1N-G	N/A	580	1674	35%
	NW-C-2N-G	N/A			
	NW-C-1S-G	-478			
	NW-C-2S-G	-580			
	NW-C-5S-G	341			
SW-C	SW-C-1N-G	-685	1013	1674	60%
	SW-C-2N-G	-1013			
	SW-C-5N-G	419			
	SW-C-1S-G	521			
	SW-C-2S-G	670			
NE-C	NE-C-1N-G	226	504	1674	30%
	NE-C-2N-G	296			
	NE-C-1S-G	-422			
	NE-C-2S-G	-504			
	NE-C-5S-G	336			
SE-C	SE-C-1N-G	-853	980	1674	59%
	SE-C-2N-G	-980			
	SE-C-5N-G	677			
	SE-C-1S-G	592			
	SE-C-2S-G	960			
NE-1/2	NE-1/2-1N-G	370	633	1715	37%
	NE-1/2-2N-G	518			
	NE-1/2-1S-G	-412			
	NE-1/2-2S-G	-633			
	NE-1/2-5S-G	383			
SE-1/2	SE-1/2-1N-G	-357	506	1715	29%
	SE-1/2-2N-G	-482			
	SE-1/2-5N-G	414			
	SE-1/2-1S-G	334			
	SE-1/2-2S-G	506			
Average measured strain over predicted strain					42%
Note:	* Actuator load was 90 k, corresponding to 14 ksi in-plane stress in the constant moment region				

Table 4.3 Out-of-plane distortion before cyclic loading

Web gap location	LVDT label	Measured out-of-plane distortion (in.) *	FEM predicted out-of-plane distortion (in.)	Measured distortion/predicted distortion
NW-1/2	LVDT NW-1/2-G	2.49E-03	1.49E-02	17%
SW-1/2	LVDT SW-1/2-G	3.54E-03	1.49E-02	24%
NW-C	LVDT NW-C-G	2.46E-03	1.50E-02	16%
SW-C	LVDT SW-C-G	1.53E-03	1.50E-02	10%
NE-C	LVDT NE-C-G	3.29E-03	1.50E-02	22%
SE-C	LVDT SE-C-G	3.23E-03	1.50E-02	21%
NE-1/2	LVDT NE-1/2-G	1.18E-03	1.49E-02	8%
SE-1/2	LVDT SE-1/2-G	2.15E-03	1.49E-02	14%
Average measured distortion over predicted distortion				17%
Note:	*	Actuator load was 90 k, corresponding to 14 ksi in-plane stress in the constant moment region		

Table 4.4 In-plane stresses before cyclic loading

Gage location	Gage label	Measured stress (ksi) *	FEM predicted stress (ksi)	Measured stress/predicted stress
N-1/4	N-1/4-1-B	-3.80	-4.09	93%
	N-1/4-2-B	-2.06	-2.25	92%
	N-1/4-3-B	-2.66	-2.65	100%
	N-1/4-4-B	2.45	2.97	83%
	N-1/4-5-B	3.08	4.03	77%
	N-1/4-6-B	2.86	2.31	124%
S-1/4	S-1/4-1-B	-4.01	-4.09	98%
	S-1/4-2-B	-1.57	-2.25	70%
	S-1/4-3-B	-2.30	-2.65	87%
	S-1/4-4-B	N/A	2.97	N/A
	S-1/4-5-B	2.72	4.03	68%
	S-1/4-6-B	2.62	2.31	114%
N-C	N-C-1-B	-11.94	-15.99	75%
	N-C-2-B	-11.90	-10.66	112%
	N-C-3-B	-10.01	-11.20	89%
	N-C-4-B	9.85	11.53	85%
	N-C-5-B	11.94	13.50	88%
	N-C-6-B	12.59	13.50	93%
S-C	S-C-1-B	-17.58	-15.99	110%
	S-C-2-B	-7.72	-10.66	72%
	S-C-3-B	-9.78	-11.20	87%
	S-C-4-B	9.86	11.53	85%
	S-C-5-B	12.81	13.50	95%
	S-C-6-B	11.91	13.50	88%
Average measured stress over predicted stress				91%
Note:	*	Actuator load was 90 k, corresponding to 14 ksi in-plane stress in the constant moment region		

Table 4.5 In-plane deflection before cyclic loading

LVDT label	Measured deflection (in.) *	FEM predicted deflection (in.)	Deflection (measured / predicted)	Measured differential deflection (in.) *	FEM predicted differential deflection (in.)	Differential deflection (measured / predicted)
NW-1/2-BD	-0.231	-0.203	114%	0.056	0.050	112%
NW-1/2-BB	-0.287	-0.254	113%			
SW-1/2-BD	-0.213	-0.203	105%	0.036	0.050	72%
SW-1/2-BB	-0.249	-0.254	98%			
NW-C-BD	-0.489	-0.388	126%	0.008	0.048	16%
NW-C-BB	-0.497	-0.436	114%			
SW-C-BD	-0.321	-0.388	83%	0.100	0.048	208%
SW-C-BB	-0.421	-0.436	97%			
NE-C-BD	-0.474	-0.388	122%	0.006	0.048	13%
NE-C-BB	-0.481	-0.436	110%			
SE-C-BD	-0.332	-0.388	85%	0.050	0.048	103%
SE-C-BB	-0.381	-0.436	87%			
NE-1/2-BD	-0.233	-0.203	115%	0.047	0.050	94%
NE-1/2-BB	-0.280	-0.254	110%			
SE-1/2-BD	-0.197	-0.203	97%	0.035	0.050	69%
SE-1/2-BB	-0.232	-0.254	92%			
Average deflection (measured/predicted)						104%
Average measured differential deflection over predicted differential deflection						86%
Note:	*	Actuator load was 90 k, corresponding to 14 ksi in-plane stress in the constant moment region				

Table 4.6 Diaphragm end channel support stresses before cyclic loading

Gage location	Gage label	Measured stress (ksi) *	Measured stress average (ksi) *	FEM predicted stress (ksi)	Measured stress/predicted stress
NW-1/2	NW-1/2-N-D	1.22	-2.63	-2.39	110%
	NW-1/2-S-D	-6.48			
NW-C	NW-C-N-D	0.69	-2.75	-2.35	117%
	NW-C-S-D	-6.19			
NE-C	NE-C-N-D	-0.03	-2.82	-2.35	120%
	NE-C-S-D	-5.61			
NE-1/2	NE-1/2-N-D	3.73	-1.61	-2.39	68%
	NE-1/2-S-D	-6.96			
Average measured stress over predicted stress					104%
Note:	*	Actuator load was 90 k, corresponding to 14 ksi in-plane stress in the constant moment region			

Table 4.7 Crack tip strains before and immediately after retrofit

Web gap location	Gage label	Crack length (in.)	Measured strain before retrofit ( $\mu\epsilon$ ) *	Measured strain after retrofit ( $\mu\epsilon$ ) *	Strain after retrofit/strain before retrofit (Absolute value)	Strain after retrofit/strain before retrofit (Absolute value)
NW-1/2	NW-1/2-nw(1)-g	0.94	501	-105	21%	16%
	NW-1/2-ne-g	1.75	967	197	20%	
	NW-1/2-se(2)-g	0.69	-603	-40	7%	
SW-1/2	SW-1/2-nw-g	1.16	-853	-296	35%	36%
	SW-1/2-ne(1)-g	0.56	-673	-308	46%	
	SW-1/2-se-g	1.81	862	244	28%	
NW-C	NW-C-ne-g	1.94	1525	441	29%	22%
	NW-C-se(1)-g	0.91	-974	-147	15%	
SW-C	SW-C-nw(1)-g	1.00	-942	-417	44%	32%
	SW-C-ne(1)-g	1.69	-883	-217	25%	
	SW-C-sw(3)-g	2.13	1173	425	36%	
	SW-C-se-g	2.31	1092	243	22%	
NE-C	NE-C-nw-g	2.81	1062	176	17%	9%
	NE-C-ne(1)-g	1.84	1518	-67	4%	
	NE-C-sw(3)-g	1.75	-1818	165	9%	
	NE-C-se-flangeweb-g	0.50	3899	-272	7%	
SE-C	SE-C-nw(1)-g **	3.25	-302	1432	473%	23%
	SE-C-ne-g	1.25	-1571	-464	30%	
	SE-C-sw-g **	4.31	1084	567	52%	
	SE-C-se-g	1.50	2282	-367	16%	
NE-1/2	NE-1/2-nw(1)-g	1.09	914	250	27%	22%
	NE-1/2-ne-g	0.81	1295	269	21%	
	NE-1/2-sw(3)-g	0.56	-485	-152	31%	
	NE-1/2-se(1)-g	0.63	1089	85	8%	
SE-1/2	SE-1/2-ne-g	1.16	-3966	N/A	N/A	14%
	SE-1/2-sw-g	1.84	1709	404	24%	
	SE-1/2-se(2)-g	0.69	1067	-48	4%	
Average strain ratio without outliers (after retrofit/before retrofit)						22%
Note: * Actuator load was 90 k, corresponding to 14 ksi in-plane stress in the constant moment region						
** Measured strain values were treated as outliers because of the type of crack formed						

Table 4.8 In-plane stresses before and immediately after retrofit

Gage location	Gage label	Stress before retrofit (ksi) *	Stress after retrofit (ksi) *	Stress ratio (after retrofit/before retrofit)
N-1/4	N-1/4-1-B	-3.07	-3.02	98%
	N-1/4-2-B	-2.42	-2.54	105%
	N-1/4-3-B	-2.50	-2.43	97%
	N-1/4-4-B	2.20	N/A	N/A
	N-1/4-5-B	2.60	2.34	90%
	N-1/4-6-B	2.99	3.05	102%
S-1/4	S-1/4-1-B	-4.03	-3.99	99%
	S-1/4-2-B	-1.77	-1.73	97%
	S-1/4-3-B	-2.33	-2.45	105%
	S-1/4-4-B	2.50	2.33	N/A
	S-1/4-5-B	2.90	2.85	98%
	S-1/4-6-B	2.58	2.64	102%
N-C	N-C-1-B	-14.73	-14.45	98%
	N-C-2-B	-7.43	-7.51	101%
	N-C-3-B	-9.36	-9.11	97%
	N-C-4-B	9.16	8.92	97%
	N-C-5-B	11.15	10.81	97%
	N-C-6-B	11.89	11.53	97%
S-C	S-C-1-B	-17.66	-17.23	98%
	S-C-2-B	-8.12	-8.12	100%
	S-C-3-B	-9.89	-9.90	100%
	S-C-4-B	9.84	9.65	98%
	S-C-5-B	12.37	11.96	97%
	S-C-6-B	13.46	13.37	99%
Average stress ratio (after retrofit/before retrofit)				95%
Note: *	Actuator load was 90 k, corresponding to 14 ksi in-plane stress in the constant moment region			

Table 4.9 In-plane deflection before and immediately after retrofit

LVDT label	Deflection before retrofit (in.)*	Deflection after retrofit (in.)*	Deflection (after retrofit/before retrofit)	Differential deflection before retrofit (in.) *	Differential deflection after retrofit (in.) *	Differential deflection (after retrofit/before retrofit)
NW-1/2-BD	-0.208	-0.221	107%	0.058	0.041	70%
NW-1/2-BB	-0.265	-0.262	99%			
SW-1/2-BD	-0.202	-0.221	109%	0.058	0.042	73%
SW-1/2-BB	-0.261	-0.263	101%			
NW-C-BD	-0.352	-0.358	102%	0.083	0.072	87%
NW-C-BB	-0.435	-0.430	99%			
SW-C-BD	-0.349	-0.384	110%	0.091	0.061	67%
SW-C-BB	-0.440	-0.445	101%			
NE-C-BD	-0.291	-0.325	112%	0.115	0.087	76%
NE-C-BB	-0.406	-0.411	101%			
SE-C-BD	-0.357	-0.399	112%	0.040	0.005	12%
SE-C-BB	-0.397	-0.403	102%			
NE-1/2-BD	-0.212	-0.222	105%	0.045	0.033	73%
NE-1/2-BB	-0.257	-0.255	99%			
SE-1/2-BD	-0.215	-0.233	109%	0.029	0.013	45%
SE-1/2-BB	-0.243	-0.246	101%			
Average differential deflection ratio (after retrofit/before retrofit)						63%
Note: *	Actuator load was 90 k, corresponding to 14 ksi in-plane stress in the constant moment region					

Table 4.10 Diaphragm end channel support stresses before and immediately after retrofit

Gage label	Average stress before retrofit (ksi) *	Average stress after retrofit (ksi) *	Average stress after retrofit/before retrofit
NW-1/2-N-D	-2.48	-2.83	114%
NW-1/2-S-D			
NW-C-N-D	-2.79	-3.04	109%
NW-C-S-D			
NE-C-N-D	-4.07	-5.01	123%
NE-C-S-D			
NE-1/2-N-D	-1.44	-1.45	101%
NE-1/2-S-D			
Average stress ratio (after retrofit/before retrofit)			112%
Note: *	Actuator load was 90 k, corresponding to 14 ksi in-plane stress in the constant moment region		

Table 5.1 Baseline specimen testing matrix

No.	Bondline thickness $t_a$ (in.)	Curing environment	Testing temperature	Surface pretreatment	Mechanically cycled prior to testing?	Data points for strength	Data points for stiffness
B1	0.020	Lab ambient air*	Lab ambient air*	No GPS	No	24	4
B2	0.020	Lab ambient air	Lab ambient air	GPS	No	20 <sup>a</sup> /15 <sup>b</sup>	5
B3	0.020	Lab ambient air	122°F	No GPS	No	5	0
B4	0.020	Lab ambient air	-40°F	No GPS	No	2****	0
B5	0.020	Cold air**	Lab ambient air	No GPS	No	5	0
B6	0.039	Lab ambient air	Lab ambient air	No GPS	No	5	5
B7	0.059	Lab ambient air	Lab ambient air	No GPS	No	10	5
B8	0.059	Lab ambient air	Lab ambient air	GPS	No	5	0
B9	0.059	Lab ambient air	122°F	No GPS	No	5	0
B10	0.059	Lab ambient air	-40°F	No GPS	No	5	0
B11	0.020	Lab ambient air	Lab ambient air	No GPS	Yes***	5	0
B12	0.020	Lab ambient air	Lab ambient air	GPS	Yes****	5	0
*	Lab ambient air was approximately 70°F for all cases						
**	In order to simulate the unfavorable field application environment in November, specimens were made outdoors at around 50°F during the daytime, left outdoors for the night and then kept in the environment chamber at 50°F for sixteen days						
***	Specimens underwent 1 million cycles between 0.2 kips and 2 kips at 15.7 Hz						
****	Though 5 specimens were tested, only 2 of them were tested at -40°F						
a	20 data points were used						
b	15 data points were used						

Table 5.2 Baseline specimen testing results

No.	Bondline thickness $t_a$ (in.)	Data points for strength	Average strength (k)	Coefficient of variation for strength	Data points for stiffness	Average stiffness (k/in.)	Coefficient of variation for stiffness
B1 (No GPS)	0.020	24	8.91	0.07	4	3246	0.06
B2 <sup>a</sup> (GPS)	0.020	20	9.13	0.11	5	3489	0.05
B2 <sup>b</sup> (GPS)	0.020	15	9.67	0.04	5	3489	0.05
B3 (No GPS)	0.020	5	5.32	0.09	0	N/A	N/A
B4 (No GPS)	0.020	2	16.46	0.17	0	N/A	N/A
B5 (No GPS)	0.020	5	4.60	0.17	0	N/A	N/A
B6 (No GPS)	0.039	5	8.41	0.13	5	2399	0.10
B7 (No GPS)	0.059	10	8.52	0.04	5	2229	0.08
B8 (GPS)	0.059	5	7.97	0.11	0	N/A	N/A
B9 (No GPS)	0.059	5	3.67	0.30	0	N/A	N/A
B10 (No GPS)	0.059	5	12.11	0.19	0	N/A	N/A
B11 (No GPS)	0.020	5	7.52	0.05	0	N/A	N/A
B12 (GPS)	0.020	5	9.53	0.02	0	N/A	N/A
a	20 data points were used						
b	15 data points were used						

Table 5.3(a) Effects of different parameters on the ultimate strength and the stiffness of baseline specimens (comparison of average values)

Investigated parameters	Comparison	Changes in ultimate strength	Changes in stiffness
The effect of GPS pretreatment on the baseline specimen	Compare No. B2 <sup>a</sup> with No. B1	2%	8%
	Compare No. B2 <sup>b</sup> with No. B1	6%	
	Compare No. B8 with No. B7	-6%	N/A
	Compare No. B12 with No. B11	27%	N/A
The effect of bondline thickness on the baseline specimen	Compare No. B6 with No. B1	-6%	-26%
	Compare No. B7 with No. B1	-4%	-31%
	Compare No. B7 with No. B6	1%	-7%
The effect of high testing temperature on the baseline specimen	Compare No. B3 with No. B1	-40%	N/A
	Compare No. B9 with No. B7	-57%	N/A
The effect of low testing temperature on the baseline specimen	Compare No. B4 with No. B1	85%	N/A
	Compare No. B10 with No. B7	42%	N/A
The effect of cold curing temperature(50°F) on the baseline specimen	Compare No. B5 with No. B1	-48%	N/A
The effect of cyclic loading on the baseline specimen	Compare No. B11 with No. B1	-16%	N/A
	Compare No. B12 with No. B2 <sup>a</sup>	4%	N/A
	Compare No. B12 with No. B2 <sup>b</sup>	-2%	N/A
a 20 data points were used			
b 15 data points were used			

Table 5.3(b) Effects of different parameters on the ultimate strength and the stiffness of baseline specimens (statistic analysis)

Investigated parameters	Comparison	Results in ultimate strength	Results in stiffness
The effect of GPS pretreatment on the baseline specimen	Compare No. B2 <sup>a</sup> with No. B1	57% ↑	92% ↑
	Compare No. B2 <sup>b</sup> with No. B1	99.9% ↑	
	Compare No. B8 with No. B7	7% ↑	N/A
	Compare No. B12 with No. B11	99.9% ↑	N/A
The effect of bondline thickness on the baseline specimen	Compare No. B6 with No. B1	62% ↓	99.9% ↓
	Compare No. B7 with No. B1	99.6% ↓	99.9% ↓
	Compare No. B7 with No. B6	59% ↓	76% ↓
The effect of high testing temperature on the baseline specimen	Compare No. B3 with No. B1	99.9% ↓	N/A
	Compare No. B9 with No. B7	99.9% ↓	N/A
The effect of low testing temperature on the baseline specimen	Compare No. B4 with No. B1	99.9% ↑	N/A
	Compare No. B10 with No. B7	98% ↑	N/A
The effect of cold curing temperature(50°F) on the baseline specimen	Compare No. B5 with No. B1	99.9% ↓	N/A
The effect of cyclic loading on the baseline specimen	Compare No. B11 with No. B1	99.9% ↓	N/A
	Compare No. B12 with No. B2 <sup>a</sup>	88% ↑	N/A
	Compare No. B12 with No. B2 <sup>b</sup>	71% ↓	N/A
“57% ↑”	denotes that one is 57% confident of an increase		
“62% ↓”	denotes that one is 62% confident of a decrease		
a	20 data points were used		
b	15 data points were used		
Note:	Each notation listed in the table is strictly limited to a comparison between the groups noted, and thus does not apply when more than one parameter is changed at a time.		

Table 5.4 Environment specimen testing matrix

Exposed environment	No.	Exposed time	Surface pretreatment	Cyclic loading? <sup>3</sup>	Data points for ultimate strength and stiffness
Air at 65°F	E1-1	180 days	No GPS	No	5
	E1-2	180 days	GPS	No	5
	E1-3	447 days	No GPS	No	5
	E1-4	447 days	GPS	No	5
	E1-5	180 days	No GPS	Yes	5
Immersion in tap water at 65°F	E2-1	92 days	No GPS	No	5
	E2-2	201 days	No GPS	No	5
Immersion in tap water at 111°F	E3-1	92 days	No GPS	No	5
	E3-2	92 days	GPS	No	5
	E3-3	210 days	No GPS	No	5
	E3-4	210 days	GPS	No	5
	E3-5	210 days	No GPS	Yes	5 <sup>4</sup>
Air at -4°F	E4-1	196 days	No GPS	No	5
	E4-2	196 days	GPS	No	5
	E4-3	382 days	No GPS	No	5
	E4-4	382 days	GPS	No	5
	E4-5	197 days	No GPS	Yes	5
Freeze and thaw chamber <sup>1</sup>	E5-1	92 days (552 cycles)	No GPS	No	5
	E5-2	193 days (1158 cycles)	No GPS	No	5
Temperature cycles <sup>2</sup> , unloaded	E6-1	197 days (14 cycles)	No GPS	No	5
	E6-2	197 days (14 cycles)	GPS	No	5
	E6-3	380 days (27 cycles)	No GPS	No	5
	E6-4	380 days (27 cycles)	GPS	No	5
	E6-5	207 days (15 cycles)	No GPS	Yes	5
	E6-6	207 days (15 cycles)	GPS	Yes	5
Temperature cycles <sup>2</sup> , loaded at 0.95 kips	E7-1	211 days (15 cycles)	No GPS	No	5 <sup>5</sup>
	E7-2	211 days (15 cycles)	GPS	No	5
	E7-3	370 days (26 cycles)	No GPS	No	5 <sup>5</sup>
	E7-4	370 days (26 cycles)	GPS	No	5
Outdoors	E8-1	184 days	No GPS	No	5
	E8-2	184 days	GPS	No	5
	E8-3	271 days	No GPS	Yes	5
Fire broke out after the listed number of days outdoors	E9-1	371 days	No GPS	No	20 <sup>6</sup>
	E9-2	374 days	GPS	No	15 <sup>6</sup>

Note:

- The specimens were immersed in tap water at 111°F for 65 hours before they were put into the freeze and thaw chamber.
- The specimens were moved between the cold chamber (-4°F) and the hot chamber (122°F) weekly.
- Specimens underwent 1 million cycles between 0.2 kips and 2 kips after the environment exposure.
- One specimen failed at 16,445 cycles and another specimen failed at 428,980 cycles.
- One specimen failed in the hot chamber after approximately 122 days of environment exposure for each of Batch E7-1 and E7-3.
- Ten of the No GPS specimens and two of the GPS specimens failed in the uncontrolled fire. The number of days of outdoor exposure before the fire was an average values of four batches for E9-1 and three batches for E9-2.

Table 5.5 Environment specimen testing results

Exposed environment	No.	Data points for strength and stiffness	Average strength (k)	Coefficient of variation for strength	Average stiffness (k/in.)	Coefficient of variation for stiffness
Air at 65°F	E1-1	5	9.08	0.02	3194	0.03
	E1-2	5	9.14	0.06	3380	0.11
	E1-3	5	9.79	0.03	3729	0.05
	E1-4	5	9.85	0.06	3714	0.05
	E1-5	5	9.66	0.06	3496	0.07
Immersion in tap water at 65°F	E2-1	5	8.32	0.05	3087	0.09
	E2-2	5	8.35	0.03	3027	0.05
Immersion in tap water at 111°F	E3-1	5	8.03	0.13	2603	0.11
	E3-2	5	8.61	0.03	2697	0.03
	E3-3	5	7.73	0.05	2609	0.05
	E3-4	5	8.43	0.06	2727	0.08
	E3-5	5 <sup>4</sup>	3.61	0.94	1345	0.92
Air at -4°F	E4-1	5	10.09	0.02	3063	0.08
	E4-2	5	10.09	0.03	2968	0.04
	E4-3	5	9.99	0.02	3463	0.03
	E4-4	5	10.25	0.04	3429	0.10
	E4-5	5	10.10	0.02	3020	0.11
Freeze and thaw chamber <sup>1</sup>	E5-1	5	8.60	0.07	2788	0.03
	E5-2	5	8.98	0.04	2966	0.04
Temperature cycles <sup>2</sup> , unloaded	E6-1	5	9.15	0.15	2644	0.23
	E6-2	5	10.31	0.02	2913	0.05
	E6-3	5	9.54	0.05	2787	0.03
	E6-4	5	9.67	0.03	2818	0.13
	E6-5	5	9.37	0.08	2894	0.07
	E6-6	5	10.12	0.02	3083	0.10
Temperature cycles <sup>2</sup> , loaded at 0.95 kips	E7-1	5 <sup>5</sup>	7.26	0.56	2213	0.56
	E7-2	5	9.33	0.05	2740	0.01
	E7-3	5 <sup>5</sup>	6.20	0.56	2066	0.56
	E7-4	5	7.41	0.37	2319	0.38
Outdoors	E8-1	5	9.10	0.02	3006	0.04
	E8-2	5	9.21	0.04	3095	0.05
	E8-3	5	9.19	0.06	2948	0.04
Fire broke out after the listed number of days outdoors	E9-1	20 <sup>6</sup>	1.03	1.54	762	1.45
	E9-2	15 <sup>6</sup>	3.43	0.73	1914	0.72

Note:

1. The specimens were immersed in tap water at 111°F for 65 hours before they were put into the freeze and thaw chamber.
2. The specimens were moved between the cold chamber (-4°F) and the hot chamber (122°F) weekly.
3. Specimens underwent 1 million cycles between 0.2 kips and 2 kips after the environment exposure.
4. One specimen failed at 16,445 cycles and another specimen failed at 428,980 cycles.
5. One specimen failed in the hot chamber after approximately 122 days of environment exposure for each of Batch E7-1 and E7-3.
6. Ten of the No GPS specimens and two of the GPS specimens failed in the uncontrolled fire. The number of days of outdoor exposure before the fire was an average values of four batches for E9-1 and three batches for E9-2.

Table 5.6(a) Effects of environment exposure on the ultimate strength and the stiffness of specimens, No GPS (comparison of average values)

Exposed environment	Investigated parameters	Comparison	Changes in ultimate strength	Changes in stiffness
Air at 65°F	180 days	Compare E1-1 with B1	2%	-2%
	447 days	Compare E1-3 with B1	10%	15%
	180 days, cyclic loading	Compare E1-5 with B1	8%	8%
Immersion in tap water at 65°F	92 days	Compare E2-1 with B1	-7%	-5%
	201 days	Compare E2-2 with B1	-6%	-7%
Immersion in tap water at 111°F	92 days	Compare E3-1 with B1	-10%	-20%
	210 days	Compare E3-3 with B1	-13%	-20%
	210 days, cyclic loading	Compare E3-5 with B1	-59%	-59%
Air at -4°F	196 days	Compare E4-1 with B1	13%	-6%
	382 days	Compare E4-3 with B1	12%	7%
	197 days, cyclic loading	Compare E4-5 with B1	13%	-7%
Freeze and thaw chamber	92 days (552 cycles)	Compare E5-1 with B1	-3%	-14%
	193 days (1158 cycles)	Compare E5-2 with B1	1%	-9%
Temperature cycles, unloaded	197 days (14 cycles)	Compare E6-1 with B1	3%	-19%
	380 days (27 cycles)	Compare E6-3 with B1	7%	-14%
	207 days (15 cycles), cyclic loading	Compare E6-5 with B1	5%	-11%
Temperature cycles, loaded at 0.95 kips	211 days (15 cycles)	Compare E7-1 with B1	-19%	-32%
	370 days (26 cycles)	Compare E7-3 with B1	-30%	-36%
Outdoors	184 days	Compare E8-1 with B1	2%	-7%
	271 days, cyclic loading	Compare E8-3 with B1	3%	-9%
Fire broke out after outdoor exposure	371 days	Compare E9-1 with B1	-88%	-77%

Table 5.6(b) Effects of environment exposure on the ultimate strength and the stiffness of specimens, No GPS (statistic analysis)

Exposed environment	Investigated parameters	Comparison	Results in	
			ultimate strength	stiffness
Air at 65°F	180 days	Compare E1-1 with B1	73% ↑	36% ↓
	447 days	Compare E1-3 with B1	99.9% ↑	99.3% ↑
	180 days, cyclic loading	Compare E1-5 with B1	95% ↑	87% ↑
Immersion in tap water at 65°F	92 days	Compare E2-1 with B1	96% ↓	67% ↓
	201 days	Compare E2-2 with B1	99.4% ↓	89% ↓
Immersion in tap water at 111°F	92 days	Compare E3-1 with B1	87% ↓	99.5% ↓
	210 days	Compare E3-3 with B1	99.9% ↓	99.8% ↓
	210 days, cyclic loading	Compare E3-5 with B1	97% ↓	97% ↓
Air at -4°F	196 days	Compare E4-1 with B1	99.9% ↑	75% ↓
	382 days	Compare E4-3 with B1	99.9% ↑	91% ↑
	197 days, cyclic loading	Compare E4-5 with B1	99.9% ↑	76% ↓
Freeze and thaw chamber	92 days (552 cycles)	Compare E5-1 with B1	64% ↓	99.1% ↓
	193 days (1158 cycles)	Compare E5-2 with B1	23% ↑	95% ↓
Temperature cycles, unloaded	197 days (14 cycles)	Compare E6-1 with B1	27% ↑	90% ↓
	380 days (27 cycles)	Compare E6-3 with B1	95% ↑	99.0% ↓
	207 days (15 cycles), cyclic loading	Compare E6-5 with B1	75% ↑	97% ↓
Temperature cycles, loaded at 0.95 kips	211 days (15 cycles)	Compare E7-1 with B1	58% ↓	86% ↓
	370 days (26 cycles)	Compare E7-3 with B1	84% ↓	91% ↓
Outdoors	184 days	Compare E8-1 with B1	72% ↑	93% ↓
	271 days, cyclic loading	Compare E8-3 with B1	66% ↑	96% ↓
Fire broke out after outdoor exposure	371 days	Compare E9-1 with B1	99.99% ↓	99.99% ↓
“73% ↑ ”	denotes that one is 73% confident of an increase			
“36% ↓ ”	denotes that one is 36% confident of a decrease			
Note:	Each notation listed in the table is strictly limited to one comparison, and thus does not apply to the whole table.			

Table 5.7(a) Effects of environment exposure on the ultimate strength and the stiffness of specimens, GPS vs. No GPS (comparison of average values)

Exposed environment	Investigated parameters	Comparison	Changes in ultimate strength	Changes in stiffness
Air at 65°F	180 days	Compare E1-2 with E1-1	1%	6%
	447 days	Compare E1-4 with E1-3	1%	0%
Immersion in tap water at 111°F	92 days	Compare E3-2 with E3-1	7%	4%
	210 days	Compare E3-4 with E3-3	9%	5%
Air at -4°F	196 days	Compare E4-2 with E4-1	0%	-3%
	382 days	Compare E4-4 with E4-3	3%	-1%
Temperature cycles, unloaded	197 days (14 cycles)	Compare E6-2 with E6-1	13%	10%
	380 days (27 cycles)	Compare E6-4 with E6-3	1%	1%
	207 days (15 cycles), cyclic loading	Compare E6-6 with E6-5	8%	7%
Temperature cycles, loaded at 0.95 kips	211 days (15 cycles)	Compare E7-2 with E7-1	29%	24%
	370 days (26 cycles)	Compare E7-4 with E7-3	20%	12%
Outdoors	184 days	Compare E8-2 with E8-1	1%	3%
Fire broke out after outdoor exposure	371~374 days	Compare E9-2 with E9-1	234%	151%

Table 5.7(b) Effects of environment exposure on the ultimate strength and the stiffness of specimens, GPS vs. No GPS (statistic analysis)

Exposed environment	Investigated parameters	Comparison	Results in ultimate strength	Results in stiffness
Air at 65°F	180 days	Compare E1-2 with E1-1	20% ↑	66% ↑
	447 days	Compare E1-4 with E1-3	17% ↑	9% ↓
Immersion in tap water at 111°F	92 days	Compare E3-2 with E3-1	73% ↑	50% ↑
	210 days	Compare E3-4 with E3-3	96% ↑	66% ↑
Air at -4°F	196 days	Compare E4-2 with E4-1	0.6% ↓	52% ↓
	382 days	Compare E4-4 with E4-3	71% ↑	15% ↓
Temperature cycles, unloaded	197 days (14 cycles)	Compare E6-2 with E6-1	85% ↑	60% ↑
	380 days (27 cycles)	Compare E6-4 with E6-3	36% ↑	14% ↑
	207 days (15 cycles), cyclic loading	Compare E6-6 with E6-5	91% ↑	71% ↑
Temperature cycles, loaded at 0.95 kips	211 days (15 cycles)	Compare E7-2 with E7-1	67% ↑	60% ↑
	370 days (26 cycles)	Compare E7-4 with E7-3	44% ↑	29% ↑
Outdoors	184 days	Compare E8-2 with E8-1	41% ↑	68% ↑
Fire broke out after outdoor exposure	371~374 days	Compare E9-2 with E9-1	99.6% ↑	98% ↑
“20% ↑”	denotes that one is 20% confident of an increase			
“52% ↓”	denotes that one is 52% confident of a decrease			
Note:	Each notation listed in the table is strictly limited to one comparison, and thus does not apply to the whole table.			

## Figures

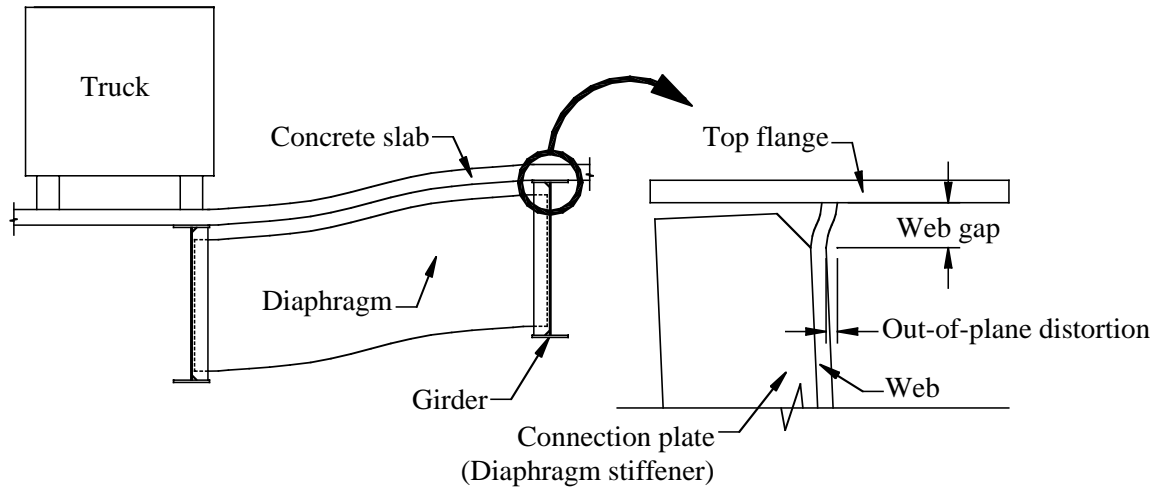


Figure 1.1 Girder differential deflection and web gap detail

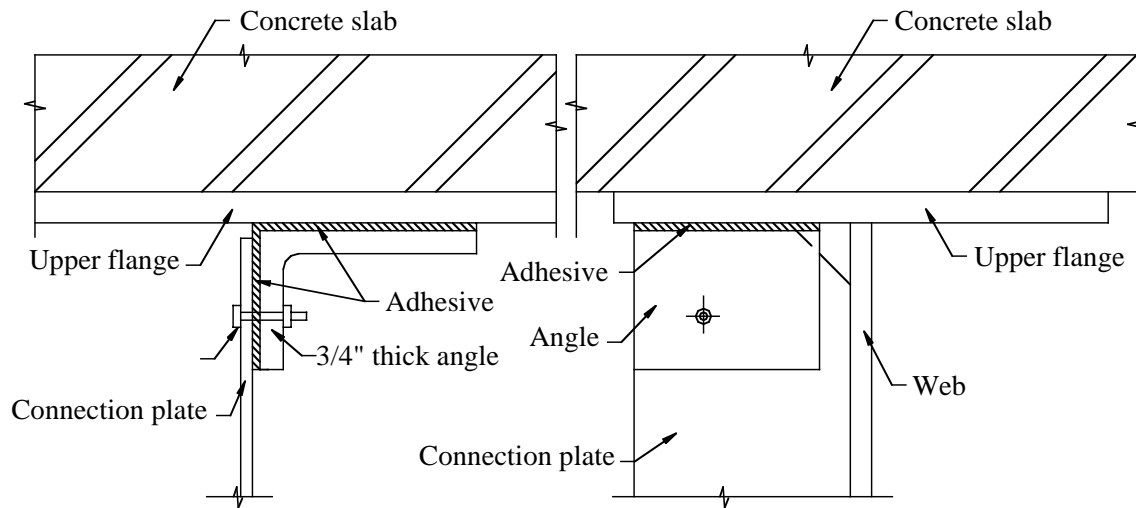


Figure 1.2 Proposed retrofit scheme with adhesives

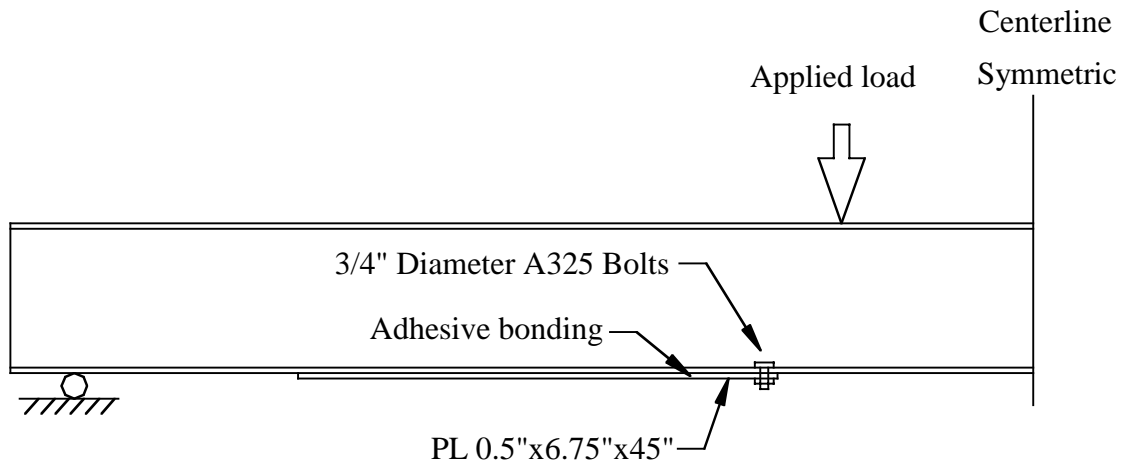


Figure 2.1 Test specimens by Albrecht (1987)

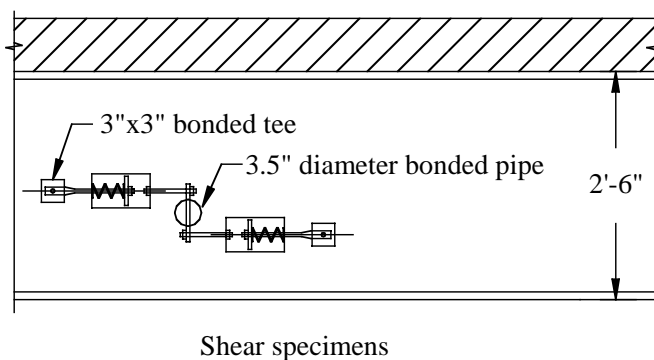
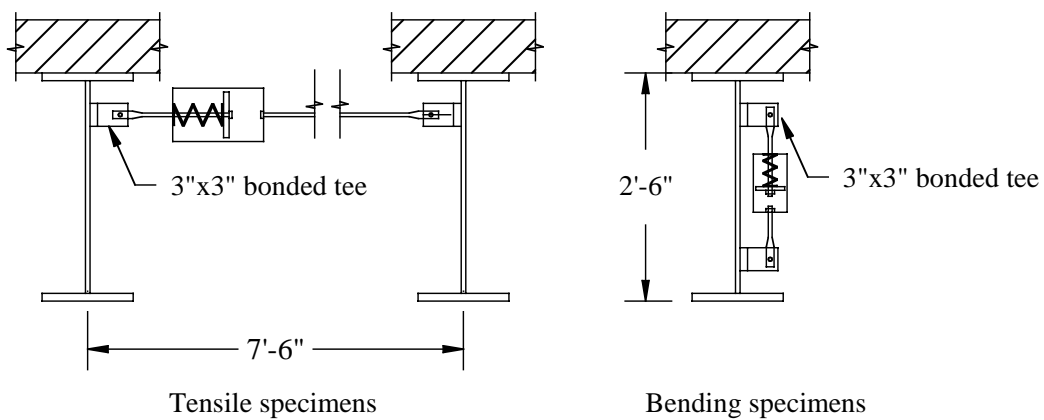


Figure 2.2 Specimens of Gasparini et al. (1990) to investigate durability of adhesives

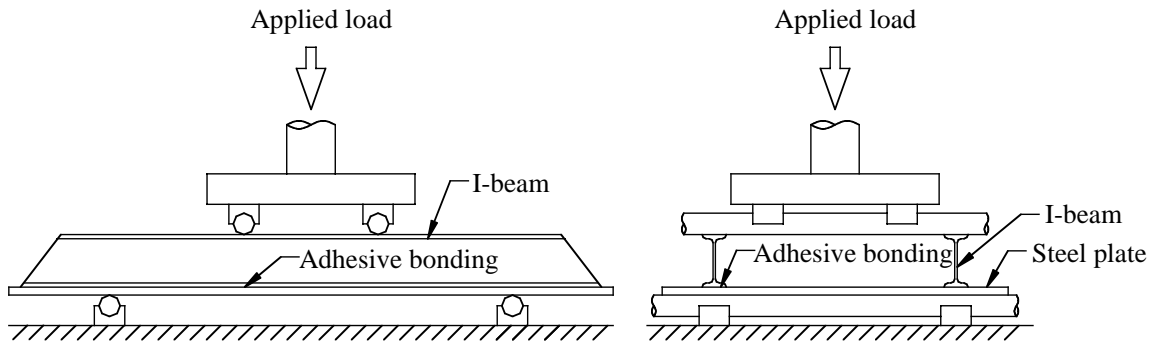


Figure 2.3 Large-scale specimens used by Hashim et al. (1990)

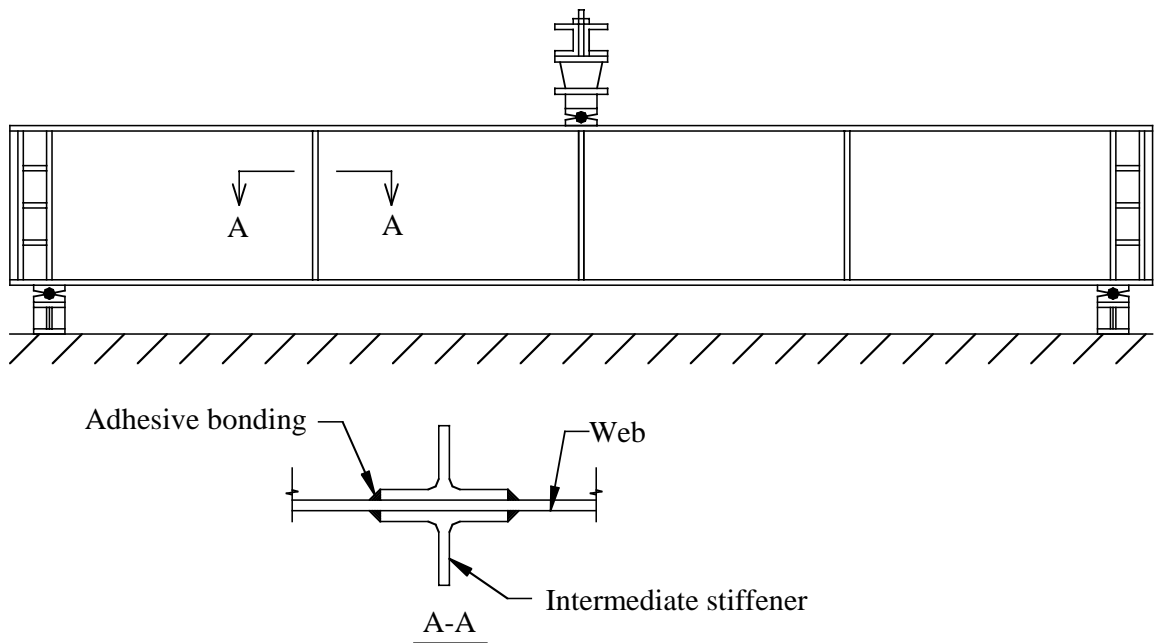


Figure 2.4 Specimens with bonded transverse intermediate stiffeners used by Martin (1992)



Bent-plate-diaphragm bridge

Cross-frame-diaphragm bridge

(a) Overview of the BPD bridge and the CFD bridge



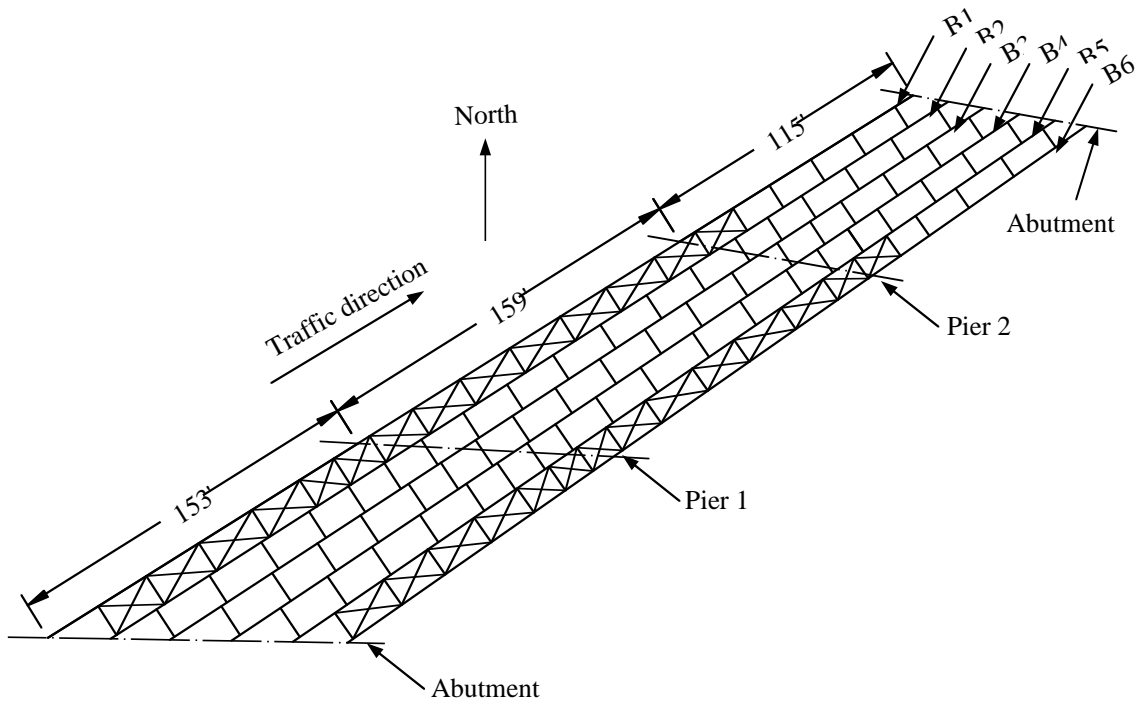
(b) Underside view of the BPD bridge (Bridge #27763)

Figure 3.1 Pictures of the field bridges

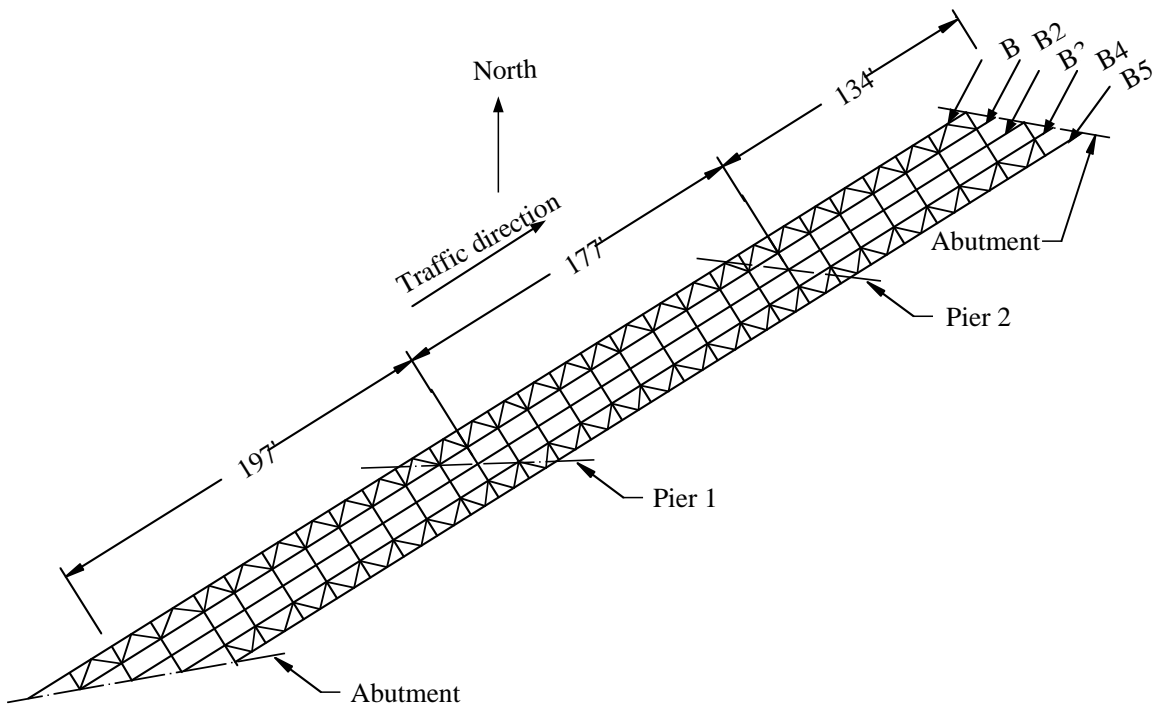


(c) Underside view of the CFD bridge (Bridge #27984)

Figure 3.1 (con't) Pictures of the field bridges

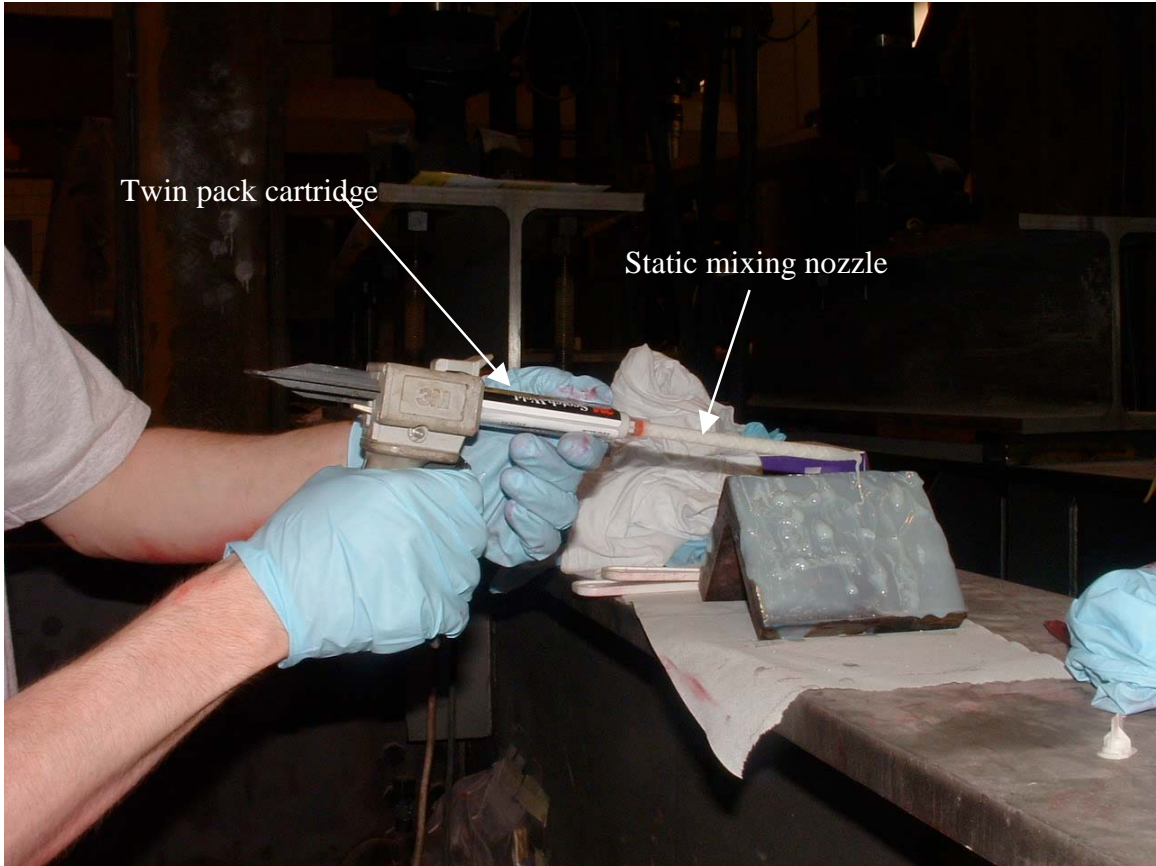


(a) Plan view of the BPD bridge



(b) Plan view of the CFD bridge

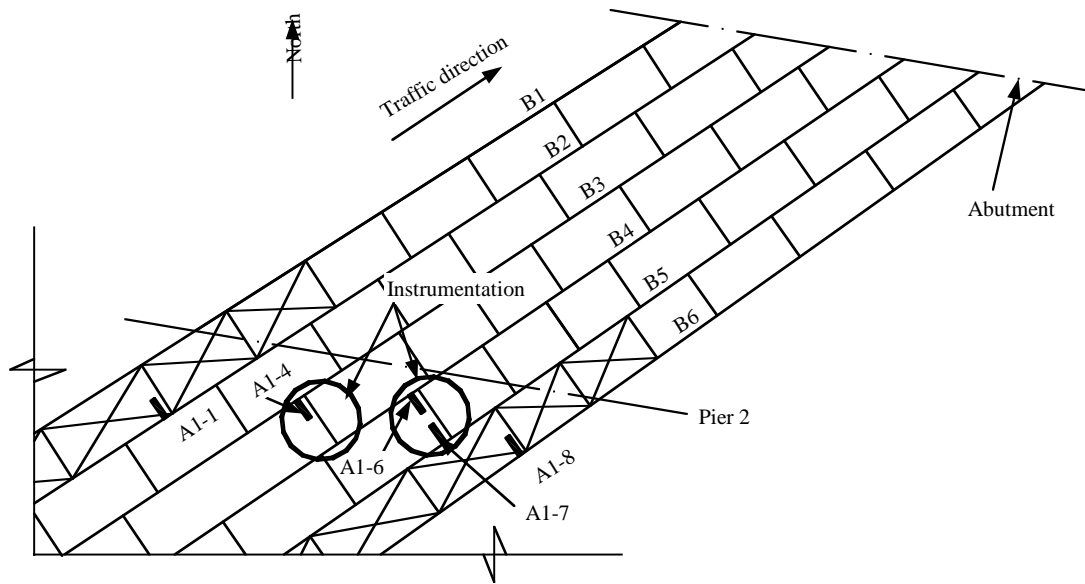
Figure 3.2 Plan view of the field bridges



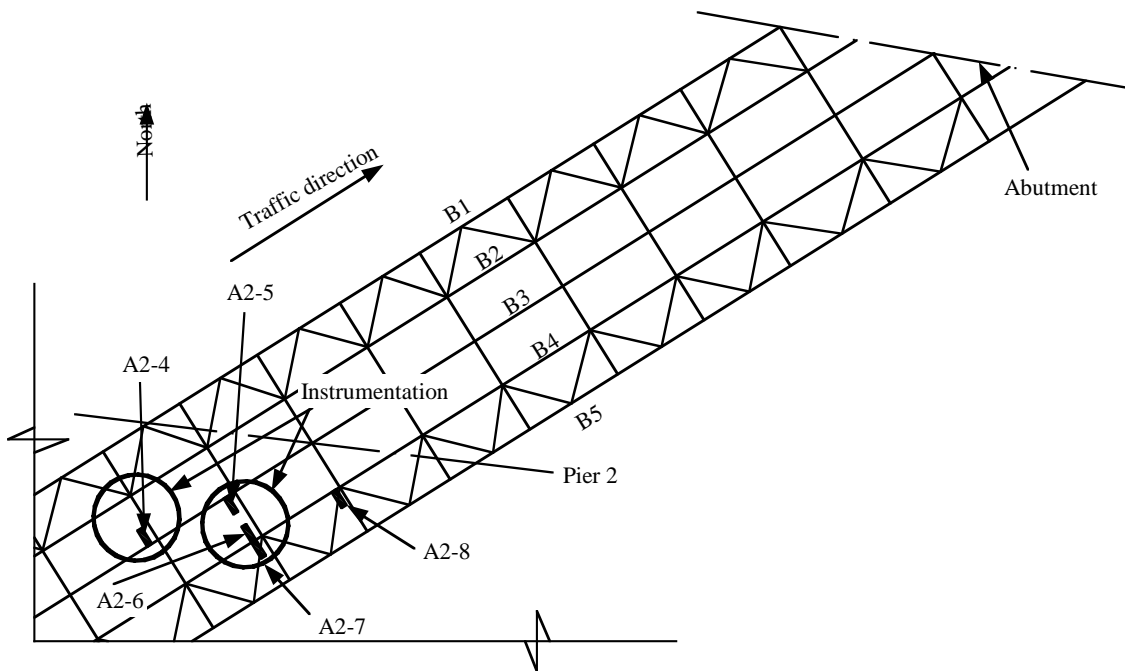
Twin pack cartridge

Static mixing nozzle

Figure 3.3 Application of DP-460 NS

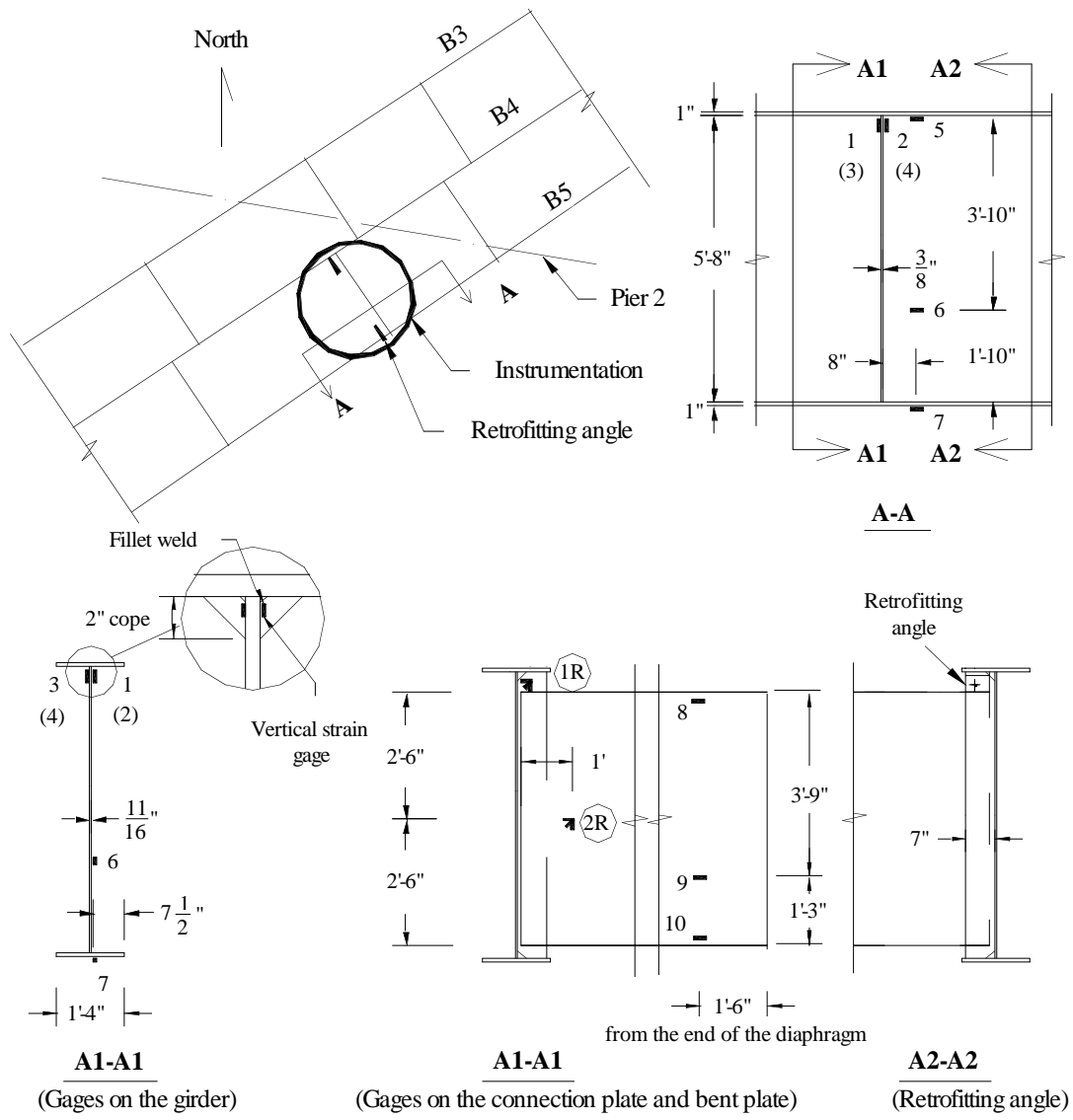


(a) Instrumentation and retrofitting plan for the BPD bridge



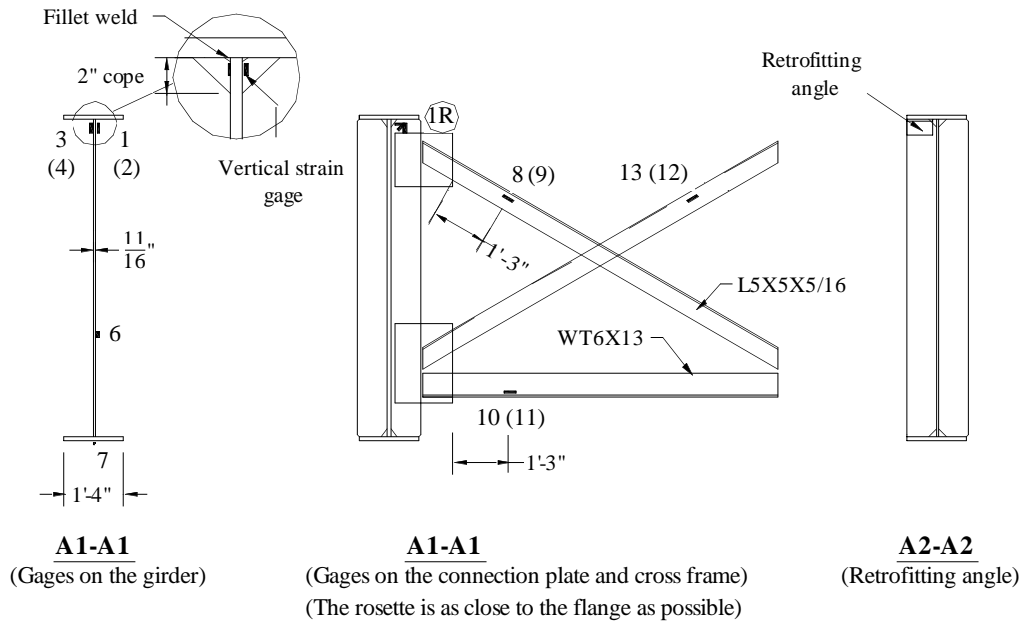
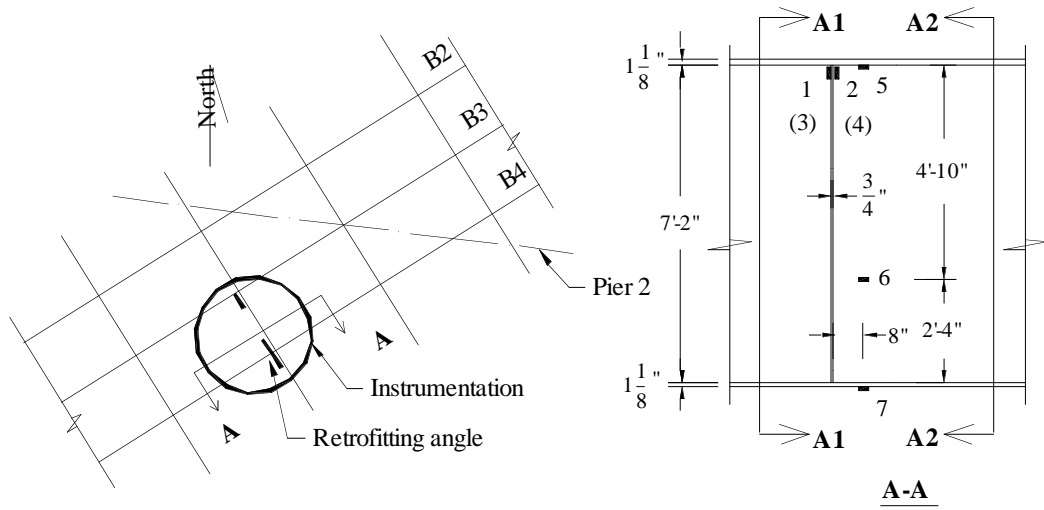
(b) Instrumentation and retrofitting plan for the CFD bridge

Figure 3.4 Instrumentation and retrofit plans for the field bridges



(a) Instrumentation for the BPD bridge

Figure 3.5 Instrument location detail for the field bridges



(b) Instrumentation for the CFD bridge

Figure 3.5 (con't) Instrument location detail for the field bridges

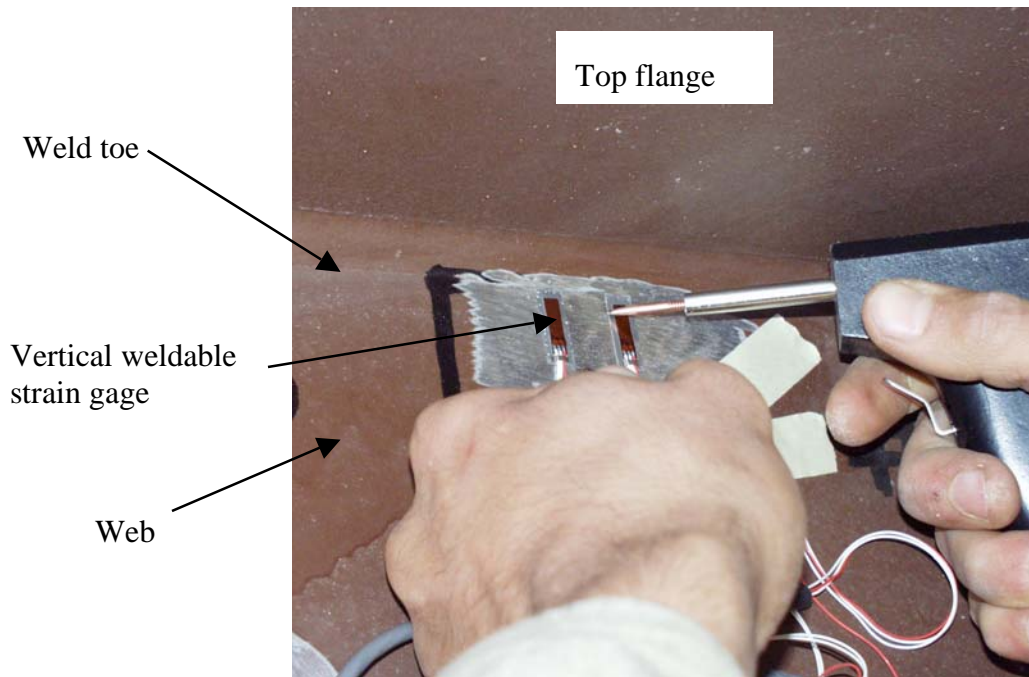


Figure 3.6 Strain gage application

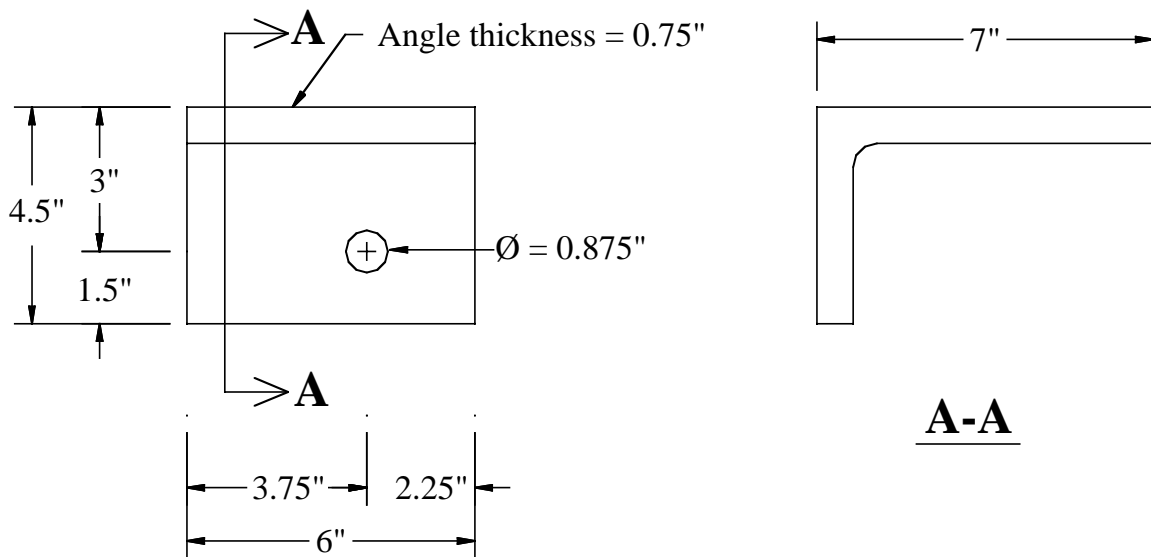


Figure 3.7 Retrofitting angle configuration

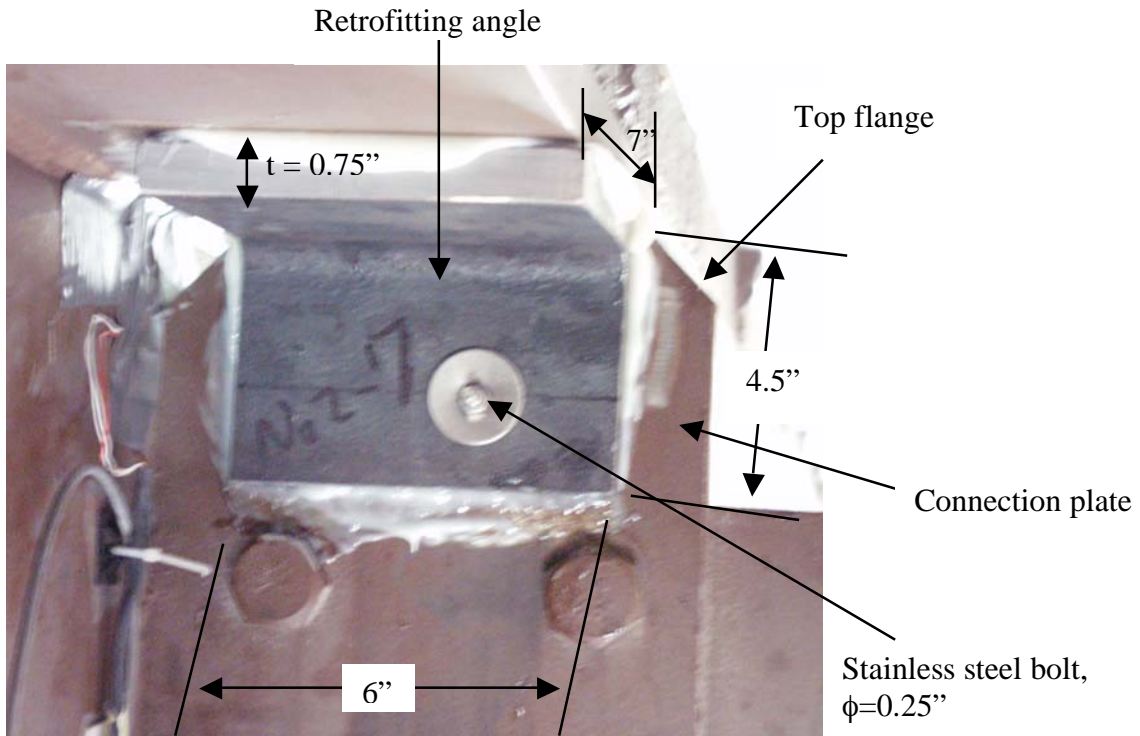


Figure 3.8 Picture of retrofitting angle

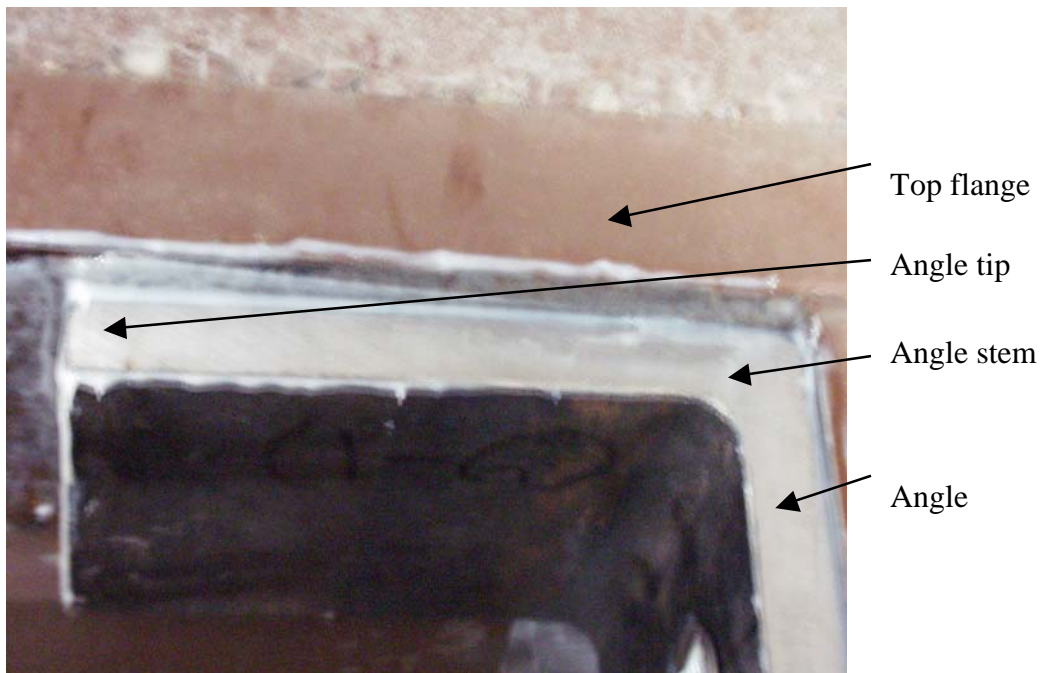


Figure 3.9 Bondline thickness of retrofitting angle

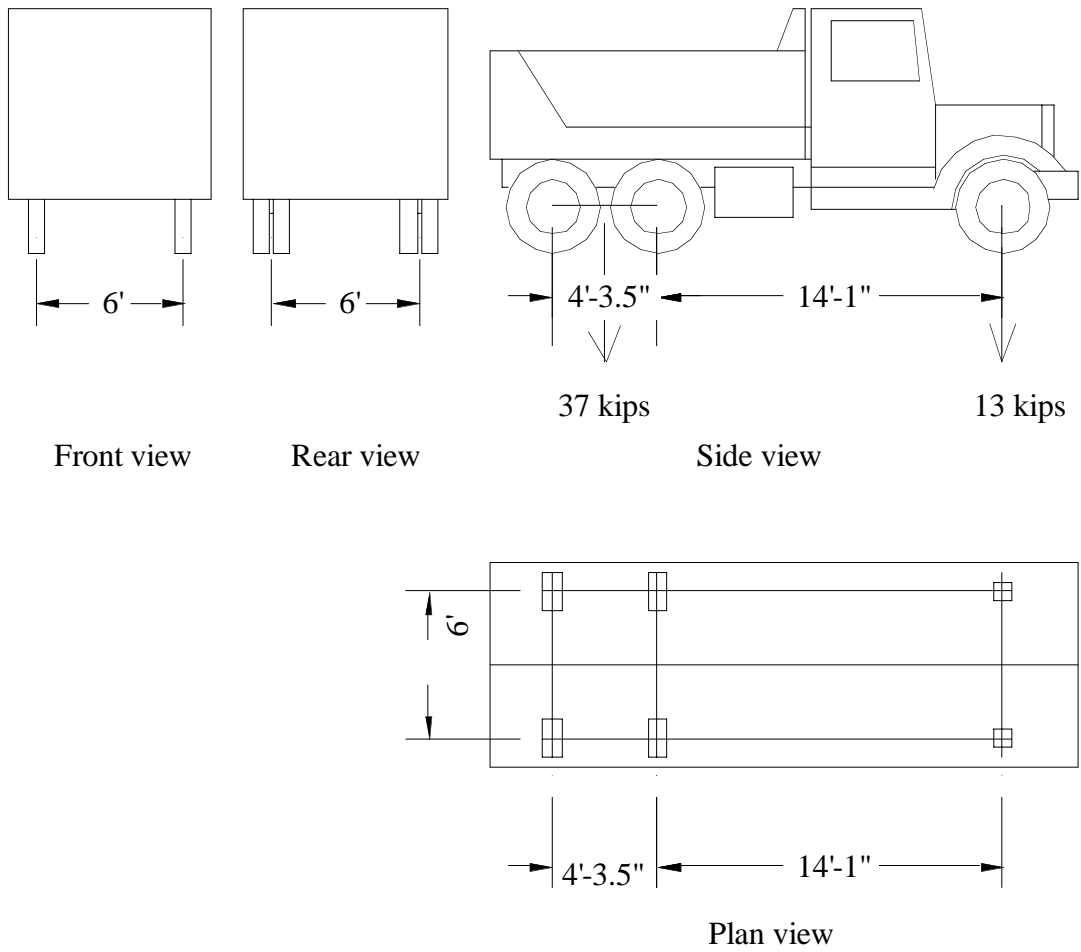


Figure 3.10 Field test truck

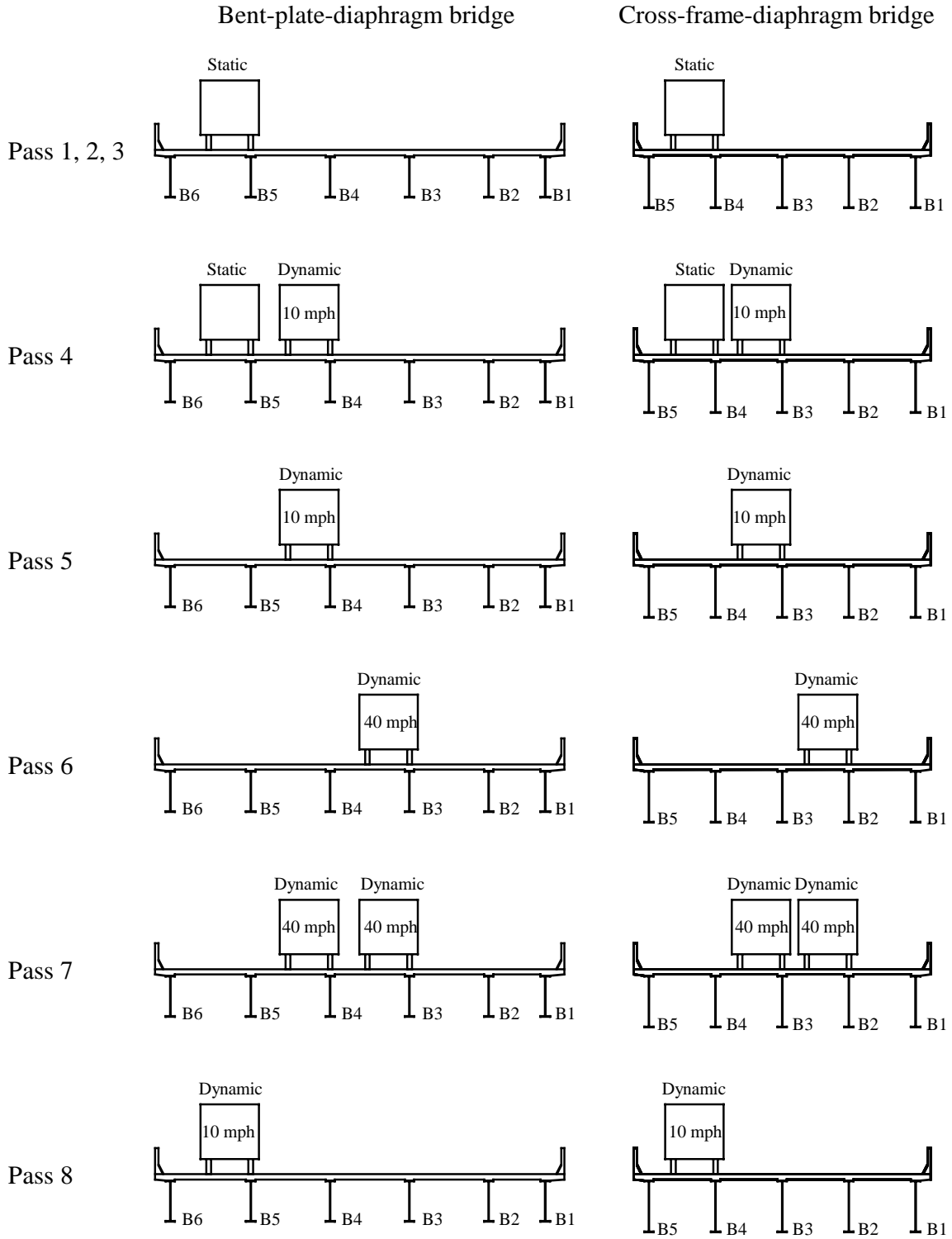


Figure 3.11 Field test truck position cross section view (with trucks moving out of the paper)

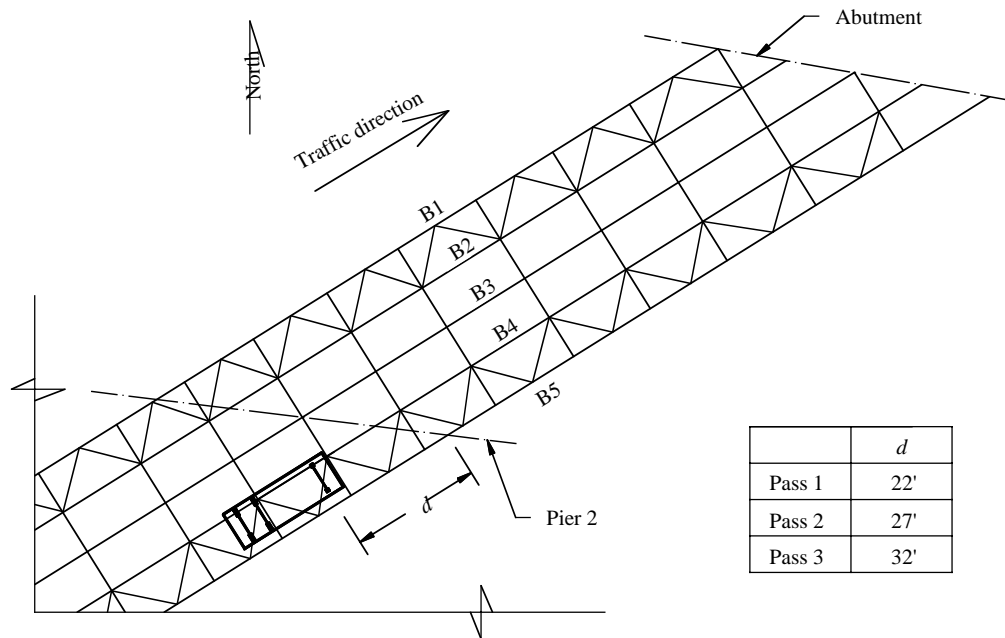
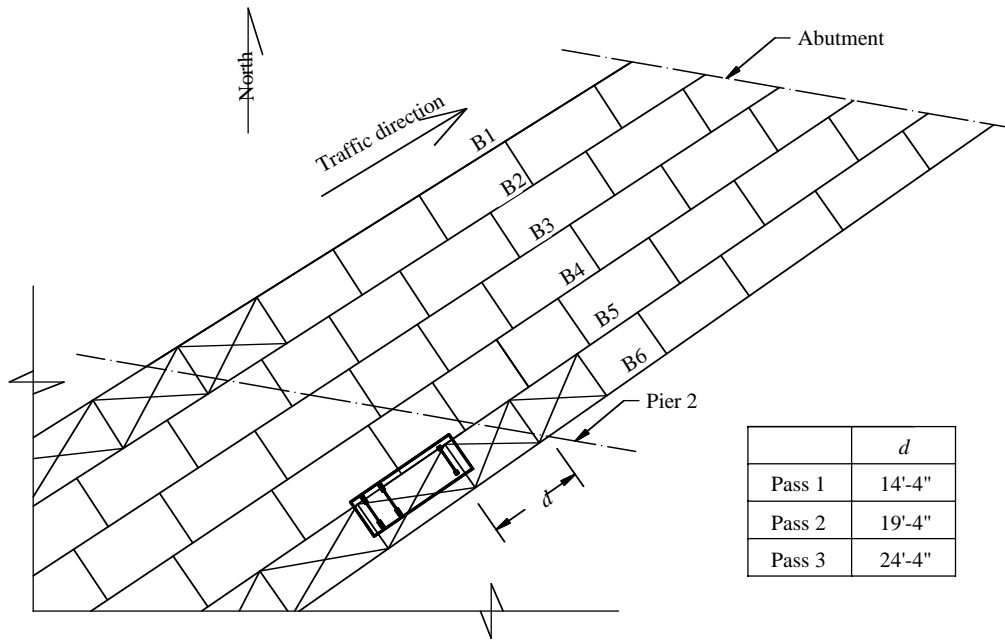
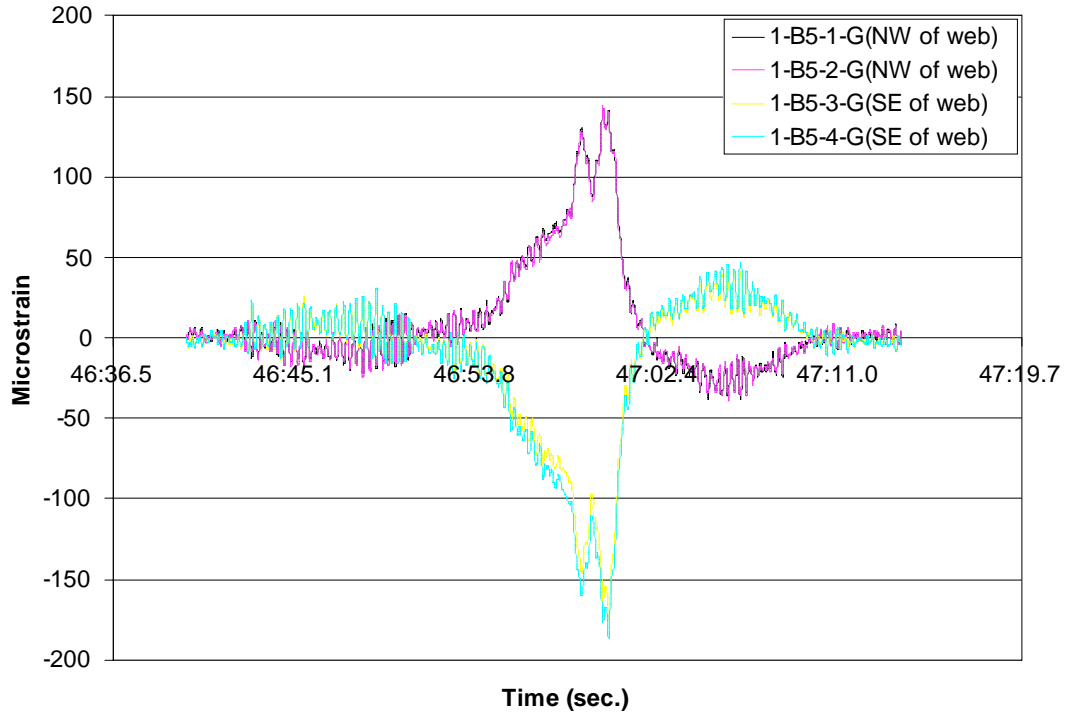
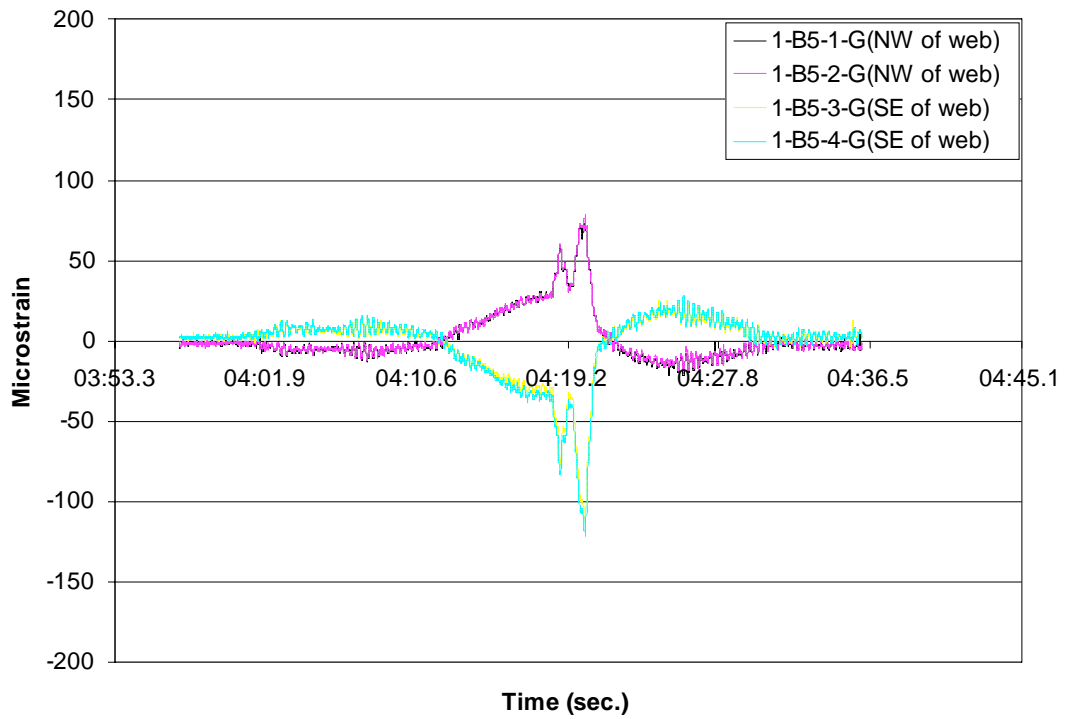


Figure 3.12 Field test truck position plan view (upper drawing: plan view of the BPD bridge; lower drawing: plan view of the CFD bridge)



(a) before retrofit (Pass 8)



(b) after retrofit (Pass 8)

Figure 3.13 Web gap strains before and after retrofit for the BPD bridge

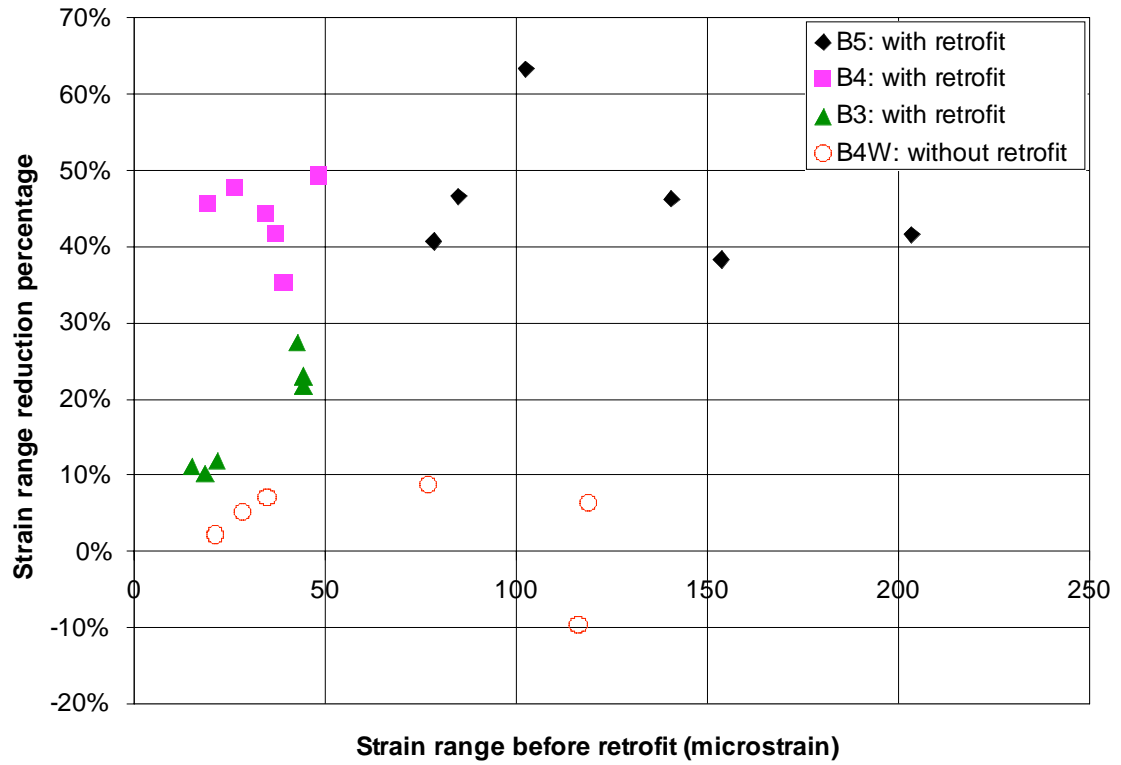


Figure 3.14 Strain range reduction vs. original strain range for the BPD bridge

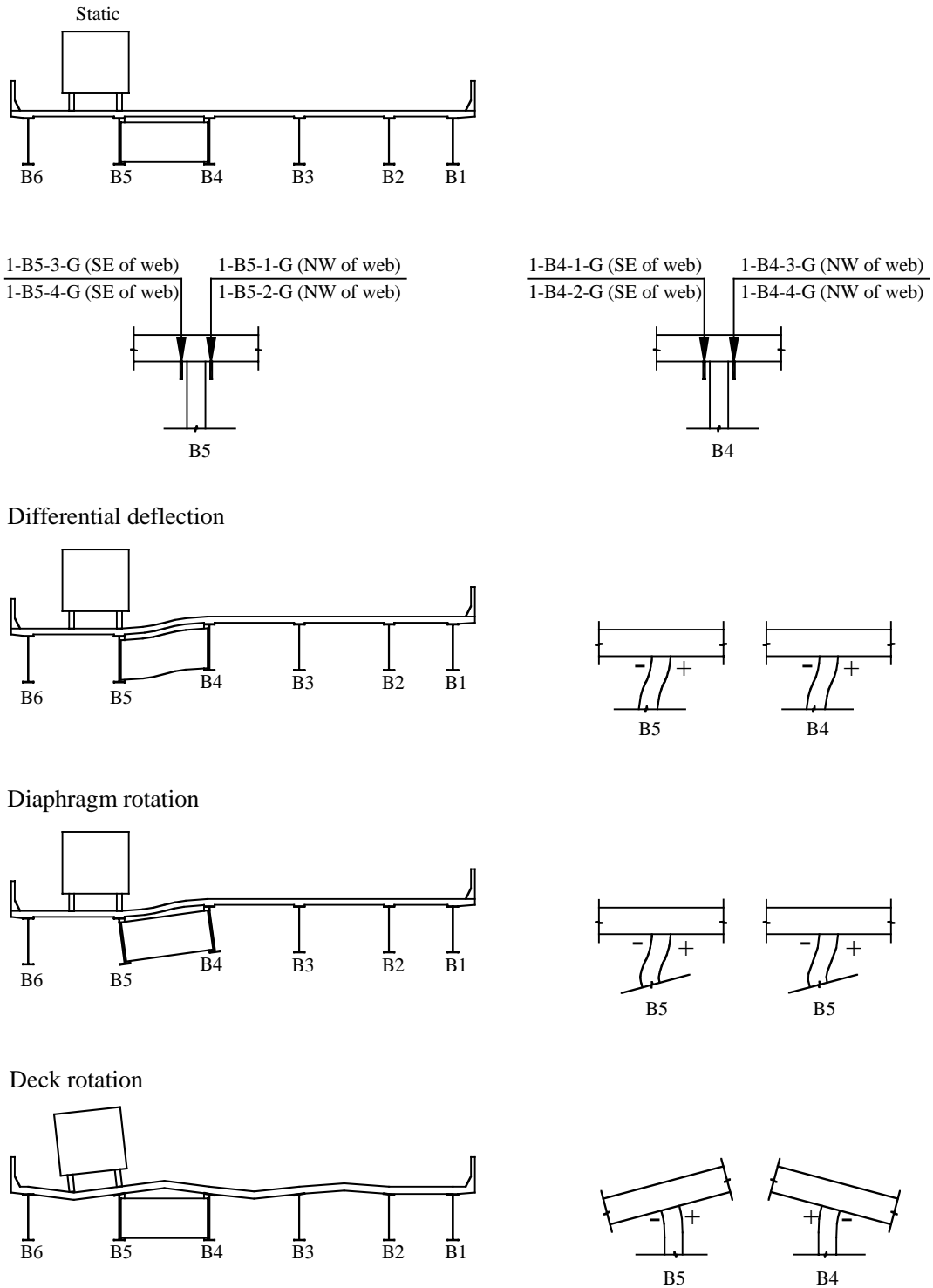
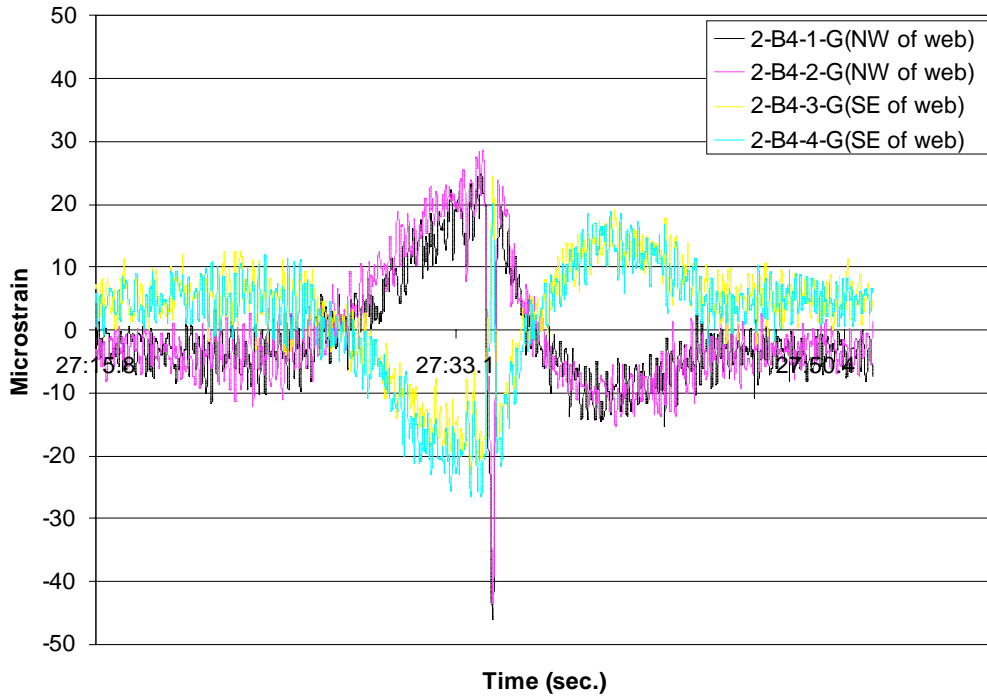
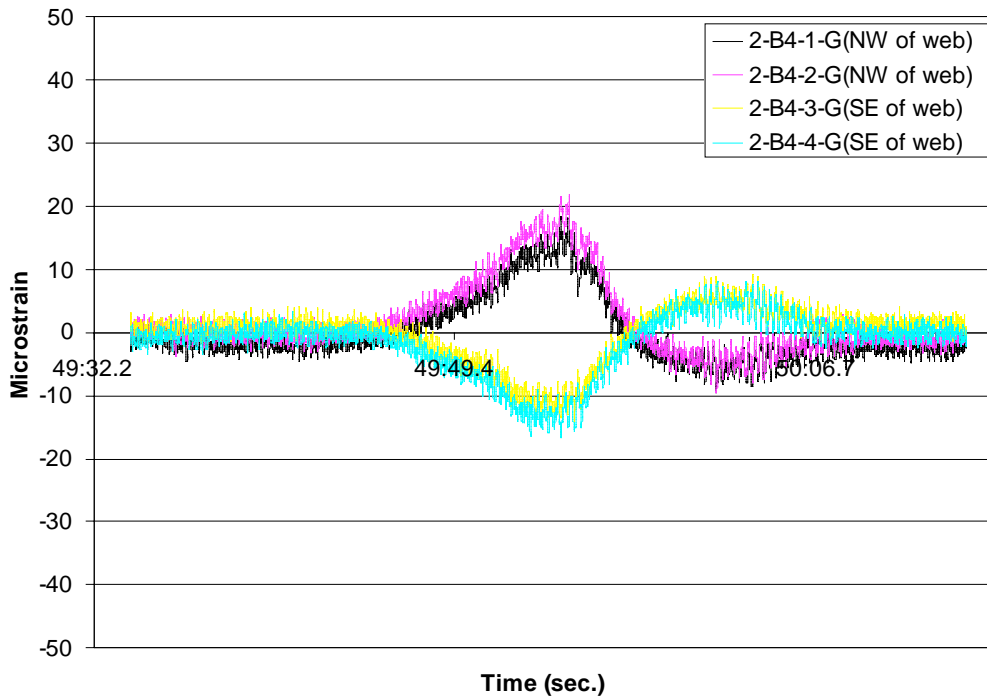


Figure 3.15 Effects of differential deflection, diaphragm rotation, and deck rotation on the BPD bridge (Note that only one diaphragm was shown for clarity)



(a) before retrofit (Pass 8)



(b) after retrofit (Pass 8)

Figure 3.16 Web gap strains for the CFD bridge before and after retrofit

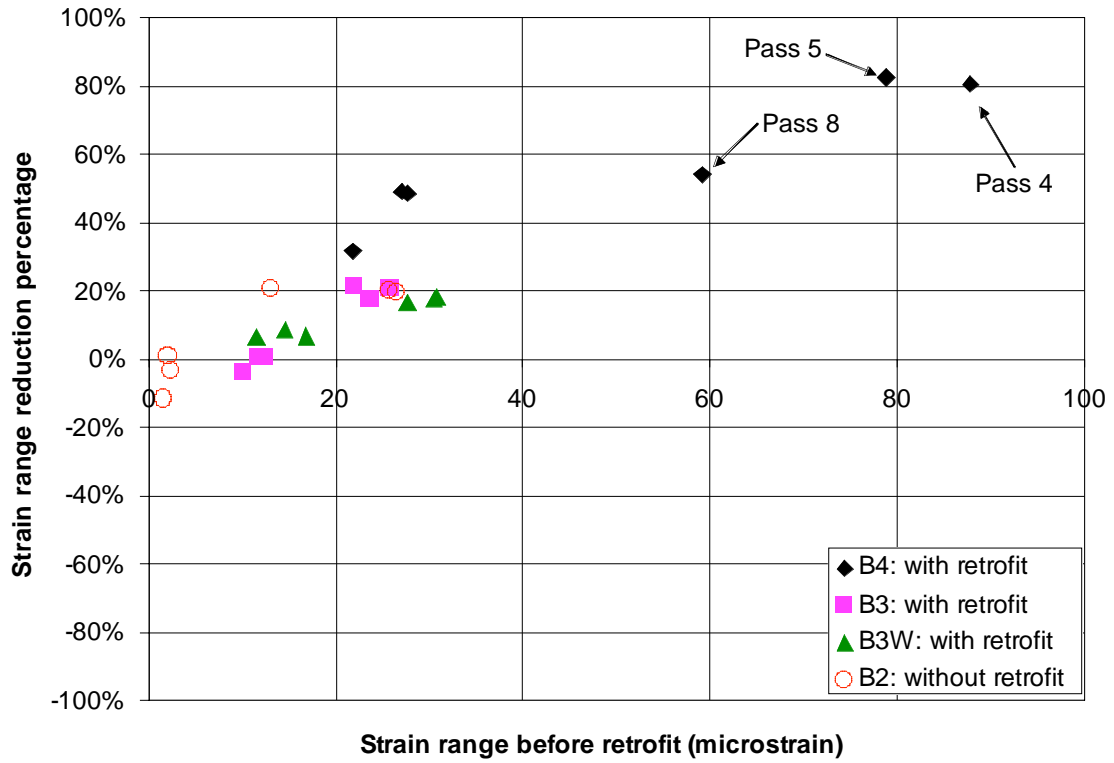


Figure 3.17 Strain range reduction vs. original strain range for the CFD bridge

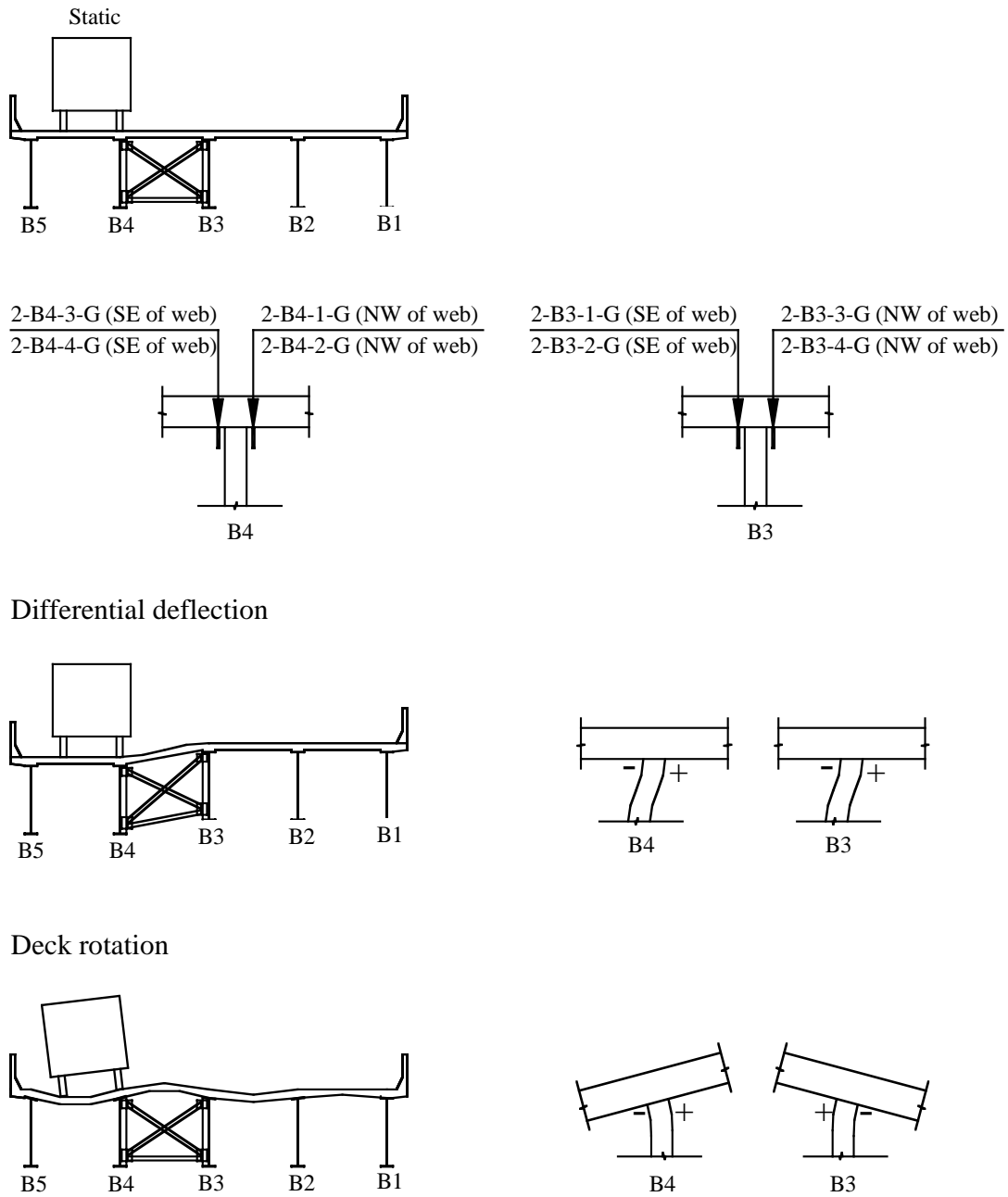


Figure 3.18 Effects of differential deflection and deck rotation on the CFD bridge (Note that only one diaphragm was shown for clarity)



Figure 3.19 Pictures of the field inspection of the adhesive-angle retrofit system 3.5 years after it was applied

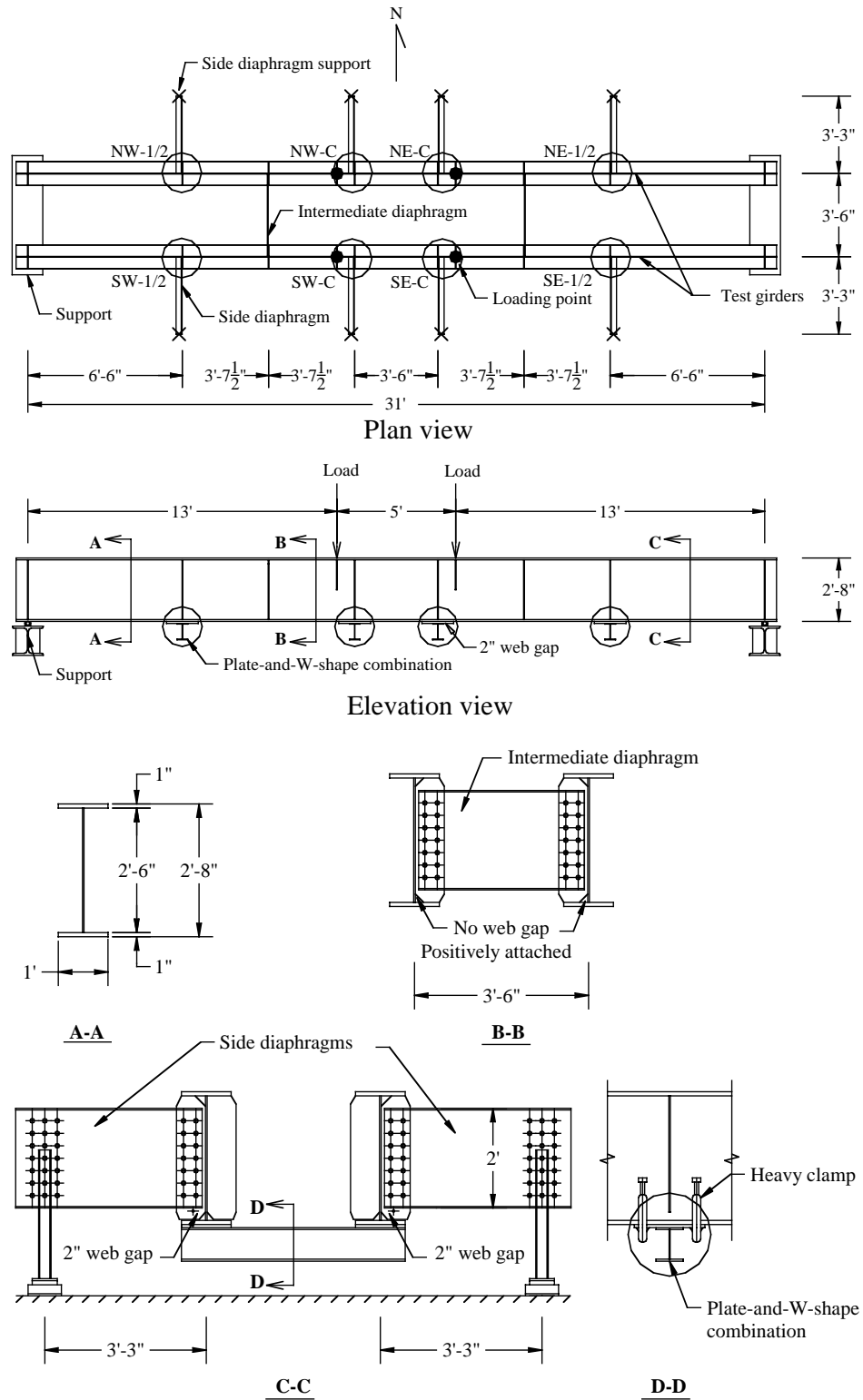


Figure 4.1 Large-scale specimen configuration

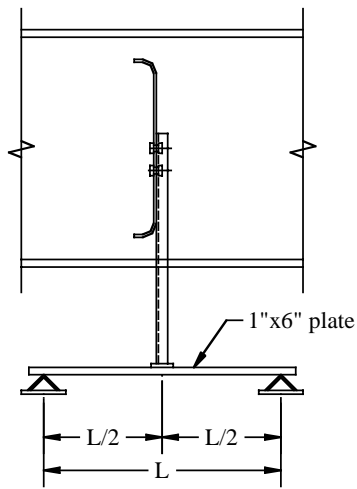


Figure 4.2 Spring support details

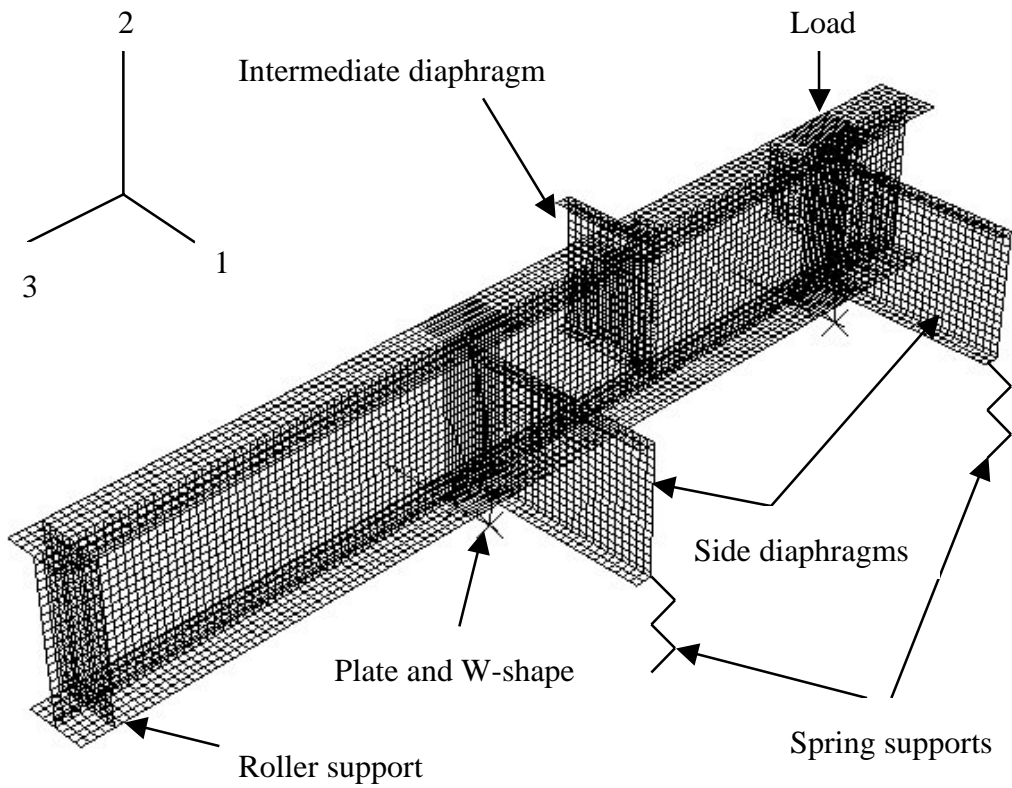


Figure 4.3 Global model of the large-scale specimen

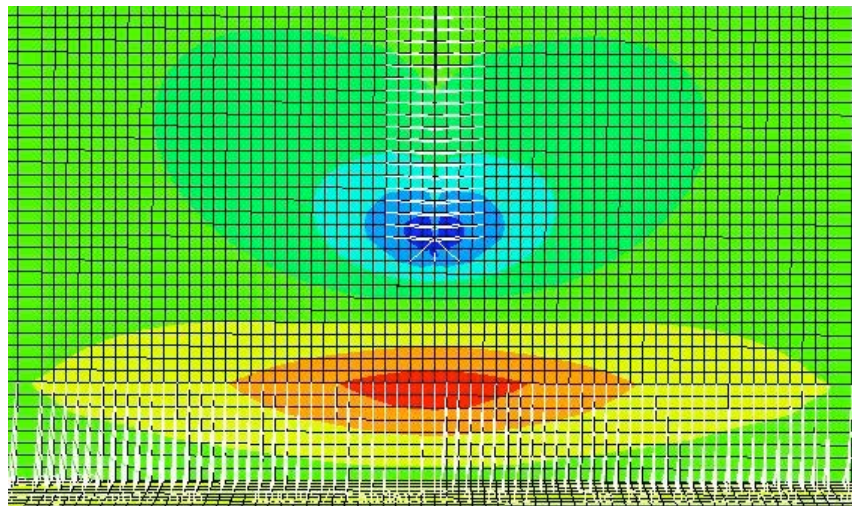
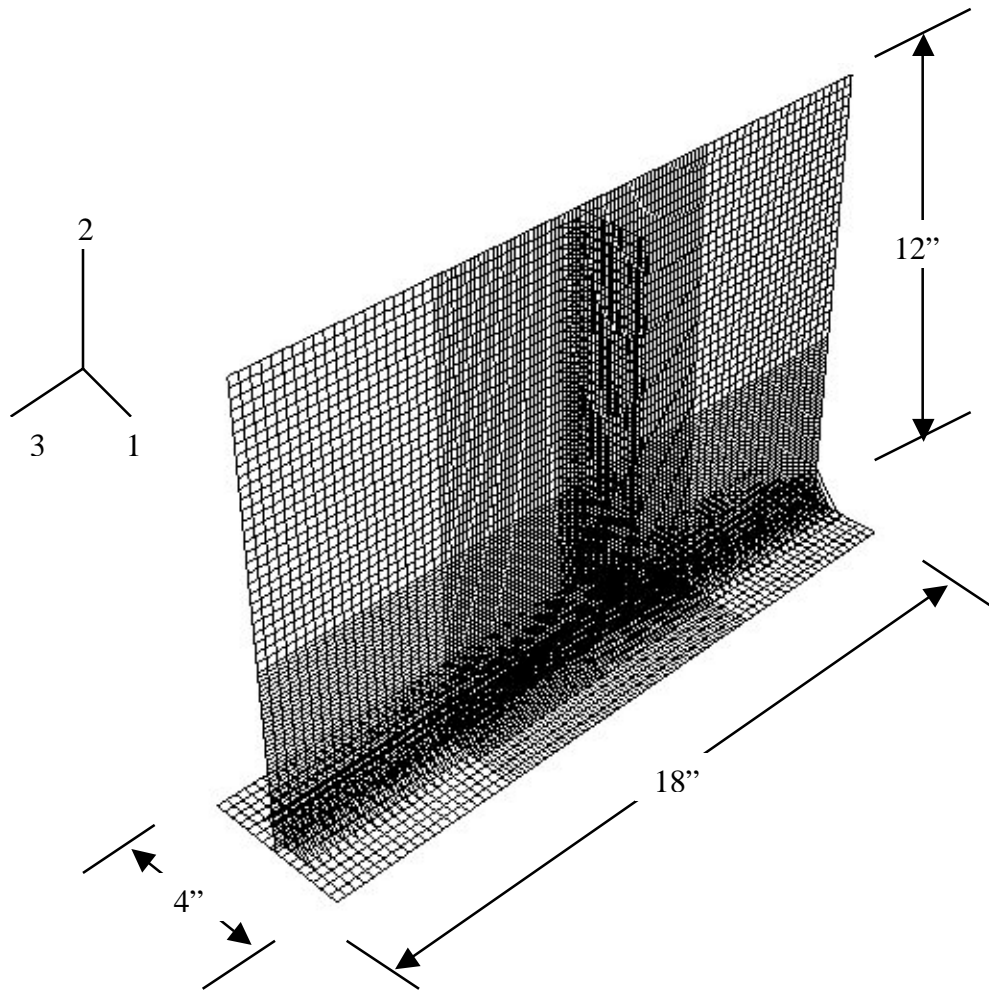
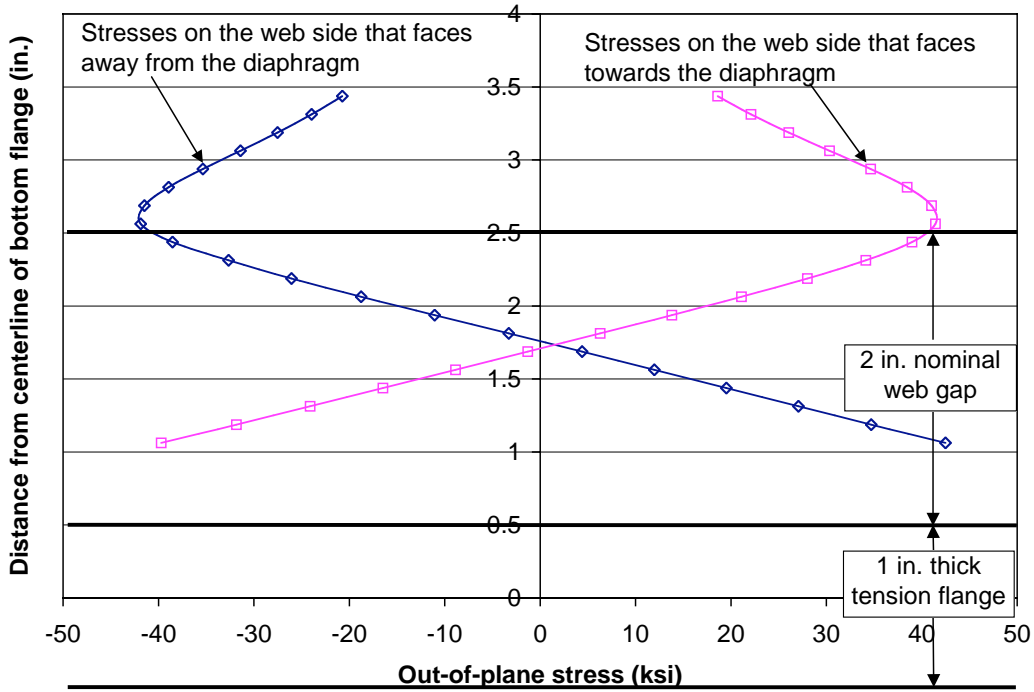
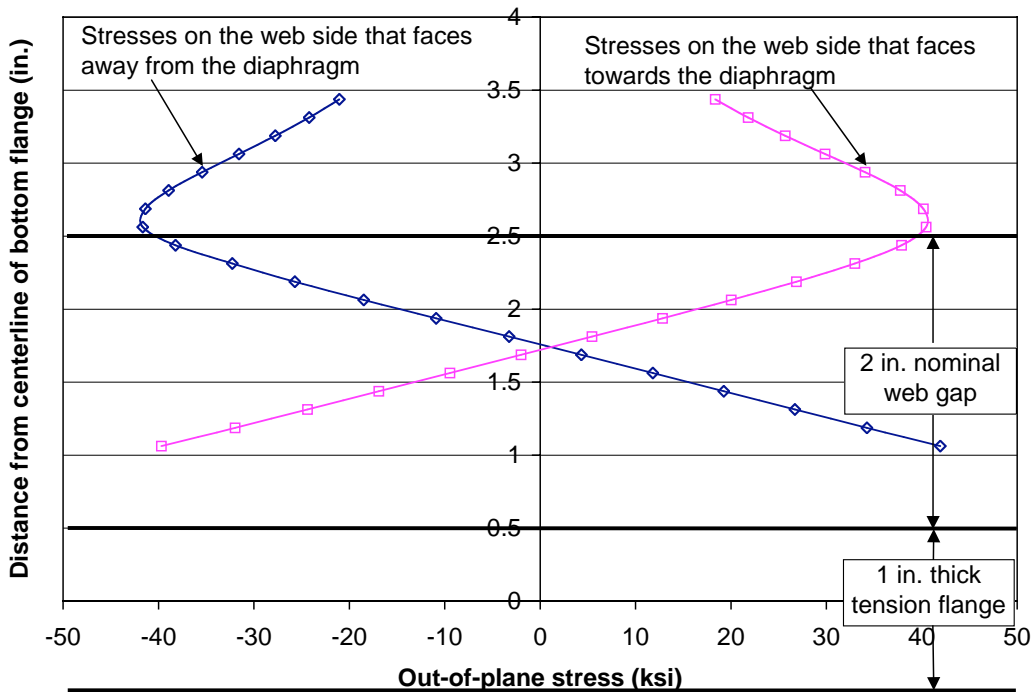


Figure 4.4 Submodel of the web gap region for the large-scale specimen

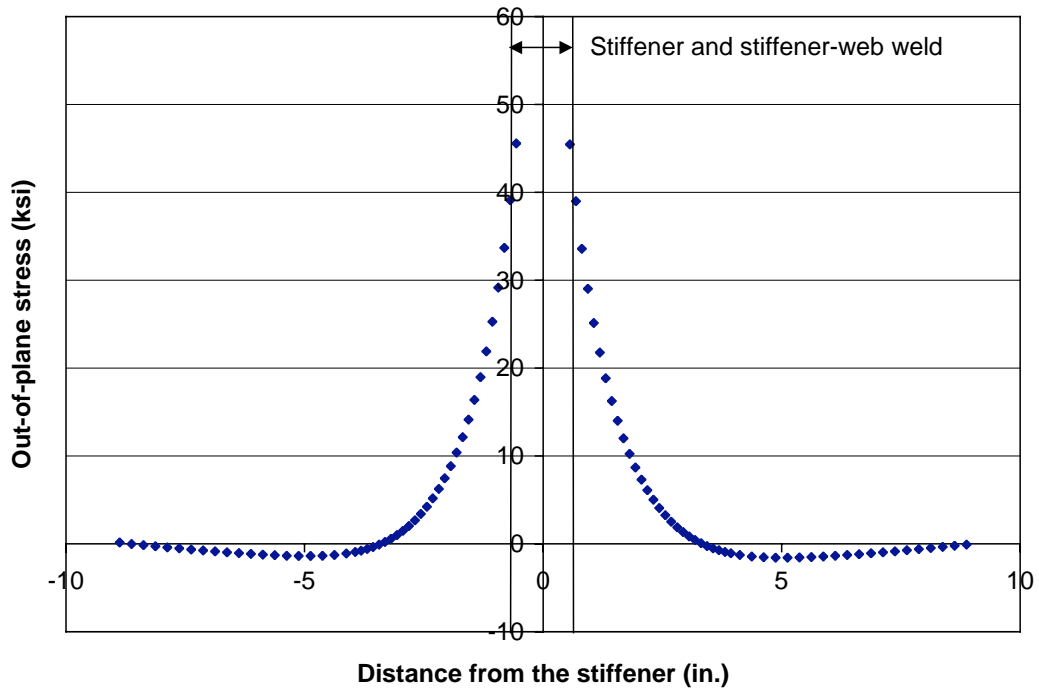


(a) in the constant moment region where in-plane stress was 12 ksi (upper graph)

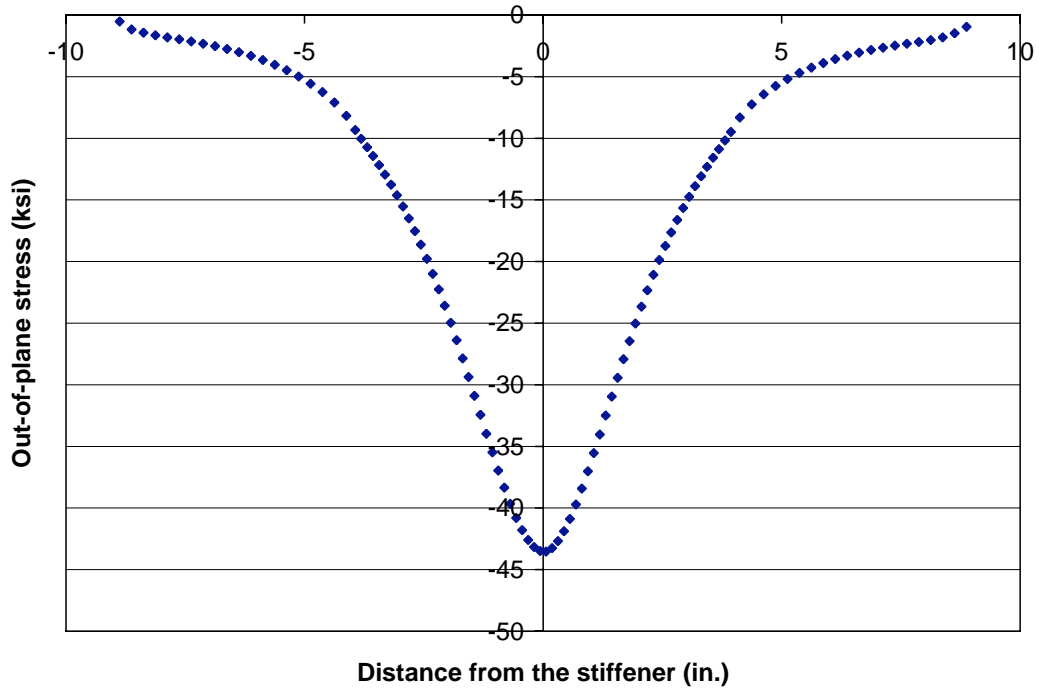


(b) where in-plane stress was 6 ksi (lower graph)

Figure 4.5 Out-of-plane stresses predicted by the FEA at web gaps



(a) at the stiffener end



(b) along the flange-web fillet weld toe

Figure 4.6 Out-of-plane stresses predicted by the FEA at web gap where in-plane stress was 6 ksi

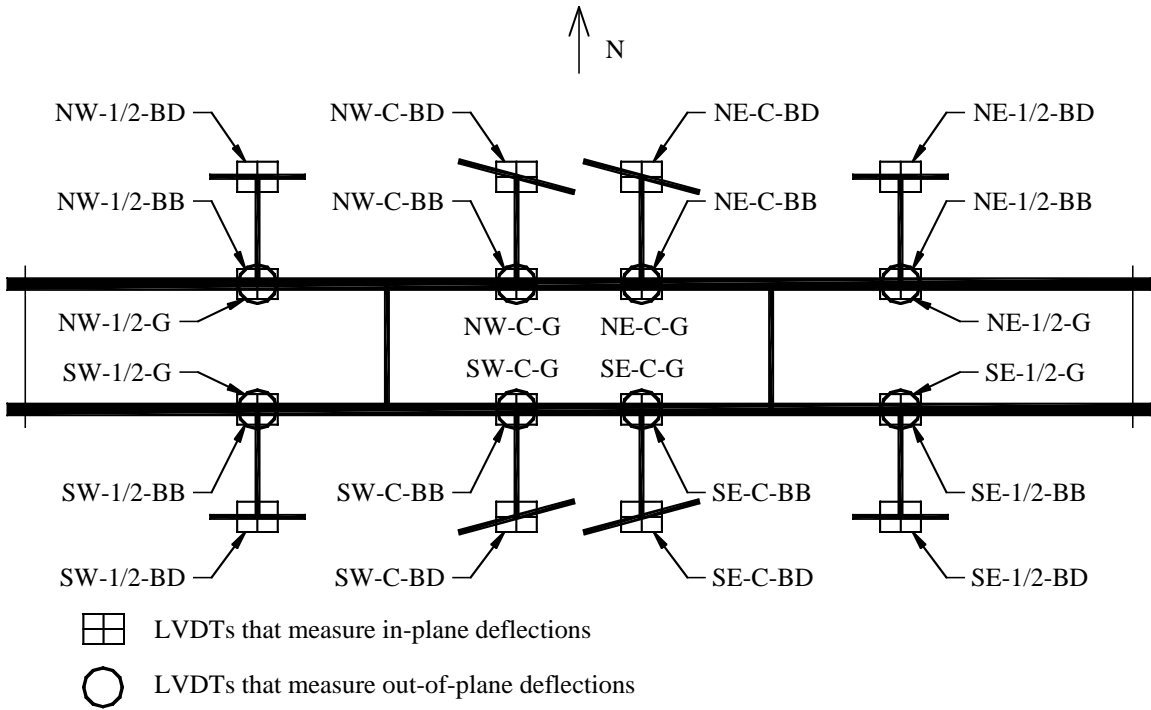


Figure 4.7 LVDT locations

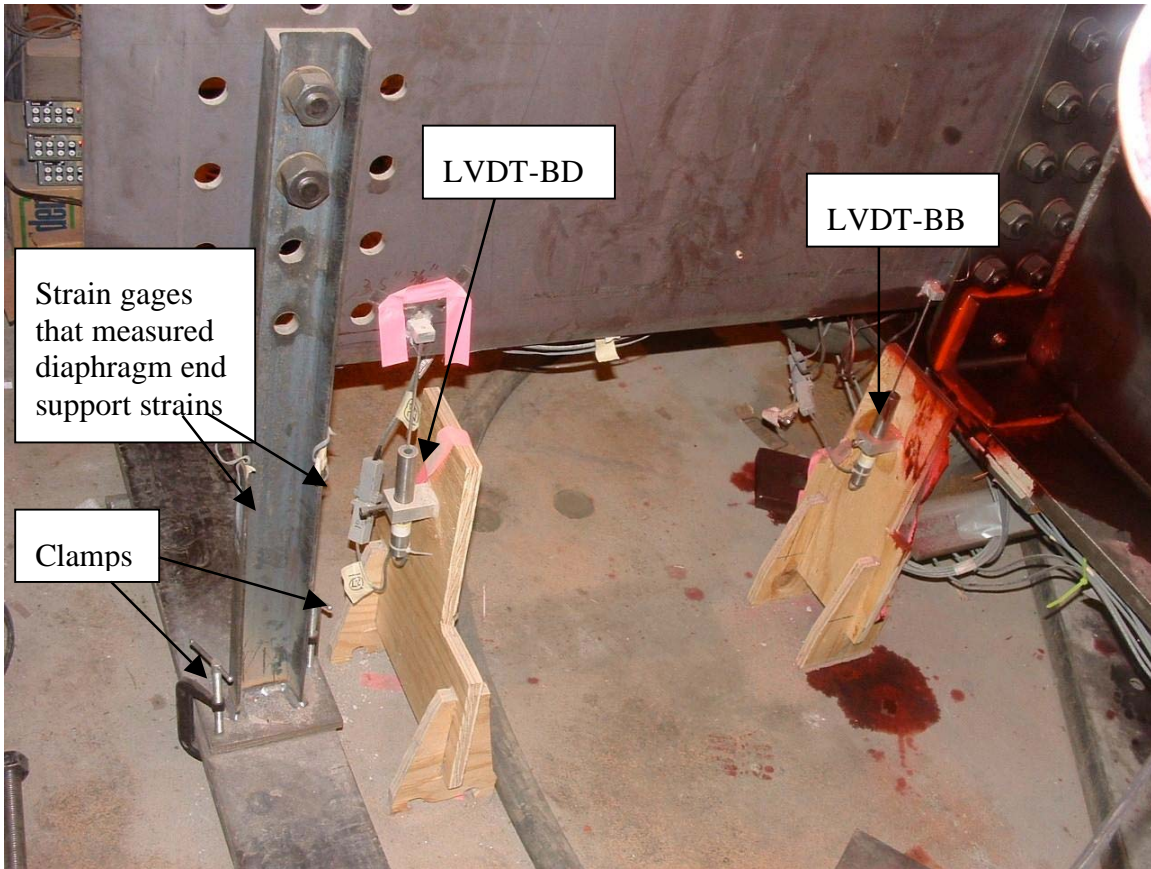


Figure 4.8 LVDTs that measure in-plane deflections and strain gages that measure diaphragm end support strains

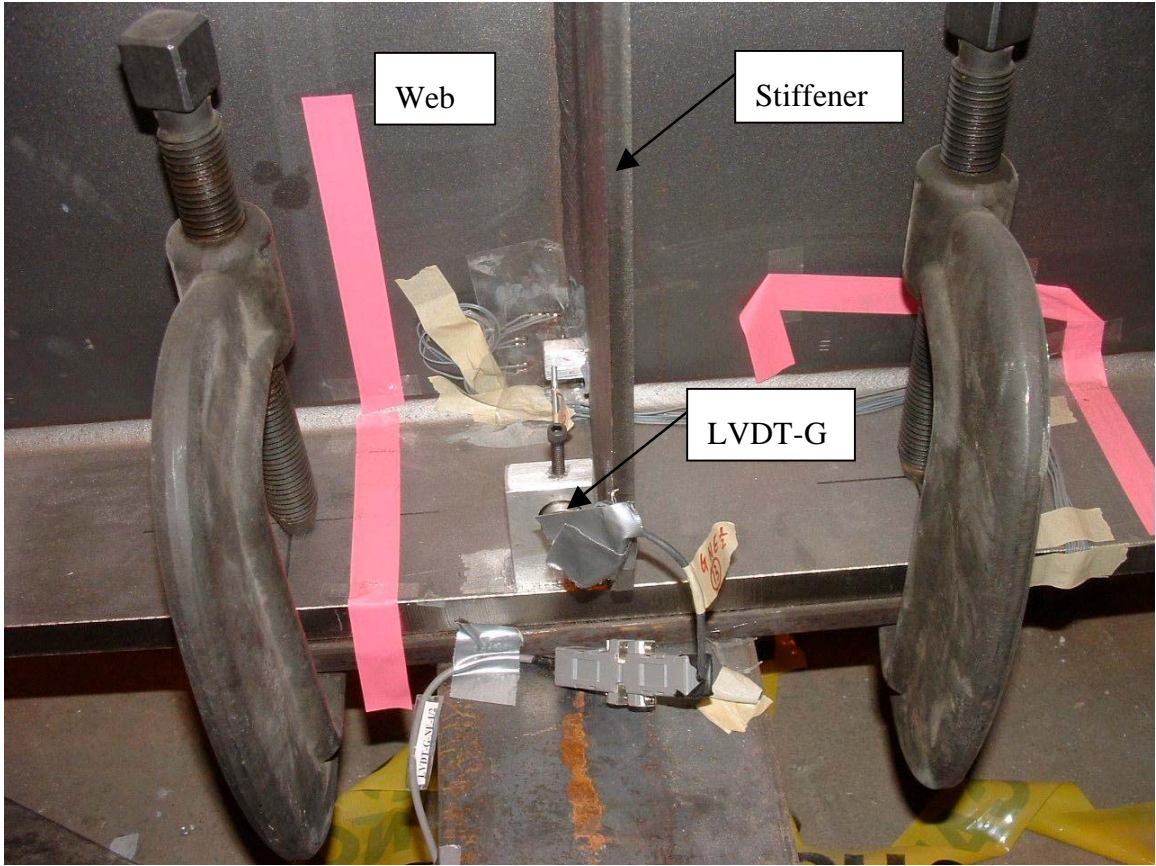


Figure 4.9 LVDTs that measure out-of-plane deflections

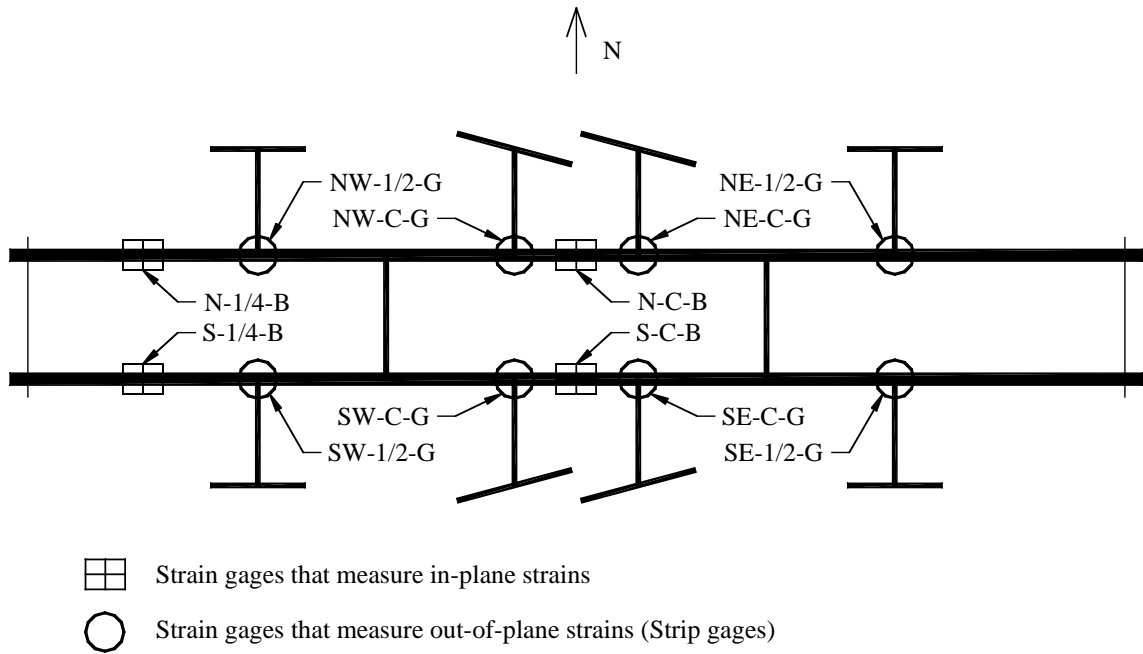


Figure 4.10 Strain gage locations

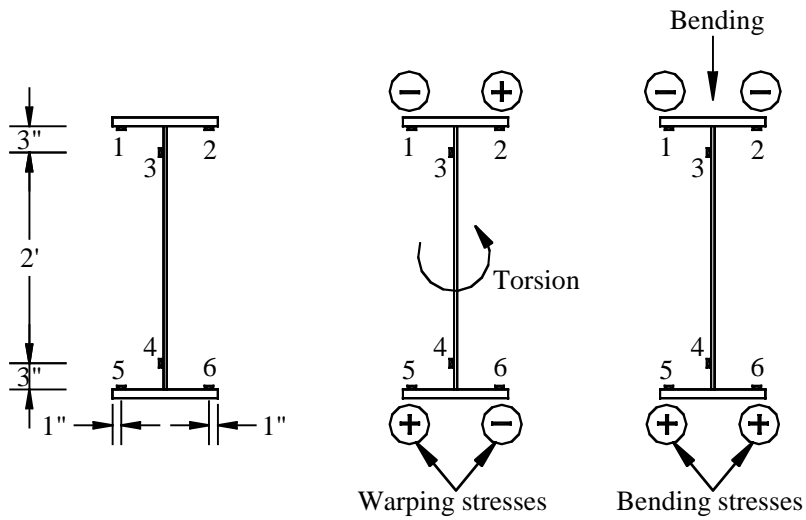


Figure 4.11 Strain gages that measure in-plane strains (Gages 1 and 5 are situated on the south side of the south girder, or north side of the north girder)

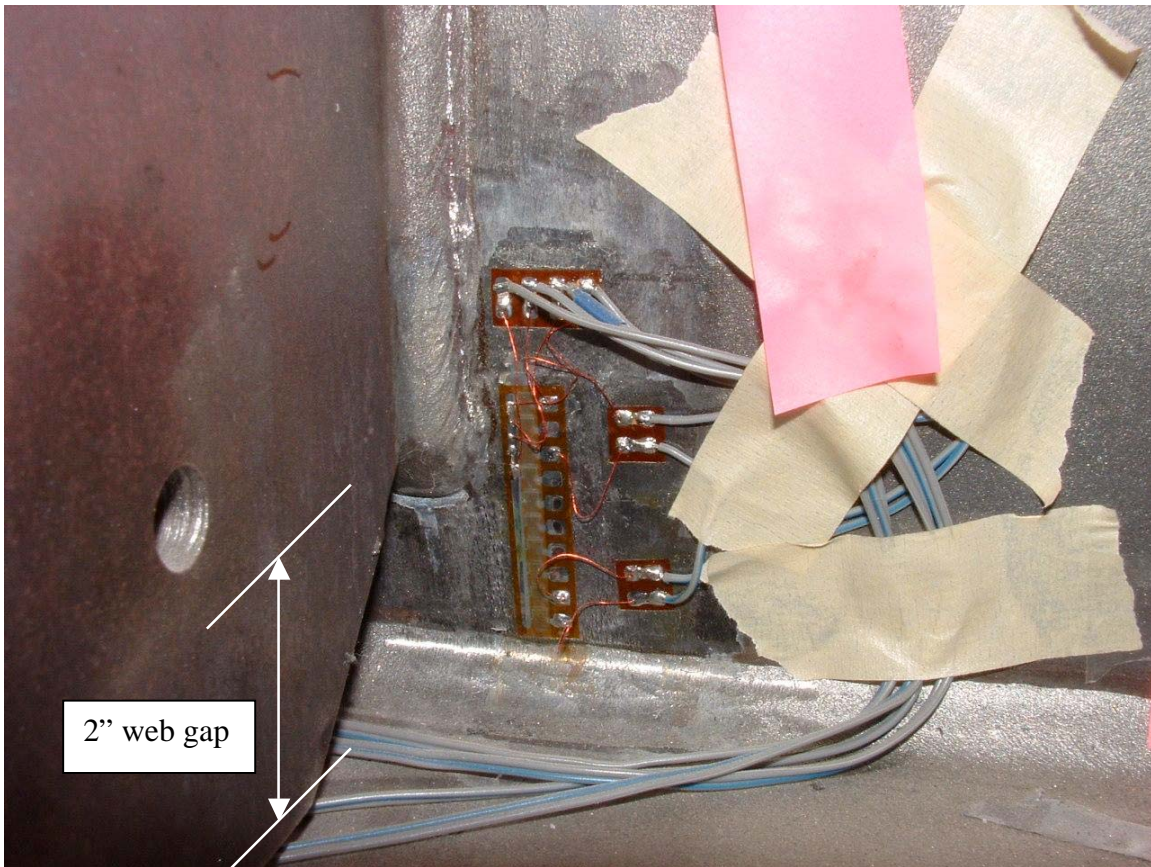
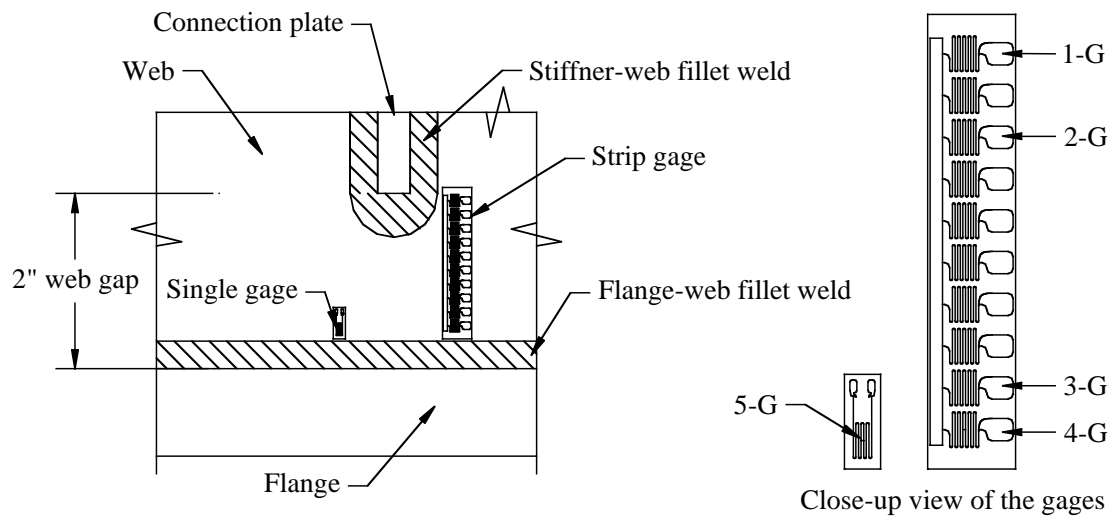
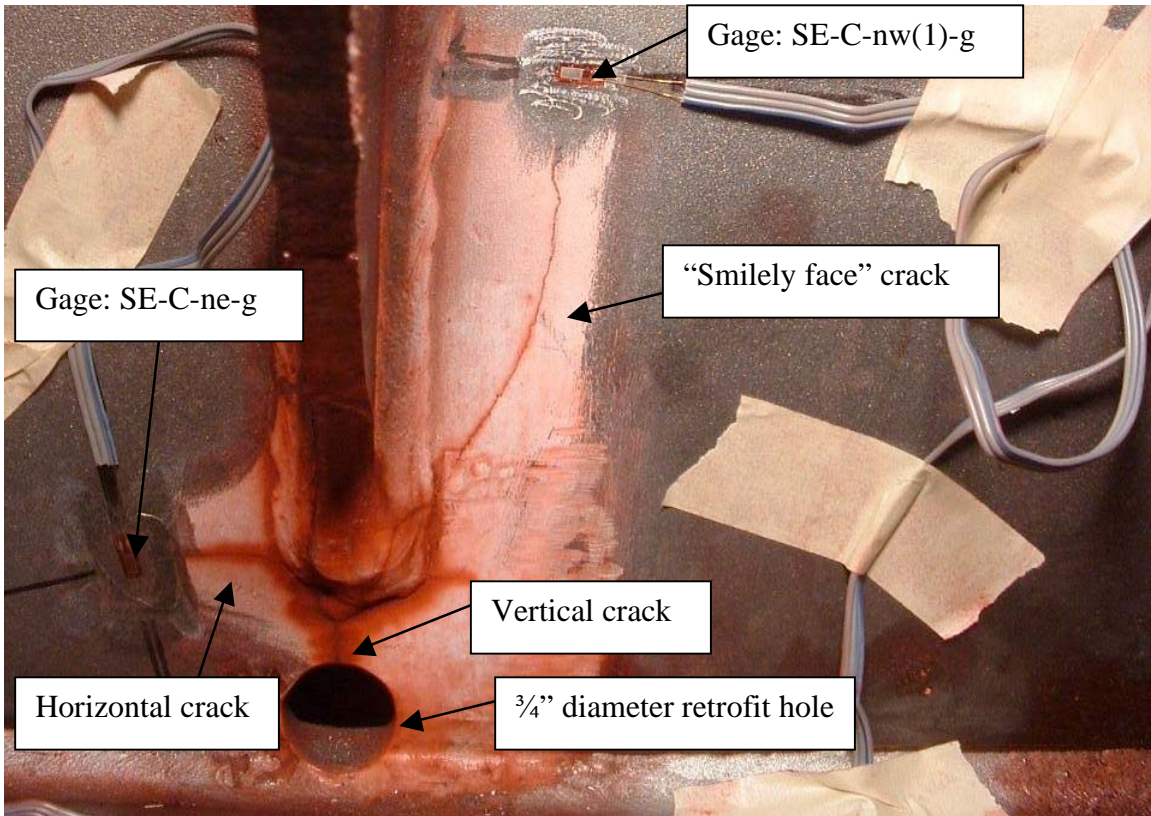
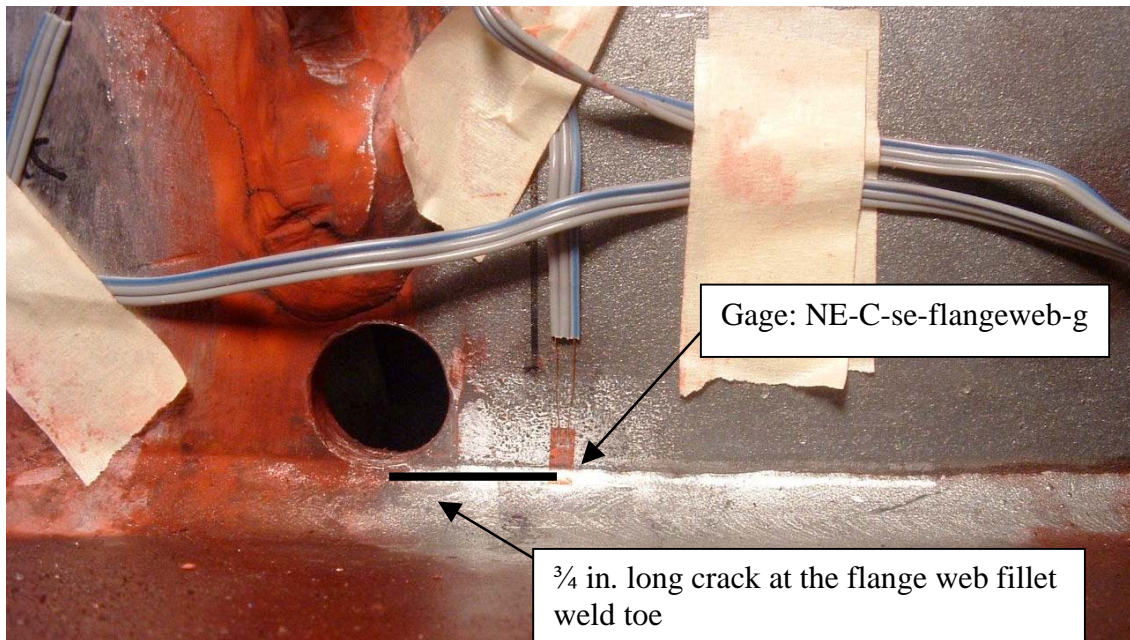


Figure 4.12 Strain gages that measure out-of-plane strains



(a) SE-C



(b) NE-C

Figure 4.13 Strain gages that measure strains at the tip of the crack for web gaps

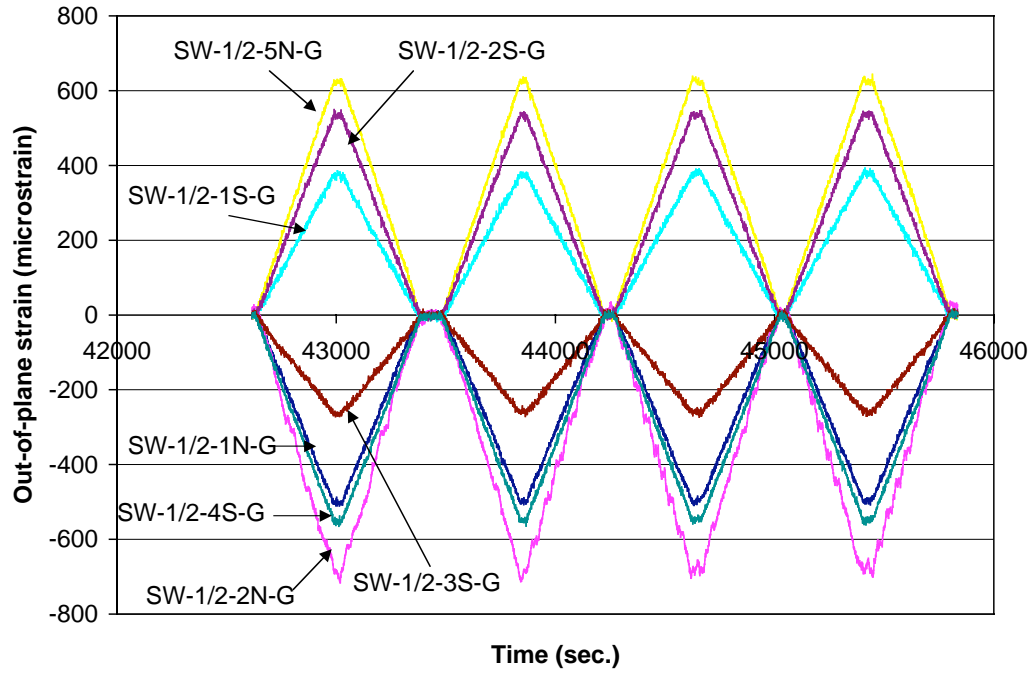


Figure 4.14 Measured out-of-plane strains at SW-1/2 web gap before cyclic loading

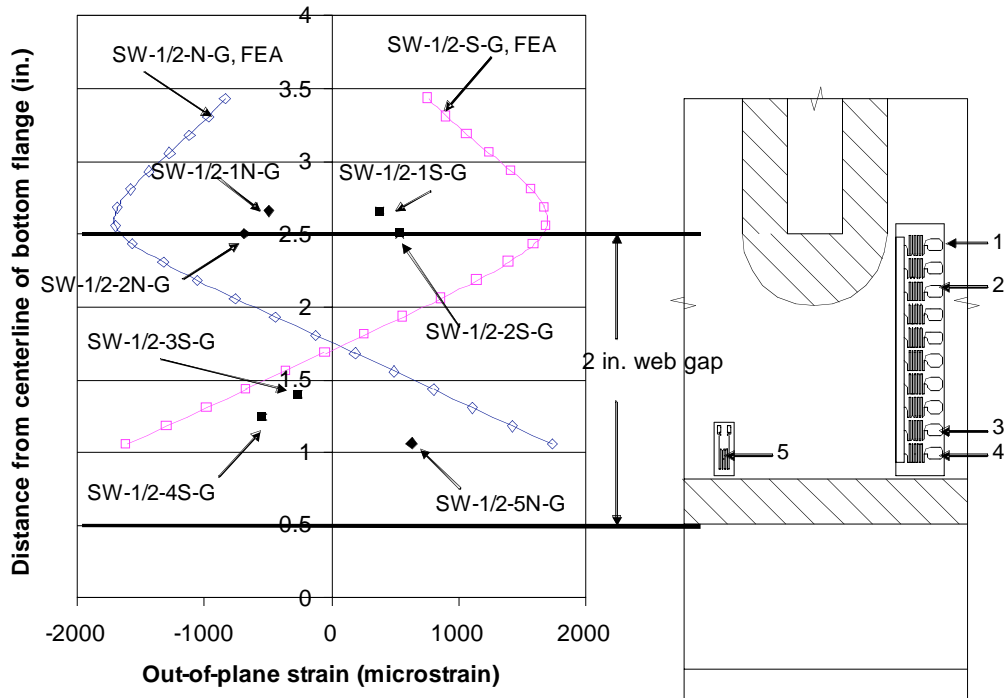
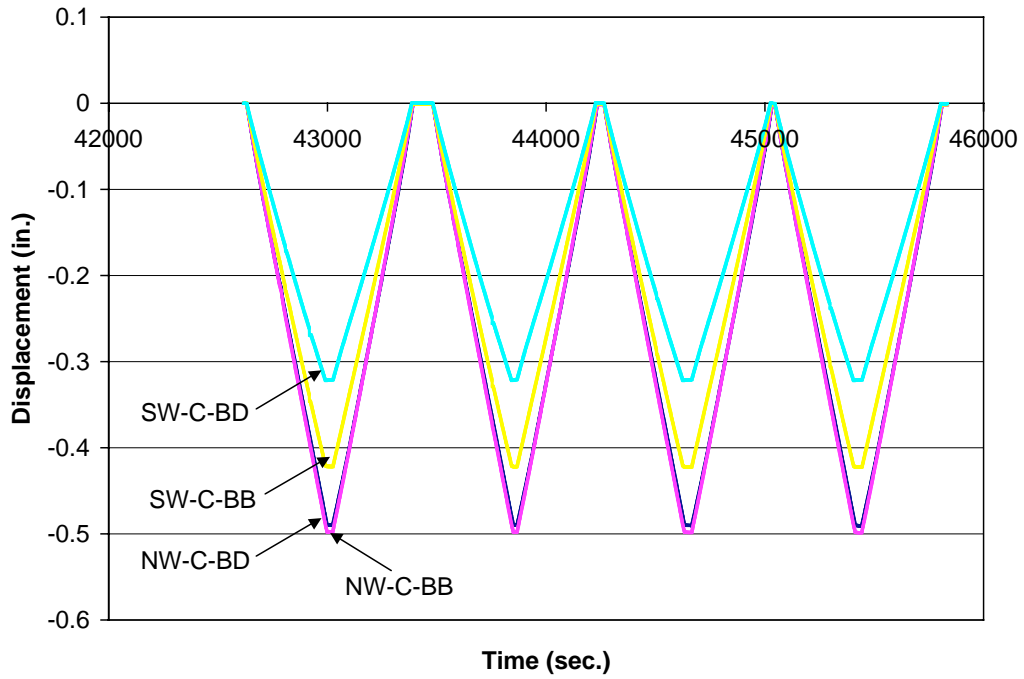
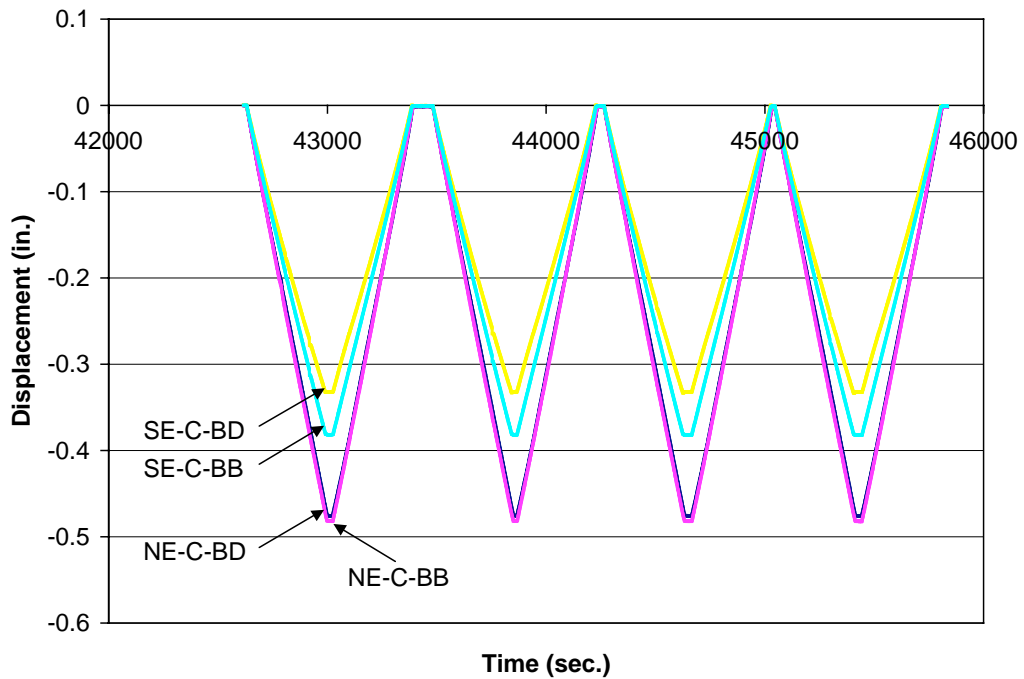


Figure 4.15 Comparison of measured out-of-plane strains with FEA predicted out-of-plane strains at SW-1/2 web gap



(a) at NW-C and SW-C



(b) at NE-C and SE-C

Figure 4.16 In-plane deflection for LVDT locations before cyclic loading

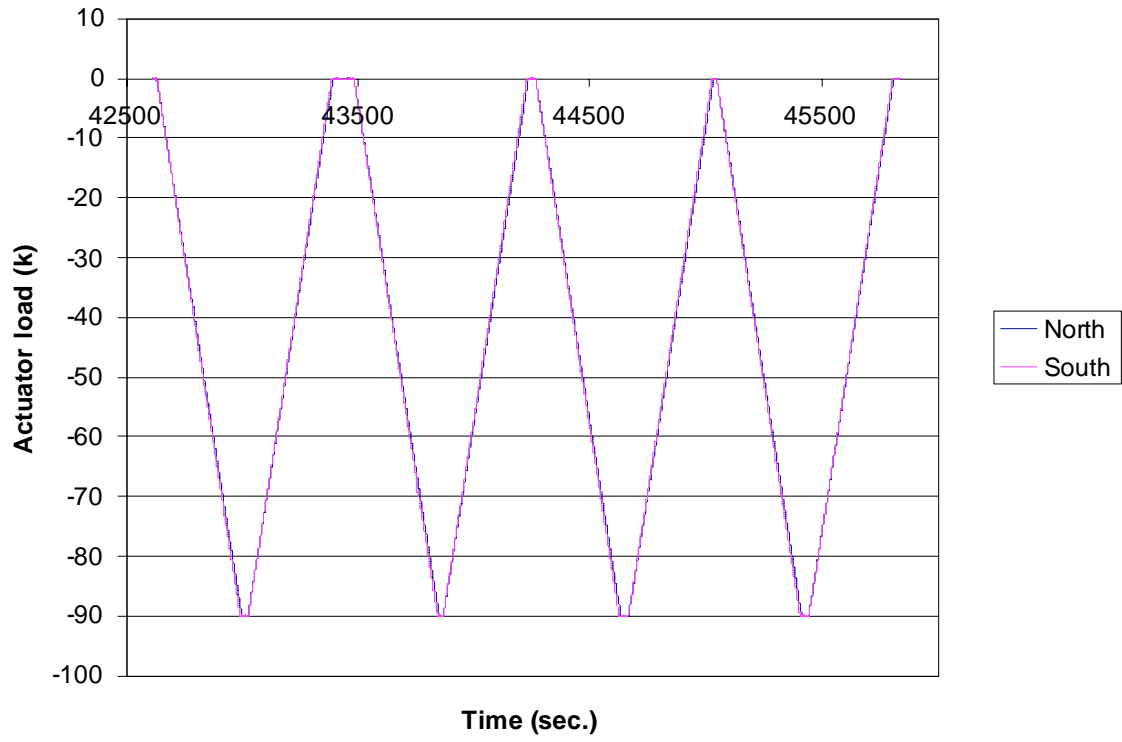


Figure 4.17 Actuator load vs. time before cyclic loading

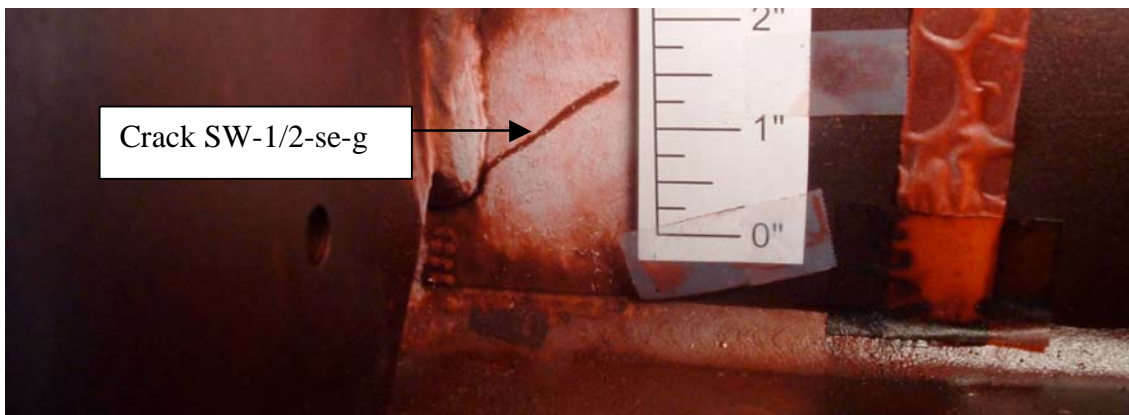
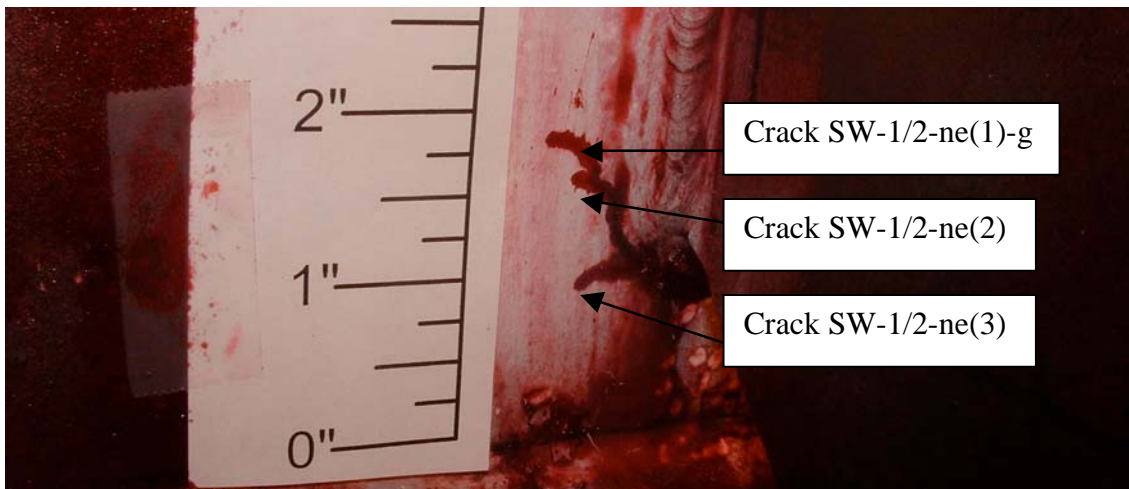
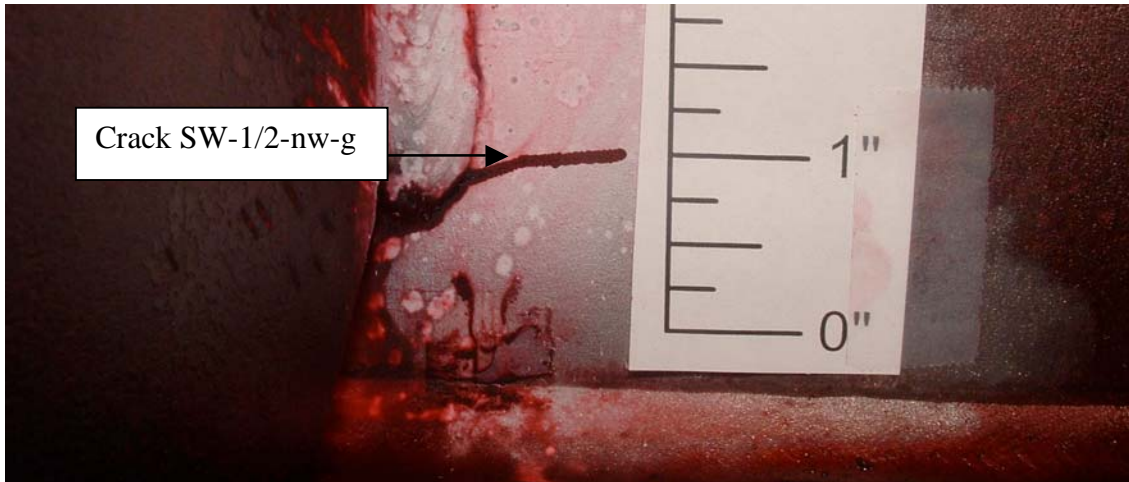
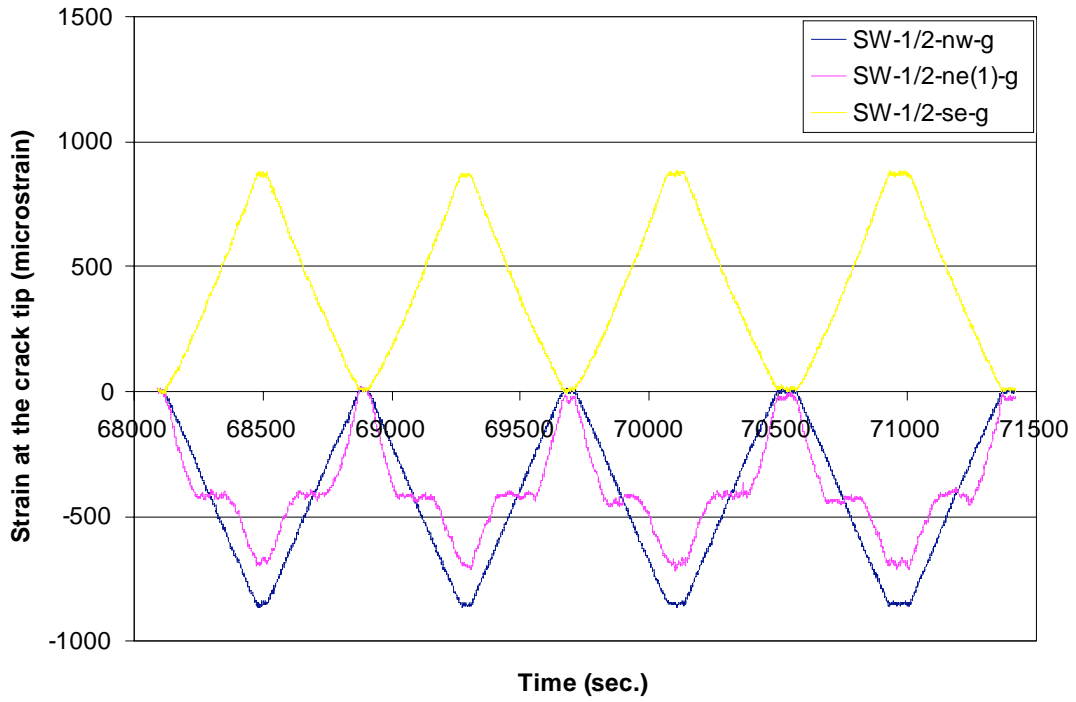
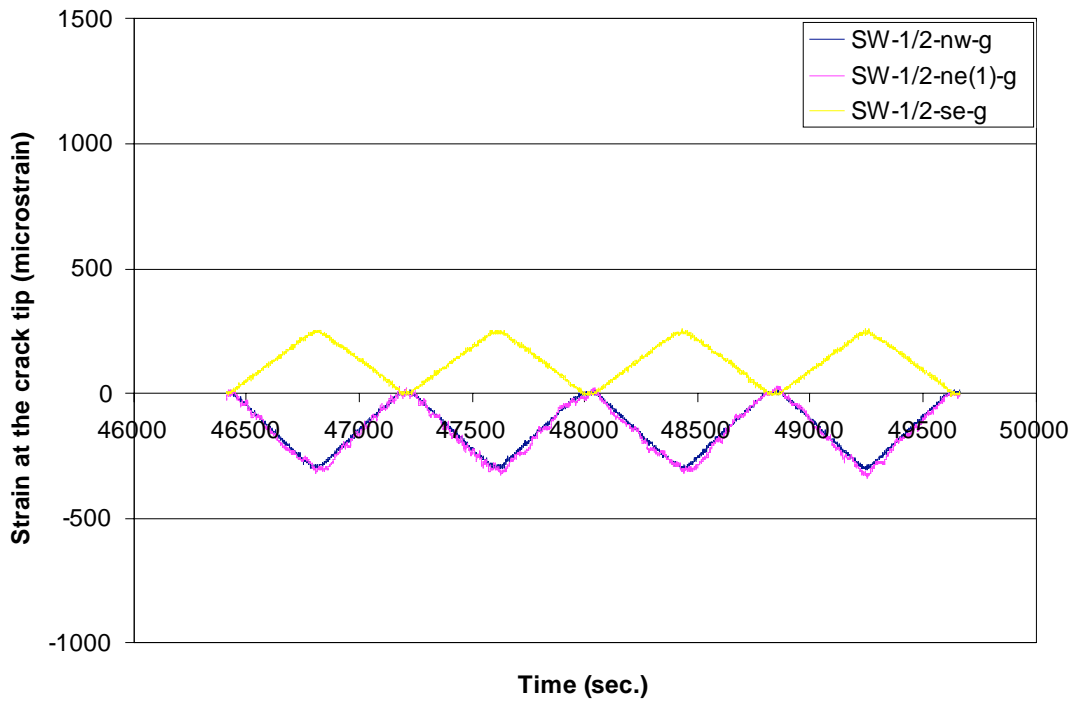


Figure 4.18 Picture of cracks at web gap SW-1/2 at 1,101,000 cycles



(a) before retrofit



(b) after retrofit

Figure 4.19 Measured strains at the crack tips at web gap SW-1/2

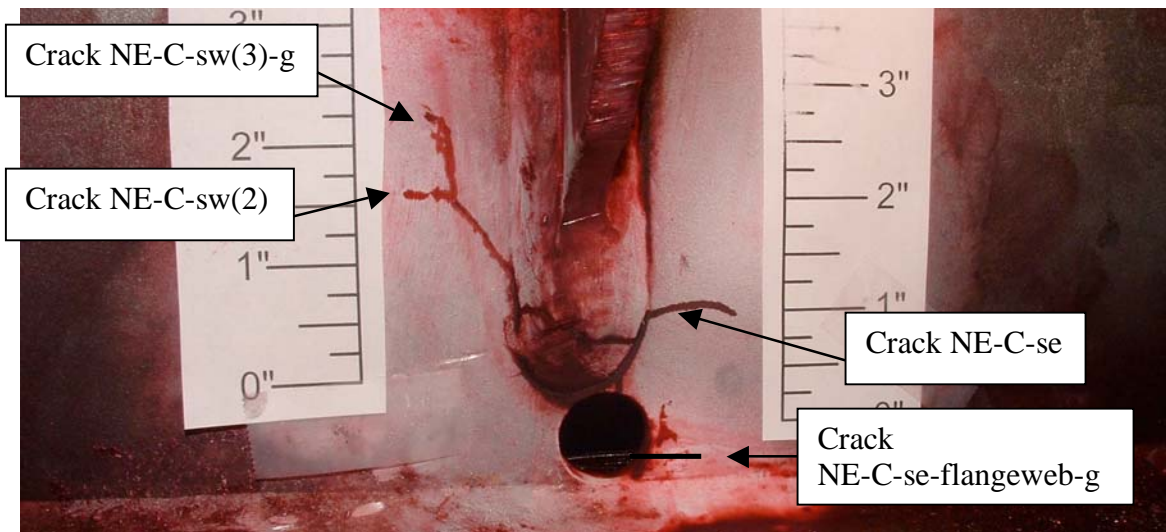
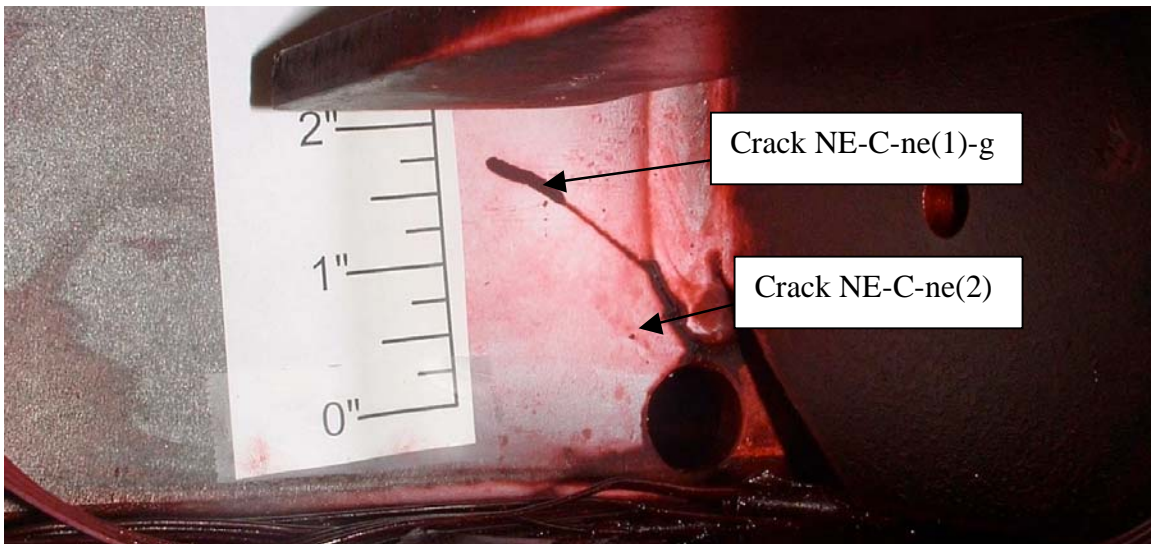
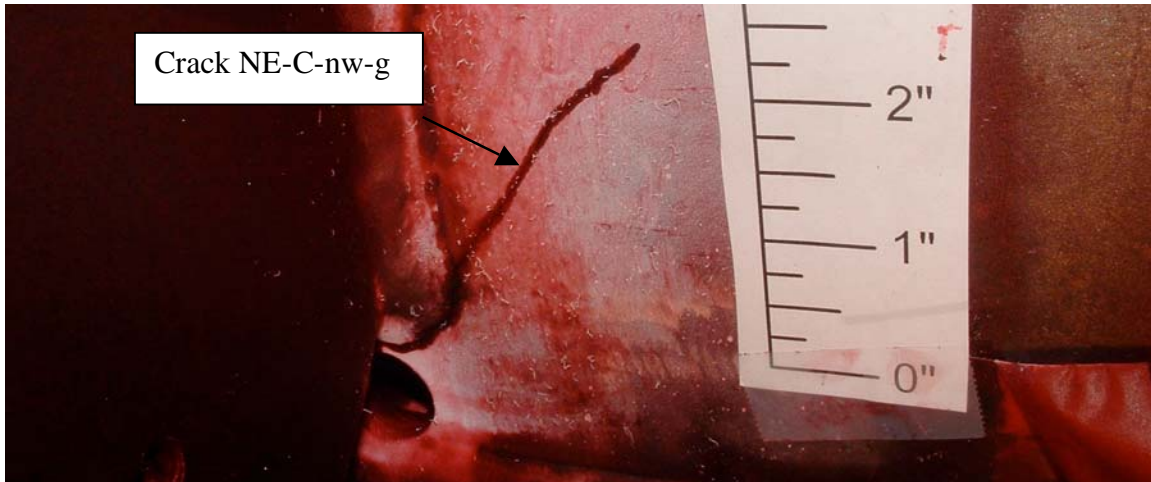
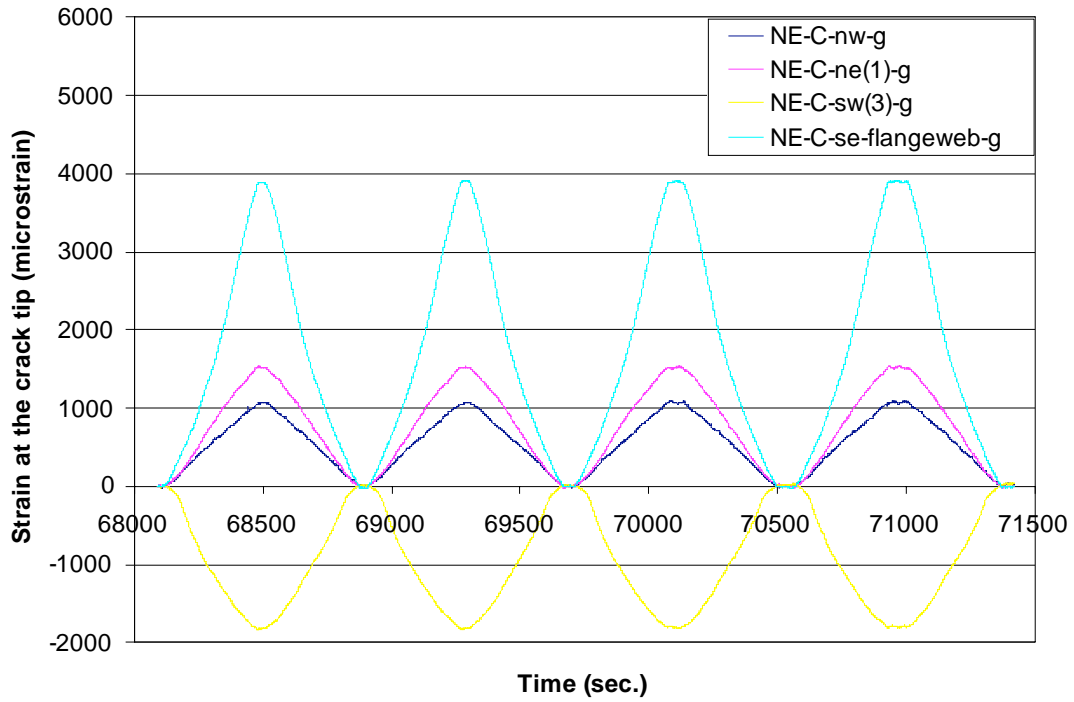
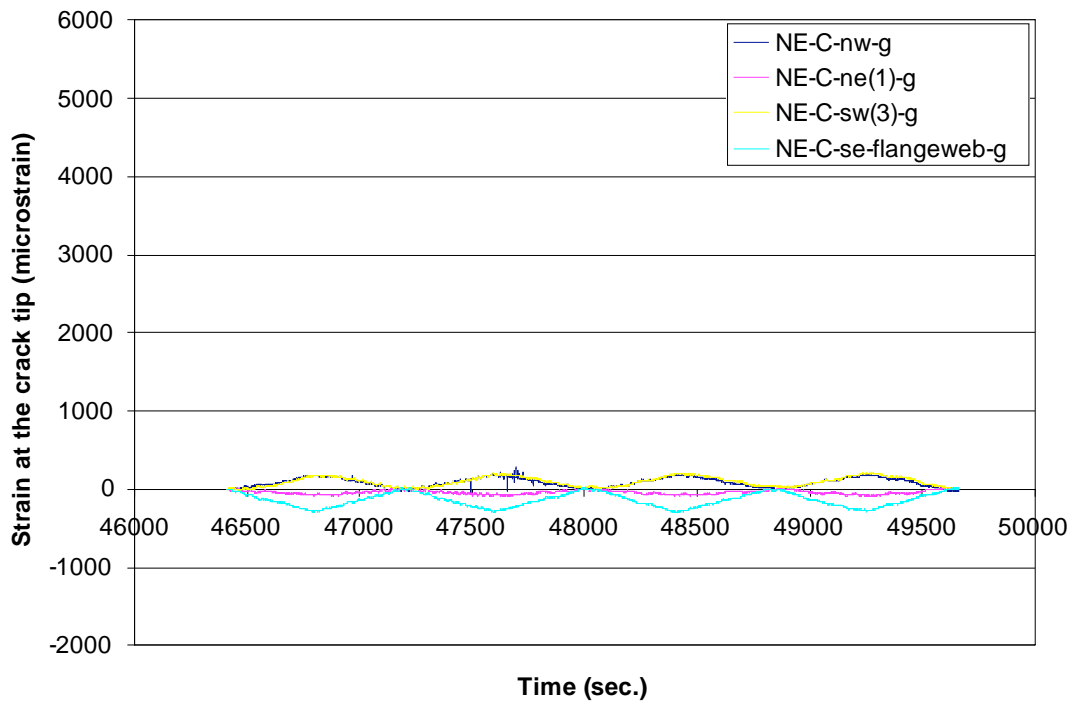


Figure 4.20 Picture of cracks at web gap NE-C at 1,101,000 cycles



(a) before retrofit



(b) after retrofit

Figure 4.21 Measured strains at the crack tips at web gap NE-C

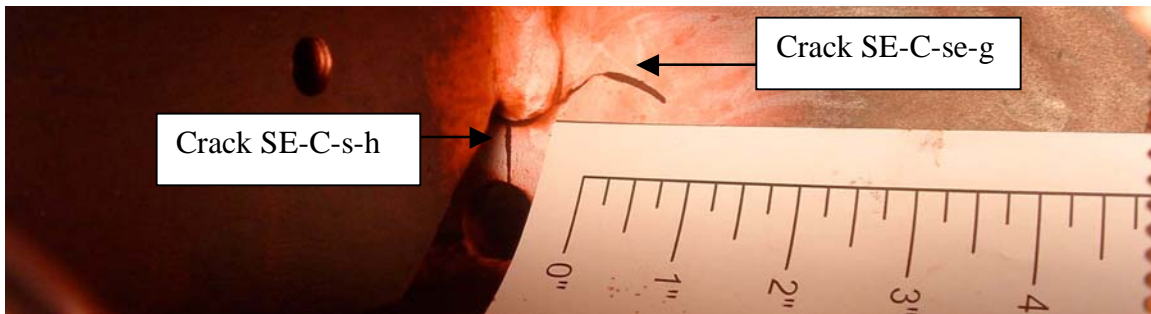
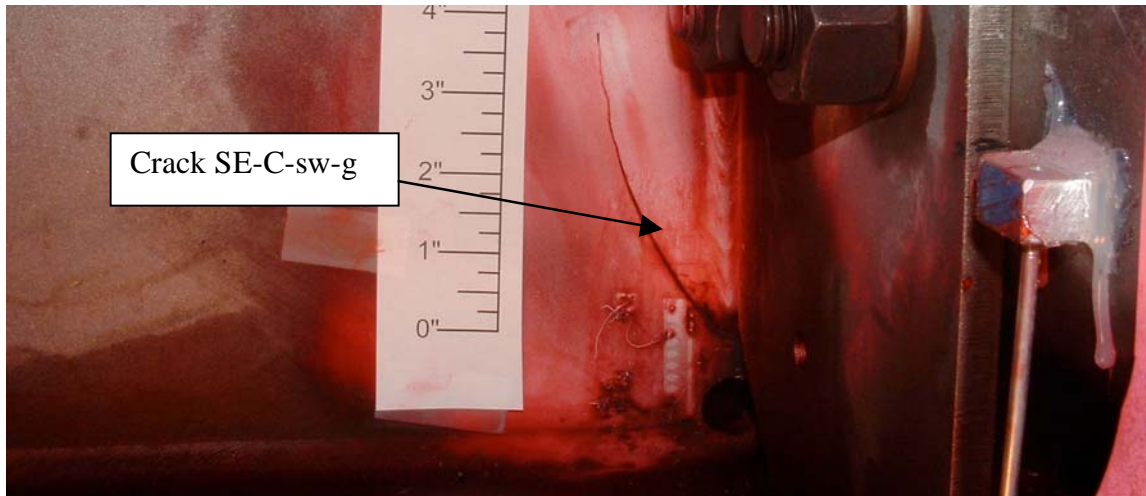
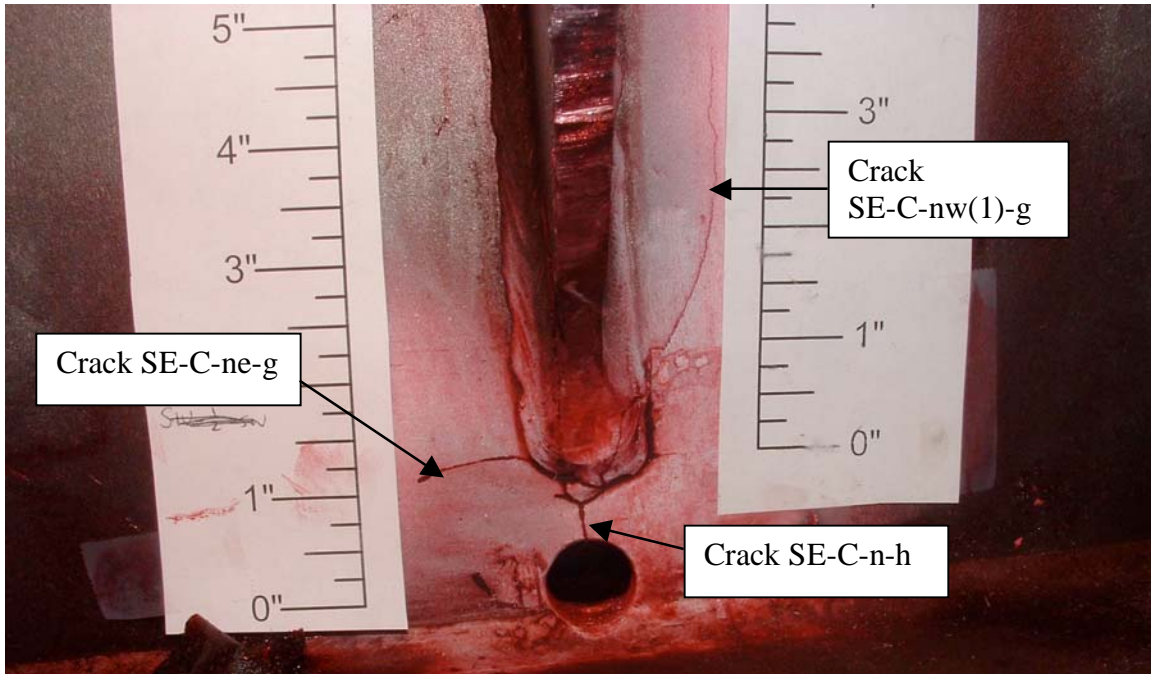
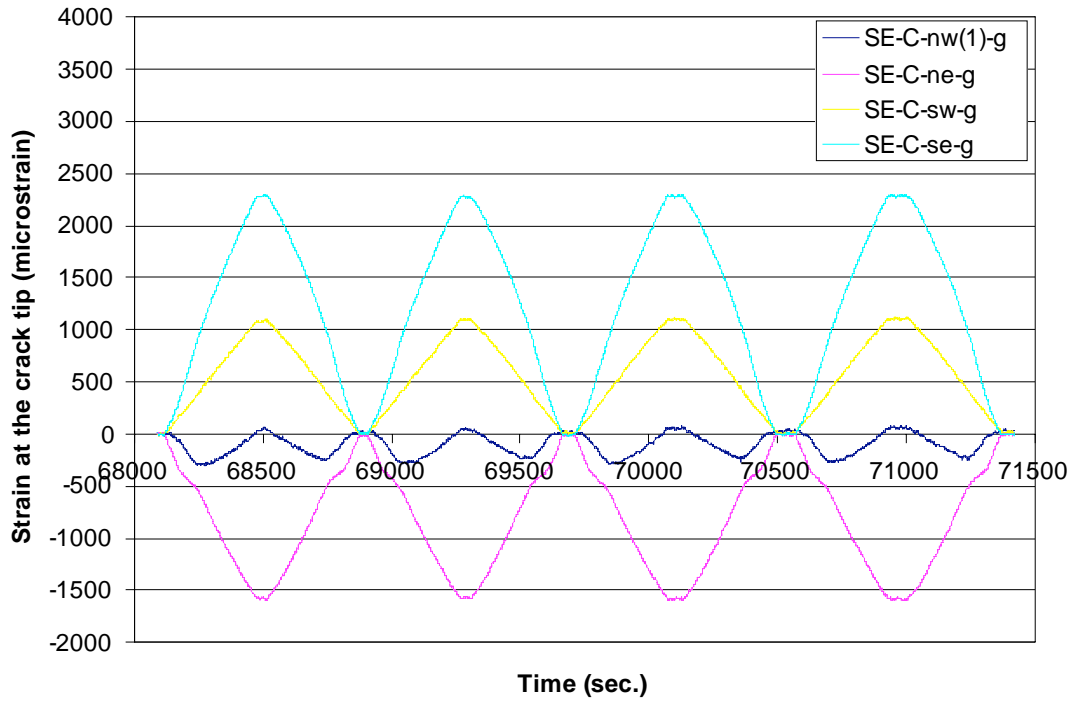
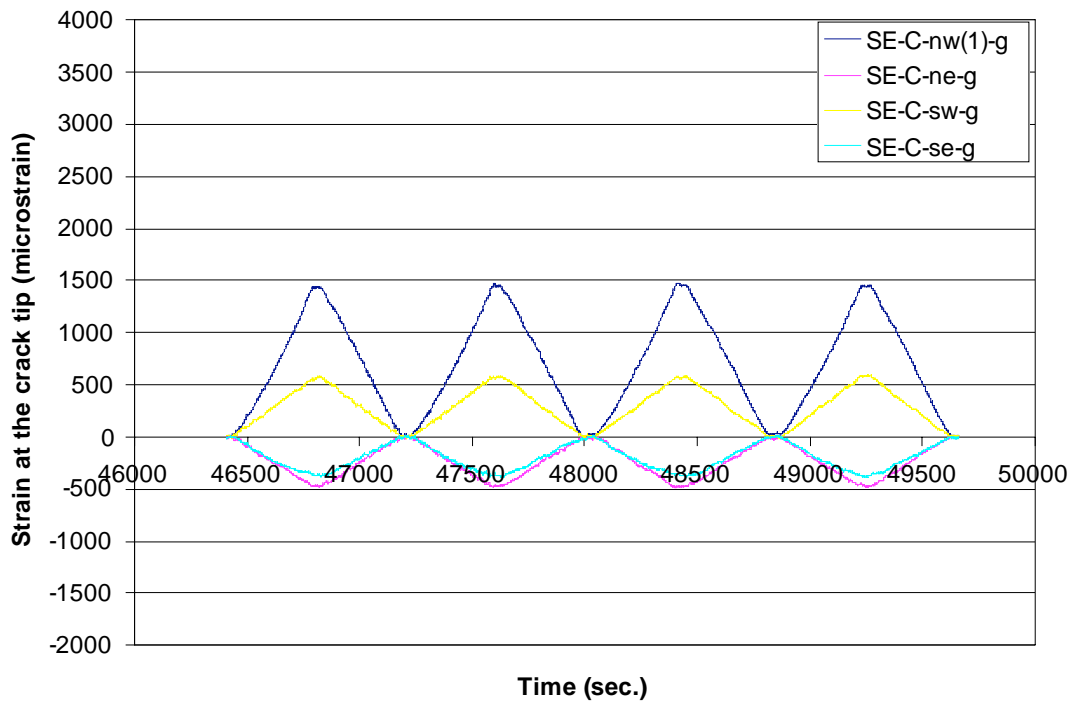


Figure 4.22 Picture of cracks at web gap SE-C at 1,101,000 cycles



(a) before retrofit



(b) after retrofit

Figure 4.23 Measured strains at the crack tips at web gap SE-C

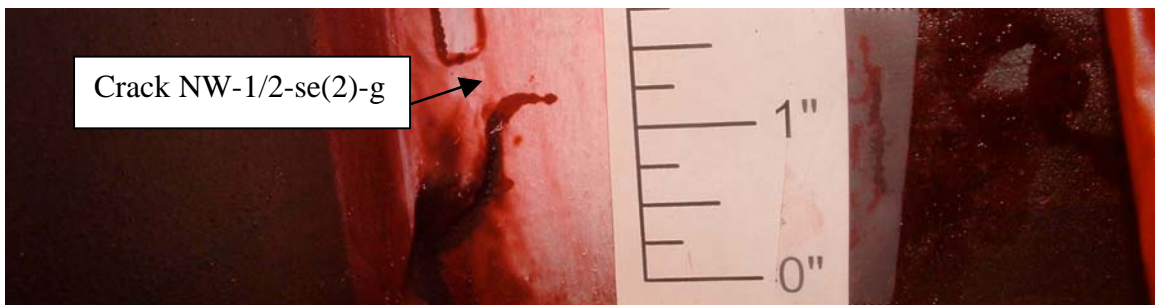
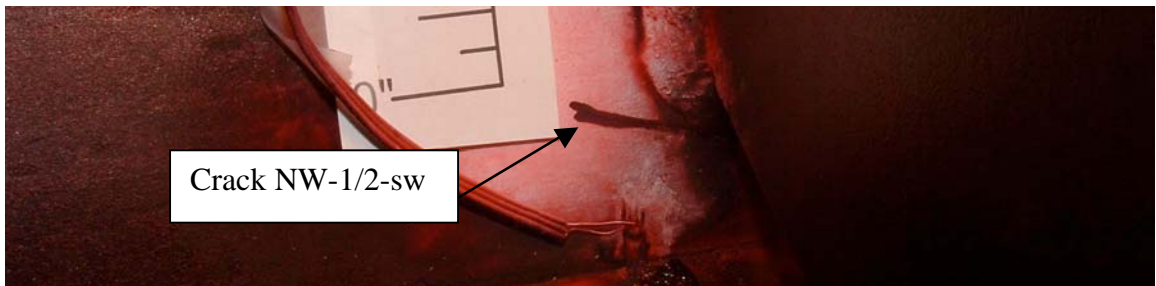
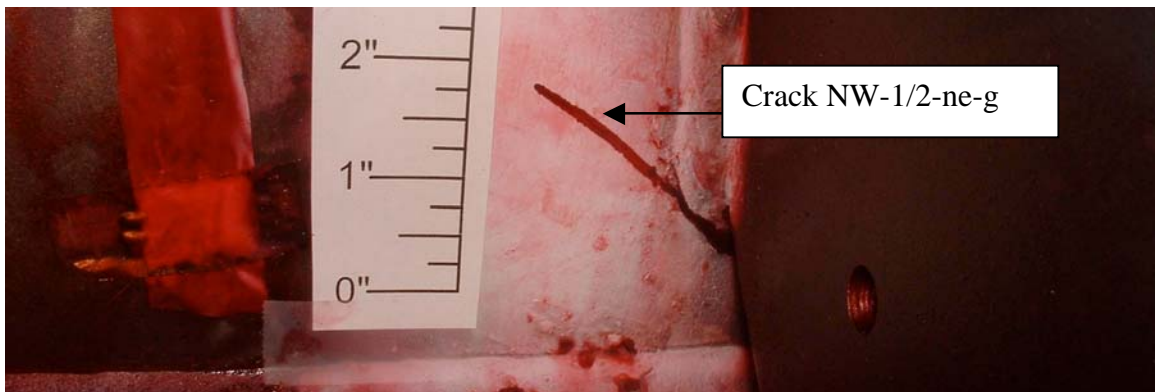
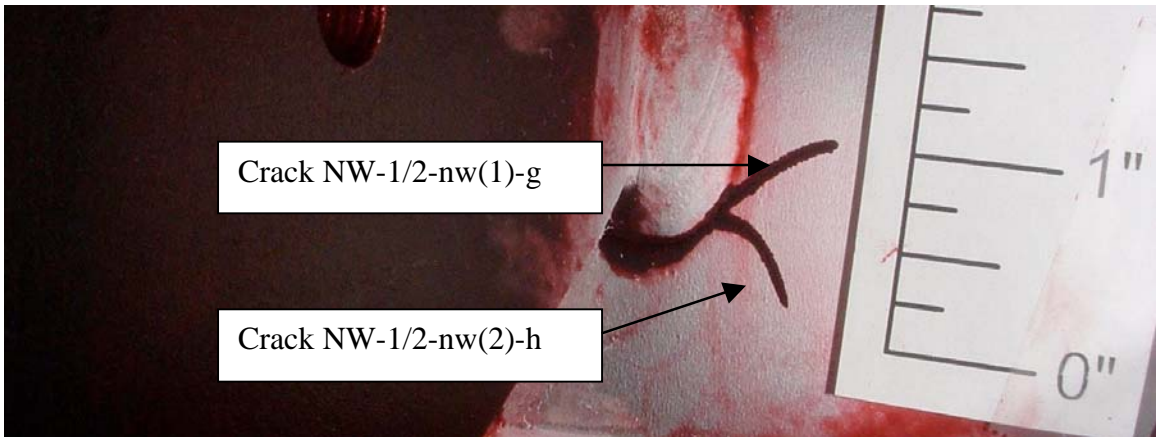
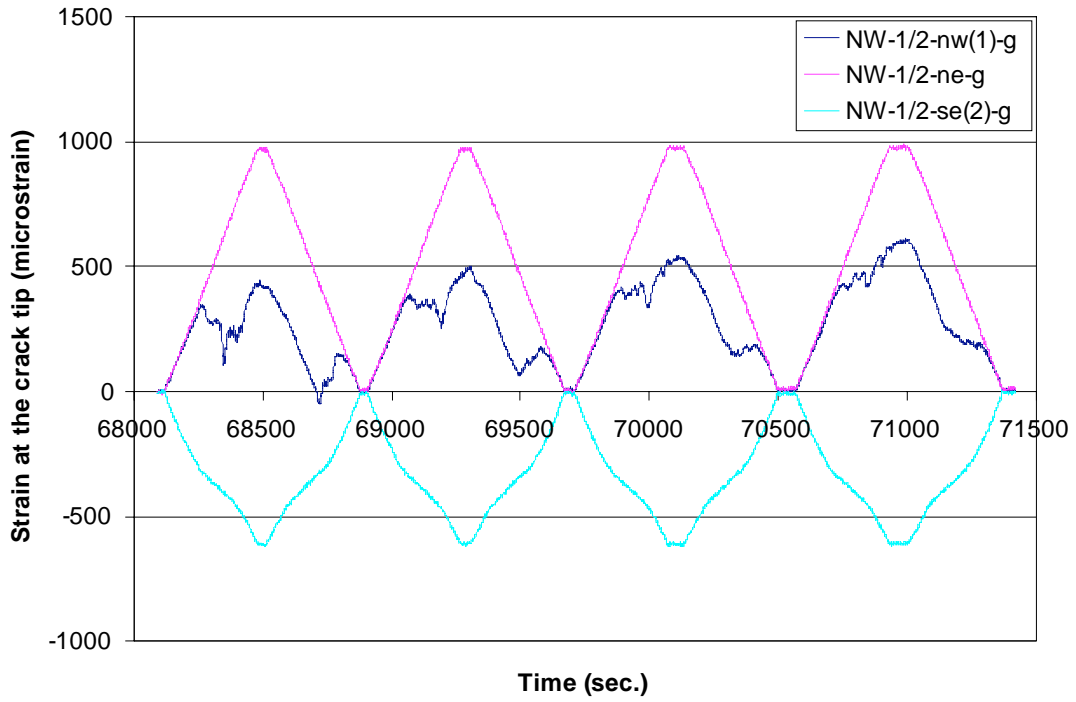
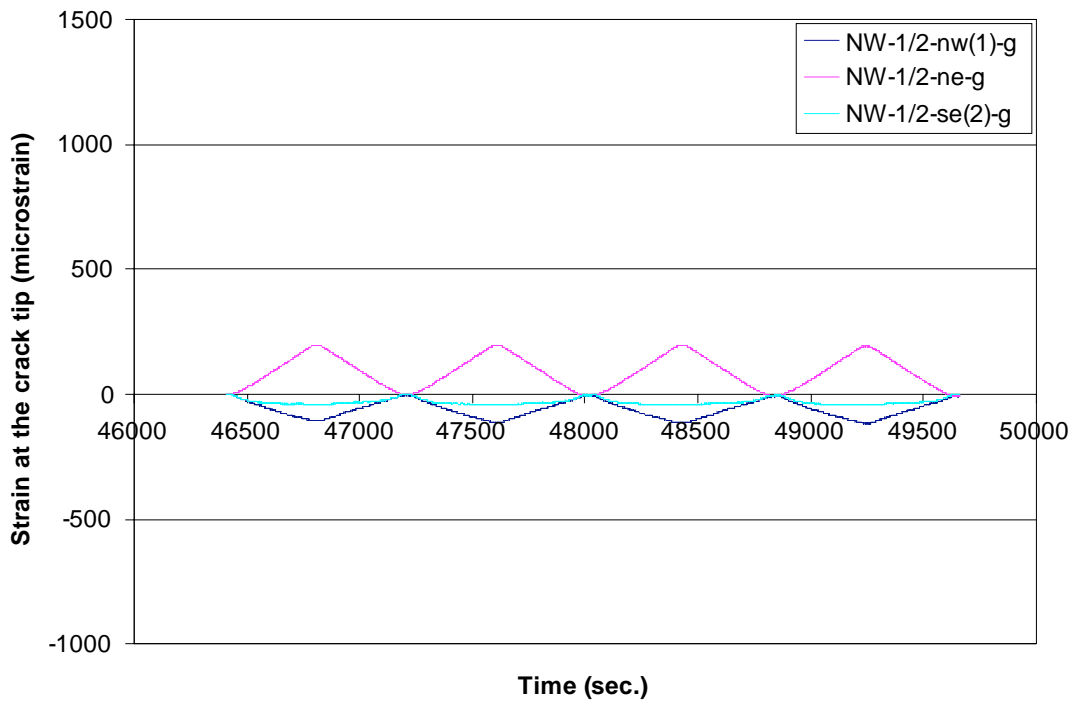


Figure 4.24 Picture of cracks at web gap NW-1/2 at 1,101,000 cycles



(a) before retrofit



(b) after retrofit

Figure 4.25 Measured strains at the crack tips at web gap NW-1/2

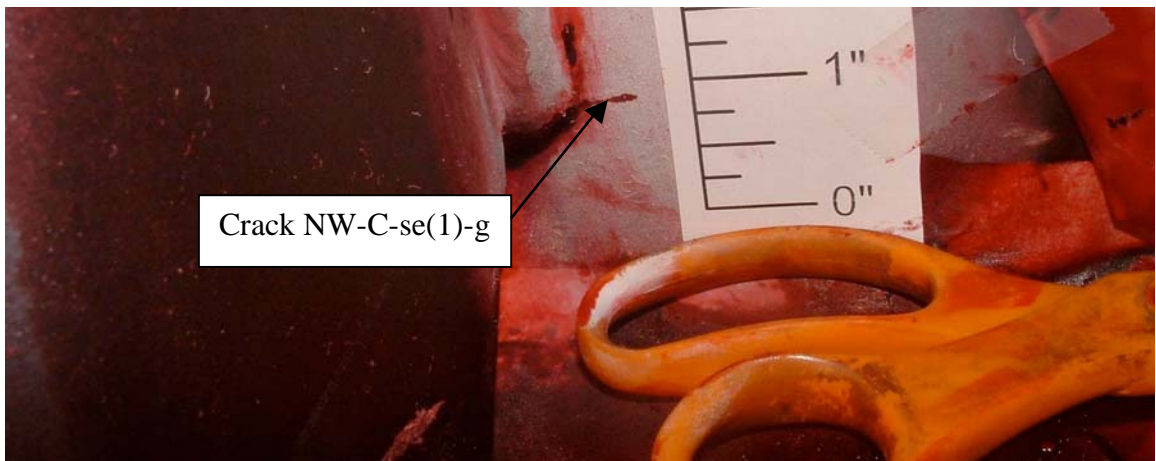
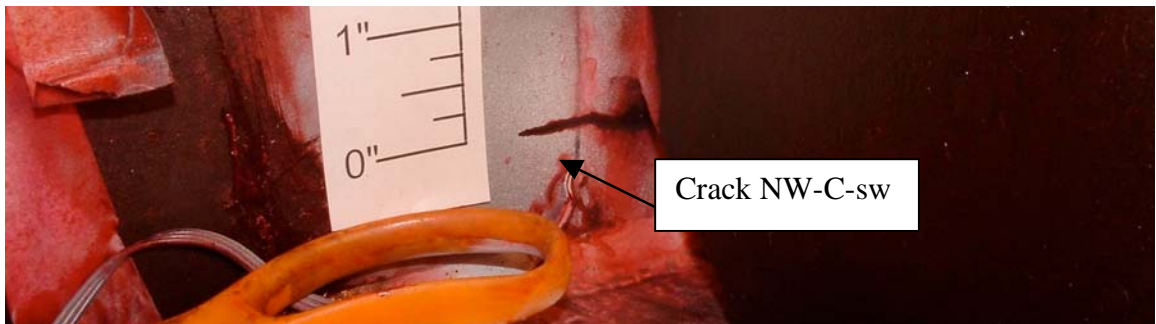
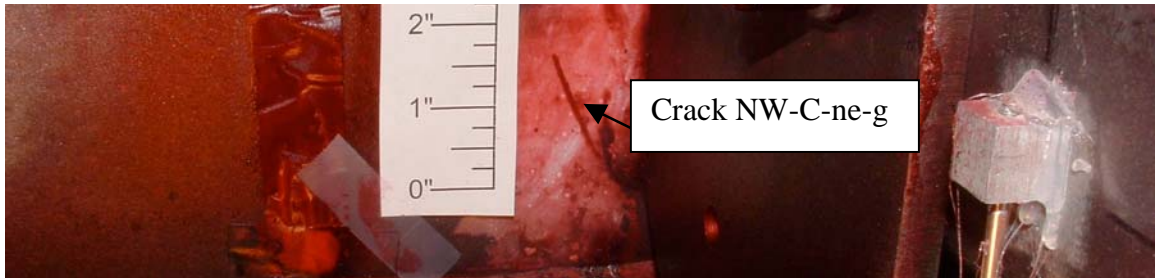
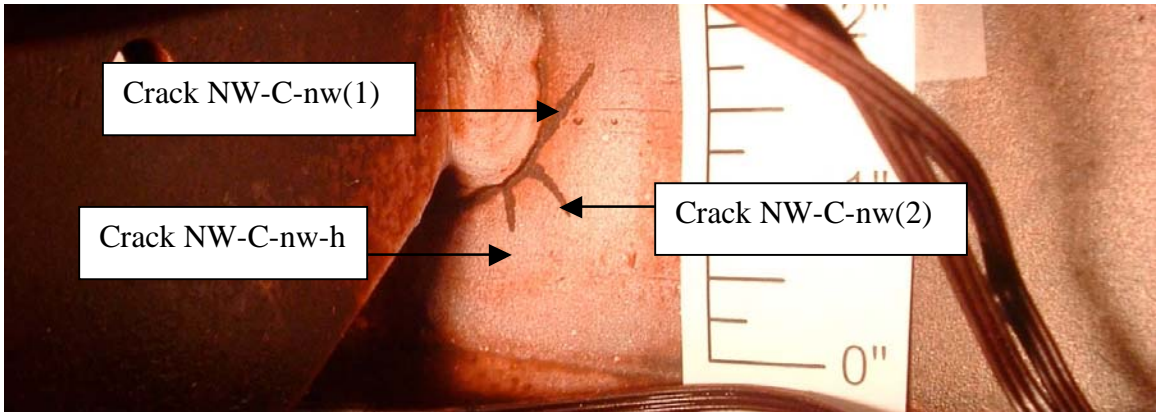
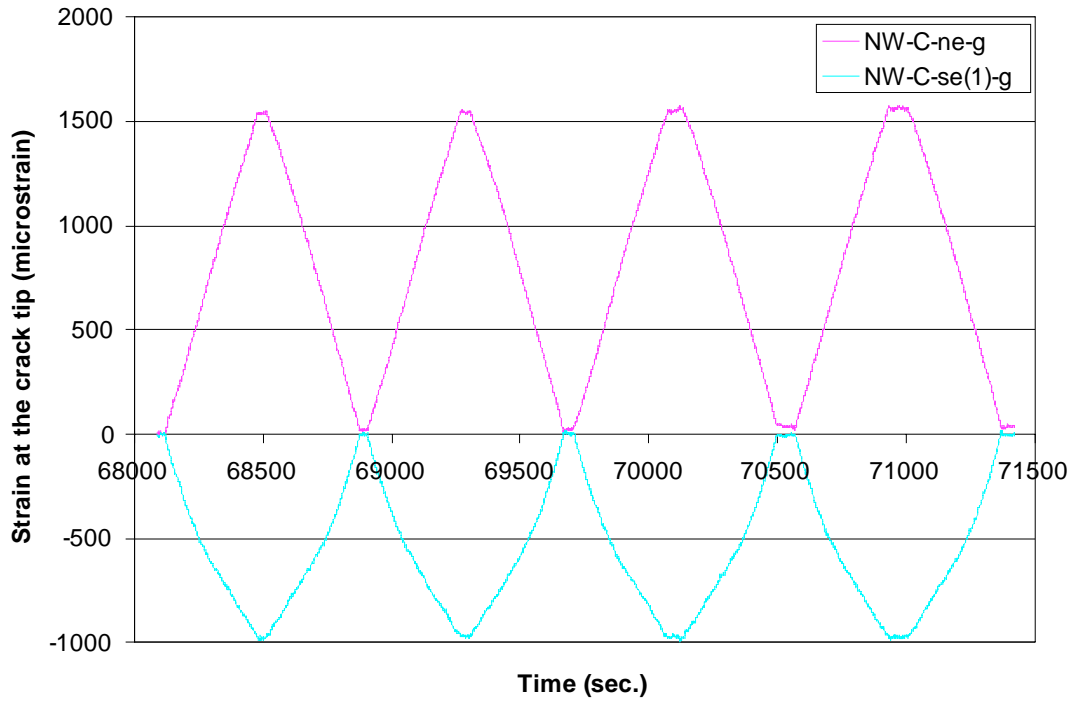
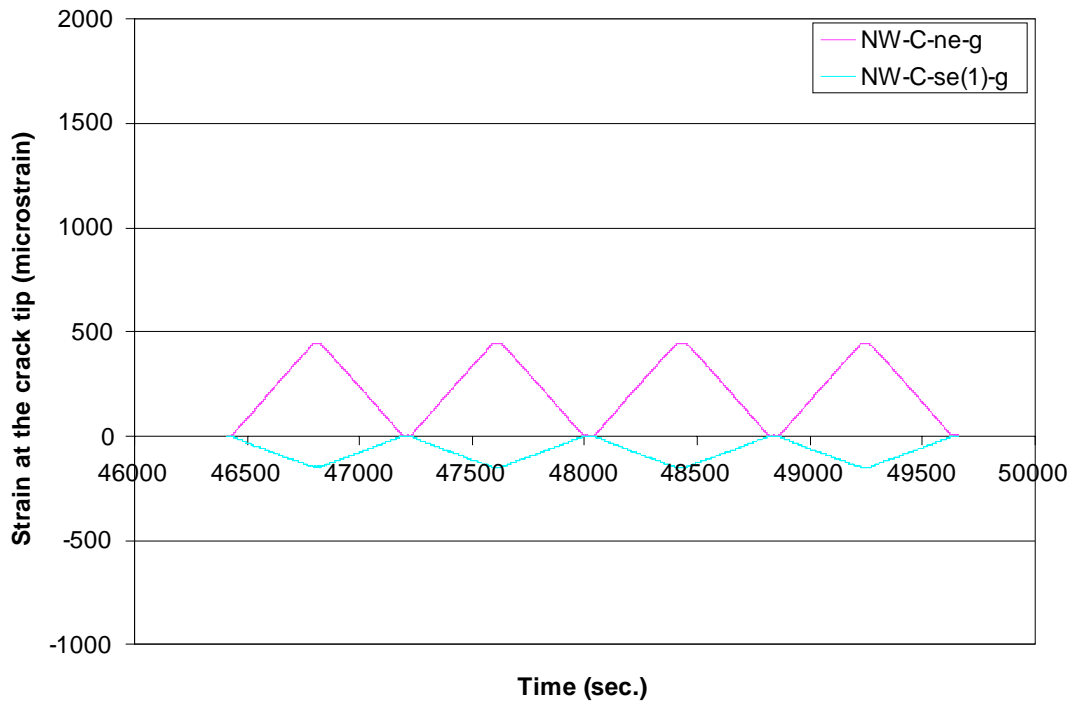


Figure 4.26 Picture of cracks at web gap NW-C at 1,101,000 cycles



(a) before retrofit



(b) after retrofit

Figure 4.27 Measured strains at the crack tips at web gap NW-C

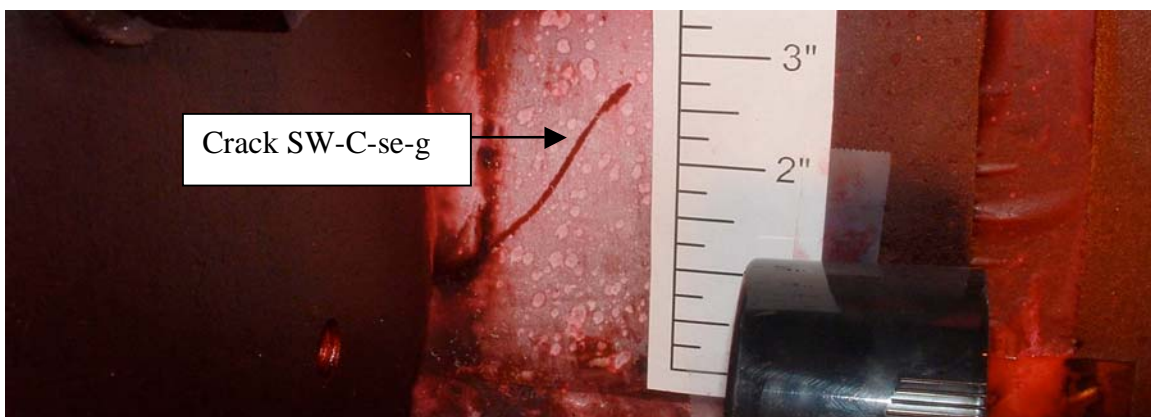
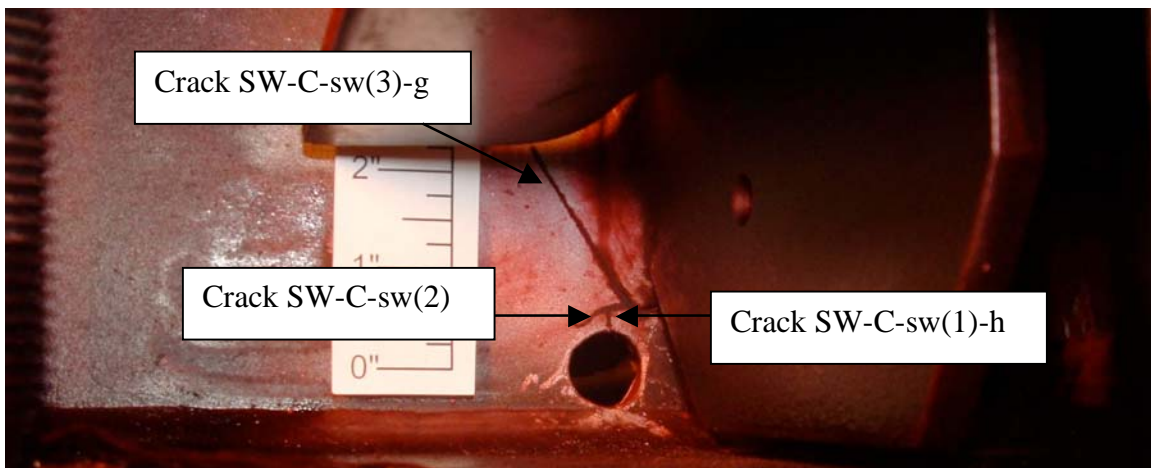
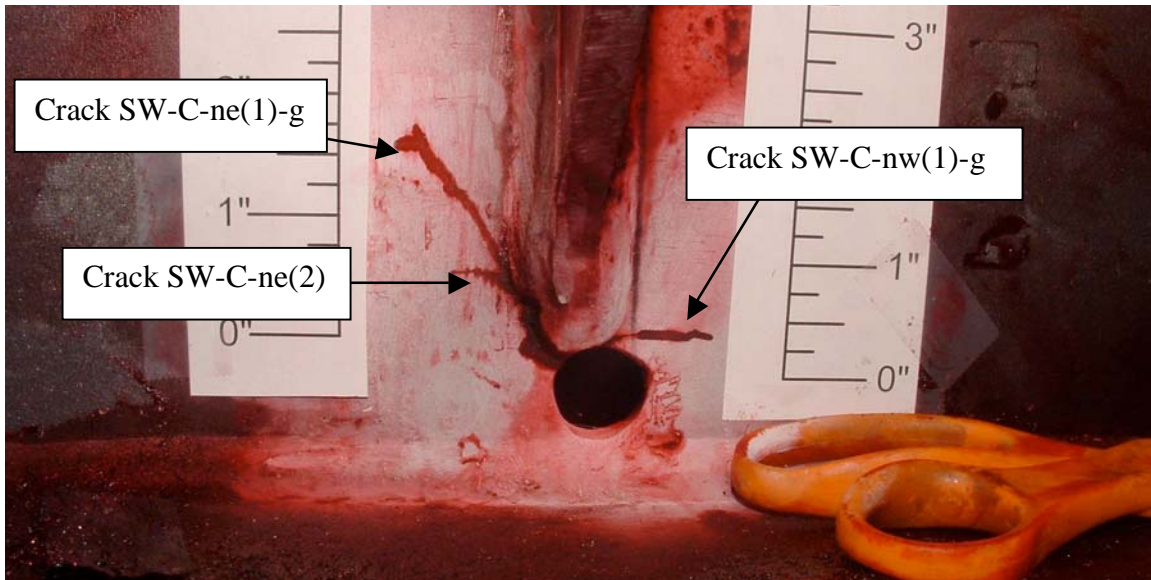
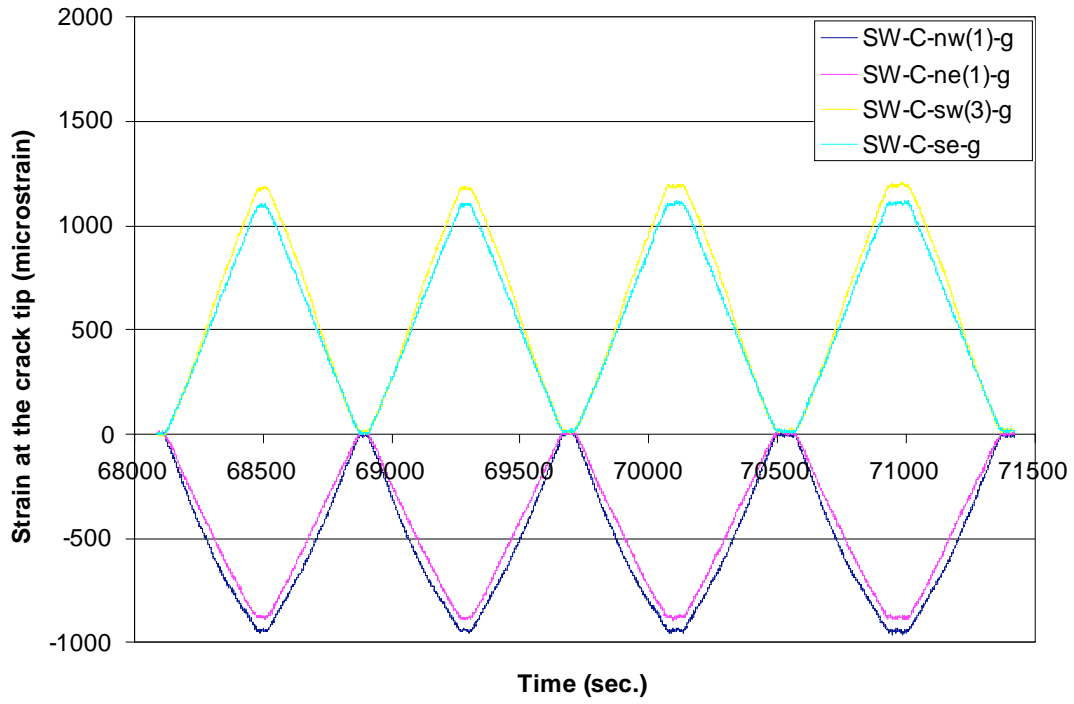
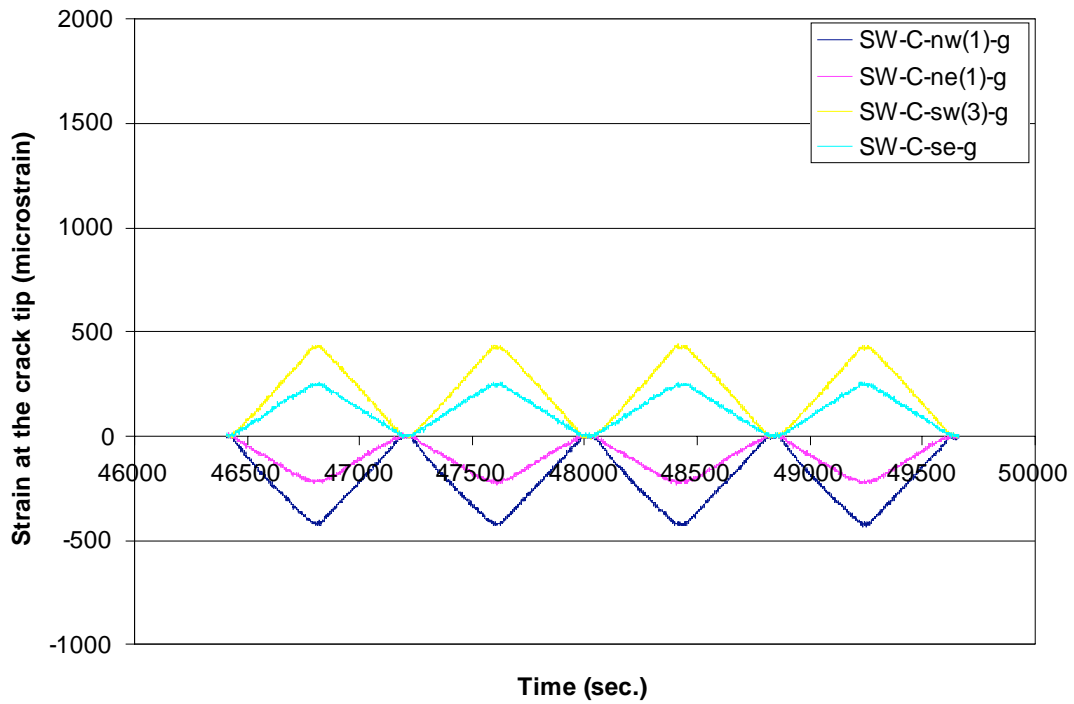


Figure 4.28 Picture of cracks at web gap SW-C at 1,101,000 cycles



(a) before retrofit



(b) after retrofit

Figure 4.29 Measured strains at the crack tips at web gap SW-C

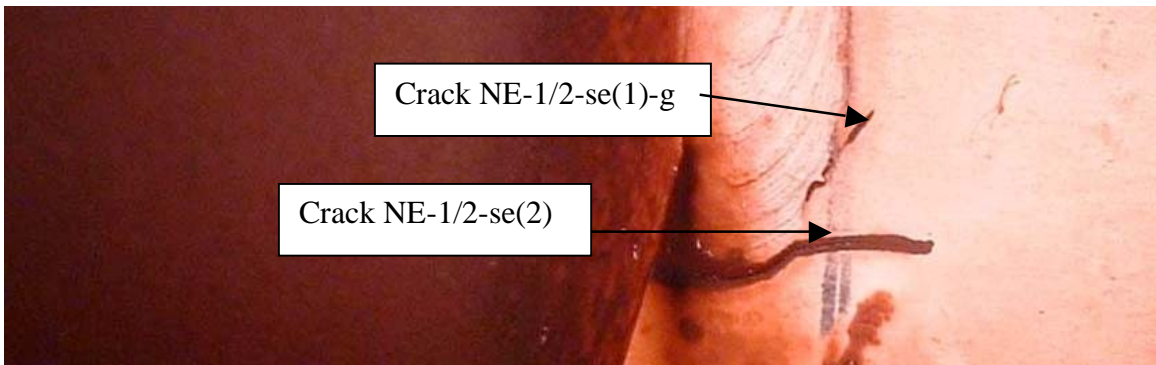
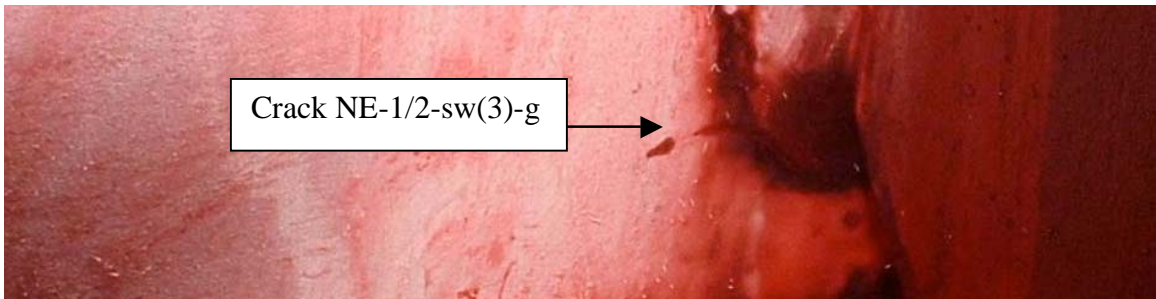
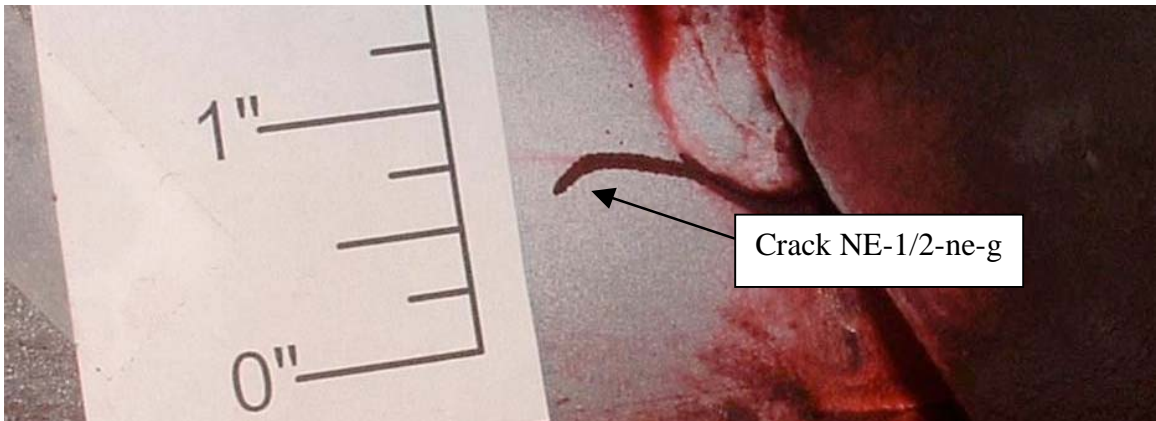
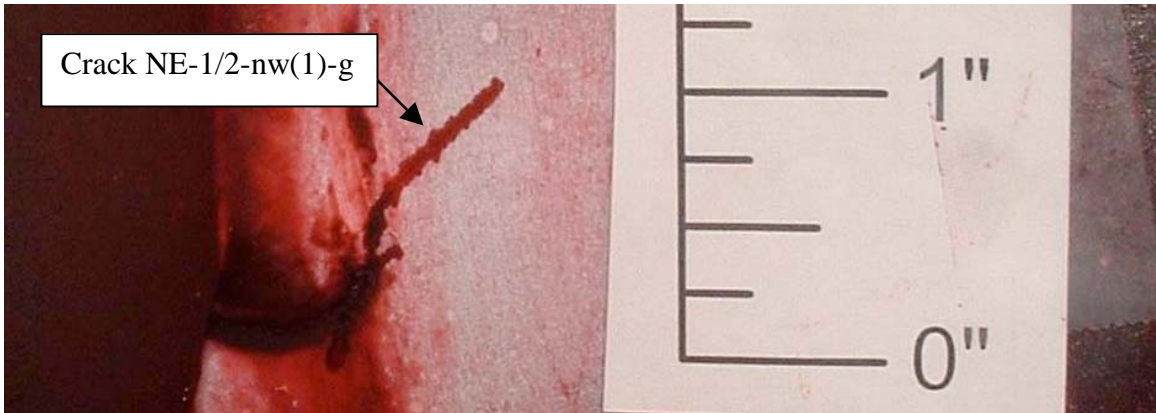
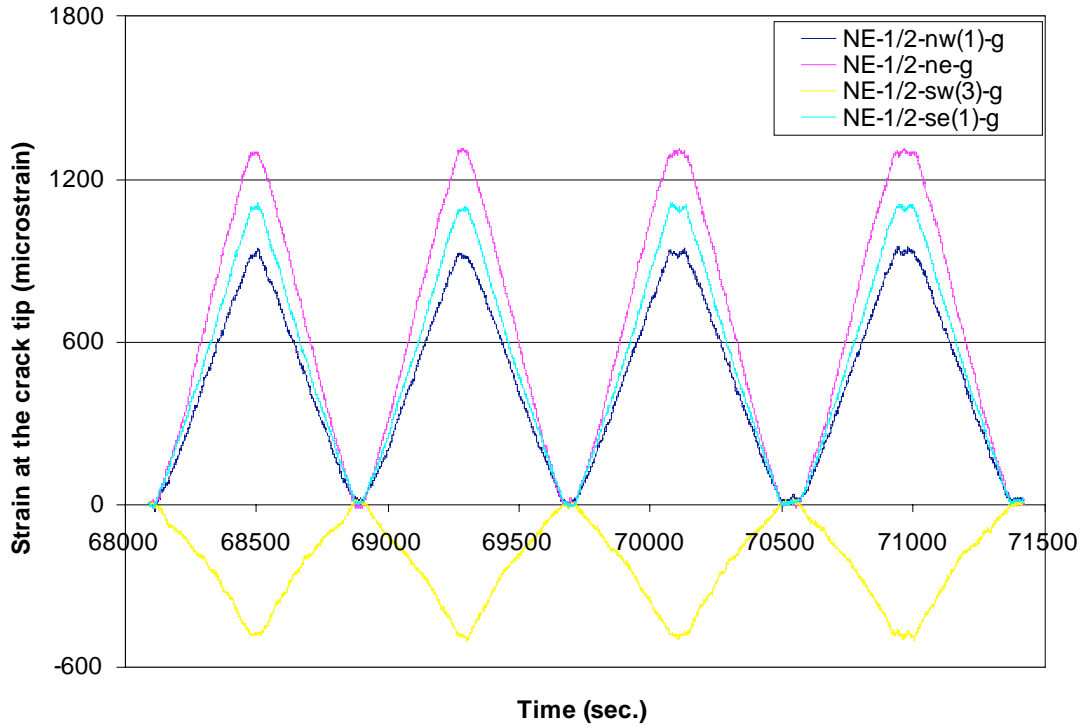
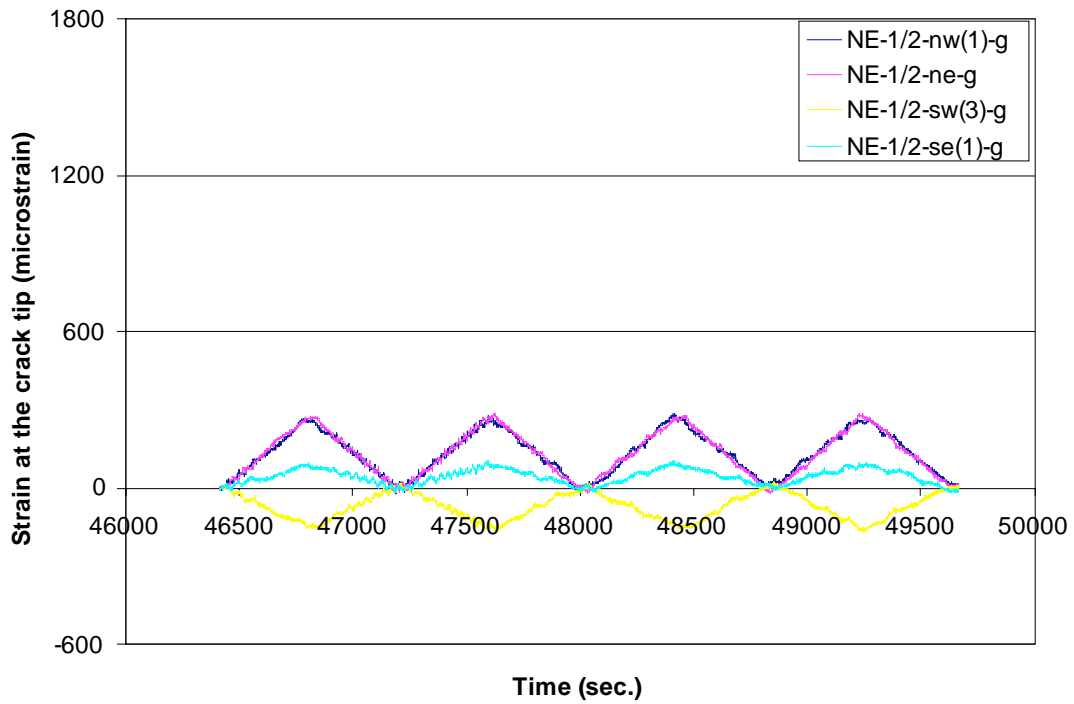


Figure 4.30 Picture of cracks at web gap NE-1/2 at 1,101,000 cycles



(a) before retrofit



(b) after retrofit

Figure 4.31 Measured strains at the crack tips at web gap NE-1/2

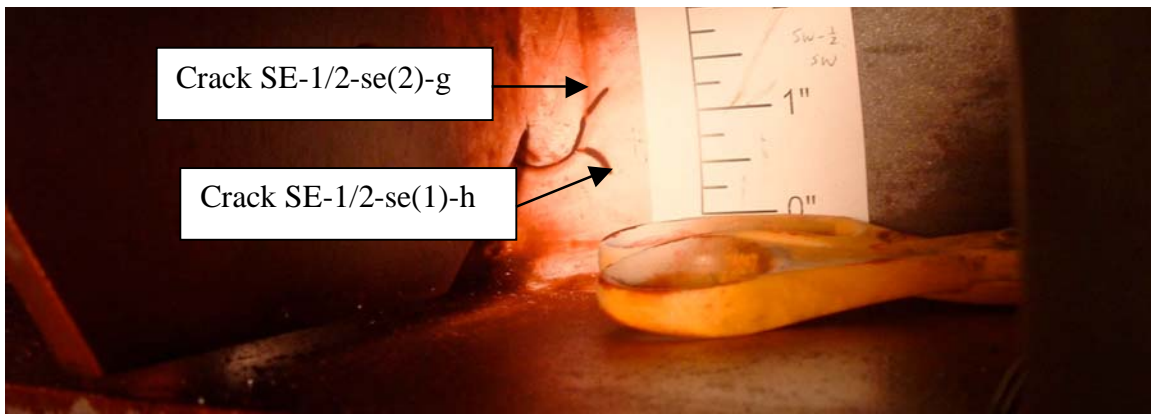
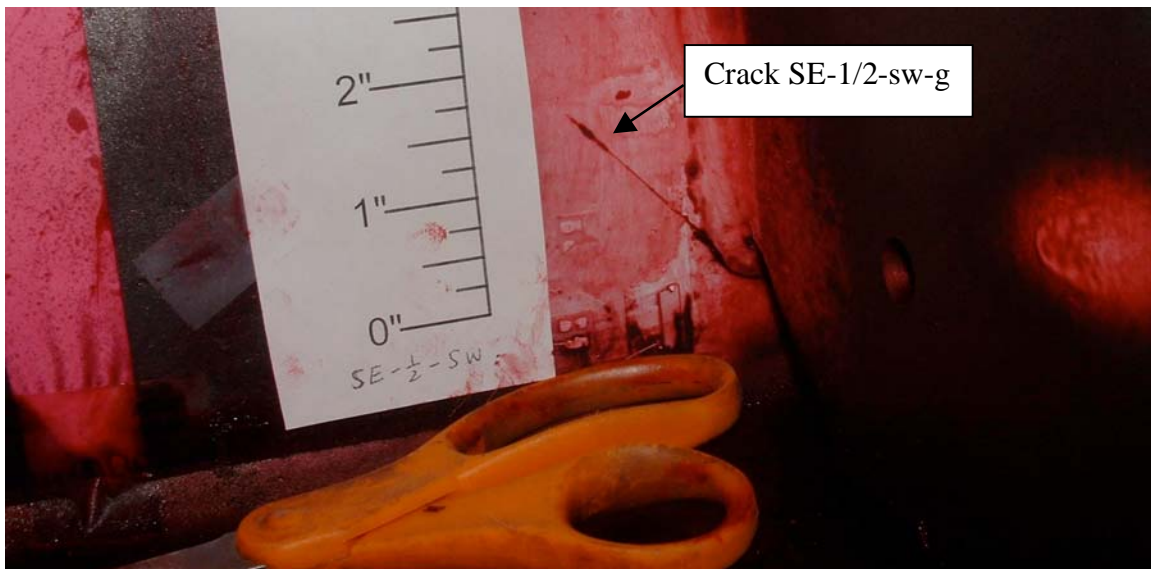
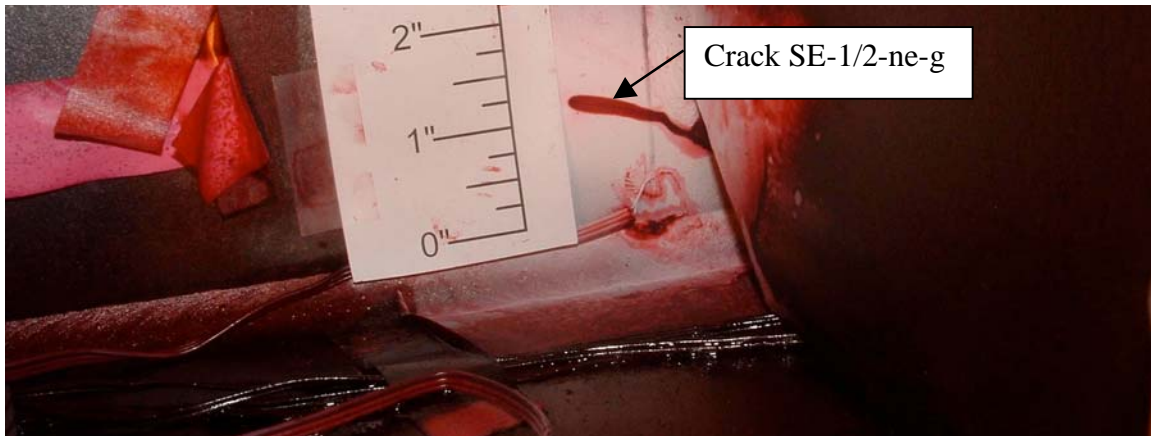
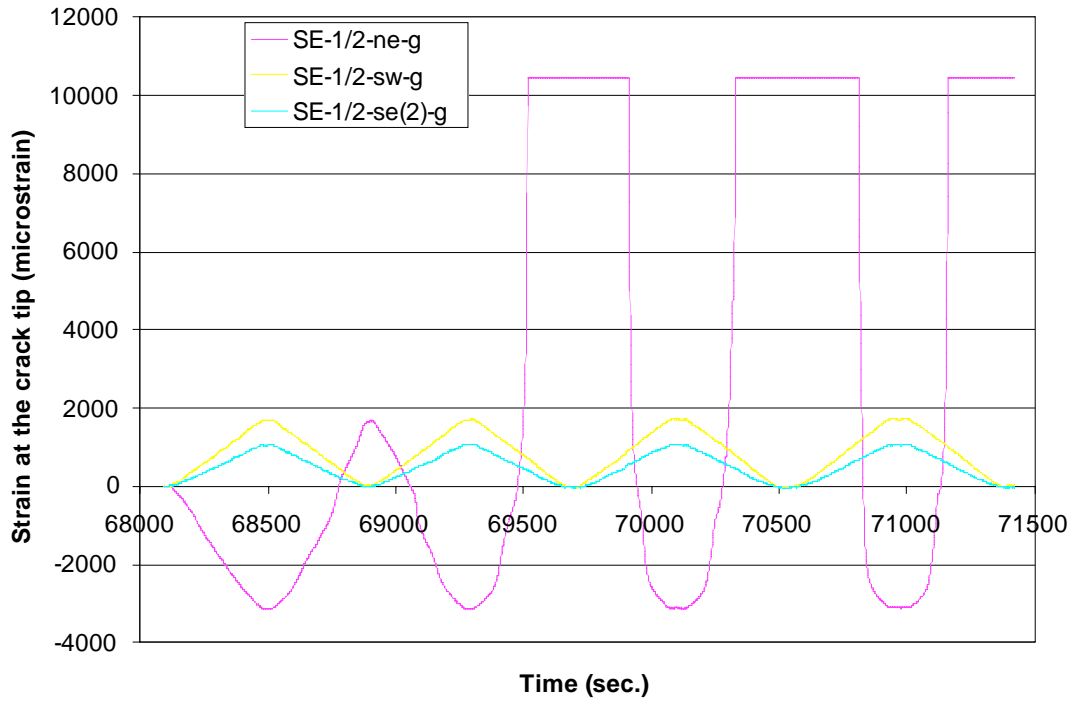
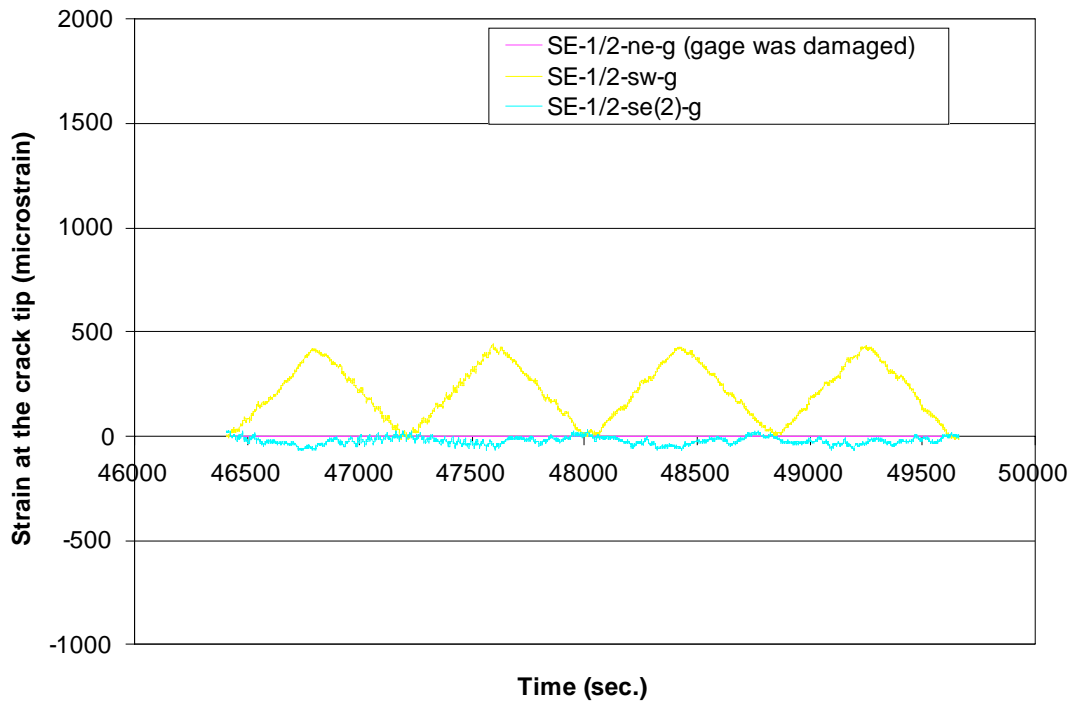


Figure 4.32 Picture of cracks at web gap SE-1/2 at 1,101,000 cycles



(a) before retrofit



(b) after retrofit

Figure 4.33 Measured strains at the crack tips at web gap SE-1/2

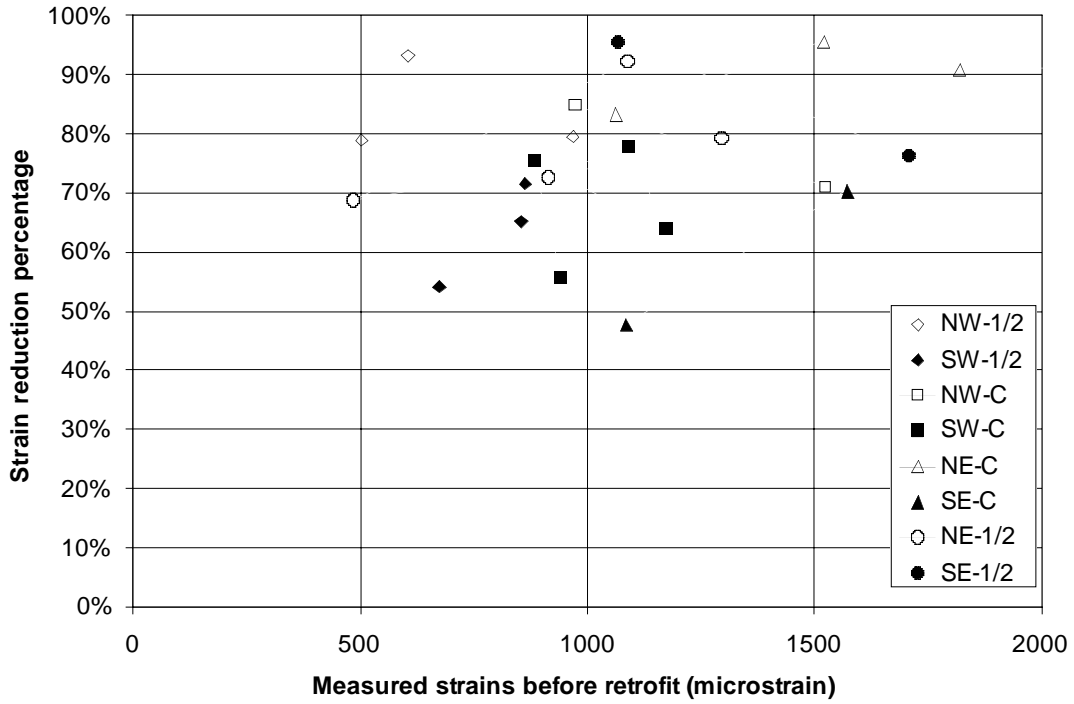


Figure 4.34 Crack tip strain reduction vs. original crack tip strain

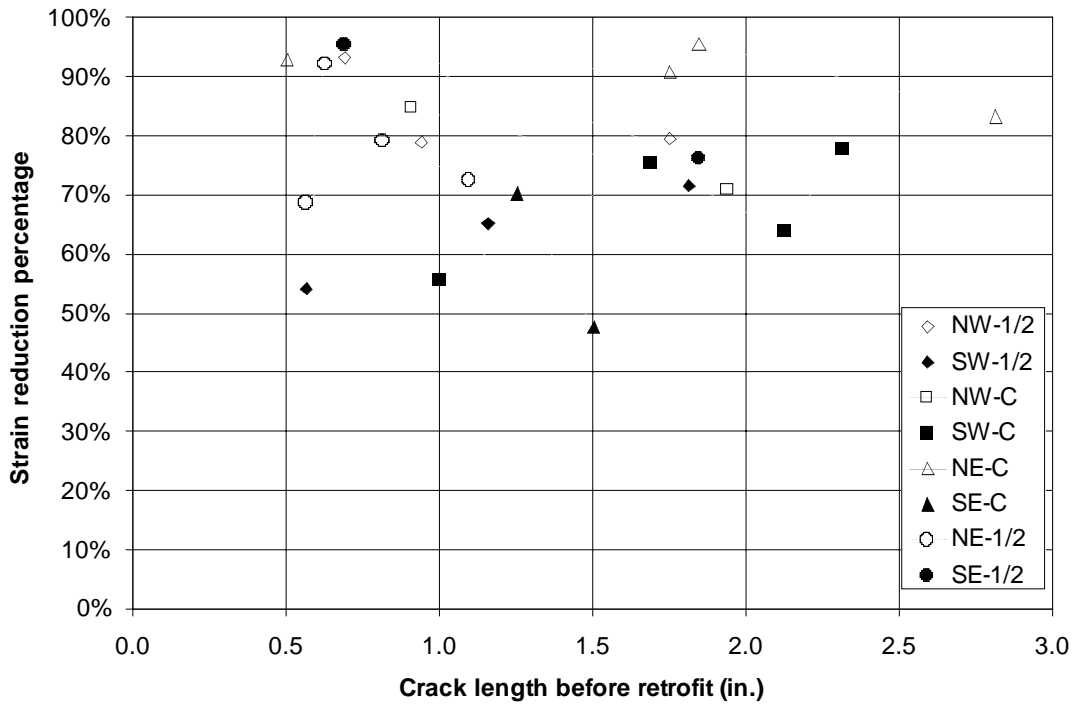


Figure 4.35 Crack tip strain reduction vs. crack length

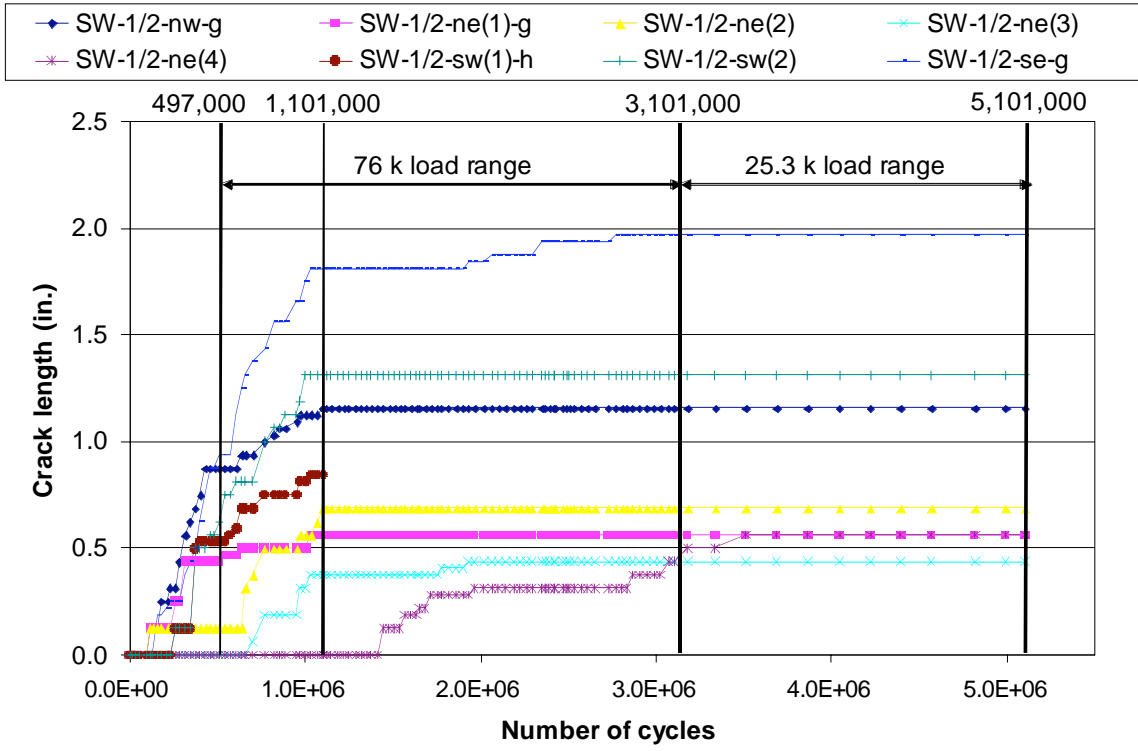


Figure 4.36 Crack growth at web gap SW-1/2

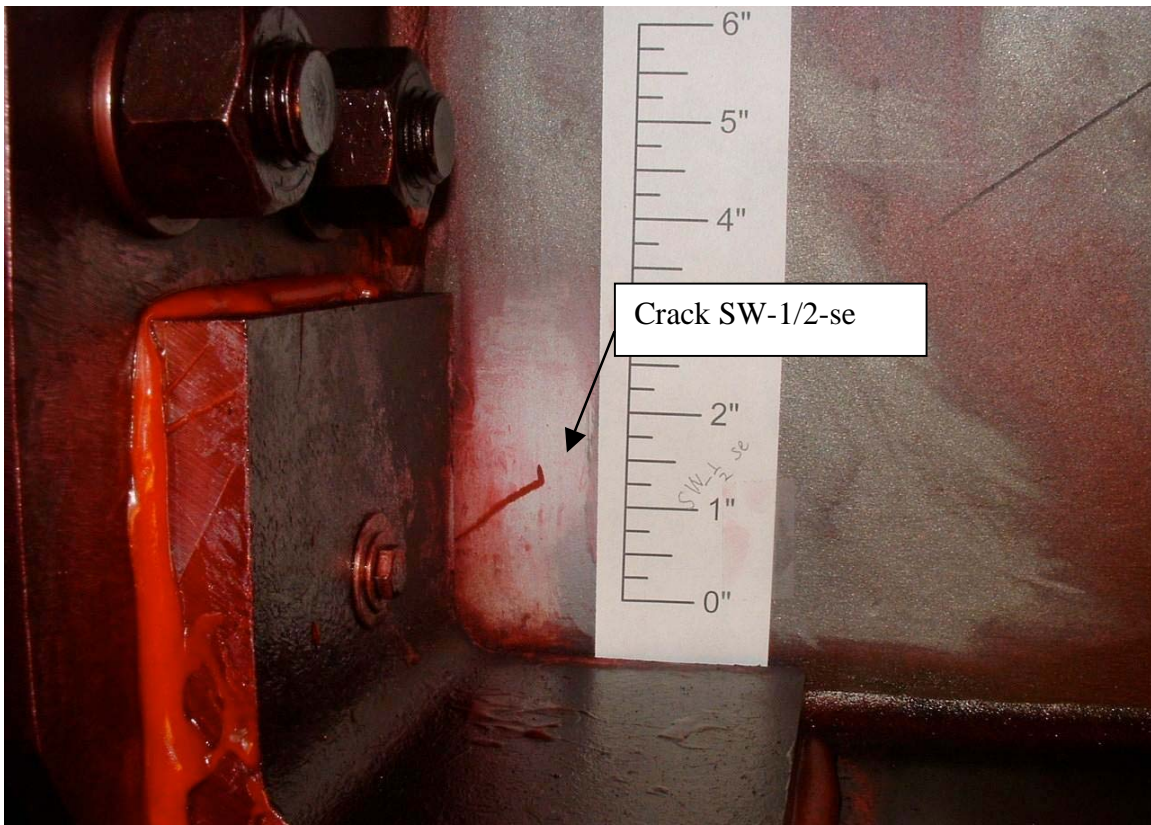
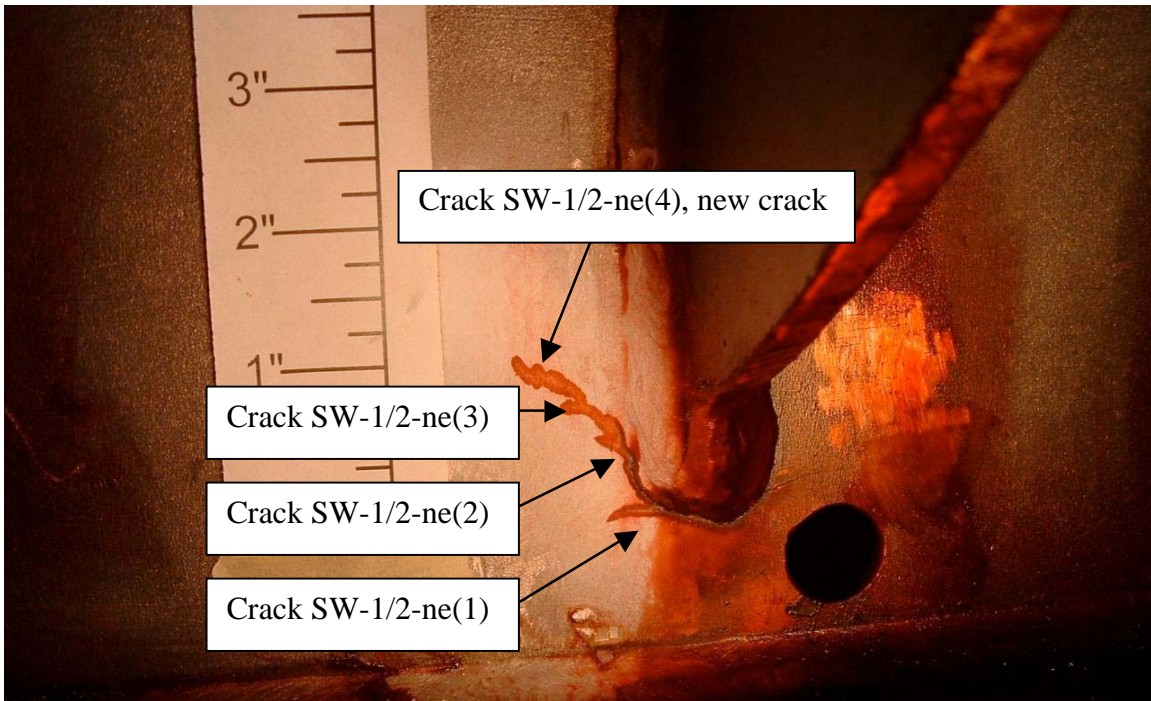


Figure 4.37 Cracks at web gap SW-1/2 at 3,101,000 cycles



Dye had penetrated a small area at the boundary of the angle

Figure 4.38 Detached angle at web gap SW-1/2

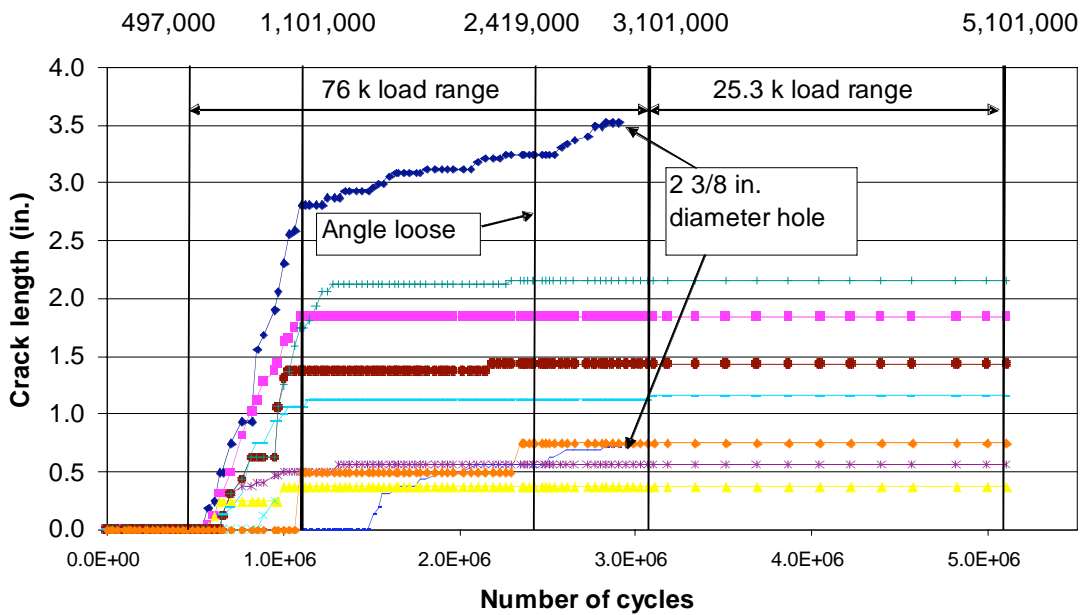
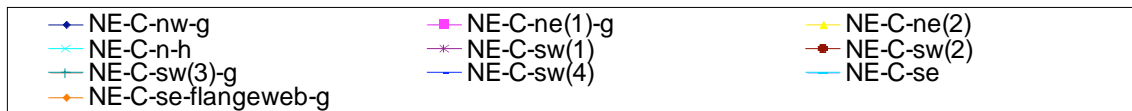
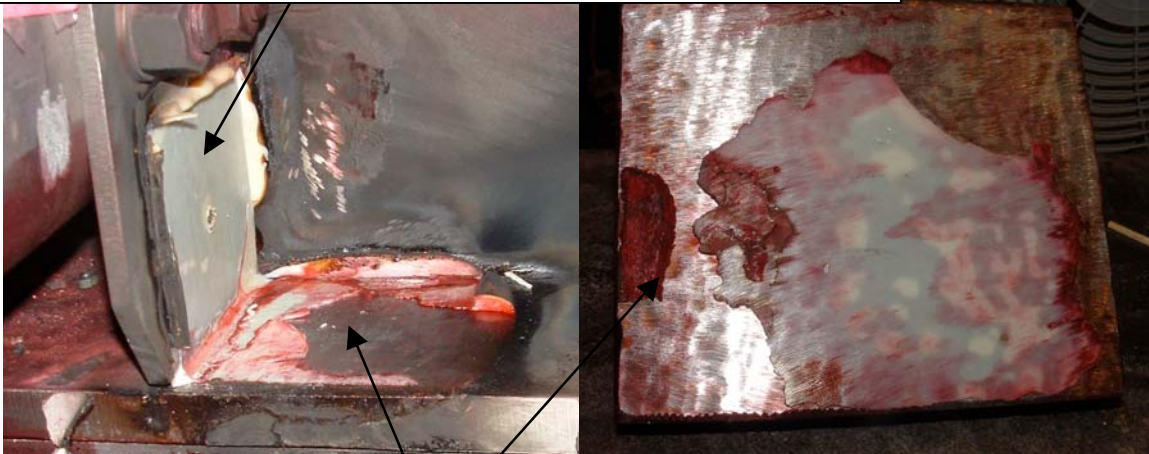


Figure 4.39 Crack growth at web gap NE-C

No adhesive deterioration on the side of the connection plate



Dye had penetrated all surface of the angle on the side of the tension flange

Figure 4.40 Detached angle at web gap NE-C

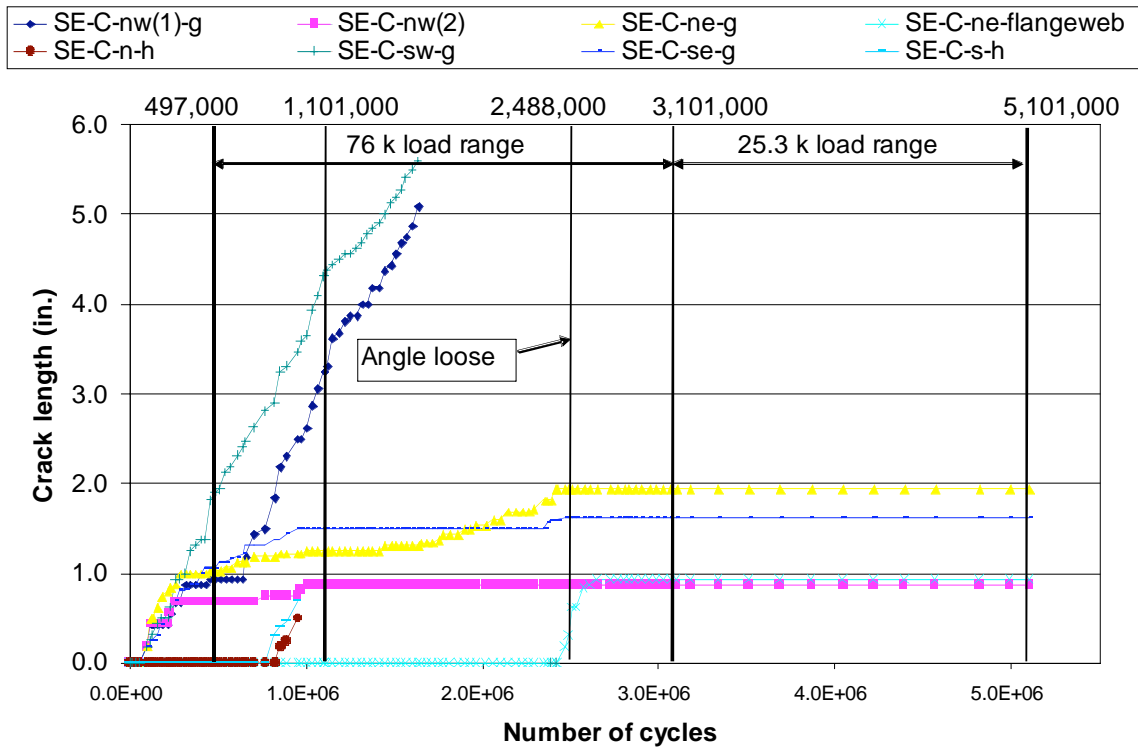
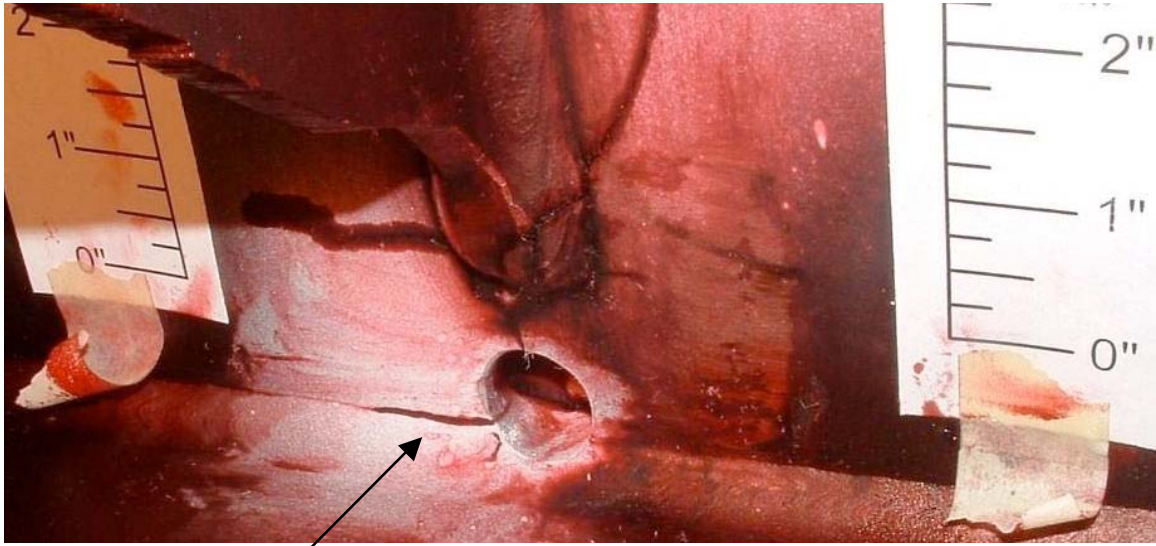


Figure 4.41 Crack growth at web gap SE-C



Crack SE-C-ne-flangeweb, new crack

Figure 4.42 New crack at web gap SE-C at 3,101,000 cycles

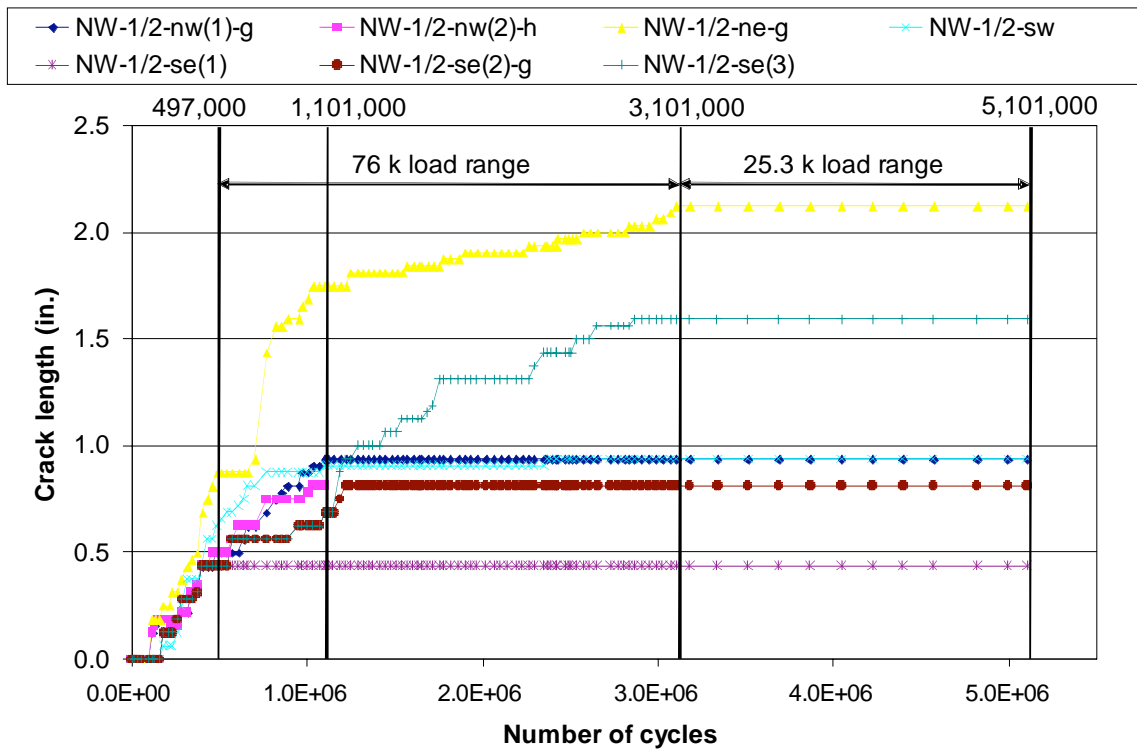


Figure 4.43 Crack growth at web gap NW-1/2

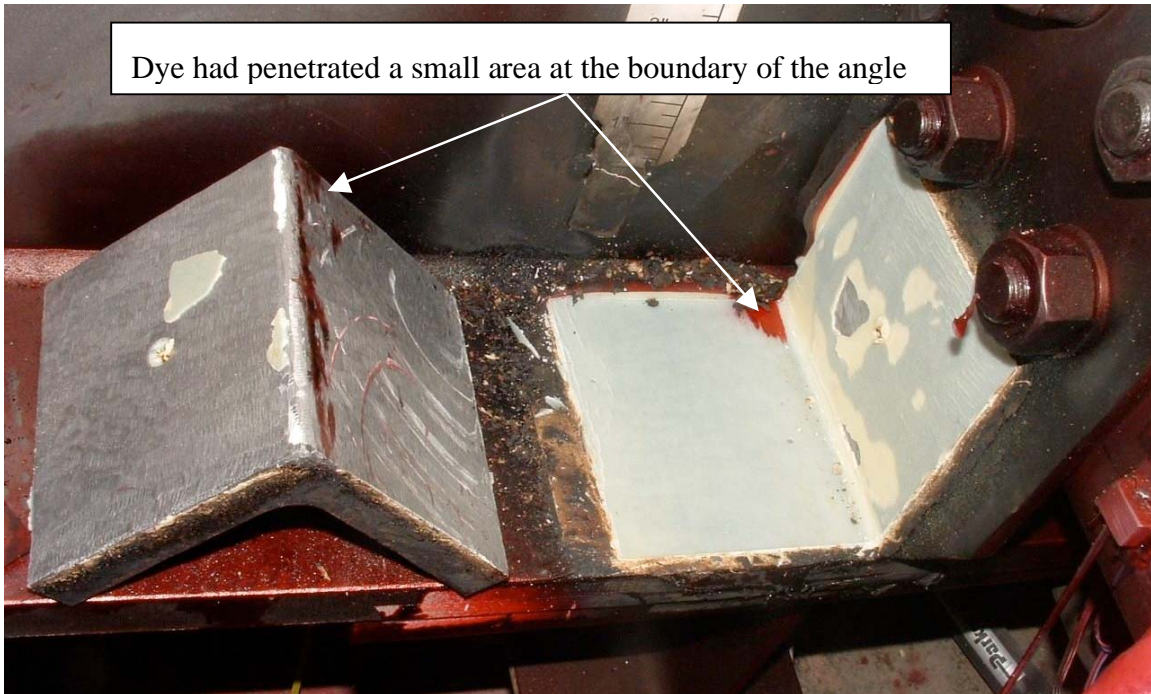


Figure 4.44 Detached angle at web gap NW-1/2

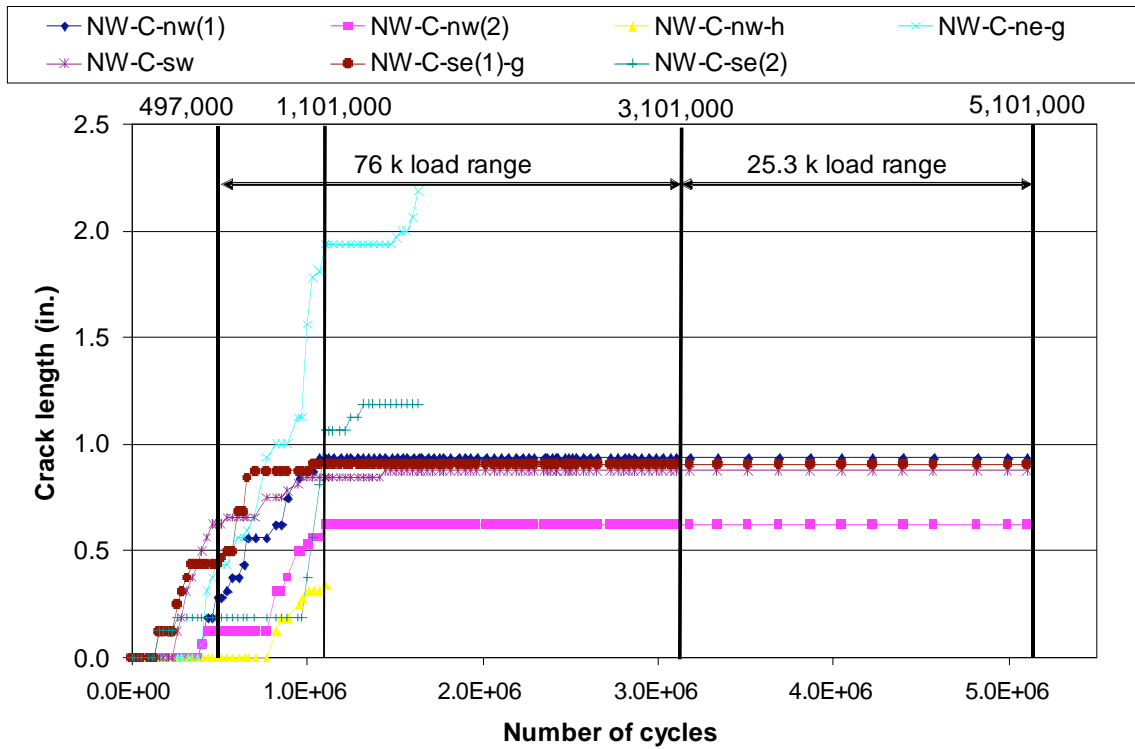


Figure 4.45 Crack growth at web gap NW-C

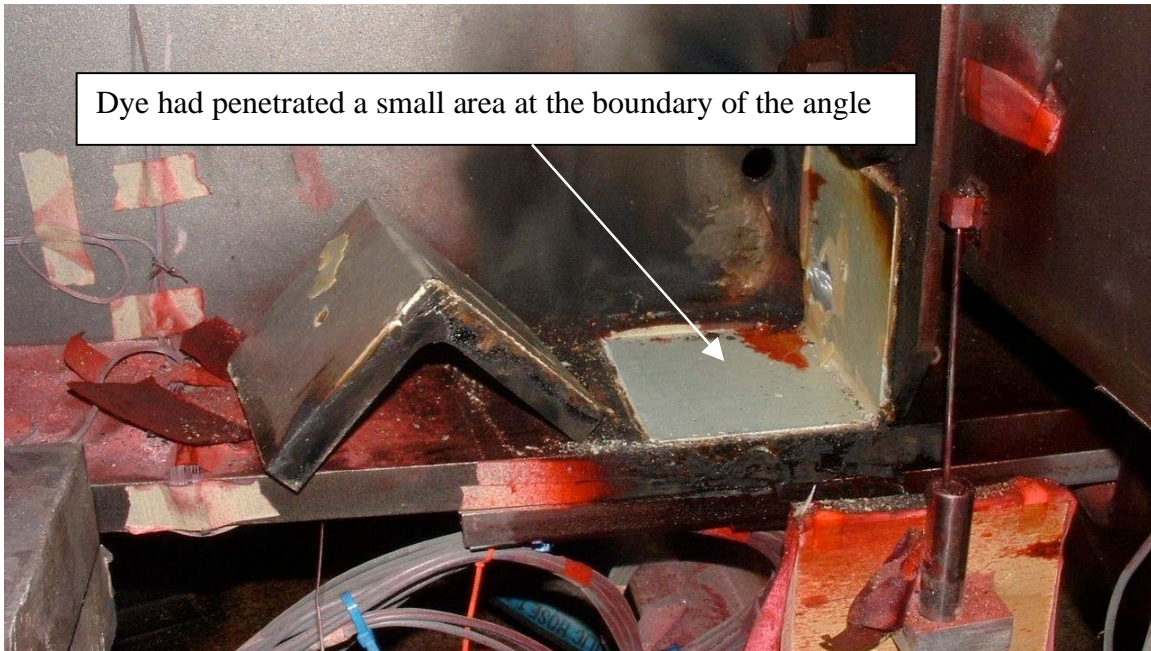


Figure 4.46 Detached angle at web gap NW-C

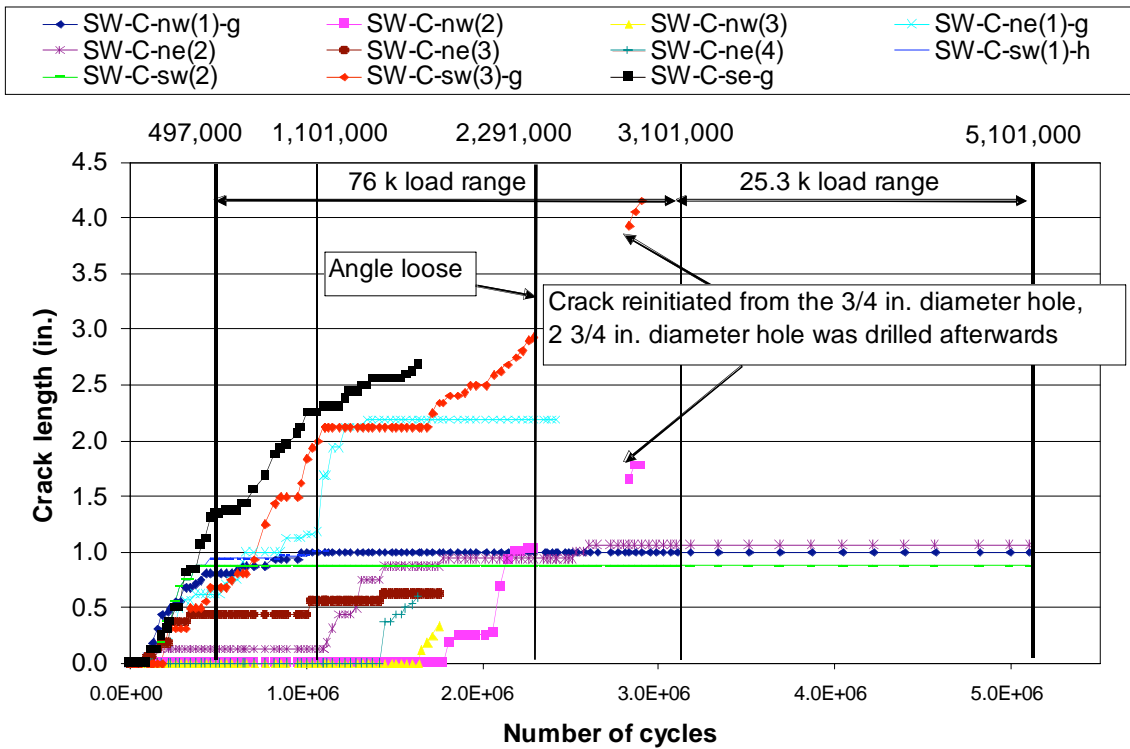


Figure 4.47 Crack growth at web gap SW-C

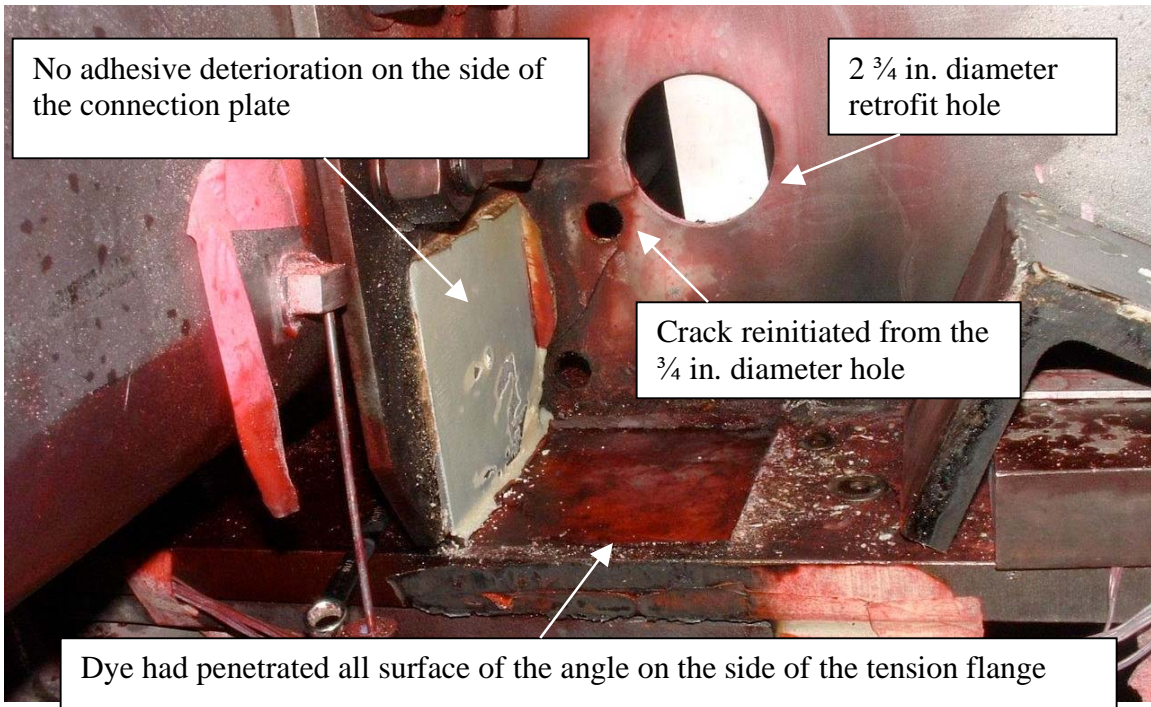


Figure 4.48 Detached angle at web gap SW-C

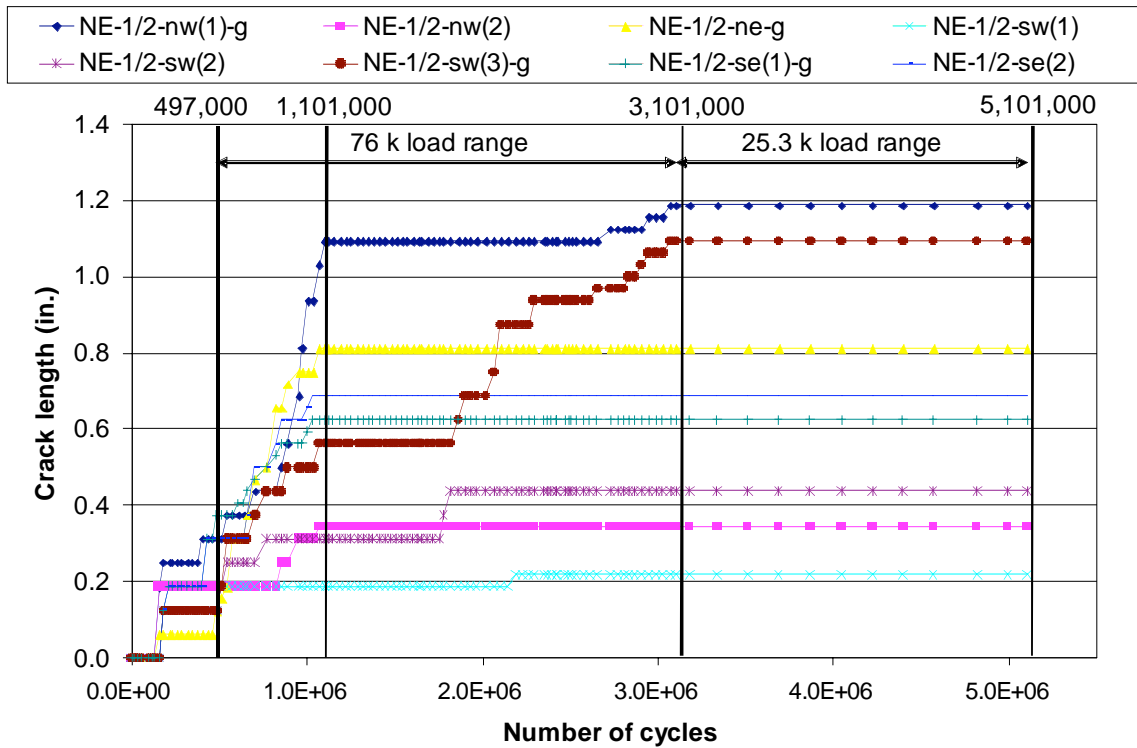


Figure 4.49 Crack growth at web gap NE-1/2



Figure 4.50 Detached angle at web gap NE-1/2

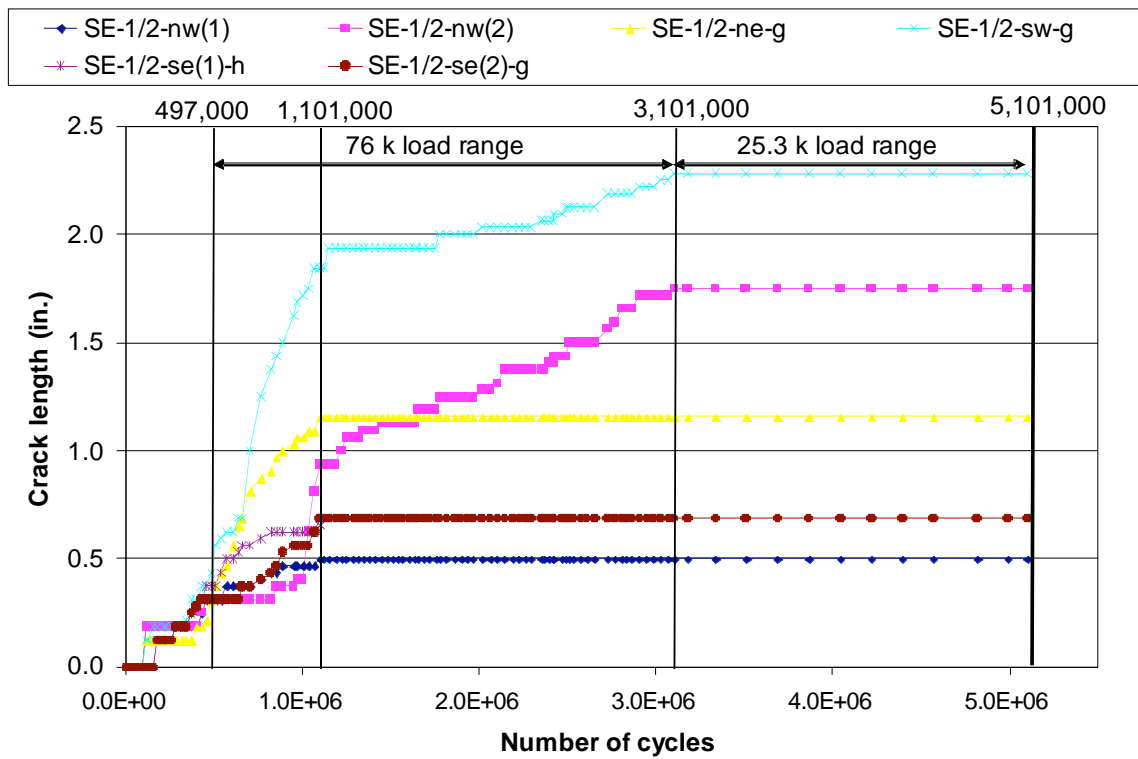


Figure 4.51 Crack growth at web gap SE-1/2

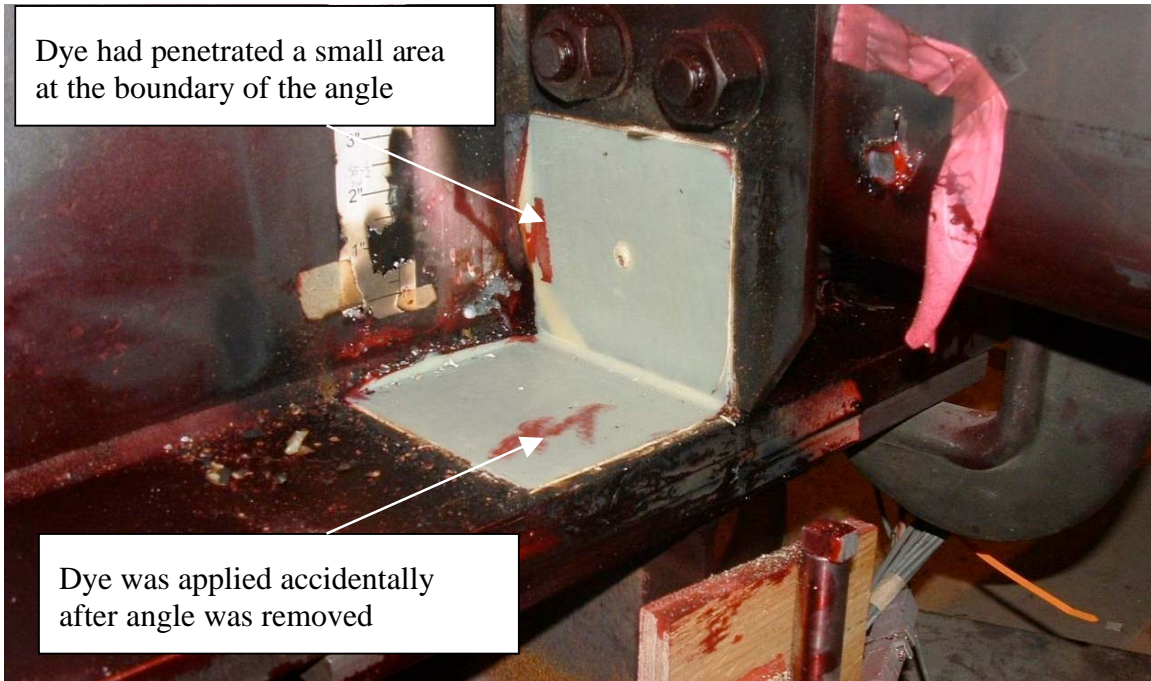


Figure 4.52 Detached angle at web gap SE-1/2

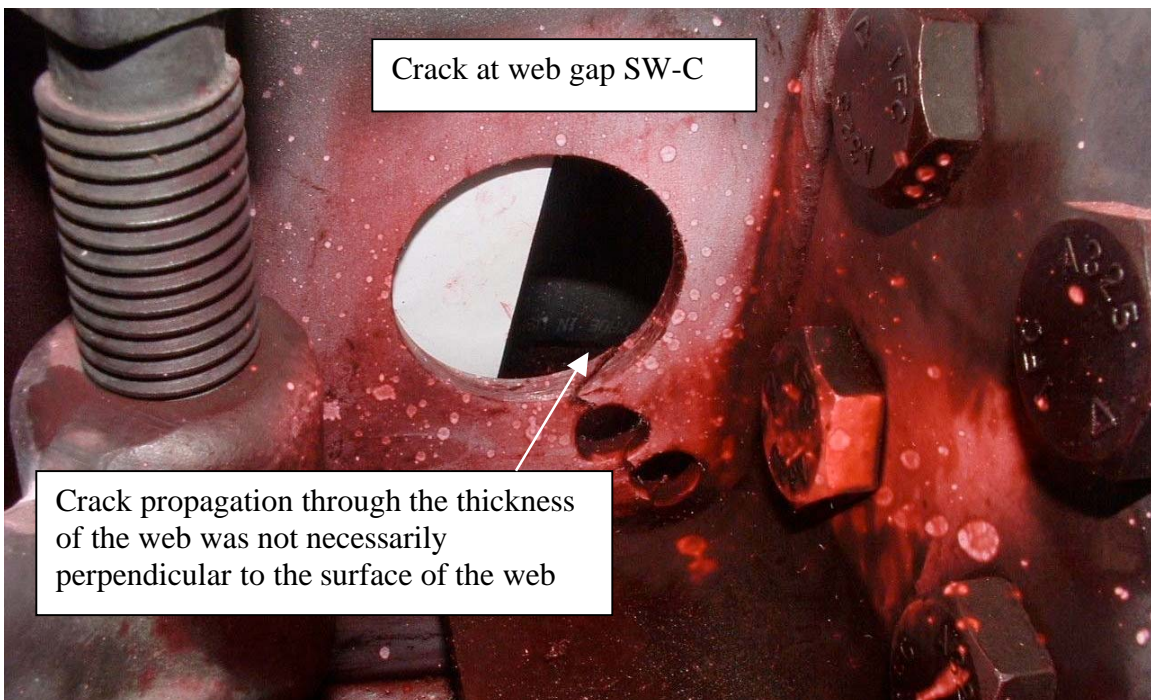
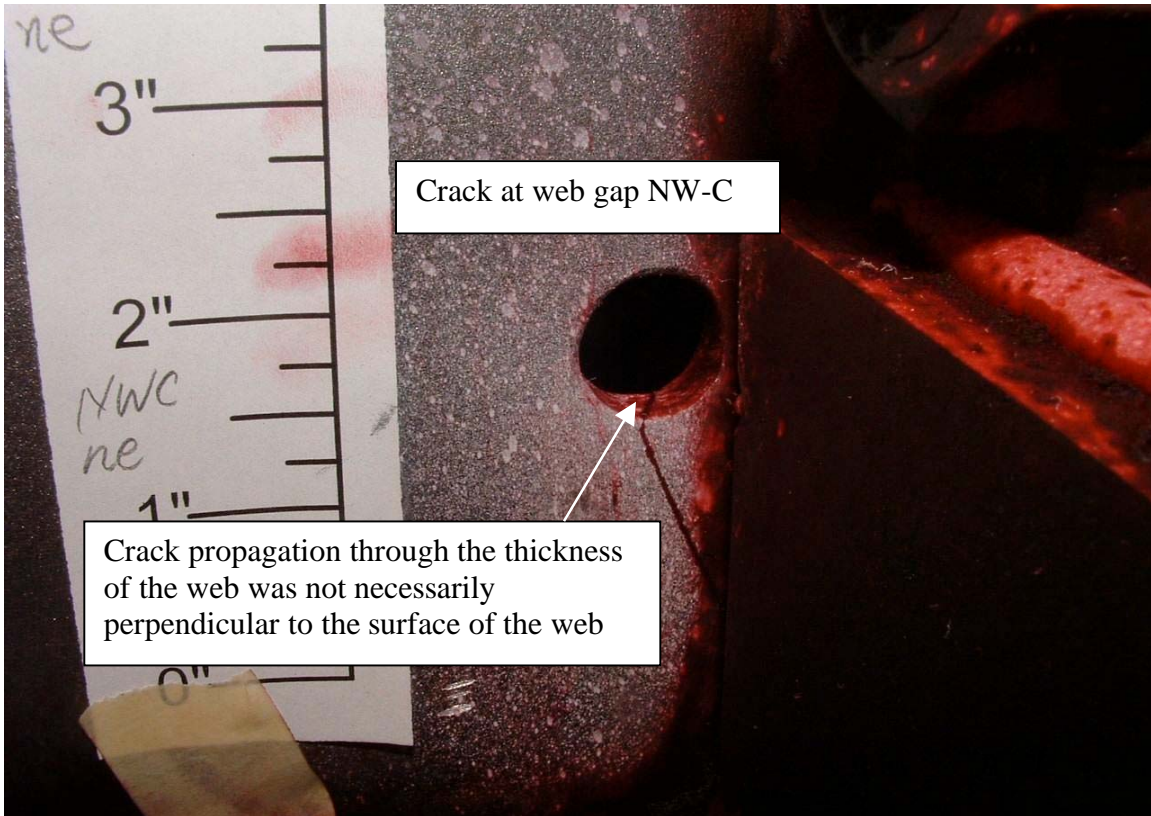


Figure 4.53 Crack propagation through the thickness of the web

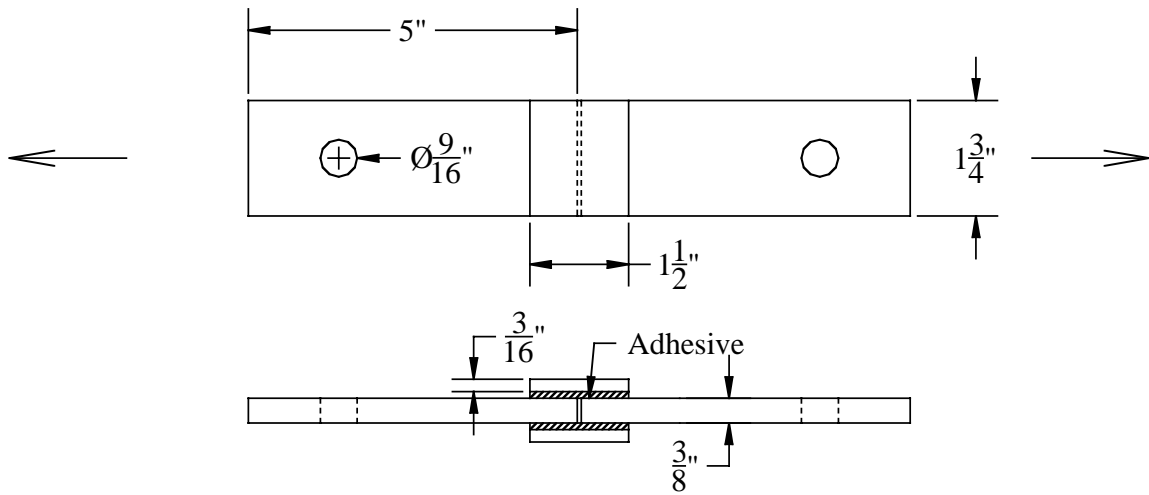


Figure 5.1 Coupon specimen dimension

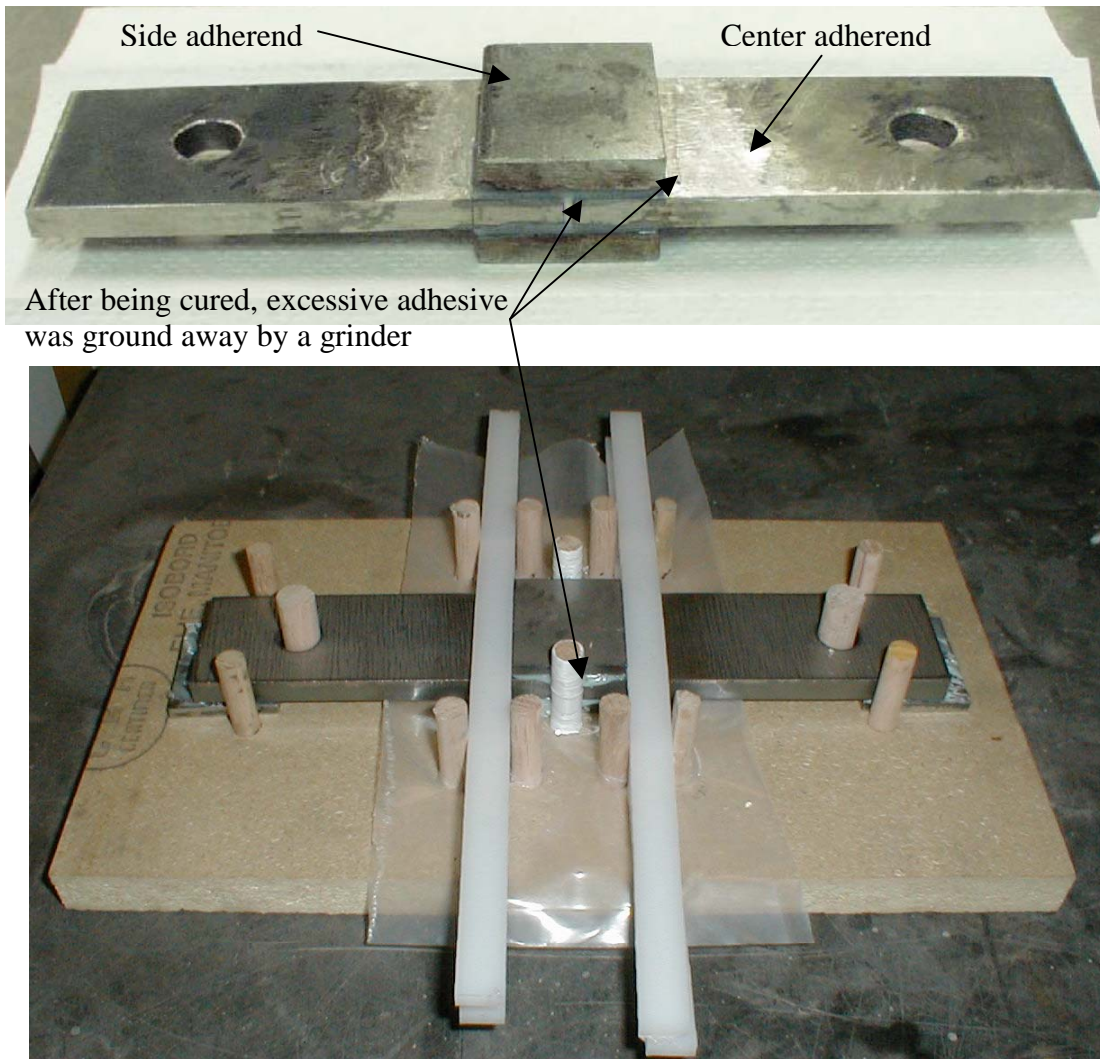


Figure 5.2 Coupon specimen fabrication

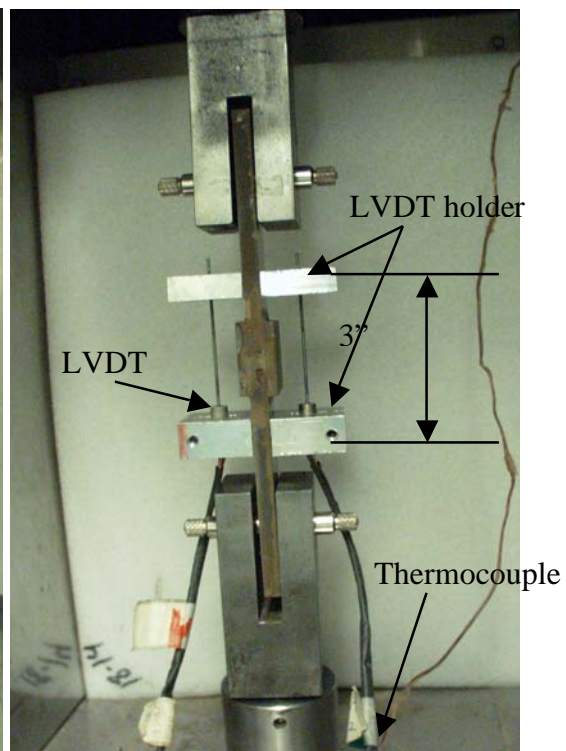
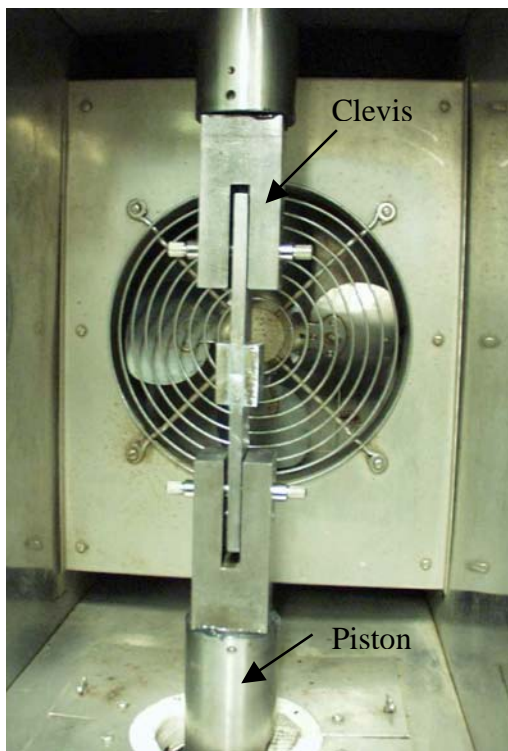


Figure 5.3 Test set up (upper picture: overall view; left lower picture: close-up view without LVDTs; right lower picture: close-up view with LVDTs)

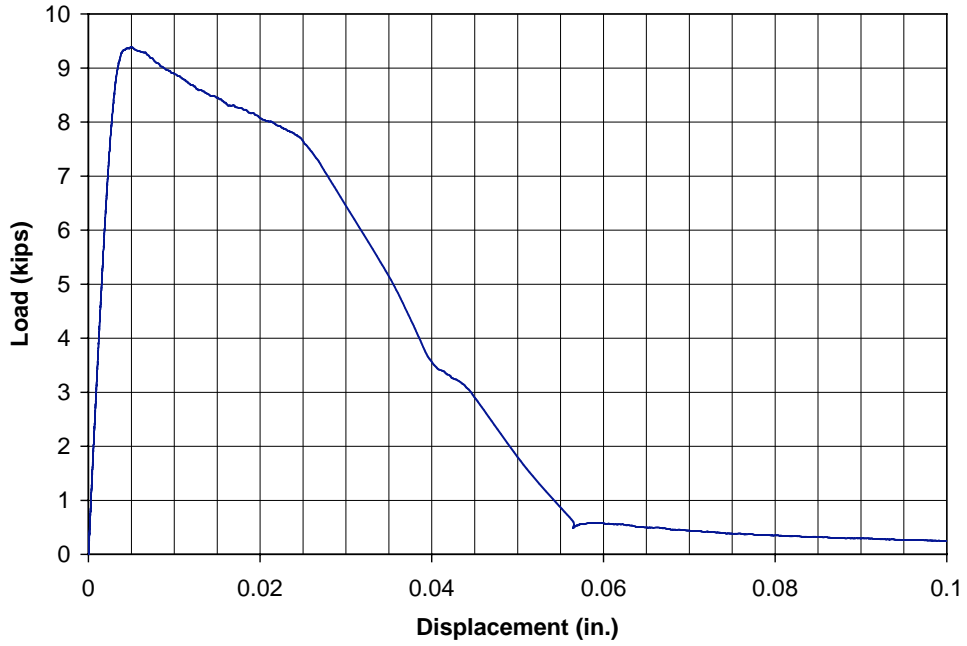


Figure 5.4 Load vs. displacement curve for a baseline specimen with bondline thickness  $t_a=0.020$  in. (Tested in lab ambient air, No GPS)

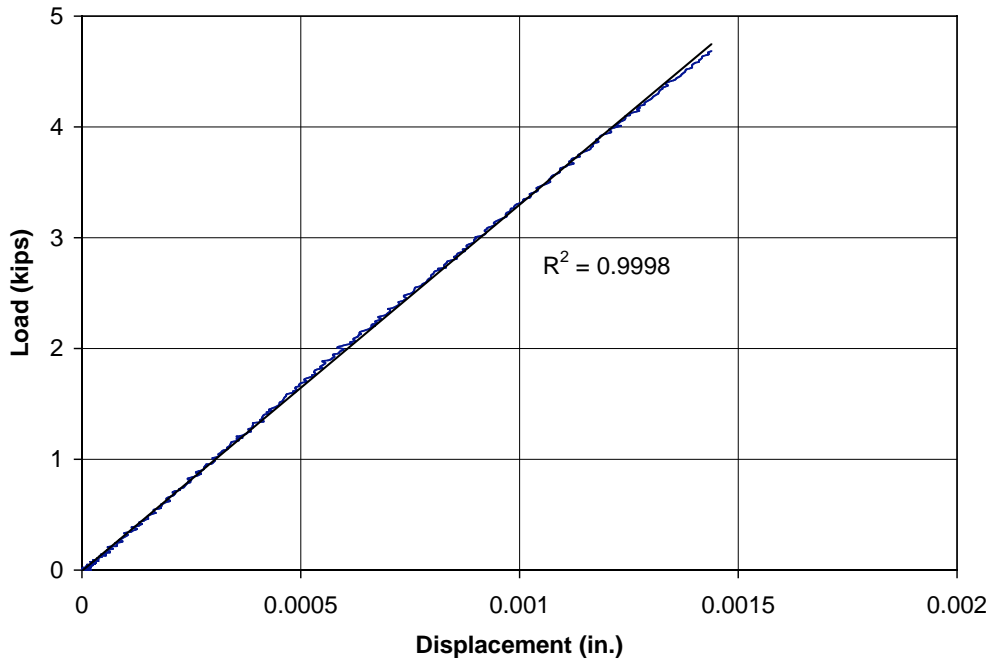


Figure 5.5 Least squares regression of load vs. displacement curve for a baseline specimen with bondline thickness  $t_a=0.020$  in. (Tested in lab ambient air, No GPS)

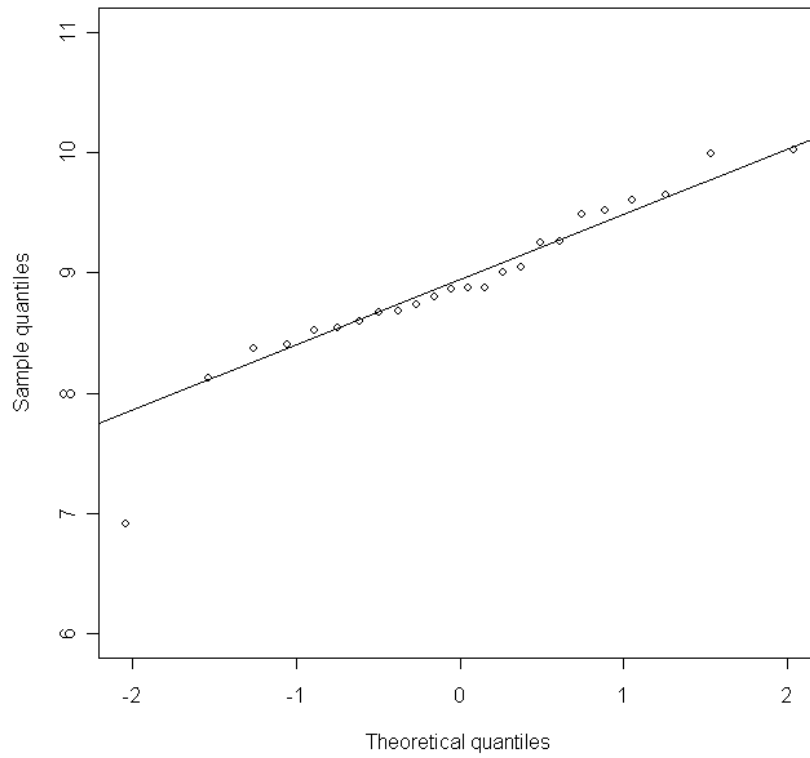
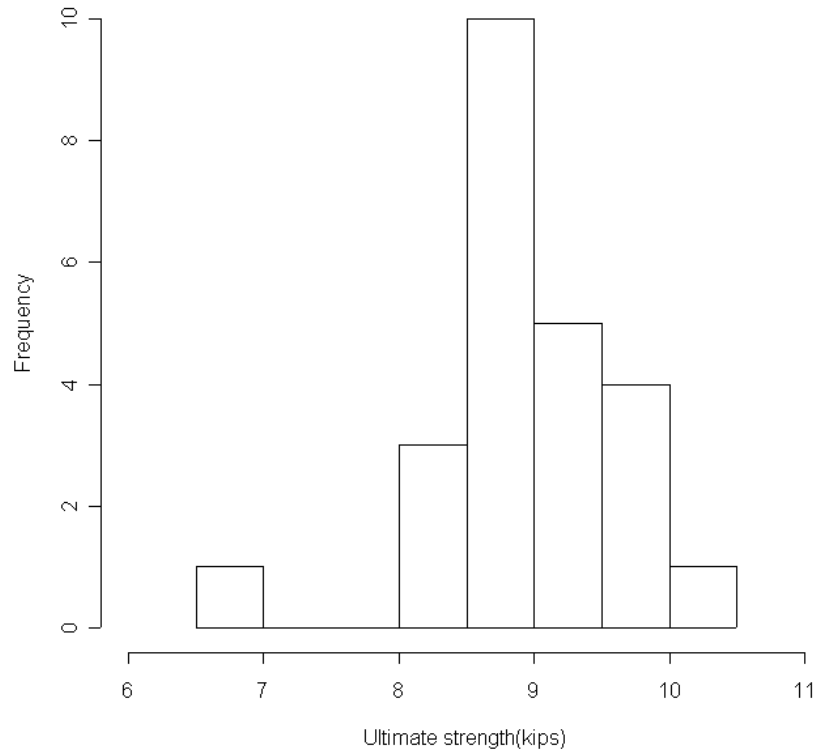
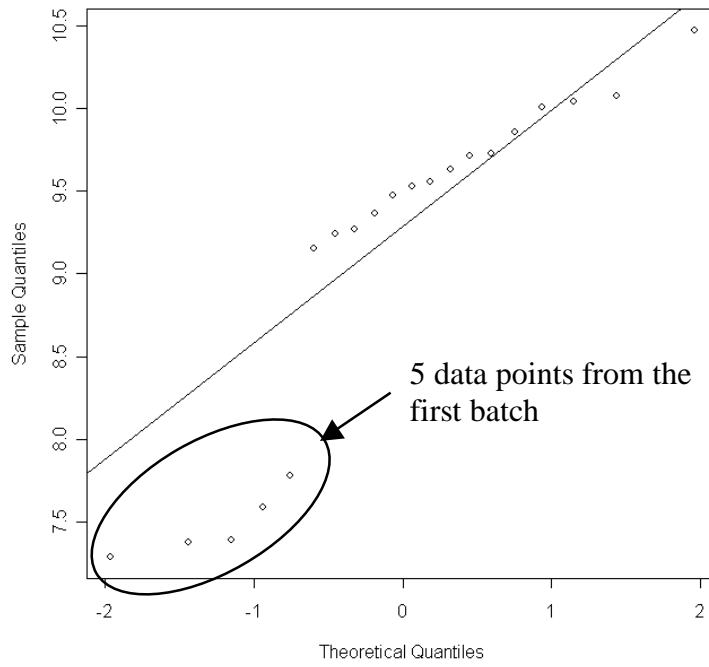
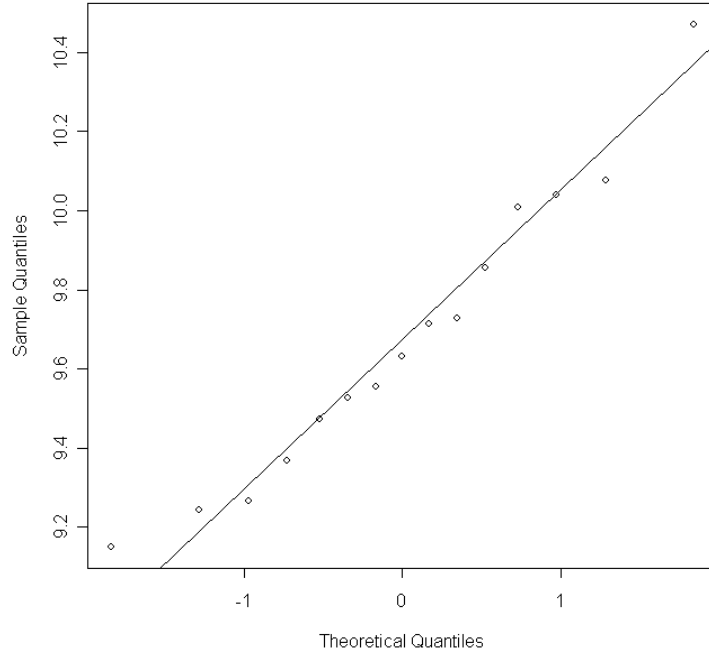


Figure 5.6 Histogram and normal quantile plot for the standard baseline specimens ( $t_a=0.020$  in., No GPS, room temperature cured, room temperature tested)

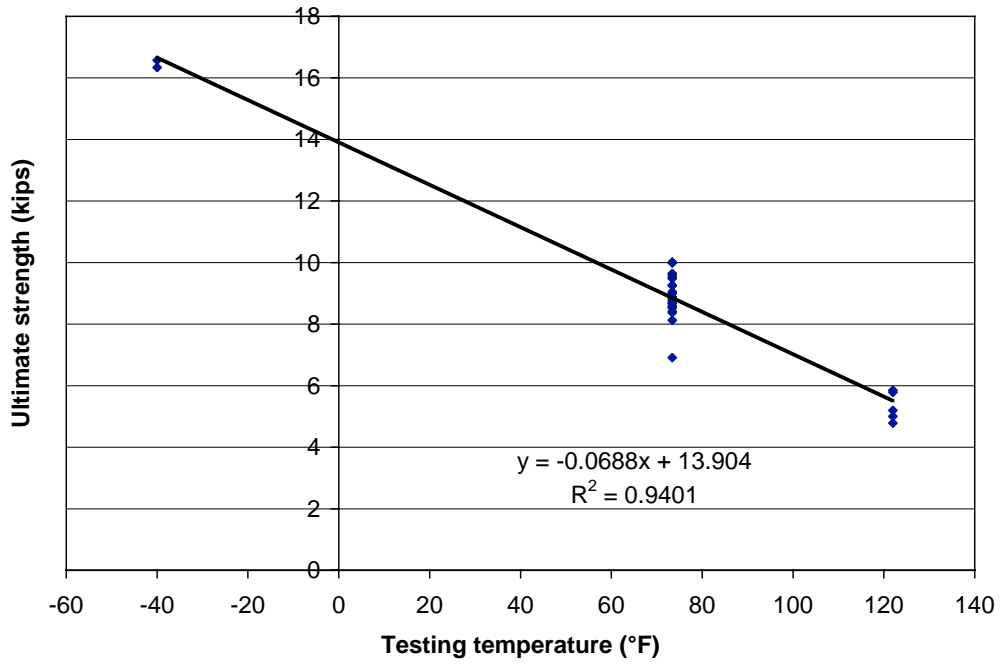


(a) 20 data points used

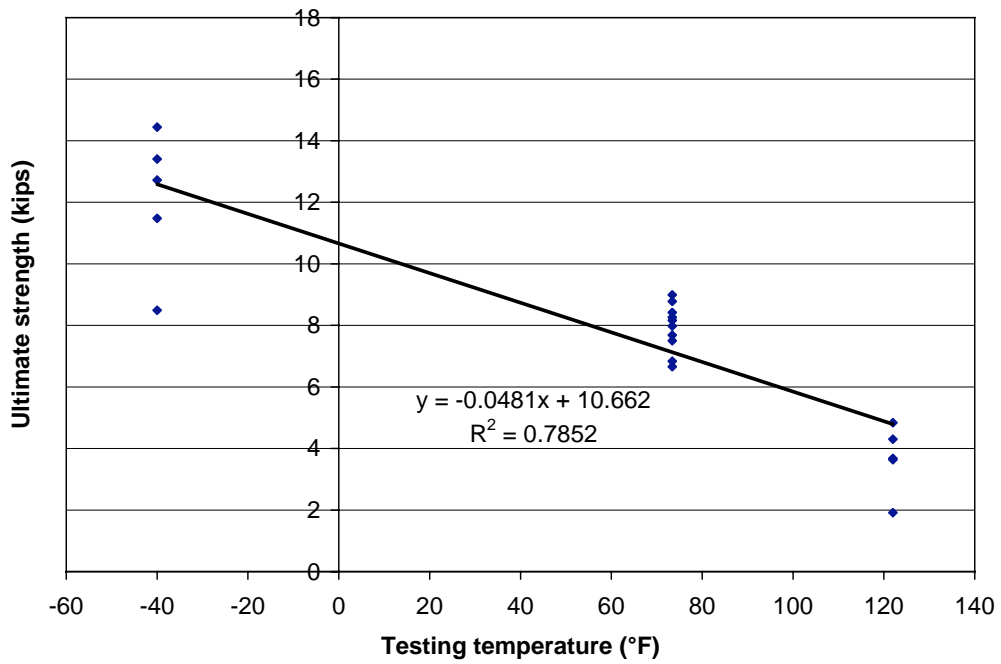


(b) 15 data points were used

Figure 5.7 Normal quantile plot for the baseline specimens with GPS ( $t_a=0.020$  in., room temperature cured, room temperature tested)



(a)  $t_a = 0.020$  in., No GPS (Only 2 specimens were tested at -40°F)



(b)  $t_a = 0.059$  in., No GPS

Figure 5.8 Ultimate strength vs. testing temperature for baseline specimens

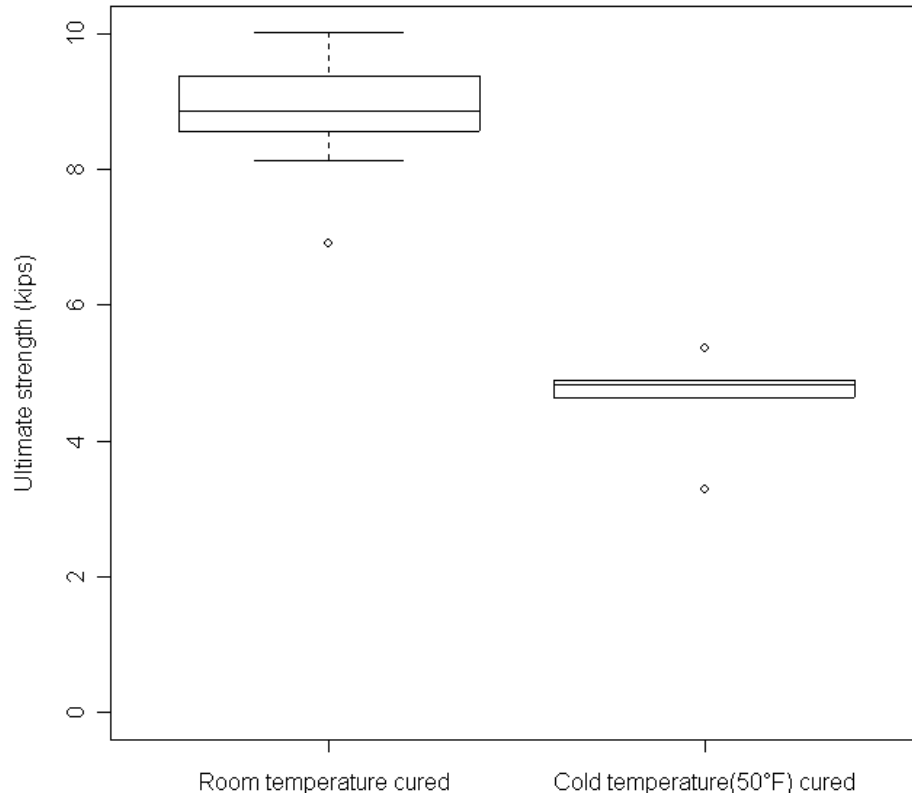


Figure 5.9 Ultimate strength of lab-ambient-air(73°F)-cured specimens and cold-air(50°F)-cured specimens (baseline specimens,  $t_a=0.020$  in., No GPS)



Figure 5.10 Failure mode of a standard baseline specimen (Room temperature cured, tested in lab ambient air, No GPS, bondline thickness  $t_a= 0.020$  in.)



Figure 5.11 Failure mode of a specimen pretreated by GPS (Room temperature cured, tested in lab ambient air, bondline thickness  $t_a= 0.020$  in.)

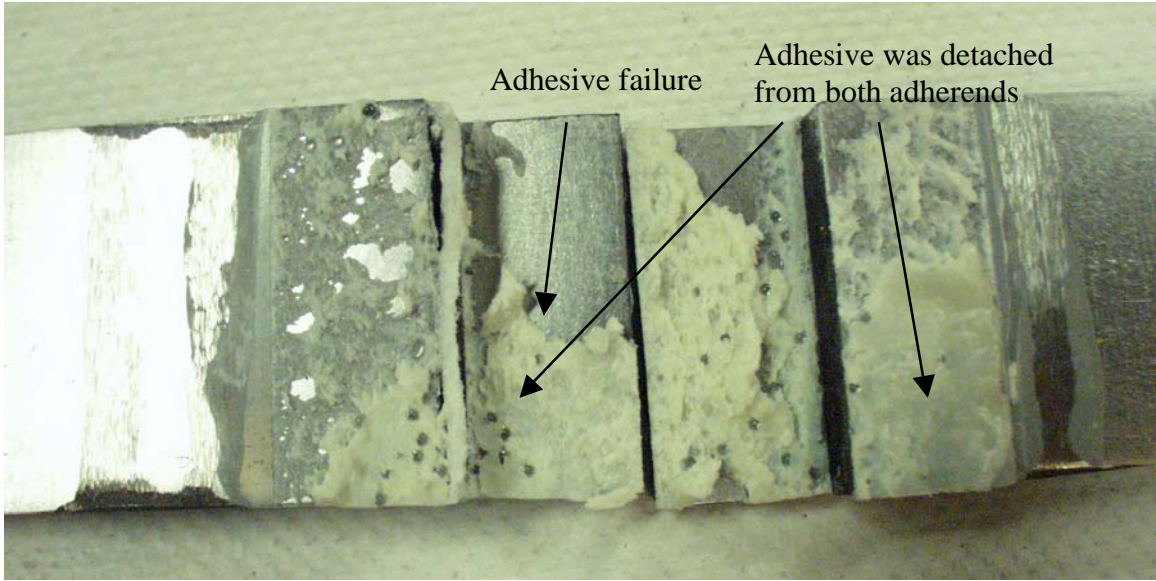


Figure 5.12 Failure mode of a specimen tested at 122°F (Room temperature cured, No GPS, bondline thickness  $t_a= 0.020$  in.)



Figure 5.13 Failure mode of a specimen tested at -40°F (Room temperature cured, No GPS, bondline thickness  $t_a= 0.020$  in.)



Figure 5.14 Failure mode of a cold temperature(50°F) cured baseline specimen (Tested in lab ambient air, No GPS, bondline thickness  $t_a= 0.020$  in.)

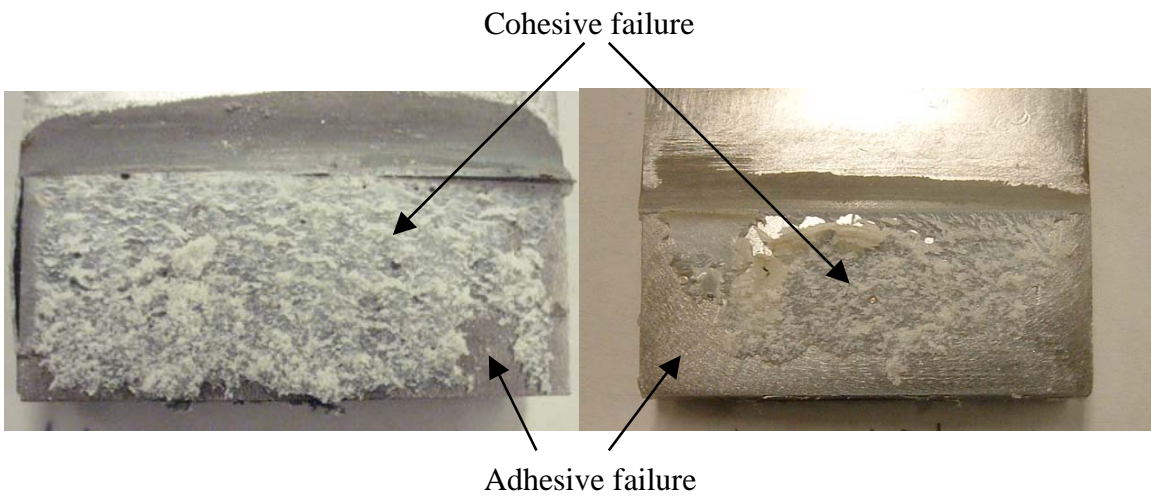


Figure 5.15 Failure mode of specimen kept in lab air at 65°F for 180 days (left) and 447 days (right) (Tested in lab ambient air, No GPS, bondline thickness  $t_a= 0.020$  in.)

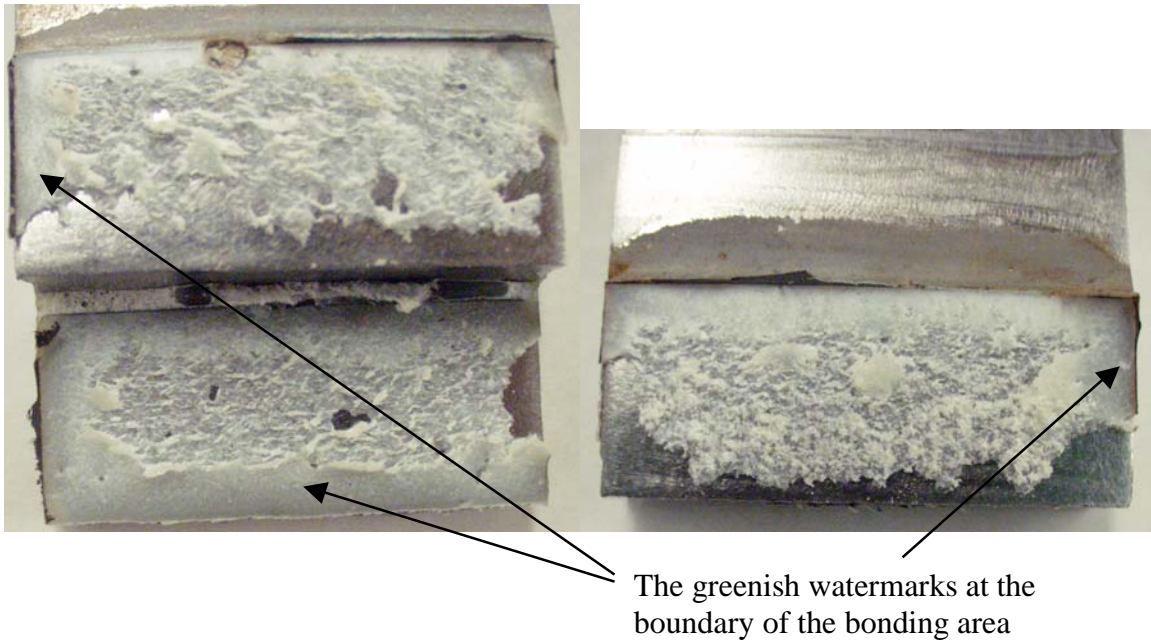


Figure 5.16 Failure mode of specimen immersed in tap water at 65°F for 92 days (left) and 201 days (right) (Tested in lab ambient air, No GPS, bondline thickness  $t_a = 0.020$  in.)

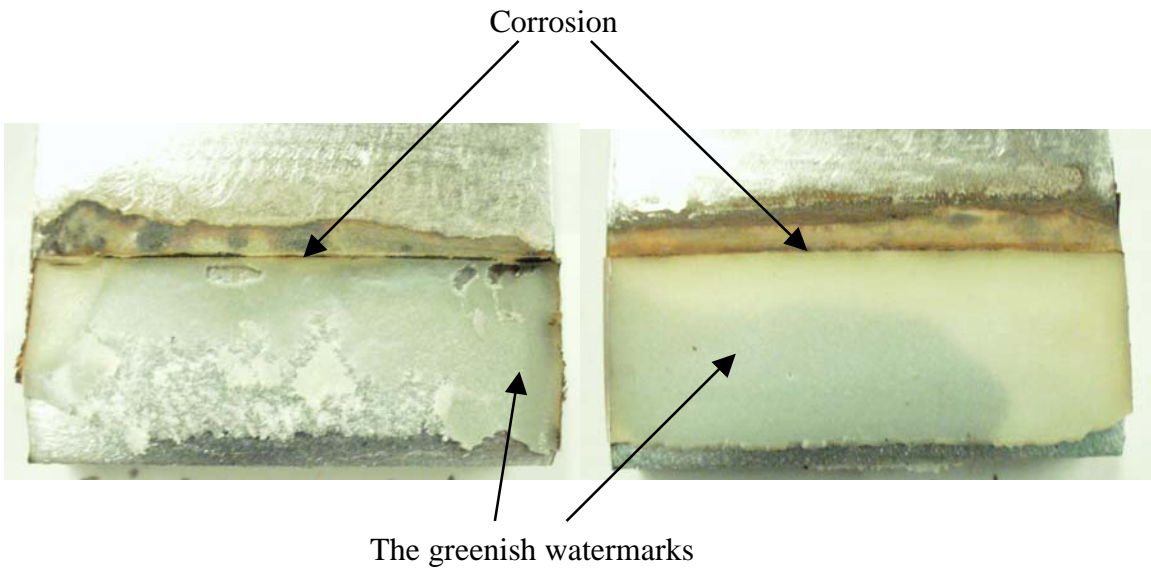


Figure 5.17 Failure mode of specimen immersed in tap water at 111°F for 92 days (left) and 210 days (right) (Tested in lab ambient air, No GPS, bondline thickness  $t_a = 0.020$  in.)

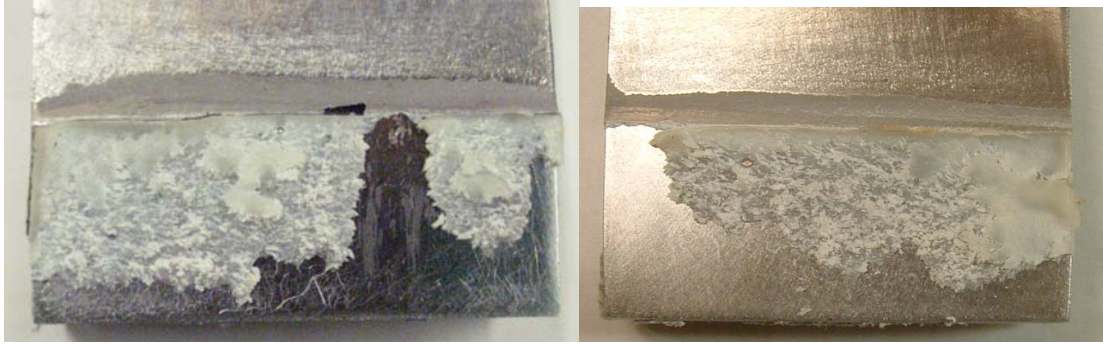


Figure 5.18 Failure mode of specimen kept in cold air at  $-4^{\circ}\text{F}$  for 196 days (left) and 382 days (right) (Tested in lab ambient air, No GPS, bondline thickness  $t_a = 0.020$  in.)

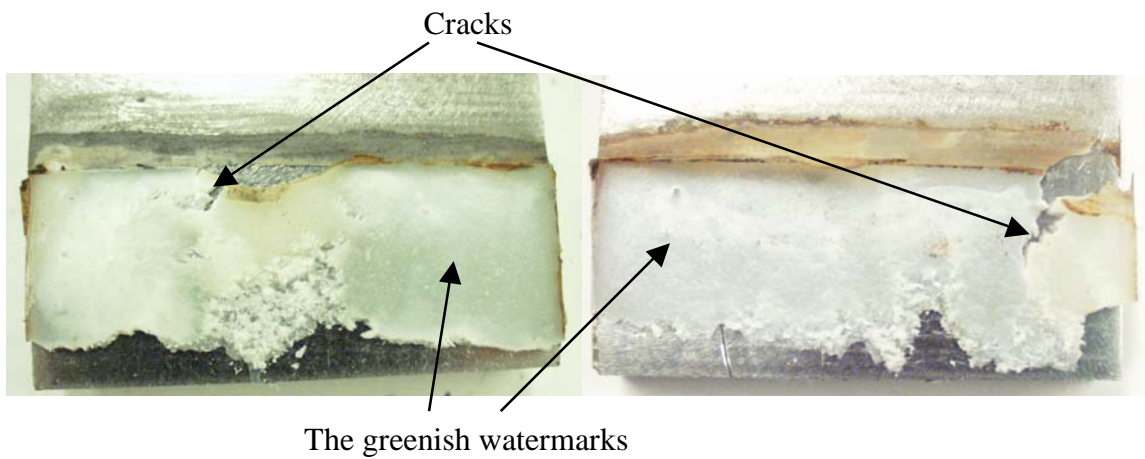


Figure 5.19 Failure mode of specimen kept in freeze and thaw chamber for 92 days (left) and 193 days (right) (Tested in lab ambient air, No GPS, bondline thickness  $t_a = 0.020$  in.)



Figure 5.20 Specimens stored in the cold chamber

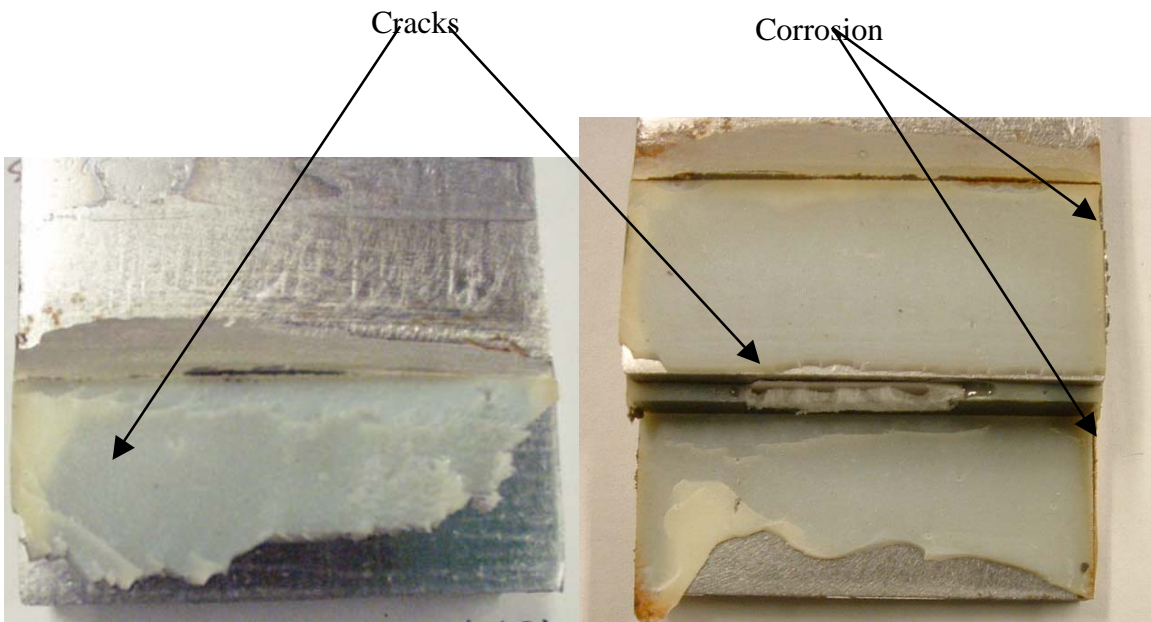


Figure 5.21 Failure mode of unloaded specimen subjected to temperature cycles between  $-4^{\circ}\text{F}$  and  $122^{\circ}\text{F}$  for 197 days (left) and 380 days (right) (Tested in lab ambient air, No GPS, bondline thickness  $t_a = 0.020$  in.)

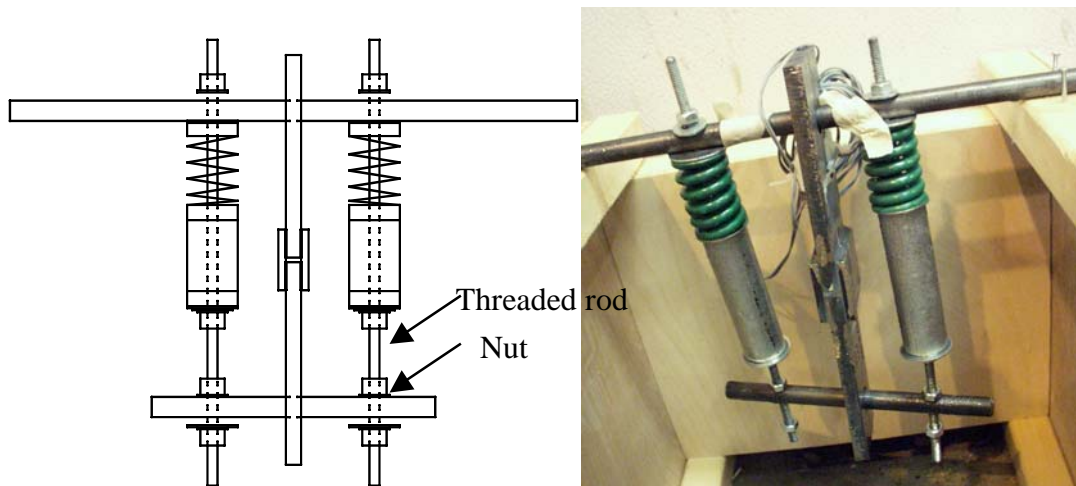


Figure 5.22 Self-equilibrium loading device

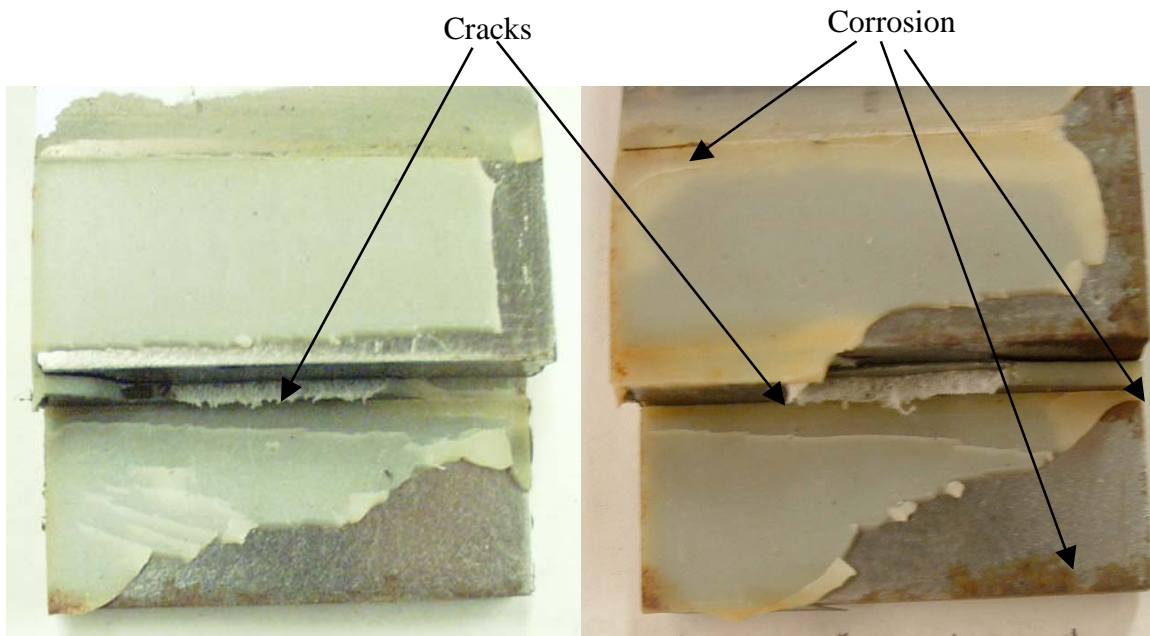


Figure 5.23 Failure mode of loaded(0.95 k) specimen subjected to temperature cycles between -4°F and 122°F for 211 days (left) and 370 days (right) (Tested in lab ambient air, No GPS, bondline thickness  $t_a = 0.020$  in.)

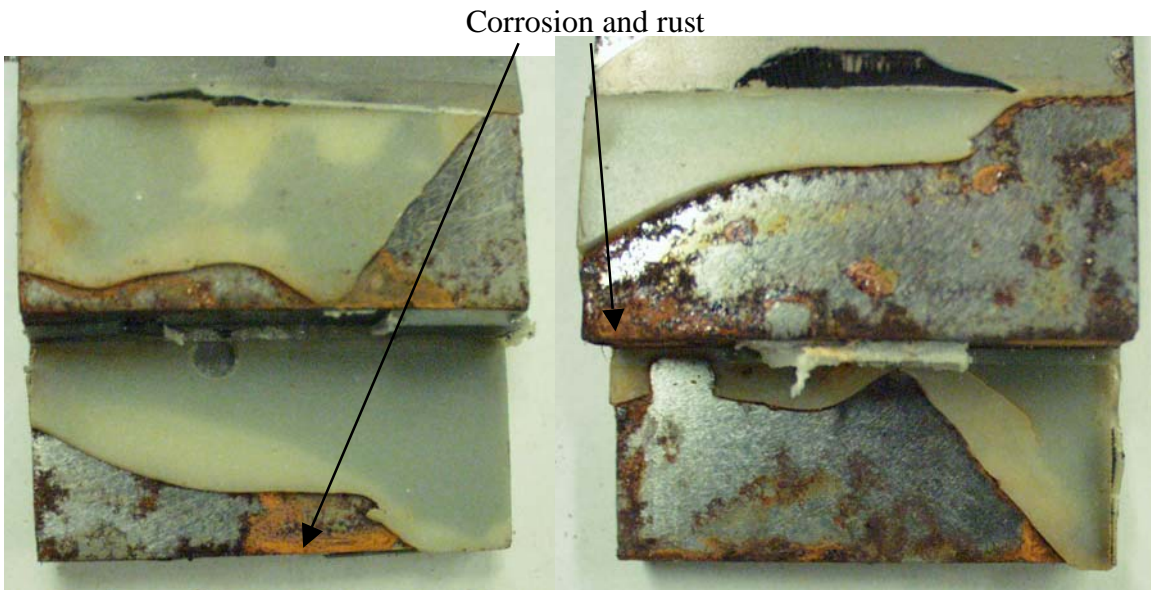


Figure 5.24 Failure mode of loaded(0.95 k) specimen subjected to temperature cycles between -4°F and 122°F (Failed in the hot chamber after 124 days of environment exposure, No GPS, bondline thickness  $t_a=0.020$  in.)

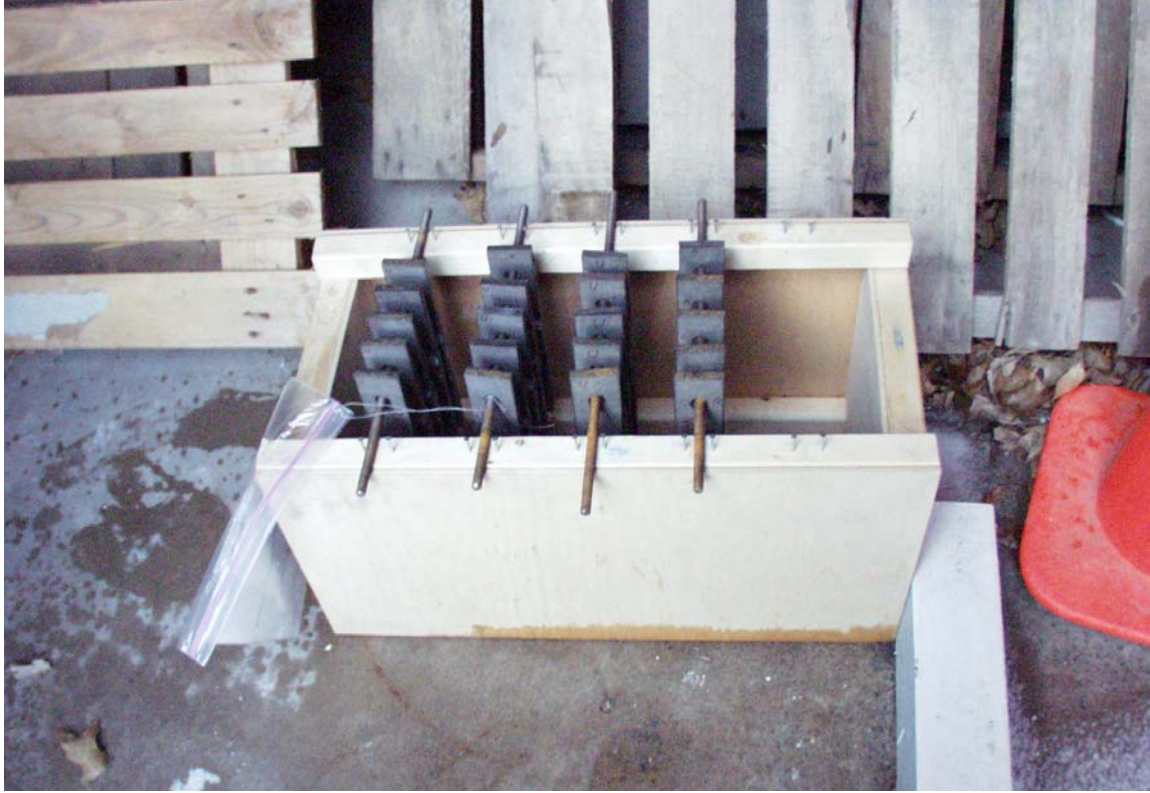


Figure 5.25 Coupon specimens kept outdoors

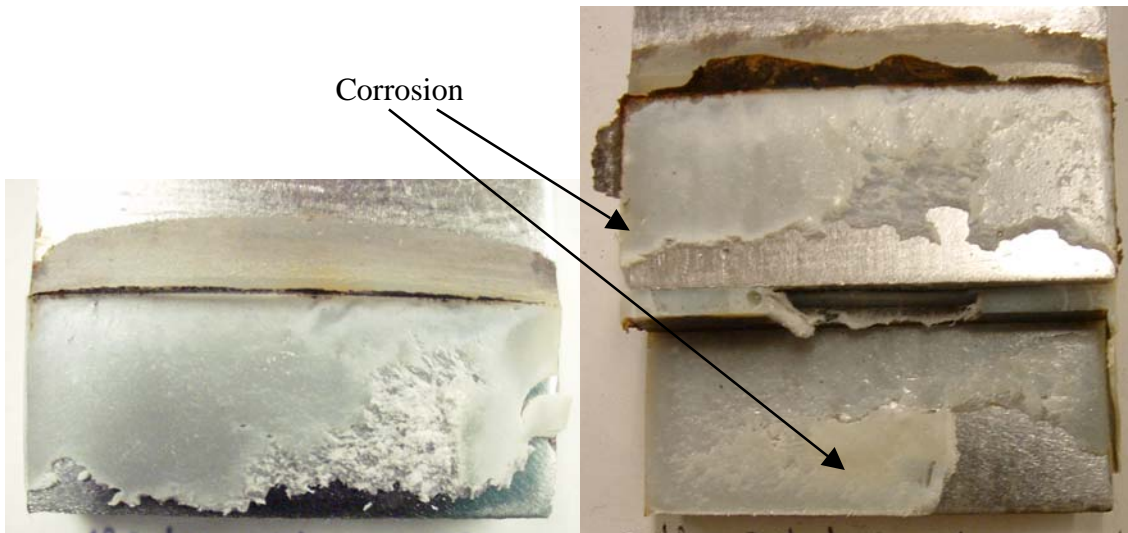


Figure 5.26 Failure mode of specimen kept outdoors for 184 days (left) and 271 days (right, cyclically loaded) (Tested in lab ambient air, No GPS, bondline thickness  $t_a = 0.020$  in.)

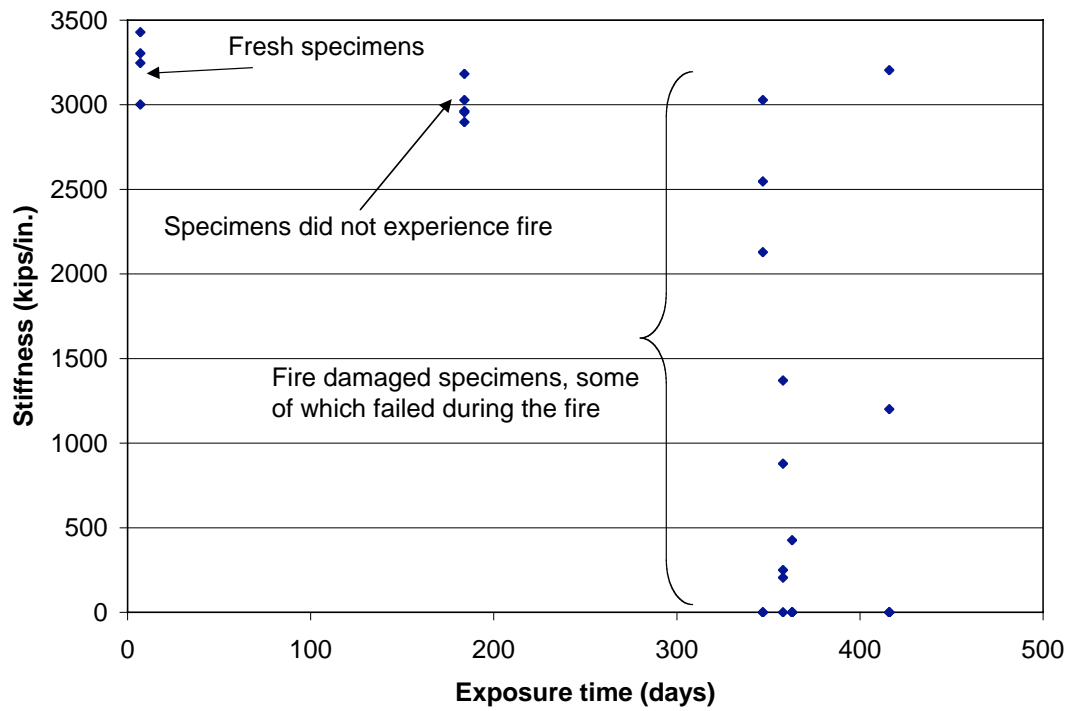
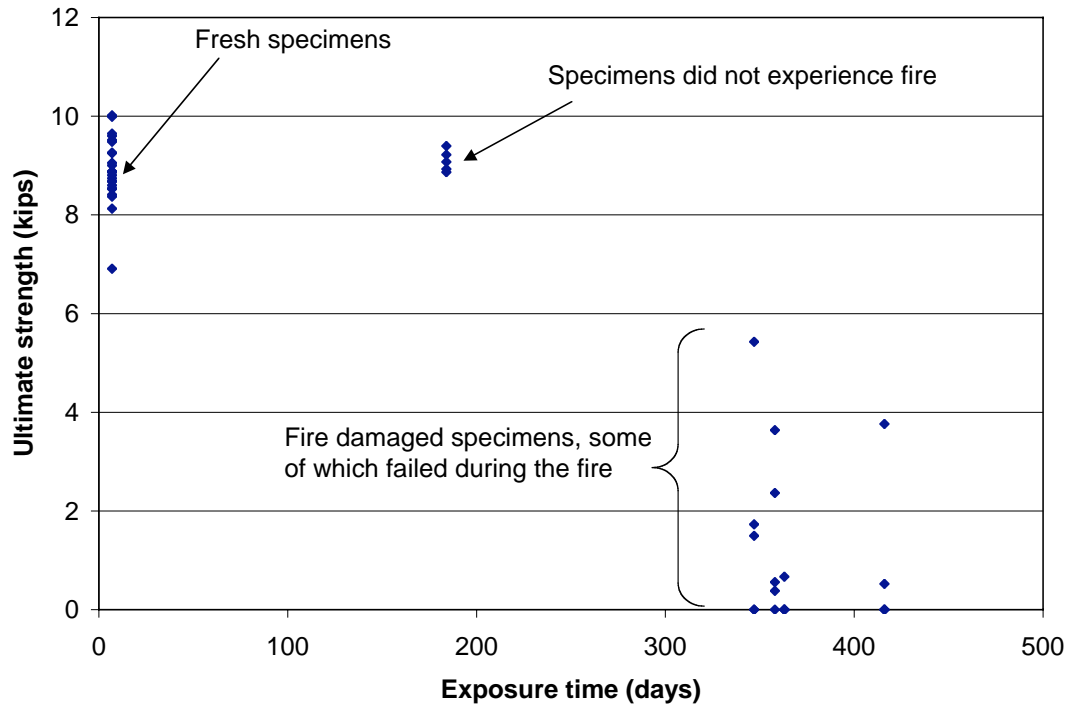


Figure 5.27 Ultimate strength and stiffness of specimens exposed to the outdoor environment and an unexpected fire (No GPS, bondline thickness  $t_a = 0.020$  in.)

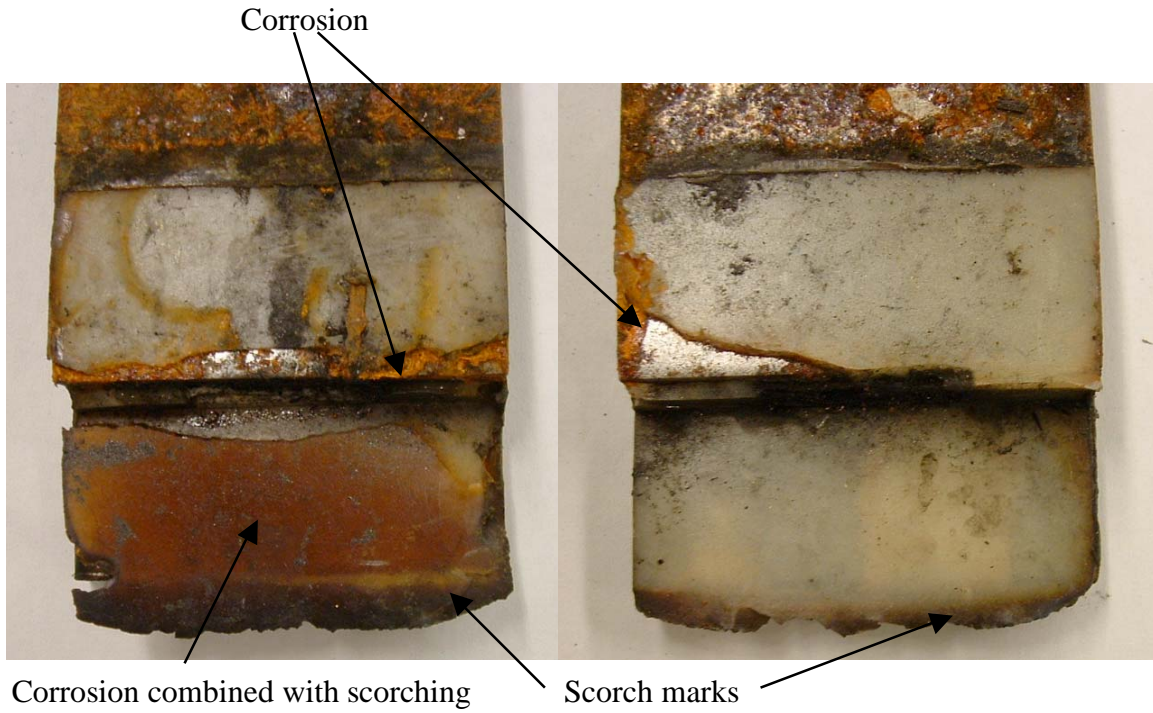


Figure 5.28 Failure mode of specimen that failed during the fire after 371 days of outdoor exposure (No GPS, bondline thickness  $t_a = 0.020$  in.)

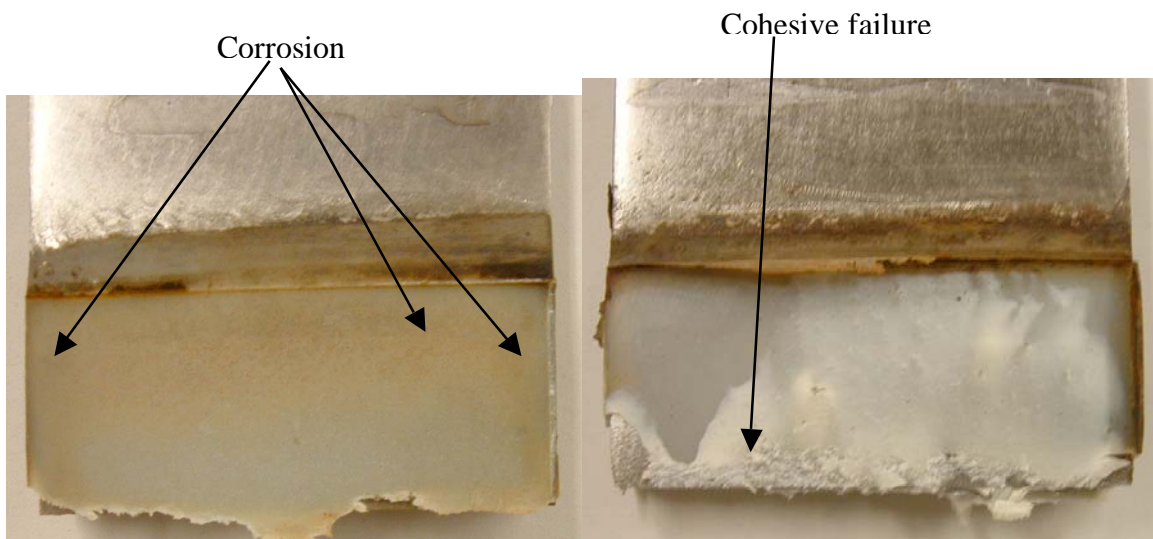


Figure 5.29 Failure mode of specimen that underwent fire after 371 days of outdoor exposure (left: ultimate strength=0.7 k, stiffness=400 k/in.; right: ultimate strength=5.4 k, stiffness=3000 k/in.)

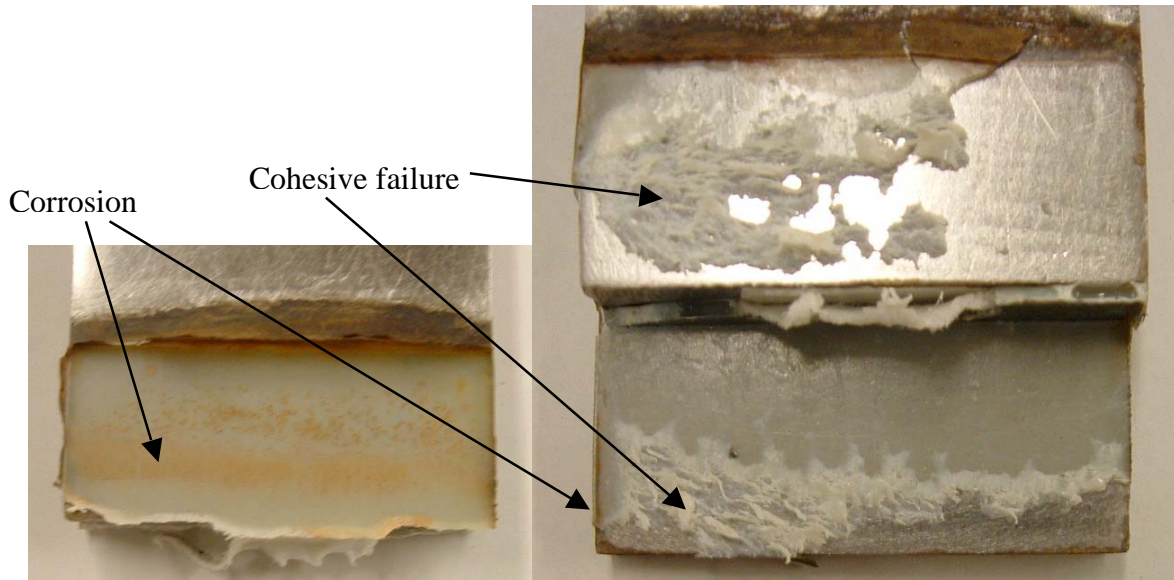


Figure 5.30 Failure mode of specimen that underwent fire after 374 days of outdoor exposure (GPS pretreated) (left: ultimate strength=1.2 k, stiffness=1800 k/in.; right: ultimate strength=7.5 k, stiffness=2800 k/in.)

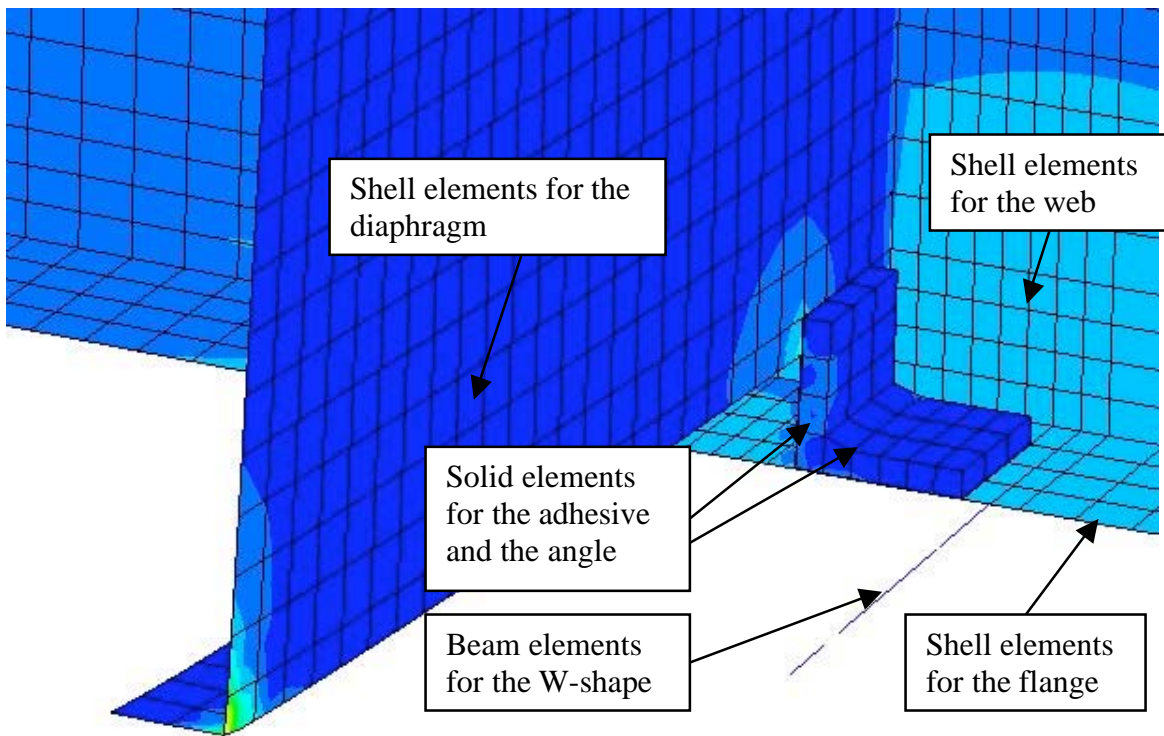


Figure 5.31 A 20-node solid element (brick element) was used to model both the adhesive and the angle for the large-scale specimen

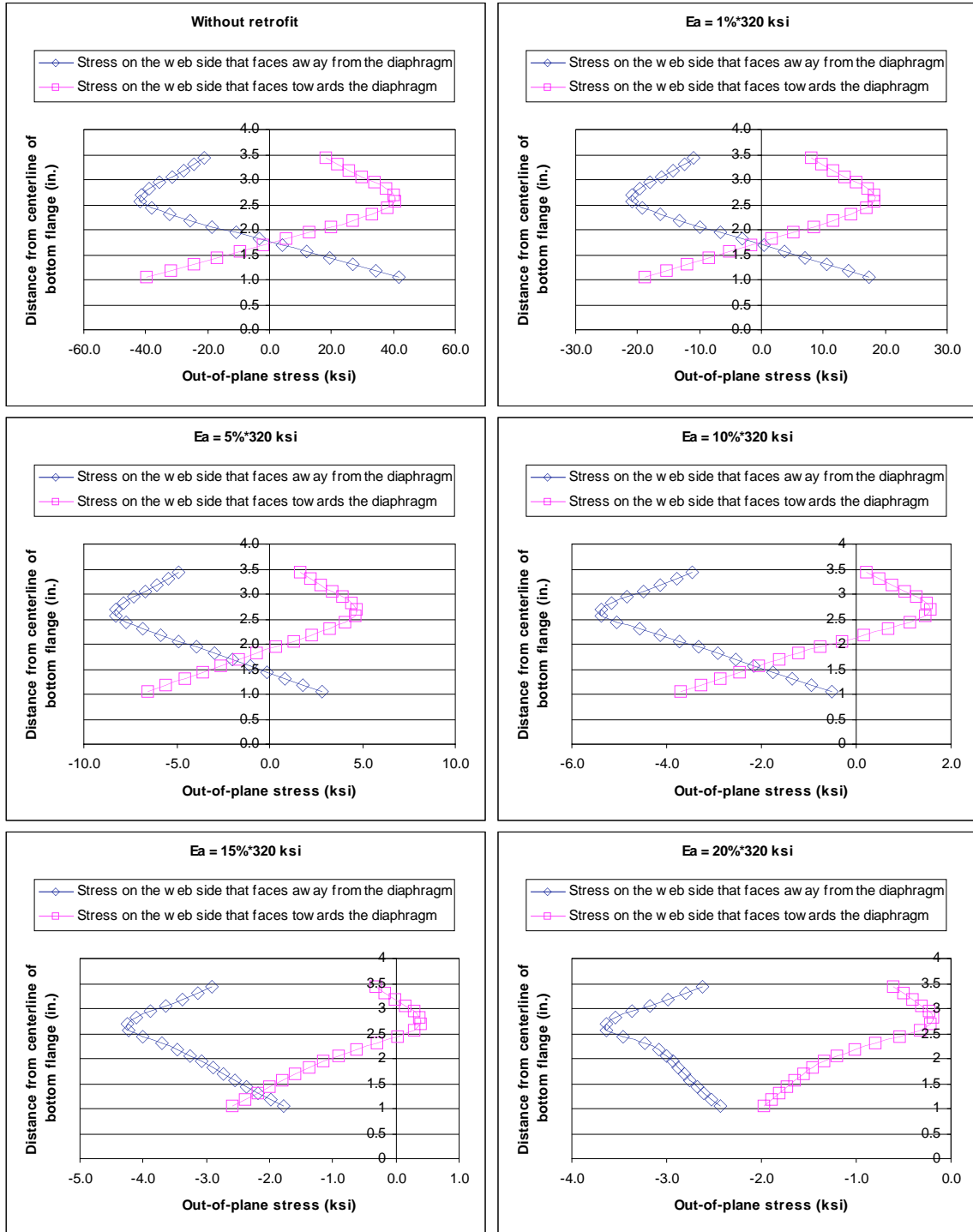


Figure 5.32 Out-of-plane stresses predicted by the FEA at web gap in the constant moment region where in-plane stress was 12 ksi (The modulus of elasticity for the adhesive is changed to investigate the influence of the adhesive stiffness on the effectiveness of the retrofit system) to be continued

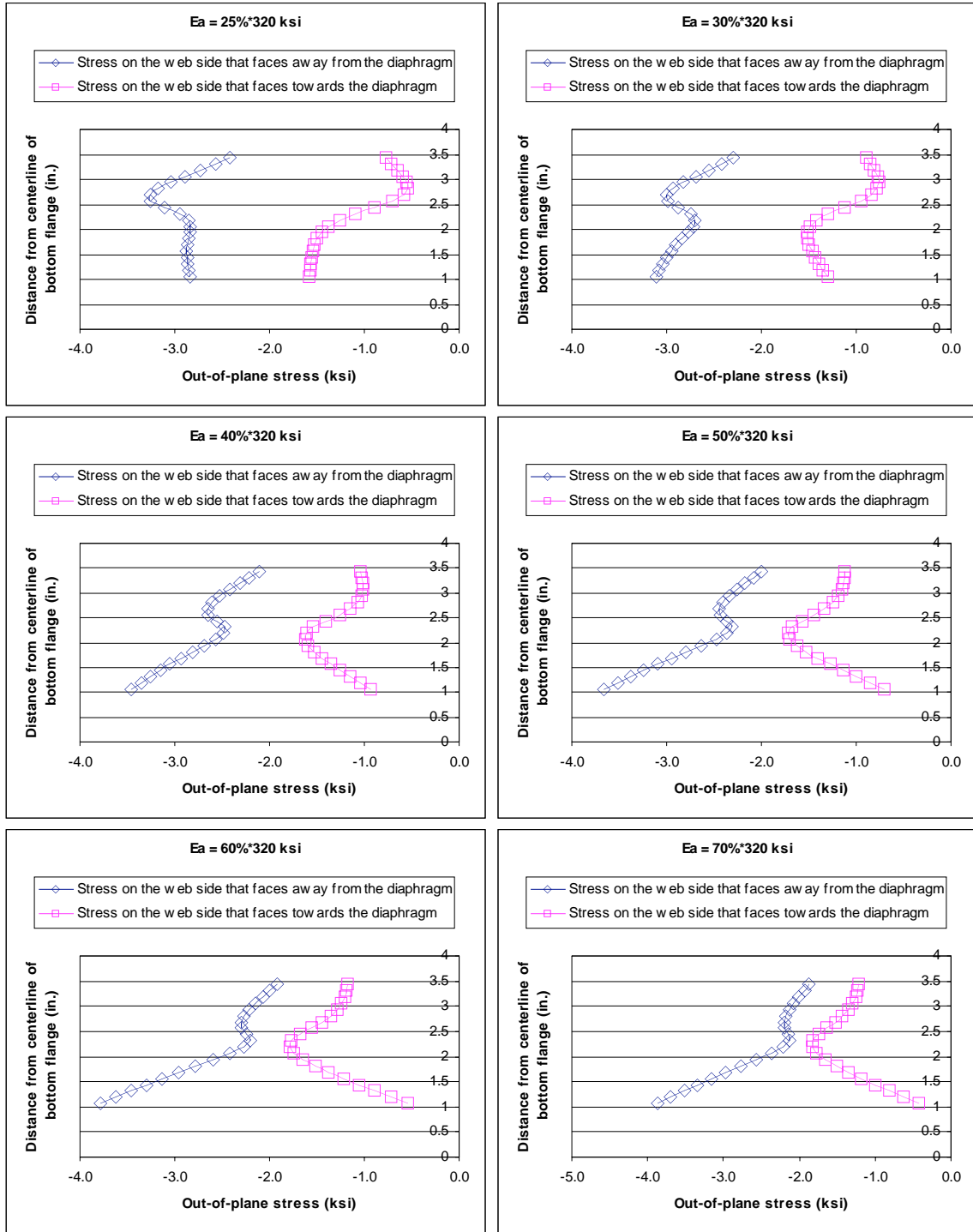


Figure 5.32 (continued) Out-of-plane stresses predicted by the FEA at web gap in the constant moment region where in-plane stress was 12 ksi (The modulus of elasticity for the adhesive is changed to investigate the influence of the adhesive stiffness on the effectiveness of the retrofit system) to be continued

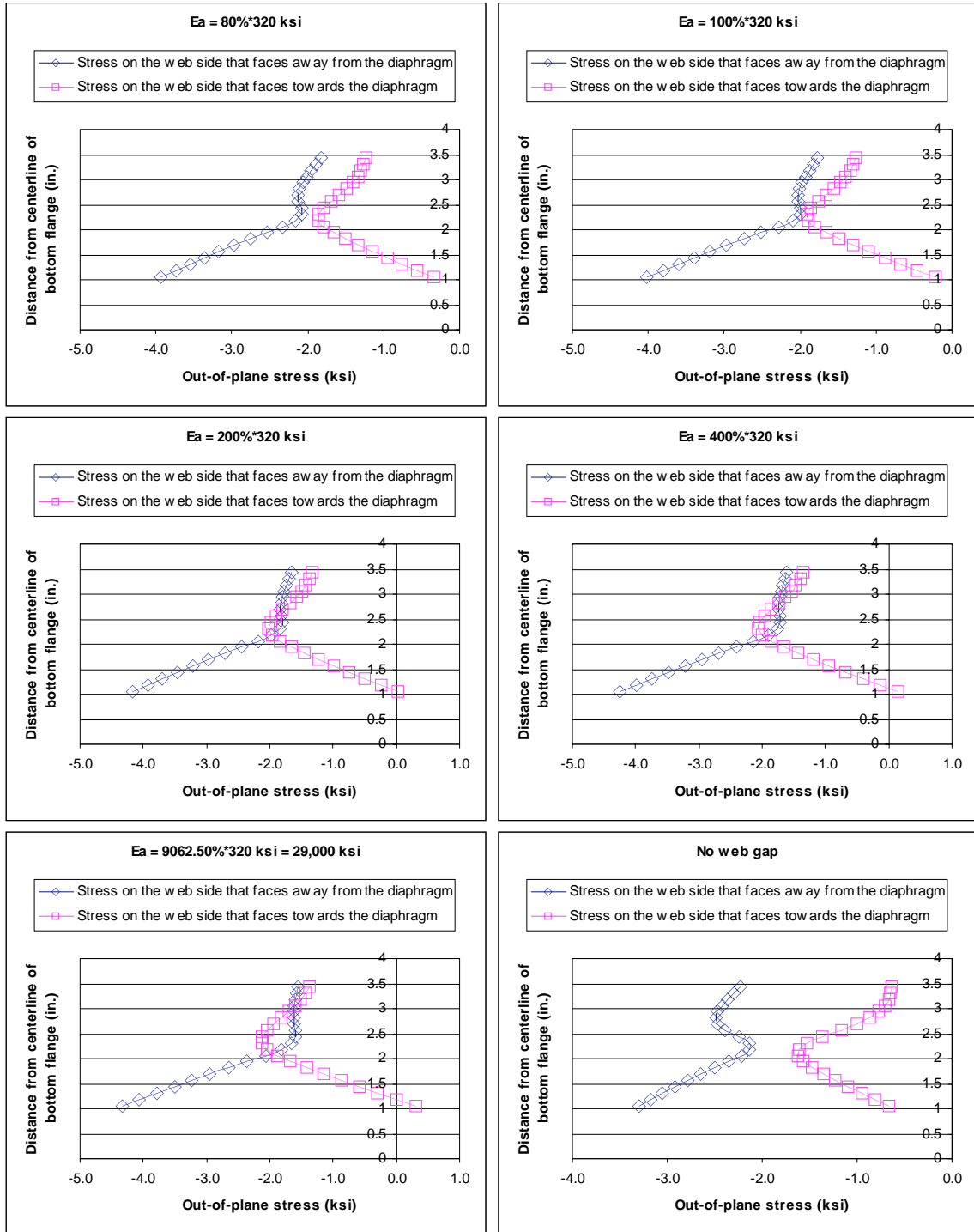


Figure 5.32 (continued) Out-of-plane stresses predicted by the FEA at web gap in the constant moment region where in-plane stress was 12 ksi (The modulus of elasticity for the adhesive is changed to investigate the influence of the adhesive stiffness on the effectiveness of the retrofit system)

## **Appendix A**

### **Gage labeling of the bridges for the field test**

Table A.1 Strain gage labeling for the BPD bridge (Bridge #27763)

Gage label	Girder	Location and position	Gage type
1-B5-1-G	B5	Web gap, vertical	Single
1-B5-2-G	B5	Web gap, vertical	Single
1-B5-3-G	B5	Web gap, vertical	Single
1-B5-4-G	B5	Web gap, vertical	Single
1-B5-5-B	B5	Girder web, 0.5" from the top flange, horizontal	Single
1-B5-6-B	B5	Girder web, 1'-10" from the bottom flange, horizontal	Single
1-B5-7-B	B5	Girder bottom flange, horizontal	Single
1-B5-R1-C	B5	Connection plate, 1st leg of rosette, horizontal	Rosette
1-B5-R2-C	B5	Connection plate, 2nd leg of rosette, 45°	Rosette
1-B5-R3-C	B5	Connection plate, 3rd leg of rosette, vertical	Rosette
1-B5-R1-D	B5	Diaphragm plate, 1st leg of rosette, horizontal	Rosette
1-B5-R2-D	B5	Diaphragm plate, 2nd leg of rosette, 45°	Rosette
1-B5-R3-D	B5	Diaphragm plate, 3rd leg of rosette, vertical	Rosette
1-B4-1-G	B4	Web gap, vertical	Single
1-B4-2-G	B4	Web gap, vertical	Single
1-B4-3-G	B4	Web gap, vertical	Single
1-B4-4-G	B4	Web gap, vertical	Single
1-B4-5-B	B4	Girder web, 0.5" from the top flange, horizontal	Single
1-B4-6-B	B4	Girder web, 1'-10" from the bottom flange, horizontal	Single
1-B4-7-B	B4	Girder bottom flange, horizontal	Single
1-B4-8-D	B4	Diaphragm web, as close to the top flange as possible, horizontal	Single
1-B4-9-D	B4	Diaphragm web, 1'-3" from the bottom flange, horizontal	Single
1-B4-10-D	B4	Diaphragm web, as close to the bottom flange as possible, horizontal	Single
1-B4-R1-C	B4	Connection plate, 1st leg of rosette, horizontal	Rosette
1-B4-R2-C	B4	Connection plate, 2nd leg of rosette, 45°	Rosette
1-B4-R3-C	B4	Connection plate, 3rd leg of rosette, vertical	Rosette
1-B4-R1-D	B4	Diaphragm plate, 1st leg of rosette, horizontal	Rosette
1-B4-R2-D	B4	Diaphragm plate, 2nd leg of rosette, 45°	Rosette
1-B4-R3-D	B4	Diaphragm plate, 3rd leg of rosette, vertical	Rosette
1-B4W-1-G	B4	Web gap on the west side of the same girder, vertical	Single
1-B4W-2-G	B4	Web gap on the west side of the same girder, vertical	Single
1-B4W-3-G	B4	Web gap on the west side of the same girder, vertical	Single
1-B4W-4-G	B4	Web gap on the west side of the same girder, vertical	Single
1-B3-1-G	B3	Web gap, vertical	Single
1-B3-2-G	B3	Web gap, vertical	Single
1-B3-3-G	B3	Web gap, vertical	Single
1-B3-4-G	B3	Web gap, vertical	Single
1-B3-5-B	B3	Girder web, 0.5" from the top flange, horizontal	Single
1-B3-6-B	B3	Girder web, 1'-10" from the bottom flange, horizontal	Single
1-B3-7-B	B3	Girder bottom flange, horizontal	Single

Table A.2 Strain gage labeling for the CFD bridge (Bridge #27984)

Gage label	Girder	Location and position	Gage type
2-B4-1-G	B4	Web gap, vertical	Single
2-B4-2-G	B4	Web gap, vertical	Single
2-B4-3-G	B4	Web gap, vertical	Single
2-B4-4-G	B4	Web gap, vertical	Single
2-B4-5-B	B4	Girder web, 0.5" from the top flange, horizontal	Single
2-B4-6-B	B4	Girder web, 2'-4" from the bottom flange, horizontal	Single
2-B4-7-B	B4	Girder bottom flange, horizontal	Single
2-B4-8-D	B4	Diaphragm, web chord, parallel to the chord	Single
2-B4-9-D	B4	Diaphragm, web chord, parallel to the chord	Single
2-B4-10-D	B4	Diaphragm, lower chord, parallel to the chord, i.e., horizontal	Single
2-B4-11-D	B4	Diaphragm, lower chord, parallel to the chord, i.e., horizontal	Single
2-B4-R1-C	B4	Connection plate, 1st leg of rosette, horizontal	Rosette
2-B4-R2-C	B4	Connection plate, 2nd leg of rosette, 45°	Rosette
2-B4-R3-C	B4	Connection plate, 3rd leg of rosette, vertical	Rosette
2-B3-1-G	B3	Web gap, vertical	Single
2-B3-2-G	B3	Web gap, vertical	Single
2-B3-3-G	B3	Web gap, vertical	Single
2-B3-4-G	B3	Web gap, vertical	Single
2-B3-5-B	B3	Girder web, 0.5" from the top flange, horizontal	Single
2-B3-6-B	B3	Girder web, 2'-4" from the bottom flange, horizontal	Single
2-B3-7-B	B3	Girder bottom flange, horizontal	Single
2-B3-12-D	B3	Diaphragm, web chord, parallel to the chord	Single
2-B3-13-D	B3	Diaphragm, web chord, parallel to the chord	Single
2-B3-R1-C	B3	Connection plate, 1st leg of rosette, horizontal	Rosette
2-B3-R2-C	B3	Connection plate, 2nd leg of rosette, 45°	Rosette
2-B3-R3-C	B3	Connection plate, 3rd leg of rosette, vertical	Rosette
2-B3W-1-G	B3	Web gap, vertical	Single
2-B3W-2-G	B3	Web gap, vertical	Single
2-B3W-3-G	B3	Web gap, vertical	Single
2-B3W-4-G	B3	Web gap, vertical	Single
2-B3W-8-D	B3	Diaphragm, web chord, parallel to the chord	Single
2-B3W-9-D	B3	Diaphragm, web chord, parallel to the chord	Single
2-B3W-10-D	B3	Diaphragm, lower chord, parallel to the chord, i.e., horizontal	Single
2-B3W-11-D	B3	Diaphragm, lower chord, parallel to the chord, i.e., horizontal	Single
2-B2-1-G	B2	Web gap, vertical	Single
2-B2-2-G	B2	Web gap, vertical	Single
2-B2-3-G	B2	Web gap, vertical	Single
2-B2-4-G	B2	Web gap, vertical	Single
2-B2-5-B	B2	Girder web, 0.5" from the top flange, horizontal	Single
2-B2-6-B	B2	Girder web, 2'-4" from the bottom flange, horizontal	Single
2-B2-7-B	B2	Girder bottom flange, horizontal	Single
2-B2-12-D	B2	Diaphragm, web chord, parallel to the chord	Single
2-B2-13-D	B2	Diaphragm, web chord, parallel to the chord	Single

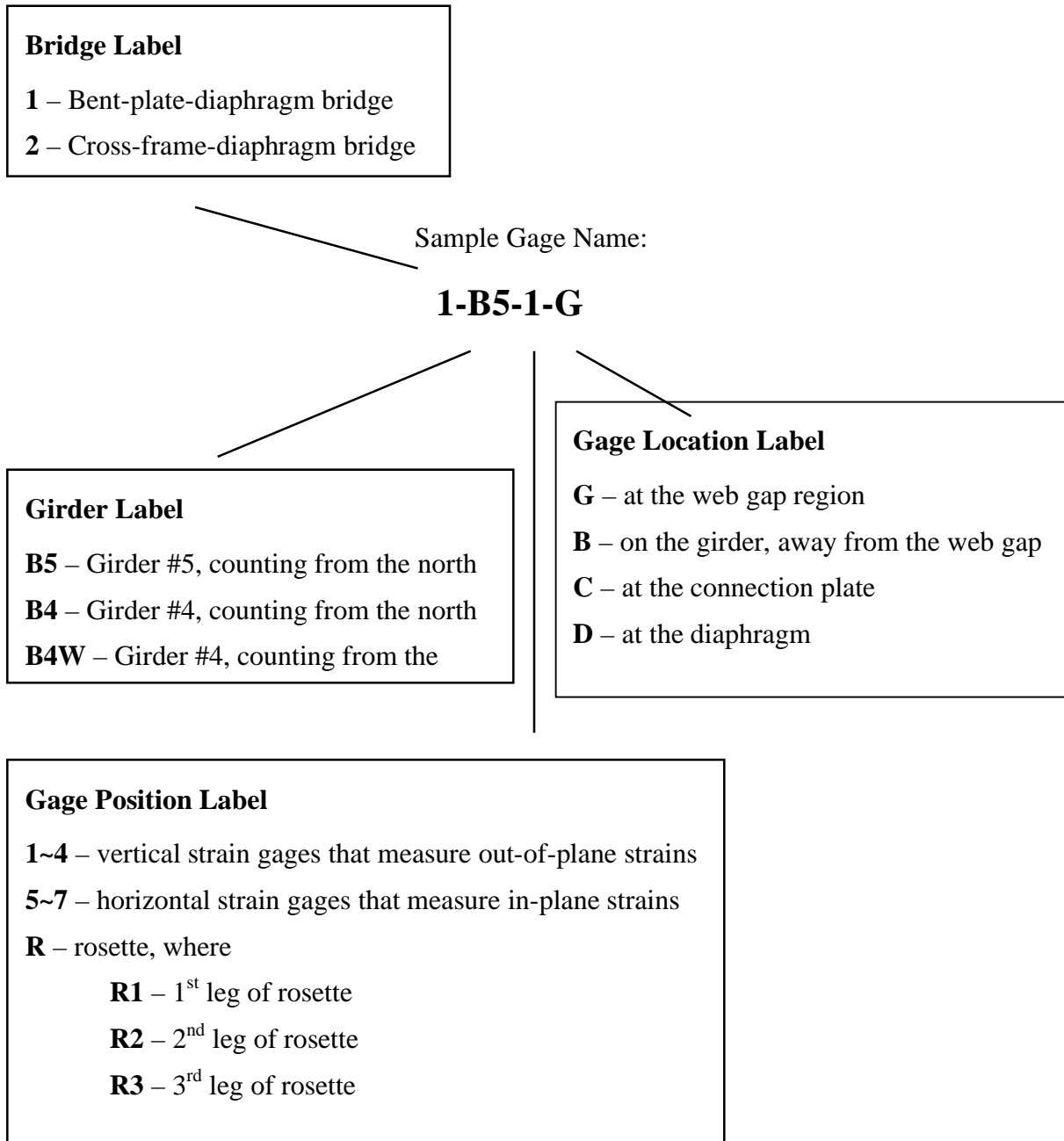


Figure A.1 Gage labeling of the bridges for the field test

## **Appendix B**

**The procedure of applying the retrofitting angles in the field test**

The following describes the procedure of applying retrofit angles in the field:

7. The surfaces of the retrofitting angle, the top flange and the connection plate were ground smooth.
8. The surfaces were wiped with acetone until no black oxide appeared when a new piece of white rag was used to wipe the surface. Since the black color of the oxide was most discernable in the white background, white rags were used.
9. DP-460NS adhesive was applied and spread over the surface of the retrofitting angle. A thin layer of adhesive was applied and spread over the surface of the top flange and connection plate.
10. Twenty to forty 0.020 in. diameter glass beads were sprayed onto each adhesive covered surface of the angle for all angles except Angle A2-8.
11. The retrofitting angle was pressed hard against the top flange while the bolt was tightened to snug tight, or until the glass beads began breaking.

It should be mentioned that the temperature recommended for the use of this adhesive is around 70°F. It was November when the angles were bonded to the bridges. The daytime temperature was approximately 50°F and the adhesive became so thick that the two parts could not be squeezed out through the manufacture supplied static mixing nozzle. As a result, the two parts were squeezed out directly from the cartridge to the angle surface, and then they were mixed with a spatula. Though efforts were made to mix them as thoroughly as possible, there were likely areas of incomplete mix. This application represented the worst situation of field application and should provide the lower bound performance of the adhesive. In some cases, a heat gun was used to facilitate squeezing the adhesives out and mixing them. Sometimes, a heat gun was also used to heat the angle for five minutes after the angle was put on to facilitate curing of the adhesive.

## **Appendix C**

**Strain ranges at web gap before/after retrofit in the field test**

Table C.1(a) Web gap strain ranges on B5 before/after retrofit for the bent-plate-diaphragm bridge (Retrofit angle was applied)

Gage Label	Pass 1 (static)			Pass 2 (static)		
	before ( $\mu\epsilon$ )	after ( $\mu\epsilon$ )	after/before ratio	before ( $\mu\epsilon$ )	after ( $\mu\epsilon$ )	after/before ratio
1-B5-1-G	95	36	38%	131	64	49%
1-B5-2-G	93	36	39%	131	65	50%
1-B5-3-G	-103	-36	35%	-143	-84	59%
1-B5-4-G	-118	-41	35%	-157	-90	57%
Gage Label	Pass 3 (static)			Pass 4 (10 mph)		
	before ( $\mu\epsilon$ )	after ( $\mu\epsilon$ )	after/before ratio	before ( $\mu\epsilon$ )	after ( $\mu\epsilon$ )	after/before ratio
1-B5-1-G	137	75	55%	75	39	52%
1-B5-2-G	137	77	56%	74	36	49%
1-B5-3-G	-164	-112	68%	91	52	57%
1-B5-4-G	-176	-118	67%	99	55	56%
Gage Label	Pass 5 (10 mph)			Pass 6 (40 mph)		
	before ( $\mu\epsilon$ )	after ( $\mu\epsilon$ )	after/before ratio	before ( $\mu\epsilon$ )	after ( $\mu\epsilon$ )	after/before ratio
1-B5-1-G	70	38	54%	95	51	54%
1-B5-2-G	68	37	54%	95	49	52%
1-B5-3-G	85	55	65%	109	65	60%
1-B5-4-G	90	57	63%	124	70	56%
Gage Label	Pass 7 (40 mph)			Pass 8 (10 mph)		
	before ( $\mu\epsilon$ )	after ( $\mu\epsilon$ )	after/before ratio	before ( $\mu\epsilon$ )	after ( $\mu\epsilon$ )	after/before ratio
1-B5-1-G	125	53	42%	180	95	53%
1-B5-2-G	122	52	43%	183	96	52%
1-B5-3-G	143	69	48%	217	139	64%
1-B5-4-G	157	76	48%	233	149	64%

Note:

- All values presented here are averages if one pass was conducted more than once.
- Description of the passes (refer to Figures 3.11 and 3.12 for more information)
 

Pass 1~3	One truck stayed with left front wheel at specific locations on B5
Pass 4	One truck stayed at position of Pass 2, and one truck traveled at 10 mph with left wheels on B4
Pass 5	One truck traveled at 10 mph with left wheels on B4
Pass 6	One truck traveled at 40 mph on the left lane with right wheels as close to B3 as possible
Pass 7	One truck traveled at 40 mph on the left lane with right wheels as close to B3 as possible, the other truck traveled side by side at 40 mph with left wheels on B4
Pass 8	One truck traveled at 10 mph with left wheels on B5
- For Pass 1~3, strain values are provided; for other passes, strain range values are provided.

Table C.1(b) Web gap strain ranges on B4 before/after retrofit for the bent-plate-diaphragm bridge (Retrofit angle was applied)

Gage Label	Pass 1 (static)			Pass 2 (static)		
	before ( $\mu\epsilon$ )	after ( $\mu\epsilon$ )	after/before ratio	before ( $\mu\epsilon$ )	after ( $\mu\epsilon$ )	after/before ratio
1-B4-1-G	-33	-18	55%	-25	-13	52%
1-B4-2-G	-33	-17	52%	-25	-12	48%
1-B4-3-G	38	22	58%	29	16	55%
1-B4-4-G	34	20	59%	26	14	54%
Gage Label	Pass 3 (static)			Pass 4 (10 mph)		
	before ( $\mu\epsilon$ )	after ( $\mu\epsilon$ )	after/before ratio	before ( $\mu\epsilon$ )	after ( $\mu\epsilon$ )	after/before ratio
1-B4-1-G	-18	-10	56%	33	17	52%
1-B4-2-G	-18	-9	50%	34	15	44%
1-B4-3-G	22	12	55%	40	27	68%
1-B4-4-G	19	11	58%	40	28	70%
Gage Label	Pass 5 (10 mph)			Pass 6 (40 mph)		
	before ( $\mu\epsilon$ )	after ( $\mu\epsilon$ )	after/before ratio	before ( $\mu\epsilon$ )	after ( $\mu\epsilon$ )	after/before ratio
1-B4-1-G	37	20	54%	22	15	68%
1-B4-2-G	36	19	53%	23	15	65%
1-B4-3-G	41	32	78%	24	16	67%
1-B4-4-G	42	31	74%	24	19	79%
Gage Label	Pass 7 (40 mph)			Pass 8 (10 mph)		
	before ( $\mu\epsilon$ )	after ( $\mu\epsilon$ )	after/before ratio	before ( $\mu\epsilon$ )	after ( $\mu\epsilon$ )	after/before ratio
1-B4-1-G	39	19	49%	47	24	51%
1-B4-2-G	39	17	44%	47	22	47%
1-B4-3-G	47	31	66%	50	26	52%
1-B4-4-G	48	32	67%	49	26	53%

Note:

1. All values presented here are averages if one pass was conducted more than once.

2. Description of the passes (refer to Figures 3.11 and 3.12 for more information)

Pass 1~3 One truck stayed with left front wheel at specific locations on B5

Pass 4 One truck stayed at position of Pass 2, and one truck traveled at 10 mph with left wheels on B4

Pass 5 One truck traveled at 10 mph with left wheels on B4

Pass 6 One truck traveled at 40 mph on the left lane with right wheels as close to B3 as possible

Pass 7 One truck traveled at 40 mph on the left lane with right wheels as close to B3 as possible, the other truck traveled side by side at 40 mph with left wheels on B4

Pass 8 One truck traveled at 10 mph with left wheels on B5

3. For Pass 1~3, strain values are provided; for other passes, strain range values are provided.

Table C.1(c) Web gap strain ranges on B4W before/after retrofit for the bent-plate-diaphragm bridge (Retrofit angle was not applied)

Gage Label	Pass 1 (static)			Pass 2 (static)		
	before ( $\mu\epsilon$ )	after ( $\mu\epsilon$ )	after/before ratio	before ( $\mu\epsilon$ )	after ( $\mu\epsilon$ )	after/before ratio
1-B4W-1-G	31	29	94%	25	24	96%
1-B4W-2-G	33	31	94%	27	26	96%
1-B4W-3-G	-38	-35	92%	-31	-29	94%
1-B4W-4-G	-37	-34	92%	-30	-28	93%
Gage Label	Pass 3 (static)			Pass 4 (10 mph)		
	before ( $\mu\epsilon$ )	after ( $\mu\epsilon$ )	after/before ratio	before ( $\mu\epsilon$ )	after ( $\mu\epsilon$ )	after/before ratio
1-B4W-1-G	19	19	100%	111	98	88%
1-B4W-2-G	20	20	100%	110	103	94%
1-B4W-3-G	-23	-22	96%	126	124	98%
1-B4W-4-G	-23	-22	96%	129	122	95%
Gage Label	Pass 5 (10 mph)			Pass 6 (40 mph)		
	before ( $\mu\epsilon$ )	after ( $\mu\epsilon$ )	after/before ratio	before ( $\mu\epsilon$ )	after ( $\mu\epsilon$ )	after/before ratio
1-B4W-1-G	102	112	110%	65	72	111%
1-B4W-2-G	105	116	110%	68	73	107%
1-B4W-3-G	130	142	109%	77	76	99%
1-B4W-4-G	128	140	109%	78	81	104%
Gage Label	Pass 7 (40 mph)			Pass 8 (10 mph)		
	before ( $\mu\epsilon$ )	after ( $\mu\epsilon$ )	after/before ratio	before ( $\mu\epsilon$ )	after ( $\mu\epsilon$ )	after/before ratio
1-B4W-1-G	77	122	158%	68	62	91%
1-B4W-2-G	81	127	157%	72	68	94%
1-B4W-3-G	99	152	154%	82	76	93%
1-B4W-4-G	99	150	152%	85	74	87%

Note:

1. All values presented here are averages if one pass was conducted more than once.

2. Description of the passes (refer to Figures 3.11 and 3.12 for more information)

Pass 1~3 One truck stayed with left front wheel at specific locations on B5

Pass 4 One truck stayed at position of Pass 2, and one truck traveled at 10 mph with left wheels on B4

Pass 5 One truck traveled at 10 mph with left wheels on B4

Pass 6 One truck traveled at 40 mph on the left lane with right wheels as close to B3 as possible

Pass 7 One truck traveled at 40 mph on the left lane with right wheels as close to B3 as possible, the other truck traveled side by side at 40 mph with left wheels on B4

Pass 8 One truck traveled at 10 mph with left wheels on B5

3. For Pass 1~3, strain values are provided; for other passes, strain range values are provided.

Table C.1(d) Web gap strain ranges on B3 before/after retrofit for the bent-plate-diaphragm bridge (Retrofit angle was applied)

Gage Label	Pass 1 (static)			Pass 2 (static)		
	before ( $\mu\epsilon$ )	after ( $\mu\epsilon$ )	after/before ratio	before ( $\mu\epsilon$ )	after ( $\mu\epsilon$ )	after/before ratio
1-B3-1-G	19	17	89%	16	15	94%
1-B3-2-G	16	15	94%	14	13	93%
1-B3-3-G	-25	-21	84%	-21	-18	86%
1-B3-4-G	-26	-22	85%	-22	-19	86%
Gage Label	Pass 3 (static)			Pass 4 (10 mph)		
	before ( $\mu\epsilon$ )	after ( $\mu\epsilon$ )	after/before ratio	before ( $\mu\epsilon$ )	after ( $\mu\epsilon$ )	after/before ratio
1-B3-1-G	13	12	92%	41	34	83%
1-B3-2-G	11	10	91%	38	31	82%
1-B3-3-G	-17	-15	88%	50	36	72%
1-B3-4-G	-18	-15	83%	47	36	77%
Gage Label	Pass 5 (10 mph)			Pass 6 (40 mph)		
	before ( $\mu\epsilon$ )	after ( $\mu\epsilon$ )	after/before ratio	before ( $\mu\epsilon$ )	after ( $\mu\epsilon$ )	after/before ratio
1-B3-1-G	40	27	68%	30	17	57%
1-B3-2-G	39	25	64%	29	16	55%
1-B3-3-G	45	36	80%	40	24	60%
1-B3-4-G	46	36	78%	39	23	59%
Gage Label	Pass 7 (40 mph)			Pass 8 (10 mph)		
	before ( $\mu\epsilon$ )	after ( $\mu\epsilon$ )	after/before ratio	before ( $\mu\epsilon$ )	after ( $\mu\epsilon$ )	after/before ratio
1-B3-1-G	51	34	67%	40	32	80%
1-B3-2-G	48	32	67%	38	26	68%
1-B3-3-G	64	40	63%	48	39	81%
1-B3-4-G	65	42	65%	50	39	78%

Note:

1. All values presented here are averages if one pass was conducted more than once.

2. Description of the passes (refer to Figures 3.11 and 3.12 for more information)

Pass 1~3 One truck stayed with left front wheel at specific locations on B5

Pass 4 One truck stayed at position of Pass 2, and one truck traveled at 10 mph with left wheels on B4

Pass 5 One truck traveled at 10 mph with left wheels on B4

Pass 6 One truck traveled at 40 mph on the left lane with right wheels as close to B3 as possible

Pass 7 One truck traveled at 40 mph on the left lane with right wheels as close to B3 as possible, the other truck traveled side by side at 40 mph with left wheels on B4

Pass 8 One truck traveled at 10 mph with left wheels on B5

3. For Pass 1~3, strain values are provided; for other passes, strain range values are provided.

Table C.2(a) Web gap strain ranges on B4 before/after retrofit for the cross-frame-diaphragm bridge (Retrofit angle was applied)

Gage Label	Pass 1 (static)			Pass 2 (static)		
	before (µε)	after (µε)	after/before ratio	before (µε)	after (µε)	after/before ratio
2-B4-1-G	26	16	62%	24	14	58%
2-B4-2-G	32	19	59%	31	17	55%
2-B4-3-G	-24	-10	42%	-24	-11	46%
2-B4-4-G	-29	-12	41%	-28	-13	46%
Gage Label	Pass 3 (static)			Pass 4 (10 mph)		
	before (µε)	after (µε)	after/before ratio	before (µε)	after (µε)	after/before ratio
2-B4-1-G	-37	9	-24%	99	17	17%
2-B4-2-G	29	13	45%	104	14	13%
2-B4-3-G	13	9	69%	76	18	24%
2-B4-4-G	8	-11	-138%	72	16	22%
Gage Label	Pass 5 (10 mph)			Pass 6 (40 mph)		
	before (µε)	after (µε)	after/before ratio	before (µε)	after (µε)	after/before ratio
2-B4-1-G	92	14	15%	22	14	64%
2-B4-2-G	90	12	13%	24	15	63%
2-B4-3-G	67	14	21%	26	14	54%
2-B4-4-G	66	13	20%	27	17	63%
Gage Label	Pass 7 (40 mph)			Pass 8 (10 mph)		
	before (µε)	after (µε)	after/before ratio	before (µε)	after (µε)	after/before ratio
2-B4-1-G	88	14	16%	71	28	39%
2-B4-2-G	81	15	19%	72	31	43%
2-B4-3-G	63	15	24%	47	23	49%
2-B4-4-G	66	15	23%	47	25	53%

Note:

- All values presented here are averages if one pass was conducted more than once.
- Description of the passes (refer to Figures 3.11 and 3.12 for more information)

Pass 1~3	One truck stayed with left front wheel at specific locations on B4
Pass 4	One truck stayed at position of Pass 2, and one truck traveled at 10 mph with left wheels on B3
Pass 5	One truck traveled at 10 mph with left wheels on B3
Pass 6	One truck traveled at 40 mph on the left lane with right wheels as close to B2 as possible
Pass 7	One truck traveled at 40 mph on the left lane with right wheels as close to B2 as possible, the other truck traveled side by side at 40 mph with left wheels on B3
Pass 8	One truck traveled at 10 mph with left wheels on B4
- For Pass 1~3, strain values are provided; for other passes, strain range values are provided.

Table C.2(b) Web gap strain ranges on B3 before/after retrofit for the cross-frame-diaphragm bridge (Retrofit angle was applied)

Gage Label	Pass 1 (static)			Pass 2 (static)		
	before ( $\mu\epsilon$ )	after ( $\mu\epsilon$ )	after/before ratio	before ( $\mu\epsilon$ )	after ( $\mu\epsilon$ )	after/before ratio
2-B3-1-G	-6	-6	100%	-6	-6	100%
2-B3-2-G	-11	-12	109%	-11	-11	100%
2-B3-3-G	15	15	100%	14	13	93%
2-B3-4-G	17	16	94%	16	15	94%
Gage Label	Pass 3 (static)			Pass 4 (10 mph)		
	before ( $\mu\epsilon$ )	after ( $\mu\epsilon$ )	after/before ratio	before ( $\mu\epsilon$ )	after ( $\mu\epsilon$ )	after/before ratio
2-B3-1-G	-5	-5	100%	18	13	72%
2-B3-2-G	-9	-10	111%	20	18	90%
2-B3-3-G	13	12	92%	24	17	71%
2-B3-4-G	14	13	93%	26	21	81%
Gage Label	Pass 5 (10 mph)			Pass 6 (40 mph)		
	before ( $\mu\epsilon$ )	after ( $\mu\epsilon$ )	after/before ratio	before ( $\mu\epsilon$ )	after ( $\mu\epsilon$ )	after/before ratio
2-B3-1-G	18	14	78%	11	10	91%
2-B3-2-G	22	20	91%	12	11	92%
2-B3-3-G	26	19	73%	14	10	71%
2-B3-4-G	28	25	89%	14	12	86%
Gage Label	Pass 7 (40 mph)			Pass 8 (10 mph)		
	before ( $\mu\epsilon$ )	after ( $\mu\epsilon$ )	after/before ratio	before ( $\mu\epsilon$ )	after ( $\mu\epsilon$ )	after/before ratio
2-B3-1-G	16	13	81%	19	15	79%
2-B3-2-G	19	16	84%	24	21	88%
2-B3-3-G	25	19	76%	30	21	70%
2-B3-4-G	26	24	92%	29	24	83%

Note:

1. All values presented here are averages if one pass was conducted more than once.

2. Description of the passes (refer to Figures 3.11 and 3.12 for more information)

Pass 1~3 One truck stayed with left front wheel at specific locations on B4

Pass 4 One truck stayed at position of Pass 2, and one truck traveled at 10 mph with left wheels on B3

Pass 5 One truck traveled at 10 mph with left wheels on B3

Pass 6 One truck traveled at 40 mph on the left lane with right wheels as close to B2 as possible

Pass 7 One truck traveled at 40 mph on the left lane with right wheels as close to B2 as possible, the other truck traveled side by side at 40 mph with left wheels on B3

Pass 8 One truck traveled at 10 mph with left wheels on B4

3. For Pass 1~3, strain values are provided; for other passes, strain range values are provided.

Table C.2(c) Web gap strain ranges on B3W before/after retrofit for the cross-frame-diaphragm bridge (Retrofit angle was applied)

Gage Label	Pass 1 (static)			Pass 2 (static)		
	before ( $\mu\epsilon$ )	after ( $\mu\epsilon$ )	after/before ratio	before ( $\mu\epsilon$ )	after ( $\mu\epsilon$ )	after/before ratio
2-B3W-1-G	19	17	89%	17	14	82%
2-B3W-2-G	18	16	89%	16	13	81%
2-B3W-3-G	-16	-16	100%	-14	-14	100%
2-B3W-4-G	-14	-13	93%	-12	-12	100%
Gage Label	Pass 3 (static)			Pass 4 (10 mph)		
	before ( $\mu\epsilon$ )	after ( $\mu\epsilon$ )	after/before ratio	before ( $\mu\epsilon$ )	after ( $\mu\epsilon$ )	after/before ratio
2-B3W-1-G	13	11	85%	35	28	80%
2-B3W-2-G	13	11	85%	30	27	90%
2-B3W-3-G	-11	-11	100%	24	18	75%
2-B3W-4-G	-10	-9	90%	22	19	86%
Gage Label	Pass 5 (10 mph)			Pass 6 (40 mph)		
	before ( $\mu\epsilon$ )	after ( $\mu\epsilon$ )	after/before ratio	before ( $\mu\epsilon$ )	after ( $\mu\epsilon$ )	after/before ratio
2-B3W-1-G	38	31	82%	27	23	85%
2-B3W-2-G	31	26	84%	17	8	47%
2-B3W-3-G	28	22	79%	24	26	108%
2-B3W-4-G	25	21	84%	18	13	72%
Gage Label	Pass 7 (40 mph)			Pass 8 (10 mph)		
	before ( $\mu\epsilon$ )	after ( $\mu\epsilon$ )	after/before ratio	before ( $\mu\epsilon$ )	after ( $\mu\epsilon$ )	after/before ratio
2-B3W-1-G	42	24	57%	38	30	79%
2-B3W-2-G	33	29	88%	29	24	83%
2-B3W-3-G	30	15	50%	29	25	86%
2-B3W-4-G	26	14	54%	26	21	81%

Note:

1. All values presented here are averages if one pass was conducted more than once.

2. Description of the passes (refer to Figures 3.11 and 3.12 for more information)

Pass 1~3 One truck stayed with left front wheel at specific locations on B4

Pass 4 One truck stayed at position of Pass 2, and one truck traveled at 10 mph with left wheels on B3

Pass 5 One truck traveled at 10 mph with left wheels on B3

Pass 6 One truck traveled at 40 mph on the left lane with right wheels as close to B2 as possible

Pass 7 One truck traveled at 40 mph on the left lane with right wheels as close to B2 as possible, the other truck traveled side by side at 40 mph with left wheels on B3

Pass 8 One truck traveled at 10 mph with left wheels on B4

3. For Pass 1~3, strain values are provided; for other passes, strain range values are provided.

Table C.2(d) Web gap strain ranges on B2 before/after retrofit for the cross-frame-diaphragm bridge (Retrofit angle was not applied)

Gage Label	Pass 1 (static)			Pass 2 (static)		
	before ( $\mu\epsilon$ )	after ( $\mu\epsilon$ )	after/before ratio	before ( $\mu\epsilon$ )	after ( $\mu\epsilon$ )	after/before ratio
2-B2-1-G	2	2	100%	2	1	50%
2-B2-2-G	2	2	100%	2	1	50%
2-B2-3-G	-2	-3	150%	-2	-3	150%
2-B2-4-G	-2	-2	100%	-2	-3	150%
Gage Label	Pass 3 (static)			Pass 4 (10 mph)		
	before ( $\mu\epsilon$ )	after ( $\mu\epsilon$ )	after/before ratio	before ( $\mu\epsilon$ )	after ( $\mu\epsilon$ )	after/before ratio
2-B2-1-G	1	1	100%	21	16	76%
2-B2-2-G	1	1	100%	27	22	81%
2-B2-3-G	-2	-2	100%	26	21	81%
2-B2-4-G	-2	-3	150%	31	25	81%
Gage Label	Pass 5 (10 mph)			Pass 6 (40 mph)		
	before ( $\mu\epsilon$ )	after ( $\mu\epsilon$ )	after/before ratio	before ( $\mu\epsilon$ )	after ( $\mu\epsilon$ )	after/before ratio
2-B2-1-G	22	16	73%	19	17	89%
2-B2-2-G	27	22	81%	21	22	105%
2-B2-3-G	25	21	84%	18	20	111%
2-B2-4-G	29	24	83%	24	29	121%
Gage Label	Pass 7 (40 mph)			Pass 8 (10 mph)		
	before ( $\mu\epsilon$ )	after ( $\mu\epsilon$ )	after/before ratio	before ( $\mu\epsilon$ )	after ( $\mu\epsilon$ )	after/before ratio
2-B2-1-G	24	22	92%	12	10	83%
2-B2-2-G	30	31	103%	14	12	86%
2-B2-3-G	27	30	111%	12	10	83%
2-B2-4-G	35	34	97%	14	9	64%

Note:

1. All values presented here are averages if one pass was conducted more than once.

2. Description of the passes (refer to Figures 3.11 and 3.12 for more information)

Pass 1~3 One truck stayed with left front wheel at specific locations on B4

Pass 4 One truck stayed at position of Pass 2, and one truck traveled at 10 mph with left wheels on B3

Pass 5 One truck traveled at 10 mph with left wheels on B3

Pass 6 One truck traveled at 40 mph on the left lane with right wheels as close to B2 as possible

Pass 7 One truck traveled at 40 mph on the left lane with right wheels as close to B2 as possible, the other truck traveled side by side at 40 mph with left wheels on B3

Pass 8 One truck traveled at 10 mph with left wheels on B4

3. For Pass 1~3, strain values are provided; for other passes, strain range values are provided.

## **Appendix D**

### **In-plane strain ranges before/after retrofit in the field test**

Table D.1(a) In-plane strain ranges on B5 before/after retrofit for the bent-plate-diaphragm bridge (Retrofit angle was applied)

Gage Label	Pass 1 (static)			Pass 2 (static)		
	before ( $\mu\epsilon$ )	after ( $\mu\epsilon$ )	after/before ratio	before ( $\mu\epsilon$ )	after ( $\mu\epsilon$ )	after/before ratio
1-B5-5-B (0.5" from top flange)	-8	-7	88%	-5	-5	100%
1-B5-6-B (1'-10" from bottom flange)	13	12	92%	14	14	100%
1-B5-7-B (bottom flange)	23	21	91%	26	25	96%
Gage Label	Pass 3 (static)			Pass 4 (10 mph)		
	before ( $\mu\epsilon$ )	after ( $\mu\epsilon$ )	after/before ratio	before ( $\mu\epsilon$ )	after ( $\mu\epsilon$ )	after/before ratio
1-B5-5-B (0.5" from top flange)	-4	-3	75%	12	14	117%
1-B5-6-B (1'-10" from bottom flange)	13	13	100%	30	26	87%
1-B5-7-B (bottom flange)	26	24	92%	37	35	95%
Gage Label	Pass 5 (10 mph)			Pass 6 (40 mph)		
	before ( $\mu\epsilon$ )	after ( $\mu\epsilon$ )	after/before ratio	before ( $\mu\epsilon$ )	after ( $\mu\epsilon$ )	after/before ratio
1-B5-5-B (0.5" from top flange)	11	10	91%	7	10	143%
1-B5-6-B (1'-10" from bottom flange)	29	27	93%	12	12	100%
1-B5-7-B (bottom flange)	37	36	97%	12	14	117%
Gage Label	Pass 7 (40 mph)			Pass 8 (10 mph)		
	before ( $\mu\epsilon$ )	after ( $\mu\epsilon$ )	after/before ratio	before ( $\mu\epsilon$ )	after ( $\mu\epsilon$ )	after/before ratio
1-B5-5-B (0.5" from top flange)	13	12	92%	18	18	100%
1-B5-6-B (1'-10" from bottom flange)	35	27	77%	35	29	83%
1-B5-7-B (bottom flange)	43	36	84%	51	47	92%

Note:

1. All values presented here are averages if one pass was conducted more than once.

2. Description of the passes (refer to Figures 3.11 and 3.12 for more information)

Pass 1~3 One truck stayed with left front wheel at specific locations on B5

Pass 4 One truck stayed at position of Pass 2, and one truck traveled at 10 mph with left wheels on B4

Pass 5 One truck traveled at 10 mph with left wheels on B4

Pass 6 One truck traveled at 40 mph on the left lane with right wheels as close to B3 as possible

Pass 7 One truck traveled at 40 mph on the left lane with right wheels as close to B3 as possible, the other truck traveled side by side at 40 mph with left wheels on B4

Pass 8 One truck traveled at 10 mph with left wheels on B5

3. For Pass 1~3, strain values are provided; for other passes, strain range values are provided.

Table D.1(b) In-plane strain ranges on B4 before/after retrofit for the bent-plate-diaphragm bridge (Retrofit angle was applied)

Gage Label	Pass 1 (static)			Pass 2 (static)		
	before ( $\mu\epsilon$ )	after ( $\mu\epsilon$ )	after/before ratio	before ( $\mu\epsilon$ )	after ( $\mu\epsilon$ )	after/before ratio
1-B4-5-B (0.5" from top flange)	2	1	50%	1	0	0%
1-B4-6-B (1'-10" from bottom flange)	-8	-8	100%	-7	-7	100%
1-B4-7-B (bottom flange)	-1	-2	200%	0	-1	
Gage Label	Pass 3 (static)			Pass 4 (10 mph)		
	before ( $\mu\epsilon$ )	after ( $\mu\epsilon$ )	after/before ratio	before ( $\mu\epsilon$ )	after ( $\mu\epsilon$ )	after/before ratio
1-B4-5-B (0.5" from top flange)	1	0	0%	14	12	86%
1-B4-6-B (1'-10" from bottom flange)	-6	-6	100%	25	25	100%
1-B4-7-B (bottom flange)	0	-1		31	27	87%
Gage Label	Pass 5 (10 mph)			Pass 6 (40 mph)		
	before ( $\mu\epsilon$ )	after ( $\mu\epsilon$ )	after/before ratio	before ( $\mu\epsilon$ )	after ( $\mu\epsilon$ )	after/before ratio
1-B4-5-B (0.5" from top flange)	14	12	86%	7	6	86%
1-B4-6-B (1'-10" from bottom flange)	21	25	119%	18	14	78%
1-B4-7-B (bottom flange)	31	28	90%	13	11	85%
Gage Label	Pass 7 (40 mph)			Pass 8 (10 mph)		
	before ( $\mu\epsilon$ )	after ( $\mu\epsilon$ )	after/before ratio	before ( $\mu\epsilon$ )	after ( $\mu\epsilon$ )	after/before ratio
1-B4-5-B (0.5" from top flange)	13	11	85%	10	13	130%
1-B4-6-B (1'-10" from bottom flange)	26	26	100%	22	23	105%
1-B4-7-B (bottom flange)	31	32	103%	24	19	79%

Note:

- All values presented here are averages if one pass was conducted more than once.
- Description of the passes (refer to Figures 3.11 and 3.12 for more information)

Pass 1~3	One truck stayed with left front wheel at specific locations on B5
Pass 4	One truck stayed at position of Pass 2, and one truck traveled at 10 mph with left wheels on B4
Pass 5	One truck traveled at 10 mph with left wheels on B4
Pass 6	One truck traveled at 40 mph on the left lane with right wheels as close to B3 as possible
Pass 7	One truck traveled at 40 mph on the left lane with right wheels as close to B3 as possible, the other truck traveled side by side at 40 mph with left wheels on B4
Pass 8	One truck traveled at 10 mph with left wheels on B5
- For Pass 1~3, strain values are provided; for other passes, strain range values are provided.

Table D.1(c) In-plane strain ranges on B3 before/after retrofit for the bent-plate-diaphragm bridge (Retrofit angle was not applied)

Gage Label	Pass 1 (static)			Pass 2 (static)		
	before ( $\mu\epsilon$ )	after ( $\mu\epsilon$ )	after/before ratio	before ( $\mu\epsilon$ )	after ( $\mu\epsilon$ )	after/before ratio
1-B3-5-B (0.5" from top flange)	0	0		0	0	
1-B3-6-B (1'-10" from bottom flange)	-1	-1	100%	-1	-1	100%
1-B3-7-B (bottom flange)	0	-1		1	0	0%
Gage Label	Pass 3 (static)			Pass 4 (10 mph)		
	before ( $\mu\epsilon$ )	after ( $\mu\epsilon$ )	after/before ratio	before ( $\mu\epsilon$ )	after ( $\mu\epsilon$ )	after/before ratio
1-B3-5-B (0.5" from top flange)	0	0		13	12	92%
1-B3-6-B (1'-10" from bottom flange)	0	0		16	16	100%
1-B3-7-B (bottom flange)	1	-1	-100%	20	22	110%
Gage Label	Pass 5 (10 mph)			Pass 6 (40 mph)		
	before ( $\mu\epsilon$ )	after ( $\mu\epsilon$ )	after/before ratio	before ( $\mu\epsilon$ )	after ( $\mu\epsilon$ )	after/before ratio
1-B3-5-B (0.5" from top flange)	13	10	77%	12	9	75%
1-B3-6-B (1'-10" from bottom flange)	14	19	136%	20	19	95%
1-B3-7-B (bottom flange)	18	29	161%	27	28	104%
Gage Label	Pass 7 (40 mph)			Pass 8 (10 mph)		
	before ( $\mu\epsilon$ )	after ( $\mu\epsilon$ )	after/before ratio	before ( $\mu\epsilon$ )	after ( $\mu\epsilon$ )	after/before ratio
1-B3-5-B (0.5" from top flange)	13	13	100%	9	11	122%
1-B3-6-B (1'-10" from bottom flange)	26	24	92%	10	10	100%
1-B3-7-B (bottom flange)	40	41	103%	14	14	100%

Note:

1. All values presented here are averages if one pass was conducted more than once.

2. Description of the passes (refer to Figures 3.11 and 3.12 for more information)

Pass 1~3 One truck stayed with left front wheel at specific locations on B5

Pass 4 One truck stayed at position of Pass 2, and one truck traveled at 10 mph with left wheels on B4

Pass 5 One truck traveled at 10 mph with left wheels on B4

Pass 6 One truck traveled at 40 mph on the left lane with right wheels as close to B3 as possible

Pass 7 One truck traveled at 40 mph on the left lane with right wheels as close to B3 as possible, the other truck traveled side by side at 40 mph with left wheels on B4

Pass 8 One truck traveled at 10 mph with left wheels on B5

3. For Pass 1~3, strain values are provided; for other passes, strain range values are provided.

Table D.2(a) In-plane strain ranges on B4 before/after retrofit for the cross-frame-diaphragm bridge (Retrofit angle was applied)

Gage Label	Pass 1 (static)			Pass 2 (static)		
	before ( $\mu\epsilon$ )	after ( $\mu\epsilon$ )	after/before ratio	before ( $\mu\epsilon$ )	after ( $\mu\epsilon$ )	after/before ratio
1-B4-5-B (0.5" from top flange)	-12	-10	83%	-9	-8	89%
1-B4-6-B (2'-4" from bottom flange)	11	11	100%	11	11	100%
1-B4-7-B (bottom flange)	20	19	95%	21	20	95%
Gage Label	Pass 3 (static)			Pass 4 (10 mph)		
	before ( $\mu\epsilon$ )	after ( $\mu\epsilon$ )	after/before ratio	before ( $\mu\epsilon$ )	after ( $\mu\epsilon$ )	after/before ratio
1-B4-5-B (0.5" from top flange)	-5	-4	80%	15	10	67%
1-B4-6-B (2'-4" from bottom flange)	12	12	100%	18	15	83%
1-B4-7-B (bottom flange)	21	19	90%	27	25	93%
Gage Label	Pass 5 (10 mph)			Pass 6 (40 mph)		
	before ( $\mu\epsilon$ )	after ( $\mu\epsilon$ )	after/before ratio	before ( $\mu\epsilon$ )	after ( $\mu\epsilon$ )	after/before ratio
1-B4-5-B (0.5" from top flange)	15	11	73%	10	7	70%
1-B4-6-B (2'-4" from bottom flange)	14	16	114%	11	10	91%
1-B4-7-B (bottom flange)	20	26	130%	14	14	100%
Gage Label	Pass 7 (40 mph)			Pass 8 (10 mph)		
	before ( $\mu\epsilon$ )	after ( $\mu\epsilon$ )	after/before ratio	before ( $\mu\epsilon$ )	after ( $\mu\epsilon$ )	after/before ratio
1-B4-5-B (0.5" from top flange)	13	14	108%	19	15	79%
1-B4-6-B (2'-4" from bottom flange)	19	20	105%	24	20	83%
1-B4-7-B (bottom flange)	31	37	119%	39	35	90%

Note:

1. All values presented here are averages if one pass was conducted more than once.

2. Description of the passes (refer to Figures 3.11 and 3.12 for more information)

Pass 1~3 One truck stayed with left front wheel at specific locations on B4

Pass 4 One truck stayed at position of Pass 2, and one truck traveled at 10 mph with left wheels on B3

Pass 5 One truck traveled at 10 mph with left wheels on B3

Pass 6 One truck traveled at 40 mph on the left lane with right wheels as close to B2 as possible

Pass 7 One truck traveled at 40 mph on the left lane with right wheels as close to B2 as possible, the other truck traveled side by side at 40 mph with left wheels on B3

Pass 8 One truck traveled at 10 mph with left wheels on B4

3. For Pass 1~3, strain values are provided; for other passes, strain range values are provided.

Table D.2(b) In-plane strain ranges on B3 before/after retrofit for the cross-frame-diaphragm bridge (Retrofit angle was applied)

Gage Label	Pass 1 (static)			Pass 2 (static)		
	before ( $\mu\epsilon$ )	after ( $\mu\epsilon$ )	after/before ratio	before ( $\mu\epsilon$ )	after ( $\mu\epsilon$ )	after/before ratio
1-B3-5-B (0.5" from top flange)	-1	0	0%	-1	-1	100%
1-B3-6-B (2'-4" from bottom flange)	4	4	100%	4	4	100%
1-B3-7-B (bottom flange)	7	7	100%	7	7	100%
Gage Label	Pass 3 (static)			Pass 4 (10 mph)		
	before ( $\mu\epsilon$ )	after ( $\mu\epsilon$ )	after/before ratio	before ( $\mu\epsilon$ )	after ( $\mu\epsilon$ )	after/before ratio
1-B3-5-B (0.5" from top flange)	-1	0	0%	17	11	65%
1-B3-6-B (2'-4" from bottom flange)	5	5	100%	24	20	83%
1-B3-7-B (bottom flange)	7	8	114%	31	27	87%
Gage Label	Pass 5 (10 mph)			Pass 6 (40 mph)		
	before ( $\mu\epsilon$ )	after ( $\mu\epsilon$ )	after/before ratio	before ( $\mu\epsilon$ )	after ( $\mu\epsilon$ )	after/before ratio
1-B3-5-B (0.5" from top flange)	13	10	77%	10	7	70%
1-B3-6-B (2'-4" from bottom flange)	23	19	83%	15	14	93%
1-B3-7-B (bottom flange)	31	28	90%	20	19	95%
Gage Label	Pass 7 (40 mph)			Pass 8 (10 mph)		
	before ( $\mu\epsilon$ )	after ( $\mu\epsilon$ )	after/before ratio	before ( $\mu\epsilon$ )	after ( $\mu\epsilon$ )	after/before ratio
1-B3-5-B (0.5" from top flange)	15	19	127%	11	7	64%
1-B3-6-B (2'-4" from bottom flange)	25	25	100%	16	13	81%
1-B3-7-B (bottom flange)	36	40	111%	22	20	91%

Note:

1. All values presented here are averages if one pass was conducted more than once.

2. Description of the passes (refer to Figures 3.11 and 3.12 for more information)

Pass 1~3 One truck stayed with left front wheel at specific locations on B4

Pass 4 One truck stayed at position of Pass 2, and one truck traveled at 10 mph with left wheels on B3

Pass 5 One truck traveled at 10 mph with left wheels on B3

Pass 6 One truck traveled at 40 mph on the left lane with right wheels as close to B2 as possible

Pass 7 One truck traveled at 40 mph on the left lane with right wheels as close to B2 as possible, the other truck traveled side by side at 40 mph with left wheels on B3

Pass 8 One truck traveled at 10 mph with left wheels on B4

3. For Pass 1~3, strain values are provided; for other passes, strain range values are provided.

Table D.2(c) In-plane strain ranges on B2 before/after retrofit for the cross-frame-diaphragm bridge (Retrofit angle was not applied)

Gage Label	Pass 1 (static)			Pass 2 (static)		
	before (µε)	after (µε)	after/before ratio	before (µε)	after (µε)	after/before ratio
1-B2-5-B (0.5" from top flange)	1	N/A	N/A	0	N/A	N/A
1-B2-6-B (2'-4" from bottom flange)	0	1		0	1	
1-B2-7-B (bottom flange)	7	7	100%	6	6	100%
Gage Label	Pass 3 (static)			Pass 4 (10 mph)		
	before (µε)	after (µε)	after/before ratio	before (µε)	after (µε)	after/before ratio
1-B2-5-B (0.5" from top flange)	0	N/A	N/A	8	N/A	N/A
1-B2-6-B (2'-4" from bottom flange)	0	1		16	12	75%
1-B2-7-B (bottom flange)	5	5	100%	27	21	78%
Gage Label	Pass 5 (10 mph)			Pass 6 (40 mph)		
	before (µε)	after (µε)	after/before ratio	before (µε)	after (µε)	after/before ratio
1-B2-5-B (0.5" from top flange)	8	N/A	N/A	N/A	N/A	N/A
1-B2-6-B (2'-4" from bottom flange)	7	13	186%	20	21	105%
1-B2-7-B (bottom flange)	26	24	92%	34	35	103%
Gage Label	Pass 7 (40 mph)			Pass 8 (10 mph)		
	before (µε)	after (µε)	after/before ratio	before (µε)	after (µε)	after/before ratio
1-B2-5-B (0.5" from top flange)	N/A	N/A	N/A	N/A	N/A	N/A
1-B2-6-B (2'-4" from bottom flange)	25	26	104%	13	9	69%
1-B2-7-B (bottom flange)	43	46	107%	24	21	88%

Note:

1. All values presented here are averages if one pass was conducted more than once.

2. Description of the passes (refer to Figures 3.11 and 3.12 for more information)

Pass 1~3 One truck stayed with left front wheel at specific locations on B4

Pass 4 One truck stayed at position of Pass 2, and one truck traveled at 10 mph with left wheels on B3

Pass 5 One truck traveled at 10 mph with left wheels on B3

Pass 6 One truck traveled at 40 mph on the left lane with right wheels as close to B2 as possible

Pass 7 One truck traveled at 40 mph on the left lane with right wheels as close to B2 as possible, the other truck traveled side by side at 40 mph with left wheels on B3

Pass 8 One truck traveled at 10 mph with left wheels on B4

3. For Pass 1~3, strain values are provided; for other passes, strain range values are provided.

## **Appendix E**

**Strain ranges measured by single weldable gages on the diaphragm  
before/after retrofit in the field test**

Table E.1 Strain ranges on the diaphragm between B5 and B4 before/after retrofit for the bent-plate-diaphragm bridge (Retrofit angles were applied at both web gaps on B5 and B4)

Gage Label	Pass 1 (static)			Pass 2 (static)		
	before ( $\mu\epsilon$ )	after ( $\mu\epsilon$ )	after/before ratio	before ( $\mu\epsilon$ )	after ( $\mu\epsilon$ )	after/before ratio
1-B4-8-D (bent plate top)	21	19	90%	17	14	82%
1-B4-9-D (1'-3" from bent plate bottom)	-4	-3	75%	-4	-3	75%
1-B4-10-D (bent plate bottom)	-33	-32	97%	-31	-30	97%
Gage Label	Pass 3 (static)			Pass 4 (10 mph)		
	before ( $\mu\epsilon$ )	after ( $\mu\epsilon$ )	after/before ratio	before ( $\mu\epsilon$ )	after ( $\mu\epsilon$ )	after/before ratio
1-B4-8-D (bent plate top)	13	11	85%	27	19	70%
1-B4-9-D (1'-3" from bent plate bottom)	-3	-3	100%	17	16	94%
1-B4-10-D (bent plate bottom)	-26	-26	100%	24	17	71%
Gage Label	Pass 5 (10 mph)			Pass 6 (40 mph)		
	before ( $\mu\epsilon$ )	after ( $\mu\epsilon$ )	after/before ratio	before ( $\mu\epsilon$ )	after ( $\mu\epsilon$ )	after/before ratio
1-B4-8-D (bent plate top)	20	21	105%	19	19	100%
1-B4-9-D (1'-3" from bent plate bottom)	10	11	110%	9	13	144%
1-B4-10-D (bent plate bottom)	21	22	105%	37	44	119%
Gage Label	Pass 7 (40 mph)			Pass 8 (10 mph)		
	before ( $\mu\epsilon$ )	after ( $\mu\epsilon$ )	after/before ratio	before ( $\mu\epsilon$ )	after ( $\mu\epsilon$ )	after/before ratio
1-B4-8-D (bent plate top)	18	24	133%	34	28	82%
1-B4-9-D (1'-3" from bent plate bottom)	11	14	127%	13	17	131%
1-B4-10-D (bent plate bottom)	34	44	129%	61	51	84%

Note:

1. All values presented here are averages if one pass was conducted more than once.

2. Description of the passes (refer to Figures 3.11 and 3.12 for more information)

Pass 1~3 One truck stayed with left front wheel at specific locations on B5

Pass 4 One truck stayed at position of Pass 2, and one truck traveled at 10 mph with left wheels on B4

Pass 5 One truck traveled at 10 mph with left wheels on B4

Pass 6 One truck traveled at 40 mph on the left lane with right wheels as close to B3 as possible

Pass 7 One truck traveled at 40 mph on the left lane with right wheels as close to B3 as possible, the other truck traveled side by side at 40 mph with left wheels on B4

Pass 8 One truck traveled at 10 mph with left wheels on B5

3. For Pass 1~3, strain values are provided; for other passes, strain range values are provided.

Table E.2(a) Strain ranges on the diaphragm between B4 and B3 before/after retrofit for the cross-frame-diaphragm bridge (Retrofit angles were applied at both web gaps on B4 and B3)

Gage Label	Pass 1 (static)			Pass 2 (static)		
	before ( $\mu\epsilon$ )	after ( $\mu\epsilon$ )	after/before ratio	before ( $\mu\epsilon$ )	after ( $\mu\epsilon$ )	after/before ratio
2-B4-8-D (cross frame diaphragm)	-62	-61	98%	-58	-56	97%
2-B4-9-D (cross frame diaphragm)	-65	-63	97%	-61	-59	97%
2-B4-10-D (cross frame diaphragm)	0	2		1	1	100%
2-B4-11-D (cross frame diaphragm)	-6	-4	67%	-5	-4	80%
2-B3-12-D (cross frame diaphragm)	57	57	100%	54	53	98%
2-B3-13-D (cross frame diaphragm)	51	50	98%	48	47	98%
Gage Label	Pass 3 (static)			Pass 4 (10 mph)		
	before ( $\mu\epsilon$ )	after ( $\mu\epsilon$ )	after/before ratio	before ( $\mu\epsilon$ )	after ( $\mu\epsilon$ )	after/before ratio
2-B4-8-D (cross frame diaphragm)	-49	-50	102%	28	24	86%
2-B4-9-D (cross frame diaphragm)	-52	-53	102%	27	26	96%
2-B4-10-D (cross frame diaphragm)	1	2	200%	21	22	105%
2-B4-11-D (cross frame diaphragm)	-4	-3	75%	28	27	96%
2-B3-12-D (cross frame diaphragm)	48	49	102%	28	25	89%
2-B3-13-D (cross frame diaphragm)	43	43	100%	26	23	88%
Gage Label	Pass 5 (10 mph)			Pass 6 (40 mph)		
	before ( $\mu\epsilon$ )	after ( $\mu\epsilon$ )	after/before ratio	before ( $\mu\epsilon$ )	after ( $\mu\epsilon$ )	after/before ratio
2-B4-8-D (cross frame diaphragm)	32	30	94%	33	37	112%
2-B4-9-D (cross frame diaphragm)	32	31	97%	34	36	106%
2-B4-10-D (cross frame diaphragm)	23	23	100%	29	28	97%
2-B4-11-D (cross frame diaphragm)	28	29	104%	37	37	100%
2-B3-12-D (cross frame diaphragm)	31	30	97%	26	30	115%
2-B3-13-D (cross frame diaphragm)	28	26	93%	24	28	117%
Gage Label	Pass 7 (40 mph)			Pass 8 (10 mph)		
	before ( $\mu\epsilon$ )	after ( $\mu\epsilon$ )	after/before ratio	before ( $\mu\epsilon$ )	after ( $\mu\epsilon$ )	after/before ratio
2-B4-8-D (cross frame diaphragm)	41	39	95%	89	90	101%
2-B4-9-D (cross frame diaphragm)	43	39	91%	91	93	102%
2-B4-10-D (cross frame diaphragm)	35	33	94%	29	25	86%
2-B4-11-D (cross frame diaphragm)	46	41	89%	38	35	92%
2-B3-12-D (cross frame diaphragm)	35	36	103%	71	72	101%
2-B3-13-D (cross frame diaphragm)	32	31	97%	62	64	103%

Note:

1. All values presented here are averages if one pass was conducted more than once.
2. Description of the passes (refer to Figures 3.11 and 3.12 for more information)
3. For Pass 1~3, strain values are provided; for other passes, strain range values are provided.

Table E.2(b) Strain ranges on the diaphragm between B3 and B2 before/after retrofit for the cross-frame-diaphragm bridge (Retrofit angle was only applied at web gap on B3)

Gage Label	Pass 1 (static)			Pass 2 (static)		
	before ( $\mu\epsilon$ )	after ( $\mu\epsilon$ )	after/before ratio	before ( $\mu\epsilon$ )	after ( $\mu\epsilon$ )	after/before ratio
2-B3-8-D (cross frame diaphragm)	-25	-28	112%	-23	-24	104%
2-B3-9-D (cross frame diaphragm)	-26	-29	112%	-24	-25	104%
2-B3-10-D (cross frame diaphragm)	-24	-23	96%	-22	-21	95%
2-B3-11-D (cross frame diaphragm)	-30	-29	97%	-27	-26	96%
2-B2-12-D (cross frame diaphragm)	1	1	100%	1	1	100%
2-B2-13-D (cross frame diaphragm)	0	1		1	0	
Gage Label	Pass 3 (static)			Pass 4 (10 mph)		
	before ( $\mu\epsilon$ )	after ( $\mu\epsilon$ )	after/before ratio	before ( $\mu\epsilon$ )	after ( $\mu\epsilon$ )	after/before ratio
2-B3-8-D (cross frame diaphragm)	-19	-20	105%	81	82	101%
2-B3-9-D (cross frame diaphragm)	-19	-21	111%	82	85	104%
2-B3-10-D (cross frame diaphragm)	-18	-17	94%	27	23	85%
2-B3-11-D (cross frame diaphragm)	-22	-22	100%	25	23	92%
2-B2-12-D (cross frame diaphragm)	1	1	100%	80	78	98%
2-B2-13-D (cross frame diaphragm)	1	1	100%	99	97	98%
Gage Label	Pass 5 (10 mph)			Pass 6 (40 mph)		
	before ( $\mu\epsilon$ )	after ( $\mu\epsilon$ )	after/before ratio	before ( $\mu\epsilon$ )	after ( $\mu\epsilon$ )	after/before ratio
2-B3-8-D (cross frame diaphragm)	80	84	105%	52	48	92%
2-B3-9-D (cross frame diaphragm)	86	86	100%	54	48	89%
2-B3-10-D (cross frame diaphragm)	21	21	100%	40	42	105%
2-B3-11-D (cross frame diaphragm)	20	20	100%	48	52	108%
2-B2-12-D (cross frame diaphragm)	76	72	95%	32	27	84%
2-B2-13-D (cross frame diaphragm)	94	91	97%	38	35	92%
Gage Label	Pass 7 (40 mph)			Pass 8 (10 mph)		
	before ( $\mu\epsilon$ )	after ( $\mu\epsilon$ )	after/before ratio	before ( $\mu\epsilon$ )	after ( $\mu\epsilon$ )	after/before ratio
2-B3-8-D (cross frame diaphragm)	97	54	56%	57	56	98%
2-B3-9-D (cross frame diaphragm)	101	56	55%	56	56	100%
2-B3-10-D (cross frame diaphragm)	48	41	85%	41	42	102%
2-B3-11-D (cross frame diaphragm)	56	47	84%	50	54	108%
2-B2-12-D (cross frame diaphragm)	77	64	83%	19	18	95%
2-B2-13-D (cross frame diaphragm)	92	84	91%	21	22	105%

Note:

1. All values presented here are averages if one pass was conducted more than once.
2. Description of the passes (refer to Figures 3.11 and 3.12 for more information)
3. For Pass 1~3, strain values are provided; for other passes, strain range values are provided.

## **Appendix F**

**Strain ranges measured by rosettes on the connection plate and diaphragm  
before/after retrofit in the field test**

Table F.1(a) Strain ranges measured by rosettes on B5 before/after retrofit for the bent-plate-diaphragm bridge (Retrofit angle was applied)

Gage Label	Pass 1 (static)			Pass 2 (static)		
	before (µε)	after (µε)	after/before ratio	before (µε)	after (µε)	after/before ratio
1-B5-1R1-C	-6	17	-283%	-7	13	-186%
1-B5-1R2-C	-1	22	-2200%	-1	17	-1700%
1-B5-1R3-C	2	-6	-300%	2	-7	-350%
1-B5-1R1-D	-2	-1	50%	-3	-3	100%
1-B5-1R2-D	0	0		0	0	
1-B5-1R3-D	-4	-4	100%	-5	-5	100%
Gage Label	Pass 3 (static)			Pass 4 (10 mph)		
	before (µε)	after (µε)	after/before ratio	before (µε)	after (µε)	after/before ratio
1-B5-1R1-C	-5	9	-180%	13	16	123%
1-B5-1R2-C	1	11	1100%	8	16	200%
1-B5-1R3-C	3	-7	-233%	9	13	144%
1-B5-1R1-D	-3	-4	133%	10	7	70%
1-B5-1R2-D	0	0		6	4	67%
1-B5-1R3-D	-5	-4	80%	9	8	89%
Gage Label	Pass 5 (10 mph)			Pass 6 (40 mph)		
	before (µε)	after (µε)	after/before ratio	before (µε)	after (µε)	after/before ratio
1-B5-1R1-C	12	19	158%	10	20	200%
1-B5-1R2-C	8	19	238%	8	22	275%
1-B5-1R3-C	8	13	163%	7	12	171%
1-B5-1R1-D	10	7	70%	9	8	89%
1-B5-1R2-D	5	4	80%	5	3	60%
1-B5-1R3-D	9	8	89%	9	9	100%
Gage Label	Pass 7 (40 mph)			Pass 8 (10 mph)		
	before (µε)	after (µε)	after/before ratio	before (µε)	after (µε)	after/before ratio
1-B5-1R1-C	12	19	158%	15	26	173%
1-B5-1R2-C	3	21	700%	10	32	320%
1-B5-1R3-C	7	12	171%	10	14	140%
1-B5-1R1-D	11	9	82%	9	9	100%
1-B5-1R2-D	6	3	50%	6	4	67%
1-B5-1R3-D	10	9	90%	13	11	85%

Note:

1. All values presented here are averages if one pass was conducted more than once.
2. Description of the passes (refer to Figures 3.11 and 3.12 for more information)
3. For Pass 1~3, strain values are provided; for other passes, strain range values are provided.

Table F.1(b) Strain ranges measured by rosettes on B4 before/after retrofit for the bent-plate-diaphragm bridge (Retrofit angle was applied)

Gage Label	Pass 1 (static)			Pass 2 (static)		
	before (µε)	after (µε)	after/before ratio	before (µε)	after (µε)	after/before ratio
1-B4-1R1-C	-40	-10	25%	-31	-8	26%
1-B4-1R2-C	6	12	200%	4	9	225%
1-B4-1R3-C	12	7	58%	9	5	56%
1-B4-1R1-D	-4	-3	75%	-4	-3	75%
1-B4-1R2-D	-8	-7	88%	-7	-6	86%
1-B4-1R3-D	-4	-3	75%	-5	-4	80%
Gage Label	Pass 3 (static)			Pass 4 (10 mph)		
	before (µε)	after (µε)	after/before ratio	before (µε)	after (µε)	after/before ratio
1-B4-1R1-C	-22	-6	27%	28	8	29%
1-B4-1R2-C	4	7	175%	13	9	69%
1-B4-1R3-C	8	4	50%	13	7	54%
1-B4-1R1-D	-3	-3	100%	10	8	80%
1-B4-1R2-D	-5	-6	120%	13	8	62%
1-B4-1R3-D	-4	-4	100%	12	8	67%
Gage Label	Pass 5 (10 mph)			Pass 6 (40 mph)		
	before (µε)	after (µε)	after/before ratio	before (µε)	after (µε)	after/before ratio
1-B4-1R1-C	30	9	30%	25	8	32%
1-B4-1R2-C	13	10	77%	8	9	113%
1-B4-1R3-C	12	8	67%	11	6	55%
1-B4-1R1-D	8	8	100%	9	9	100%
1-B4-1R2-D	12	9	75%	15	14	93%
1-B4-1R3-D	12	7	58%	11	8	73%
Gage Label	Pass 7 (40 mph)			Pass 8 (10 mph)		
	before (µε)	after (µε)	after/before ratio	before (µε)	after (µε)	after/before ratio
1-B4-1R1-C	31	9	29%	55	15	27%
1-B4-1R2-C	12	9	75%	14	16	114%
1-B4-1R3-C	10	7	70%	22	11	50%
1-B4-1R1-D	10	10	100%	9	9	100%
1-B4-1R2-D	14	13	93%	18	15	83%
1-B4-1R3-D	11	11	100%	15	11	73%
Note:						
1. All values presented here are averages if one pass was conducted more than once.						
2. Description of the passes (refer to Figures 3.11 and 3.12 for more information)						
3. For Pass 1~3, strain values are provided; for other passes, strain range values are provided.						

Table F.2 Strain ranges measured by rosettes on B4 and B3 before/after retrofit for the cross-frame-diaphragm bridge (Retrofit angles were applied at both web gaps on B4 and B3)

Gage Label	Pass 1 (static)			Pass 2 (static)		
	before (µε)	after (µε)	after/before ratio	before (µε)	after (µε)	after/before ratio
1-B4-1R1-C	-16	2	-13%	-15	1	-7%
1-B4-1R2-C	-6	15	-250%	-6	13	-217%
1-B4-1R3-C	6	3	50%	5	2	40%
1-B3-1R1-C	-1	-1	100%	-1	-1	100%
1-B3-1R2-C	24	22	92%	22	20	91%
1-B3-1R3-C	6	3	50%	5	2	40%
Gage Label	Pass 3 (static)			Pass 4 (10 mph)		
	before (µε)	after (µε)	after/before ratio	before (µε)	after (µε)	after/before ratio
1-B4-1R1-C	-12	1	-8%	13	10	77%
1-B4-1R2-C	-4	10	-250%	10	16	160%
1-B4-1R3-C	5	-3	-60%	13	16	123%
1-B3-1R1-C	-1	1	-100%	8	6	75%
1-B3-1R2-C	19	18	95%	24	17	71%
1-B3-1R3-C	5	2	40%	21	20	95%
Gage Label	Pass 5 (10 mph)			Pass 6 (40 mph)		
	before (µε)	after (µε)	after/before ratio	before (µε)	after (µε)	after/before ratio
1-B4-1R1-C	14	10	71%	15	8	53%
1-B4-1R2-C	11	15	136%	10	17	170%
1-B4-1R3-C	14	13	93%	11	11	100%
1-B3-1R1-C	9	6	67%	7	5	71%
1-B3-1R2-C	25	21	84%	16	14	88%
1-B3-1R3-C	22	18	82%	11	8	73%
Gage Label	Pass 7 (40 mph)			Pass 8 (10 mph)		
	before (µε)	after (µε)	after/before ratio	before (µε)	after (µε)	after/before ratio
1-B4-1R1-C	17	9	53%	28	9	32%
1-B4-1R2-C	11	16	145%	16	32	200%
1-B4-1R3-C	14	14	100%	18	14	78%
1-B3-1R1-C	7	5	71%	7	5	71%
1-B3-1R2-C	24	21	88%	38	34	89%
1-B3-1R3-C	20	6	30%	13	8	62%
Note:						
1. All values presented here are averages if one pass was conducted more than once.						
2. Description of the passes (refer to Figures 3.11 and 3.12 for more information)						
3. For Pass 1~3, strain values are provided; for other passes, strain range values are provided.						

## **Appendix G**

### **Linear Variable Differential Transformer (LVDT) labeling for the large-scale test**

Table G.1 Labeling for the LVDTs that measure in-plane deflections (vertical deflections)

LVDT label	Girder	Location and position	Measurement range
LVDT-NW-1/2-BD	North	Close to the diaphragm support	± 0.5 in.
LVDT-NW-1/2-BB	North	Close to the girder	± 0.5 in.
LVDT-SW-1/2-BD	South	Close to the diaphragm support	± 0.5 in.
LVDT-SW-1/2-BB	South	Close to the girder	± 0.5 in.
LVDT-NW-C-BD	North	Close to the diaphragm support	± 0.5 in.
LVDT-NW-C-BB	North	Close to the girder	± 0.5 in.
LVDT-SW-C-BD	South	Close to the diaphragm support	± 0.5 in.
LVDT-SW-1/2-BB	South	Close to the girder	± 0.5 in.
LVDT-NE-C-BD	North	Close to the diaphragm support	± 0.5 in.
LVDT-NE-C-BB	North	Close to the girder	± 0.5 in.
LVDT-SE-C-BD	South	Close to the diaphragm support	± 0.5 in.
LVDT-SE-C-BB	South	Close to the girder	± 0.5 in.
LVDT-NE-1/2-BD	North	Close to the diaphragm support	± 0.5 in.
LVDT-NE-1/2-BB	North	Close to the girder	± 0.5 in.
LVDT-SE-1/2-BD	South	Close to the diaphragm support	± 0.5 in.
LVDT-SE-1/2-BB	South	Close to the girder	± 0.5 in.

Table G.2 Labeling for the LVDTs that measure out-of-plane distortions (horizontal displacement)

LVDT label	Girder	Location and position	Measurement range
LVDT-NW-1/2-G	North	West side of the girder	± 0.05 in.
LVDT-SW-1/2-G	South	West side of the girder	± 0.05 in.
LVDT-NW-C-G	North	West side of the girder	± 0.05 in.
LVDT-SW-C-G	South	West side of the girder	± 0.05 in.
LVDT-NE-C-G	North	East side of the girder	± 0.05 in.
LVDT-SE-C-G	South	East side of the girder	± 0.05 in.
LVDT-NE-1/2-G	North	East side of the girder	± 0.05 in.
LVDT-SE-1/2-G	South	East side of the girder	± 0.05 in.

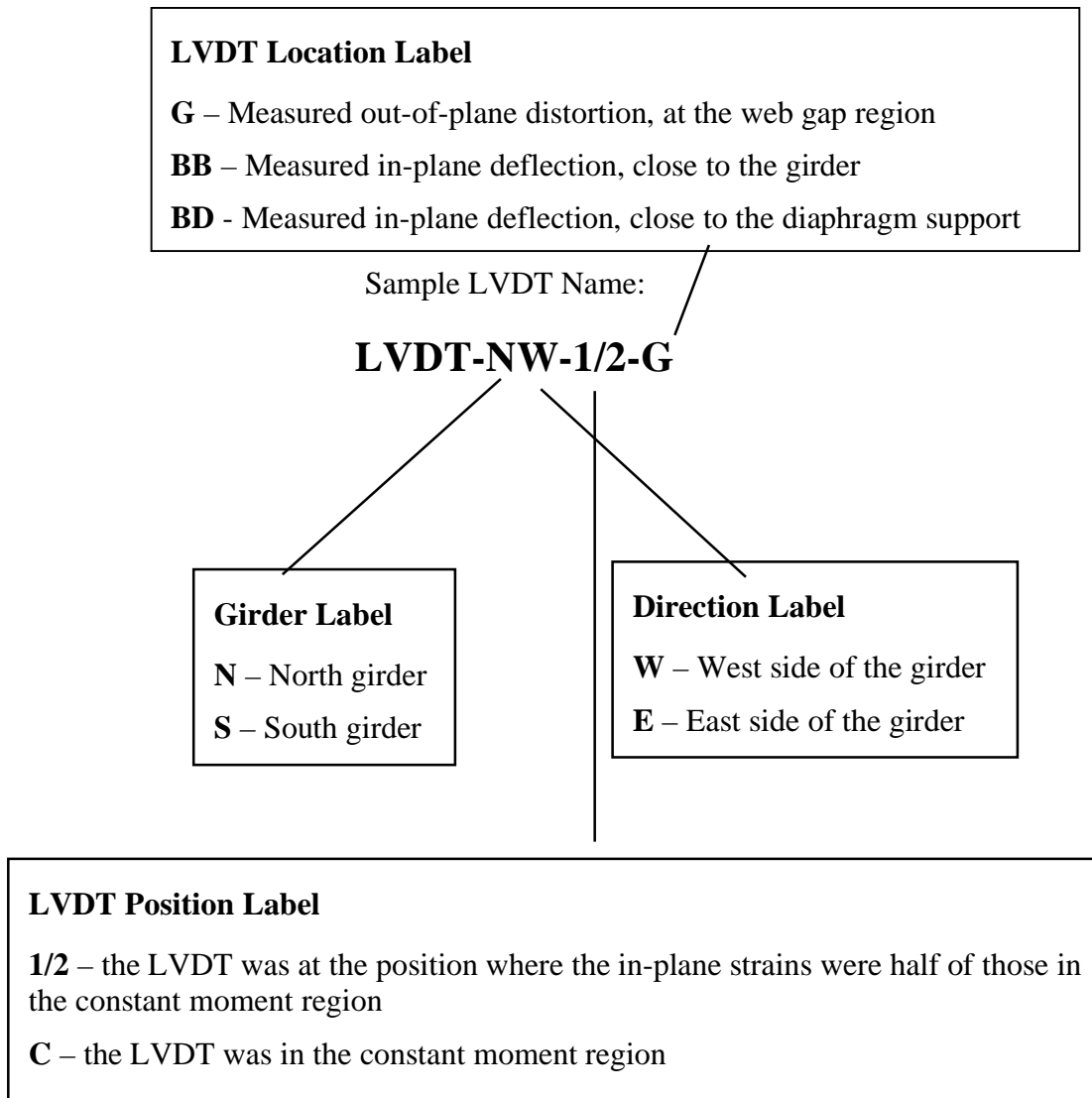


Figure G.1 Linear Variable Differential Transformer (LVDT) labeling for the large-scale test

## **Appendix H**

### **Gage labeling for the large-scale test**

Table H.1 Labeling for the strain gages that measured in-plane strains

Gage label	Girder	Location and position	Gage type
N-1/4-1-B	North	Top flange, north side	Single
N-1/4-2-B	North	Top flange, south side	Single
N-1/4-3-B	North	Web, 3 in. from the top flange, north side	Single
N-1/4-4-B	North	Web, 3 in. from the bottom flange, north side	Single
N-1/4-5-B	North	Bottom flange, north side	Single
N-1/4-6-B	North	Bottom flange, south side	Single
S-1/4-1-B	North	Top flange, south side	Single
S-1/4-2-B	North	Top flange, north side	Single
S-1/4-3-B	North	Web, 3 in. from the top flange, south side	Single
S-1/4-4-B	North	Web, 3 in. from the bottom flange, south side	Single
S-1/4-5-B	North	Bottom flange, south side	Single
S-1/4-6-B	North	Bottom flange, north side	Single
N-C-1-B	North	Top flange, north side	Single
N-C-2-B	North	Top flange, south side	Single
N-C-3-B	North	Web, 3 in. from the top flange, north side	Single
N-C-4-B	North	Web, 3 in. from the bottom flange, north side	Single
N-C-5-B	North	Bottom flange, north side	Single
N-C-6-B	North	Bottom flange, south side	Single
S-C-1-B	North	Top flange, south side	Single
S-C-2-B	North	Top flange, north side	Single
S-C-3-B	North	Web, 3 in. from the top flange, south side	Single
S-C-4-B	North	Web, 3 in. from the bottom flange, south side	Single
S-C-5-B	North	Bottom flange, south side	Single
S-C-6-B	North	Bottom flange, north side	Single

Table H.2 Labeling for the strain gages that were mounted on the vertical diaphragm supports

Gage label	Girder	Location and position	Gage type
NW-1/2-N-D	North	North side of the vertical diaphragm support	Single
NW-1/2-S-D	North	South side of the vertical diaphragm support	Single
NW-C-N-D	North	North side of the vertical diaphragm support	Single
NW-C-S-D	North	South side of the vertical diaphragm support	Single
NE-C-N-D	North	North side of the vertical diaphragm support	Single
NE-C-S-D	North	South side of the vertical diaphragm support	Single
NE-1/2-N-D	North	North side of the vertical diaphragm support	Single
NE-1/2-S-D	North	South side of the vertical diaphragm support	Single

Table H.3 Labeling for the strain gages that measured out-of-plane strains (to be continued)

Gage label	Girder	Location and position	Gage type
NW-1/2-1N-G	North	North side of the web, close to the stiffener-web weld	Strip gage
NW-1/2-2N-G	North	North side of the web, close to the stiffener-web weld	Strip gage
NW-1/2-3N-G *	North	North side of the web, close to the flange-web weld	Strip gage
NW-1/2-4N-G *	North	North side of the web, close to the flange-web weld	Strip gage
NW-1/2-1S-G	North	South side of the web, close to the stiffener-web weld	Strip gage
NW-1/2-2S-G	North	South side of the web, close to the stiffener-web weld	Strip gage
NW-1/2-3S-G *	North	South side of the web, close to the flange-web weld	Strip gage
NW-1/2-4S-G *	North	South side of the web, close to the flange-web weld	Strip gage
NW-1/2-5S-G	North	South side of the web, close to the flange-web weld	Single
SW-1/2-1N-G	South	North side of the web, close to the stiffener-web weld	Strip gage
SW-1/2-2N-G	South	North side of the web, close to the stiffener-web weld	Strip gage
SW-1/2-3N-G *	South	North side of the web, close to the flange-web weld	Strip gage
SW-1/2-4N-G *	South	North side of the web, close to the flange-web weld	Strip gage
SW-1/2-5N-G	South	North side of the web, close to the flange-web weld	Single
SW-1/2-1S-G	South	South side of the web, close to the stiffener-web weld	Strip gage
SW-1/2-2S-G	South	South side of the web, close to the stiffener-web weld	Strip gage
SW-1/2-3S-G	South	South side of the web, close to the flange-web weld	Strip gage
SW-1/2-4S-G	South	South side of the web, close to the flange-web weld	Strip gage
NW-C-1N-G	North	North side of the web, close to the stiffener-web weld	Strip gage
NW-C-2N-G	North	North side of the web, close to the stiffener-web weld	Strip gage
NW-C-3N-G *	North	North side of the web, close to the flange-web weld	Strip gage
NW-C-4N-G *	North	North side of the web, close to the flange-web weld	Strip gage
NW-C-1S-G	North	South side of the web, close to the stiffener-web weld	Strip gage
NW-C-2S-G	North	South side of the web, close to the stiffener-web weld	Strip gage
NW-C-3S-G *	North	South side of the web, close to the flange-web weld	Strip gage
NW-C-4S-G *	North	South side of the web, close to the flange-web weld	Strip gage
NW-C-5S-G	North	South side of the web, close to the flange-web weld	Single
SW-C-1N-G	South	North side of the web, close to the stiffener-web weld	Strip gage
SW-C-2N-G	South	North side of the web, close to the stiffener-web weld	Strip gage
SW-C-3N-G *	South	North side of the web, close to the flange-web weld	Strip gage
SW-C-4N-G *	South	North side of the web, close to the flange-web weld	Strip gage
SW-C-5N-G	South	North side of the web, close to the flange-web weld	Single
SW-C-1S-G	South	South side of the web, close to the stiffener-web weld	Strip gage
SW-C-2S-G	South	South side of the web, close to the stiffener-web weld	Strip gage
SW-C-3S-G *	South	South side of the web, close to the flange-web weld	Strip gage
SW-C-4S-G *	South	South side of the web, close to the flange-web weld	Strip gage
* Gage did not work in the test			



Table H.4 Labeling for the strain gages that measured the strains at the tip of the out-of-plane distortion-induced cracks

Web gap location	Gage label	Girder	Location and position	Gage type
NW-1/2	NW-1/2-nw(1)-g	North	Northwest side of the web gap, crack tip	Single
	NW-1/2-ne-g	North	Northeast side of the web gap, crack tip	Single
	NW-1/2-se(2)-g	North	Southeast side of the web gap, crack tip	Single
SW-1/2	SW-1/2-nw-g	South	Northwest side of the web gap, crack tip	Single
	SW-1/2-ne(1)-g	South	Northeast side of the web gap, crack tip	Single
	SW-1/2-se-g	South	Southeast side of the web gap, crack tip	Single
NW-C	NW-C-ne-g	North	Northeast side of the web gap, crack tip	Single
	NW-C-se(1)-g	North	Southeast side of the web gap, crack tip	Single
SW-C	SW-C-nw(1)-g	South	Northwest side of the web gap, crack tip	Single
	SW-C-ne(1)-g	South	Northeast side of the web gap, crack tip	Single
	SW-C-sw(3)-g	South	Southwest side of the web gap, crack tip	Single
	SW-C-se-g	South	Southeast side of the web gap, crack tip	Single
NE-C	NE-C-nw-g	North	Northwest side of the web gap, crack tip	Single
	NE-C-ne(1)-g	North	Northeast side of the web gap, crack tip	Single
	NE-C-sw(3)-g	North	Crack was at the flange-web weld, crack tip	Single
	NE-C-se-flangeweb-g	North	Southwest side of the web gap, crack tip	Single
SE-C	SE-C-nw(1)-g	South	Northwest side of the web gap, crack tip	Single
	SE-C-ne-g	South	Northeast side of the web gap, crack tip	Single
	SE-C-sw-g	South	Southwest side of the web gap, crack tip	Single
	SE-C-se-g	South	Southeast side of the web gap, crack tip	Single
NE-1/2	NE-1/2-nw(1)-g	North	Northwest side of the web gap, crack tip	Single
	NE-1/2-ne-g	North	Northeast side of the web gap, crack tip	Single
	NE-1/2-sw(3)-g	North	Southwest side of the web gap, crack tip	Single
	NE-1/2-se(1)-g	North	Southeast side of the web gap, crack tip	Single
SE-1/2	SE-1/2-ne-g	South	Northeast side of the web gap, crack tip	Single
	SE-1/2-sw-g	South	Southwest side of the web gap, crack tip	Single
	SE-1/2-se(2)-g	South	Southeast side of the web gap, crack tip	Single

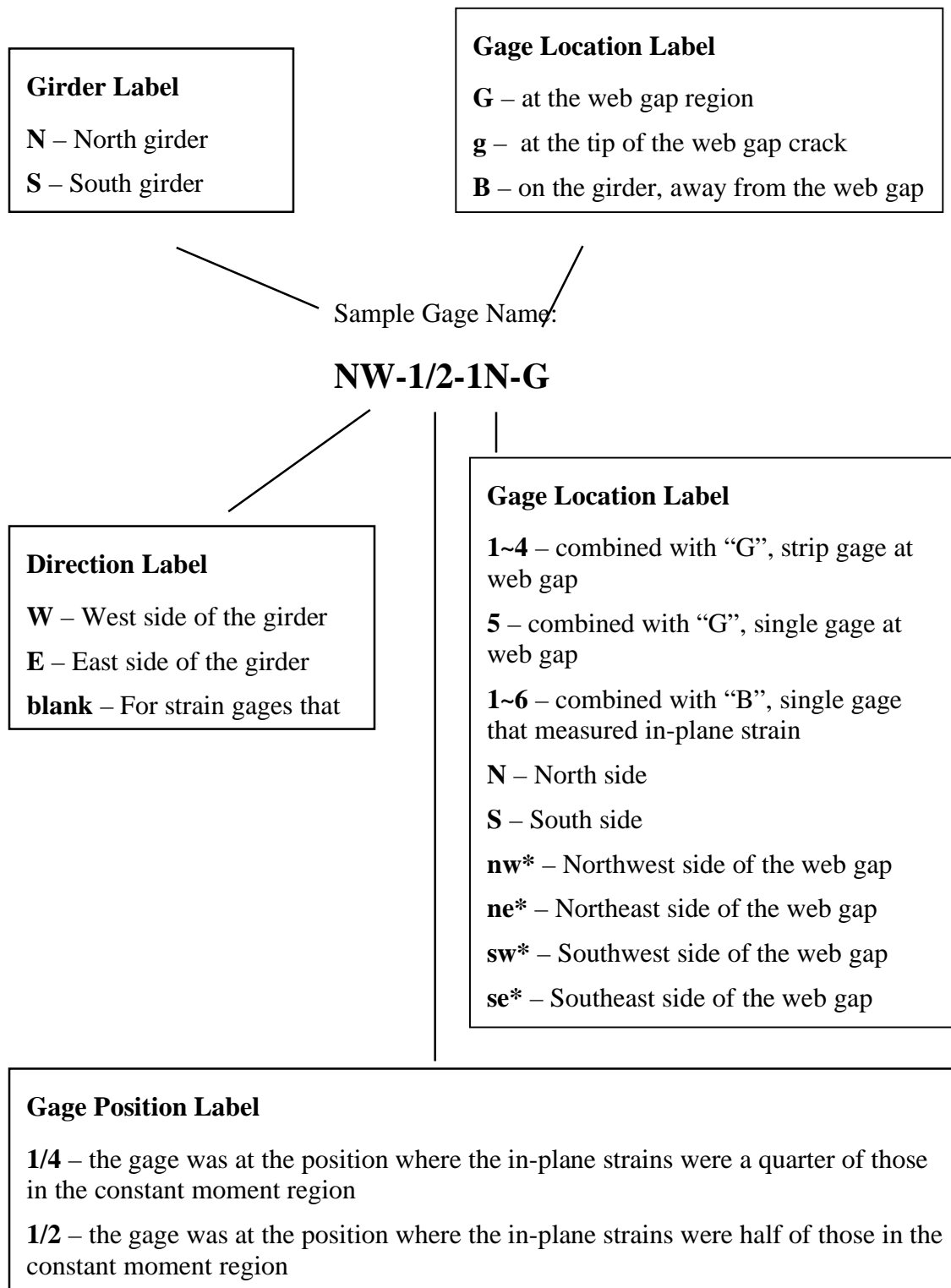


Figure H.1 Gage labeling for the large-scale test

## **Appendix I**

**The procedure of applying the retrofitting angles in the large-scale test**

The following describes the procedure of applying retrofit angles with both 3M adhesive (DP-460NS) and Hilti powder actuated fasteners (X-AL-H37 P8). For the retrofit angles that did not utilize Hilti powder actuated fasteners, steps (2) and (10) were omitted, while all the other procedures were the same. More information about Hilti powder actuated fasteners can be found at [www.hilti.com](http://www.hilti.com).

12. The  $\frac{3}{4}$  in. thick retrofitting angle was cut to the size shown in Figure I-1.
13. Fifteen  $\frac{5}{32}$  in. diameter holes were predrilled so that the nails could pass through the angle and penetrate into the tension flange. The hole size was chosen such that the 0.177 in. diameter high strength nail tip would end half way through the tension flange. Trial tests with different hole diameters were conducted. The remaining length of the fasteners was measured and subtracted from the original length, thus the embedded length could be obtained. It was believed that defect was most likely to occur at the nail tip. Since stress intensity was higher for a surface crack than for an embedded crack for the same defect size, it was targeted that nail tip would end half way through the tension flange. The distance of the predrilled holes was chosen for optimum gripping force recommended by Hilti technical support.
14. The actuator load was set at 48 k, the mean load for the cyclic loading. In other words, the adhesive-angle retrofit system would undergo a stress ratio of  $-1$  in the following cyclic loading.
15. The surfaces of the retrofitting angle, the bottom flange and the connection plate were ground to get rid of the mill scale.
16. The surface was then abraded with 220 grit sandpaper.
17. The surfaces were wiped with acetone until no black oxide appeared when a new piece of white rag was used to wipe the surface.
18. The two part DP-460NS adhesive was squeezed into the mixing nozzle from the cartridge. Then the adhesive was applied and spread over the surface of the retrofitting angle. A thin layer of adhesive was also applied and spread over the surface of the bottom flange and connection plate.
19. Twenty to forty 0.020 in. diameter glass beads were sprayed onto each adhesive covered surface of the angle.
20. The retrofitting angle was pressed hard against the bottom flange while the bolt was tightened to the point that the glass beads began breaking.
21. The X-AL-H powder actuated fasteners were shot with a semi-automatic fastening tool (DX 36M) provided by Hilti company. Collated cartridges (6.8/11 M red cartridges) were used as boosters. The fastening tool was positioned perpendicular to the surface for optimal effect.

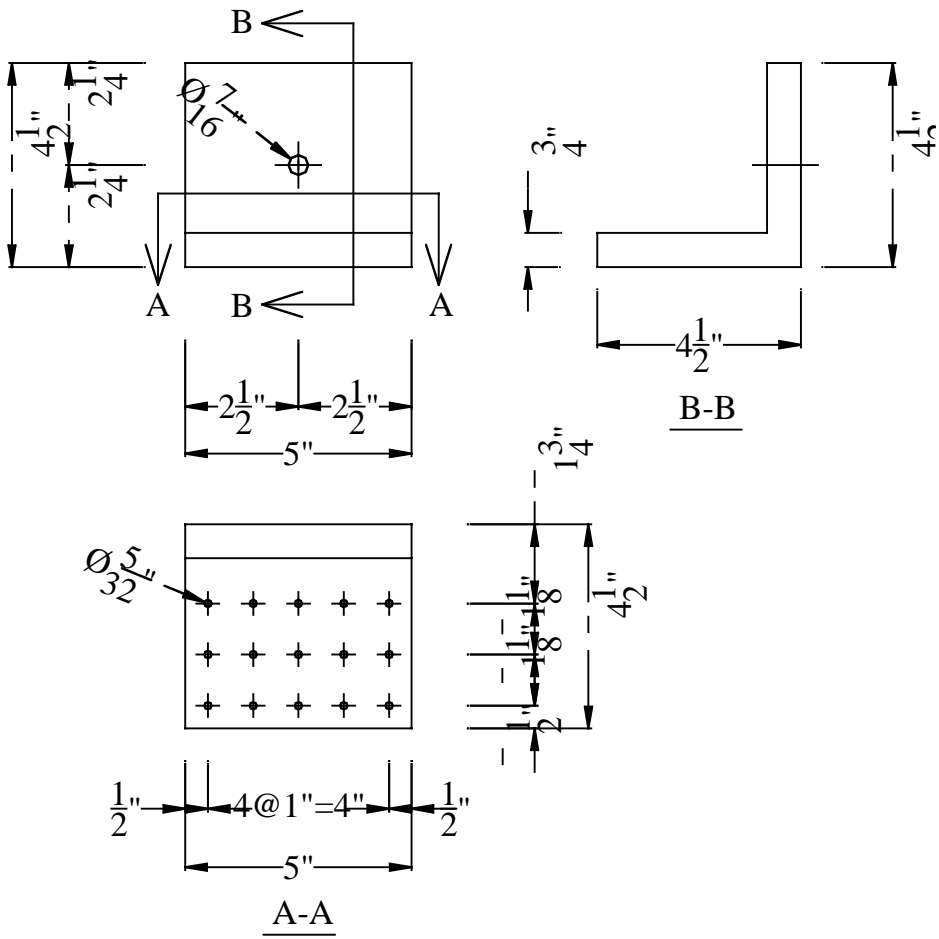


Figure I.1 Retrofit angle



Figure I.2 Picture of the retrofit angle with Hilti powder actuated fasteners

## **Appendix J**

### **Measured out-of-plane strains for the large-scale specimen**

The location and labeling of the strain gage that measured out-of-plane strains are provided in Figure 4.12 and Appendix H.

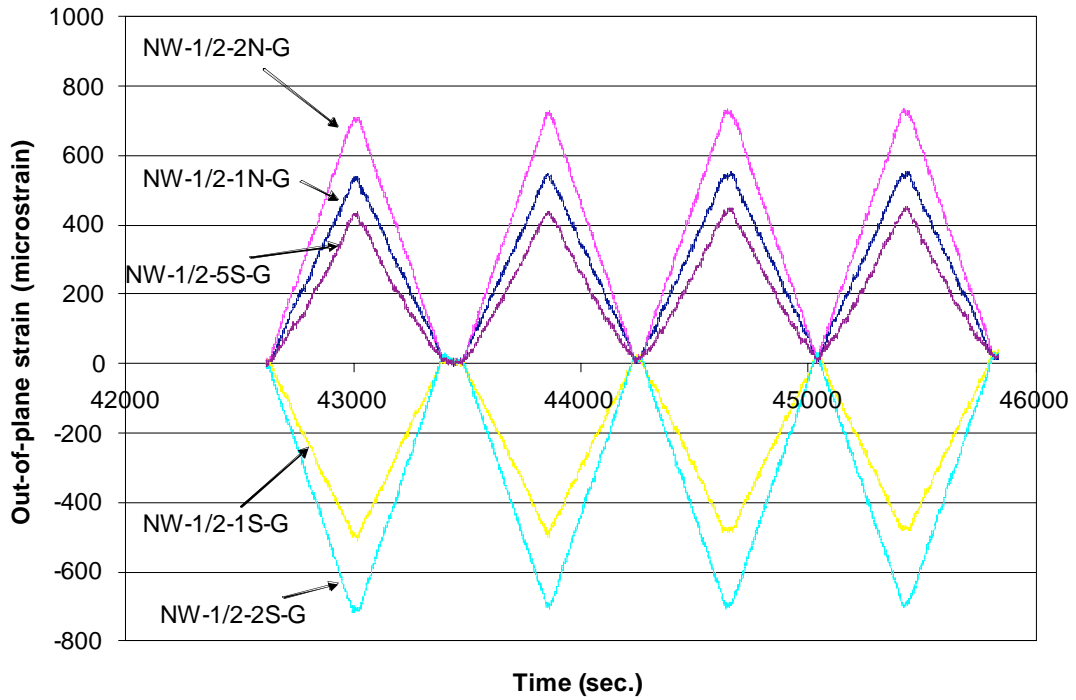


Figure J.1 Measured out-of-plane strains at web gap NW-1/2 before cyclic loading

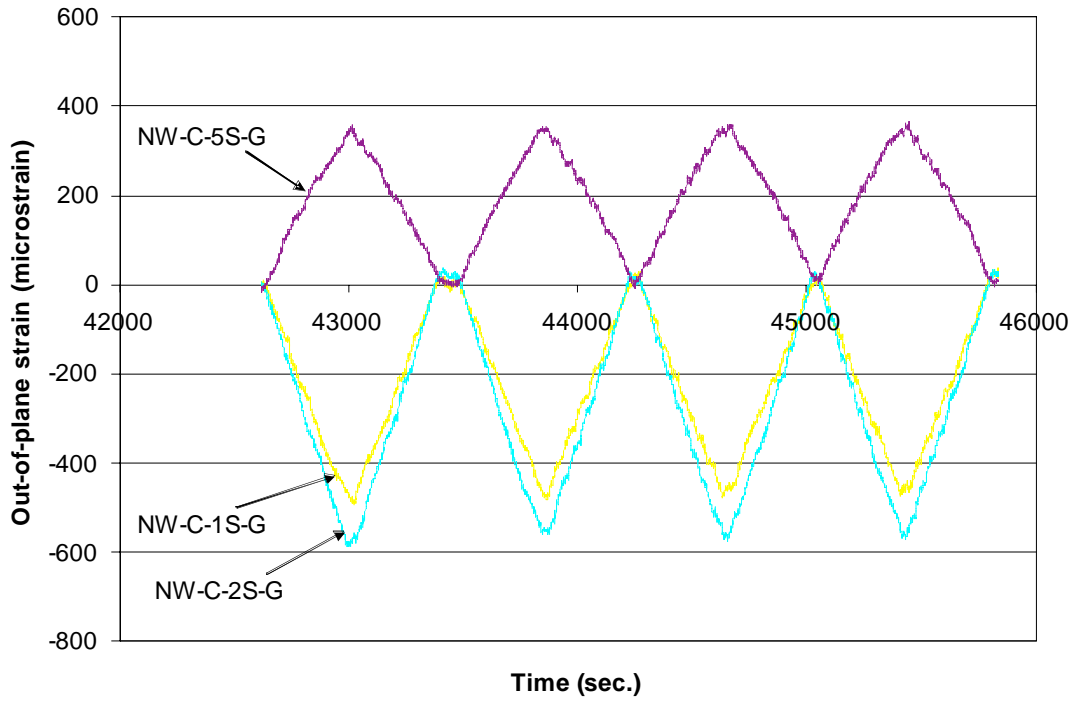


Figure J.2 Measured out-of-plane strains at web gap NW-C before cyclic loading

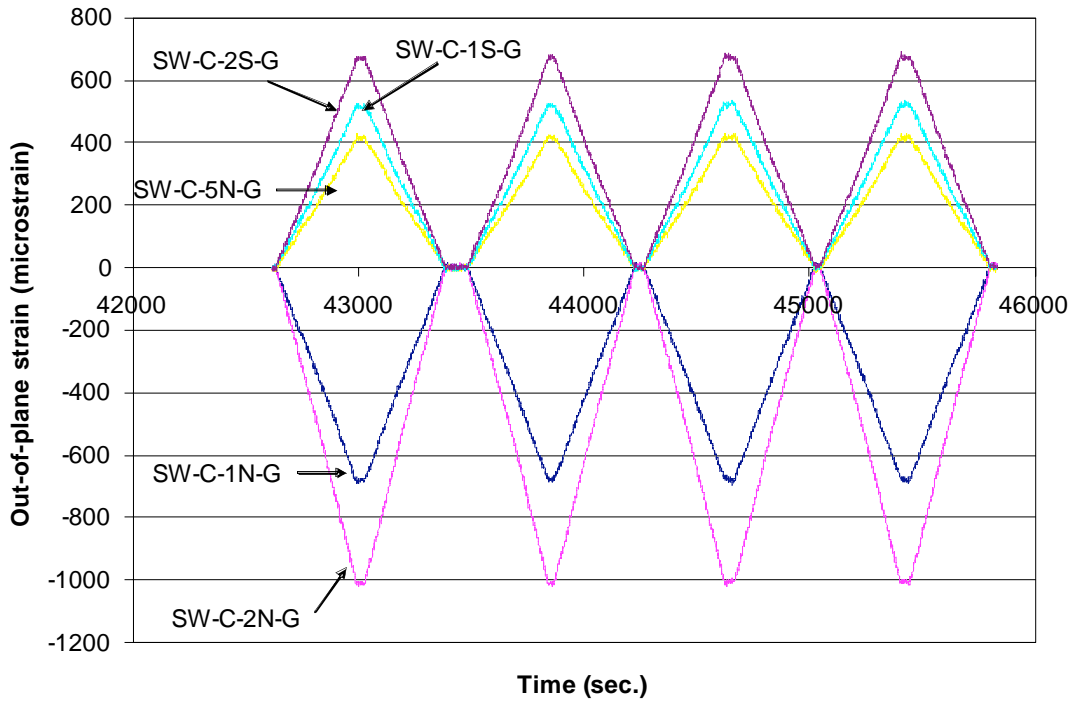


Figure J.3 Measured out-of-plane strains at web gap SW-C before cyclic loading

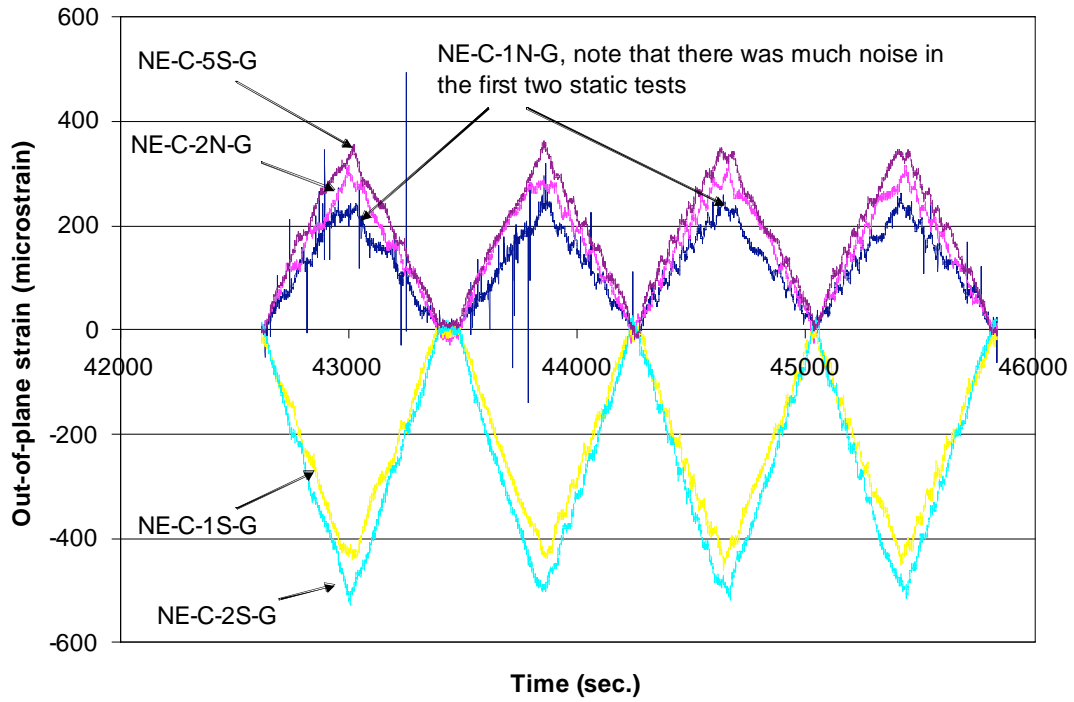


Figure J.4 Measured out-of-plane strains at web gap NE-C before cyclic loading

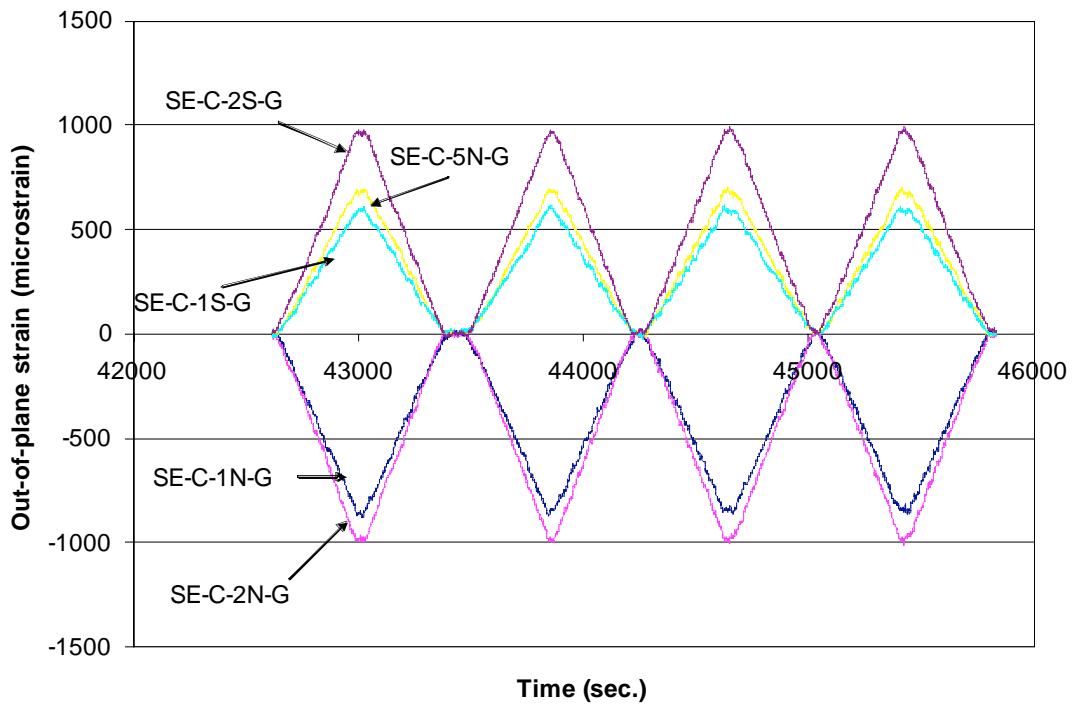


Figure J.5 Measured out-of-plane strains at web gap SE-C before cyclic loading

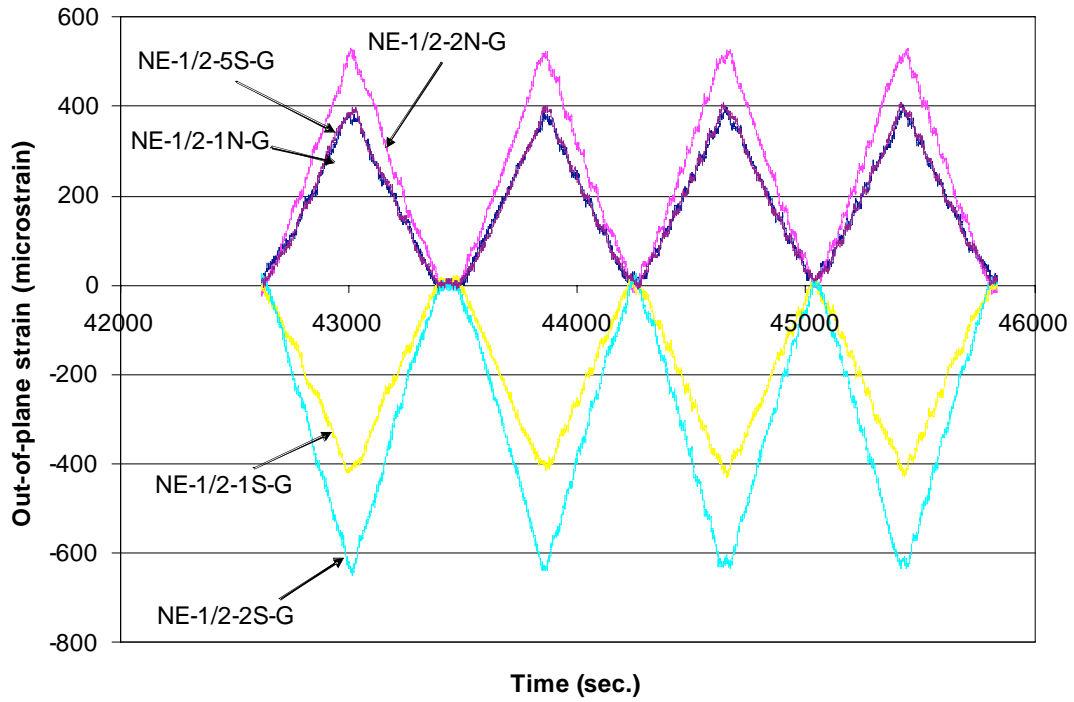


Figure J.6 Measured out-of-plane strains at web gap NE-1/2 before cyclic loading

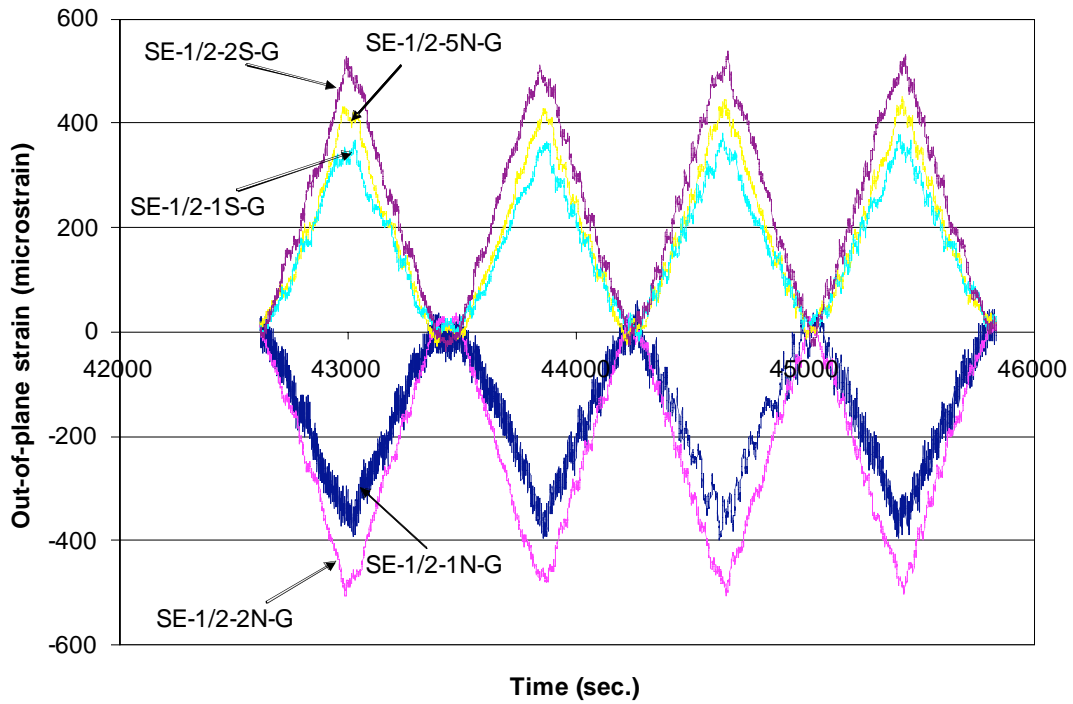


Figure J.7 Measured out-of-plane strains at web gap SE-1/2 before cyclic loading

## **Appendix K**

### **Coupon specimen fabrication procedure**

The adherends were made with A36 steel. They were manufactured by a local company using high pressure water cutting. The as-received steel pieces contained mill oil. Steps (7) and (8) were skipped for specimens without GPS pretreatment.

22. Jigs were made to keep all four pieces of the coupon specimen in position before the adhesive cured. In order to make the jigs reusable, plastic sheet and polytetrafluoroethylene(PTFE) seal tape were used at places where the adhesive might come into contact with the jig. A picture of the coupon specimen sitting in the jig is shown in Figure K.1.
23. The surface of the adherends was wiped with rags soaked in acetone.
24. The surface of the adherends was then sanded with 40 to 60 grit sandpaper by a hand electronic sanding machine, until the surface became bright.
25. Sandpaper of 220 grit was used to sand the surface until the surface became bright and shiny.
26. Mounting tape of size 3/8 in. × 1 3/4 in. was adhered to the side of one center adherend (Figure K.2). This helped to avoid adhesives squeezing between the two center adherends.
27. The adherend surface was wiped with white rags soaked in acetone until no black oxide appeared when a new piece of rag was used to wipe the surface. Since the black color of the oxide was most discernable in the white background, white rags were used.
28. Measuring cups were used to measure 1 ml of  $\gamma$ -glycidoxypropyltrimethoxy silane (GPS) and 100 ml of distilled water. GPS was then poured into the distilled water and a brush was used to stir the solution for 1 to 3 minutes. The solution was kept still for 15 to 60 minutes before it was applied to the surface of the adherend with a brush.
29. The steel plates were tilted to get rid of the excess water. After the GPS solution had dried in the ambient air, the adherends were ready for adhesive application. Note that some rust was observed at places where water residual was left on the surface.
30. DP-460NS adhesive was applied and spread over the surface of both the center adherends and the side adherends.
31. After the bottom side adherend was put into the jig, approximately 10 glass beads of 0.020 in. (or 0.039 in., or 0.059 in.) in diameter were sprinkled by hand onto the adhesive covered surface. Then the two center adherends were pressed against each other as they were lowered to fit into the jig. Afterwards, the two center adherends were pressed with fingertip pressure so that the excess adhesive between the bottom side adherend and the center adherends would squeeze out. No breaking sound of the glass beads was ever heard. Spacers were used at the far end of the center adherends so that the center adherends did not tilt.

32. The same procedure was followed to adhere the top side adherend to the center adherends.
33. The specimens were stored in the jigs for seven days before they were taken out of the jigs.
34. The cured excess adhesive, or fillet, was ground away by a grinder.
35. The specimens were now ready for testing, or for environmental exposure.

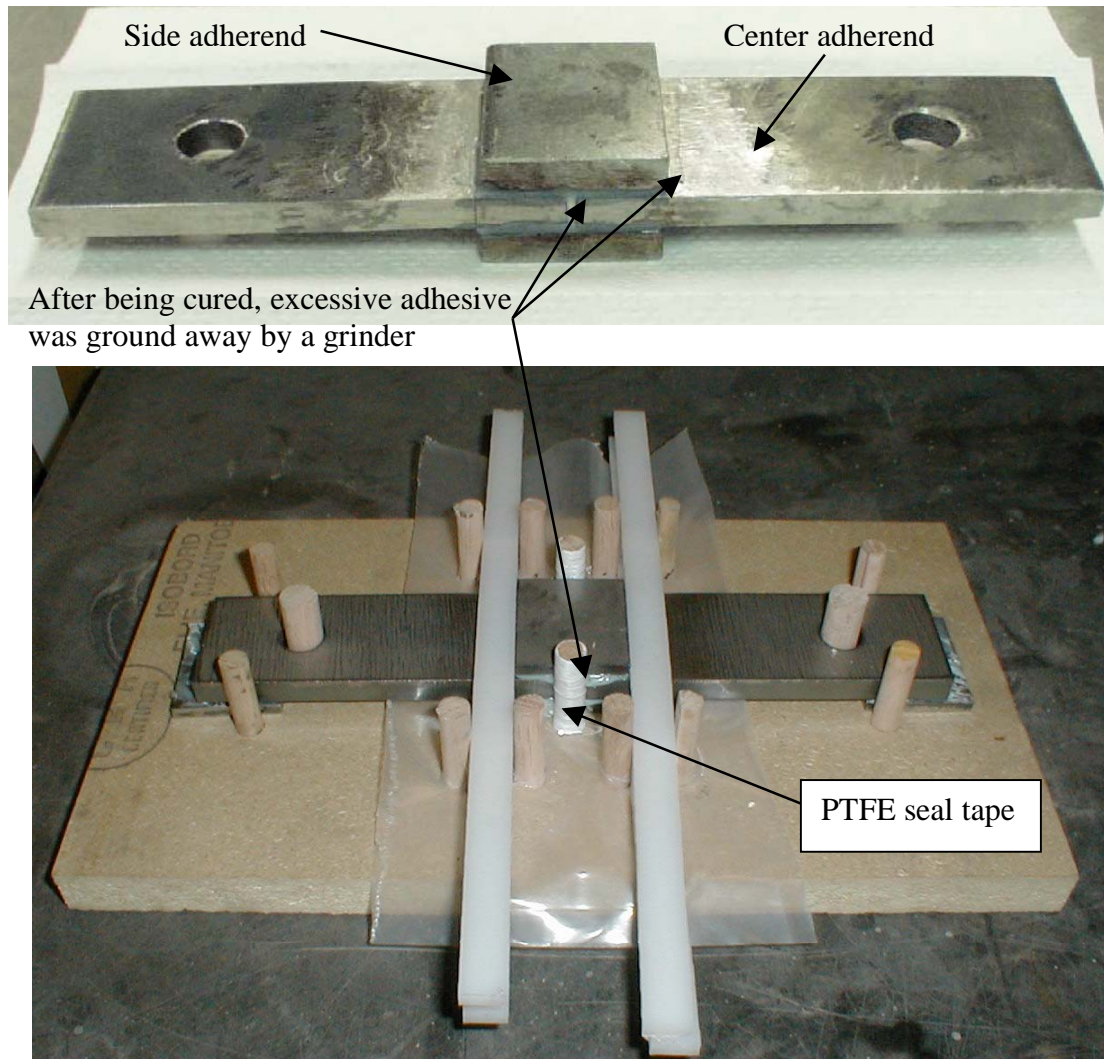


Figure K.1 Coupon specimen

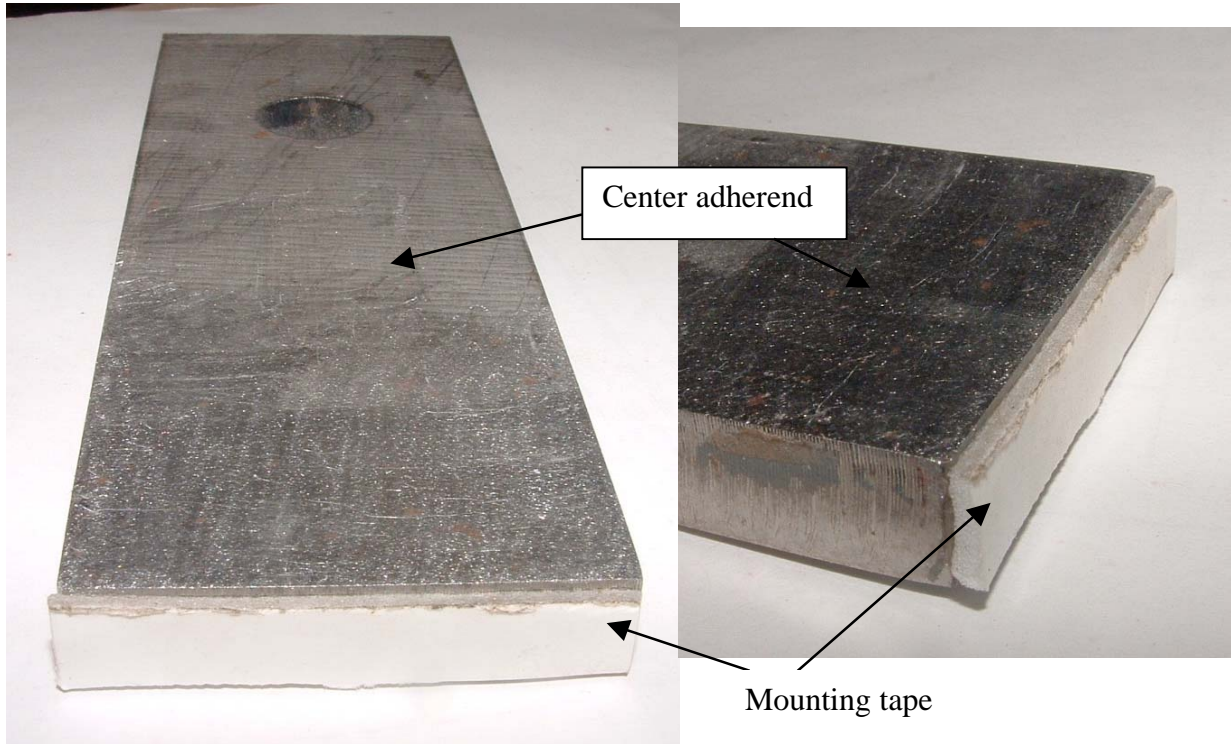


Figure K.2 Mounting tape was adhered to the side of one center adherend

## **Appendix L**

### **Strength and stiffness of the baseline coupon specimens and environmentally exposed coupon specimens**

Table L.1(a) Strength of the baseline coupon specimens

No.	Description	Mechanically cycled prior to testing?	Ultimate load (kips)				
			1	2	3	4	5
B1	Fresh-0.020" -No GPS-tested at 70°F	No	8.54	8.41	6.91	8.37	8.86
			9.05	9.65	10.02	9.99	9.26
			8.13	9.60	9.48	9.52	8.88
			8.80	9.25	8.60	8.67	8.52
			* N/A	8.69	8.74	9.00	8.88
B2	Fresh-0.020" -GPS-tested at 70°F	No	7.78	7.59	7.38	7.39	7.29
			10.08	10.01	9.53	10.47	10.04
			9.27	9.24	9.15	9.37	9.56
			* 9.71	9.47	9.85	9.63	9.73
B3	Fresh-0.020" -No GPS-tested at 122°F	No	5.01	5.20	4.78	5.85	5.78
B4	Fresh-0.020" -No GPS-tested at -40°F	No	16.57	16.34	6.30	14.26	13.75
B5	Fresh-0.020" -No GPS-cured at 50°F	No	3.27	4.63	4.89	5.37	4.83
B6	Fresh-0.039" -No GPS-tested at 70°F	No	* 6.67	9.41	8.08	8.95	8.96
B7	Fresh-0.059" -No GPS-tested at 70°F	No	7.98	6.84	7.69	7.50	6.66
			* 8.16	8.26	8.78	8.99	8.42
B8	Fresh-0.059" -GPS-tested at 70°F	No	8.64	6.89	8.31	8.79	7.23
B9	Fresh-0.059" -No GPS-tested at 122°F	No	3.68	4.84	1.92	4.30	3.64
B10	Fresh-0.059" -No GPS-tested at -40°F	No	13.41	14.44	11.48	12.72	8.49
B11	Fresh-0.020" -No GPS-tested at 70°F	Yes	8.01	7.04	7.32	7.89	7.36
B12	Fresh-0.020" -GPS-tested at 70°F	Yes	9.29	9.44	9.66	9.44	9.80
Note:	* Denotes the stiffness was taken from that corresponding batch.						

Table L.1(b) Stiffness of the baseline coupon specimens

No.	Description	Mechanically cycled prior to testing?	Stiffness up to 50% of ultimate load (kips/in.)				
			1	2	3	4	5
B1	Fresh-0.020" -No GPS-tested at 70°F	No	N/A	3429	3247	3002	3305
B2	Fresh-0.020" -No GPS-tested at 70°F	No	3516	3462	3225	3598	3644
B6	Fresh-0.039" -No GPS-tested at 70°F	No	2021	2654	2476	2323	2524
B7	Fresh-0.059" -No GPS-tested at 70°F	No	2022	2216	2139	2276	2490

Table L.2(a) Strength of the environmentally exposed coupon specimens without GPS pretreatment

No.	Description	Mechanically cycled prior to testing?	Ultimate load (kips)				
			1	2	3	4	5
E1-1	Air at 65°F for 180 d	No	9.03	8.95	8.98	9.28	9.15
E1-3	Air at 65°F for 447 d	No	9.87	9.84	9.61	10.15	9.48
E1-5	Air at 65°F for 180 d	Yes	9.01	9.91	10.54	9.22	9.63
E2-1	Immersion at 65°F for 92 d	No	7.63	8.32	8.52	8.81	8.33
E2-2	Immersion at 65°F for 201 d	No	8.04	8.25	8.35	8.72	8.41
E3-1	Immersion at 111°F for 92 d	No	6.31	8.02	8.83	8.37	8.61
E3-3	Immersion at 111°F for 210 d	No	7.17	7.47	7.96	8.03	8.02
E3-5	Immersion at 111°F for 210 d *	Yes	0.00	4.76	0.00	6.55	6.76
E4-1	Air at -4°F for 196 d	No	9.79	10.32	10.00	10.20	10.14
E4-3	Air at -4°F for 382 d	No	9.91	9.94	10.04	9.82	10.23
E4-5	Air at -4°F for 197 d	Yes	9.96	10.30	10.40	10.04	9.82
E5-1	Freeze and thaw chamber for 92 d	No	8.42	9.12	8.74	7.61	9.11
E5-2	Freeze and thaw chamber for 193 d	No	8.30	9.26	9.27	9.11	8.94
E6-1	Temperature cycles (unloaded) for 197 d	No	6.71	9.32	9.46	10.12	10.12
E6-3	Temperature cycles (unloaded) for 380 d	No	8.68	9.70	9.73	9.58	10.01
E6-5	Temperature cycles (unloaded) for 207 d	Yes	8.26	9.39	9.16	10.11	9.94
E7-1	Temperature cycles (loaded) for 211 d **	No	0.00	9.09	9.11	9.67	8.43
E7-3	Temperature cycles (loaded) for 370 d **	No	0.00	7.73	7.73	7.50	8.03
E8-1	Outdoors for 184 d	No	8.87	9.22	9.08	9.40	8.93
E8-3	Temperature cycles (loaded) for 370 d	Yes	9.02	9.36	9.67	8.36	9.54
E9-1	Fire after outdoor exposure for 371 d ***	No	0.00	0.00	1.73	1.50	5.43
			0.00	2.37	0.38	0.56	3.64
			0.00	0.67	0.00	0.00	0.00
			0.00	0.00	0.00	3.76	0.52
*	Two specimens failed during the mechanical cycling						
**	One specimen failed during the environmental exposure						
***	Ten specimens failed in the fire						

Table L.2(b) Stiffness of the environmentally exposed coupon specimens without GPS pretreatment

No.	Description	Mechanically cycled prior to testing?	Stiffness up to 50% of ultimate load (kips/in.)				
			1	2	3	4	5
E1-1	Air at 65°F for 180 d	No	3188	3238	3216	3041	3290
E1-3	Air at 65°F for 447 d	No	3694	4034	3645	3776	3499
E1-5	Air at 65°F for 180 d	Yes	3658	3561	3750	3133	3376
E2-1	Immersion at 65°F for 92 d	No	2721	3078	3177	3457	3002
E2-2	Immersion at 65°F for 201 d	No	3076	3054	2755	3179	3070
E3-1	Immersion at 111°F for 92 d	No	2137	2646	2791	2820	2622
E3-3	Immersion at 111°F for 210 d	No	2503	2455	2735	2728	2622
E3-5	Immersion at 111°F for 210 d *	Yes	0	2009	0	2330	2385
E4-1	Air at -4°F for 196 d	No	2894	3399	3212	2774	3037
E4-3	Air at -4°F for 382 d	No	3496	3548	3536	3390	3348
E4-5	Air at -4°F for 197 d	Yes	2926	2927	3600	2837	2812
E5-1	Freeze and thaw chamber for 92 d	No	2713	2800	2835	2691	2902
E5-2	Freeze and thaw chamber for 193 d	No	2850	3127	2947	3027	2878
E6-1	Temperature cycles (unloaded) for 197 d	No	1550	2737	3011	2968	2953
E6-3	Temperature cycles (unloaded) for 380 d	No	2870	2713	2707	2827	2817
E6-5	Temperature cycles (unloaded) for 207 d	Yes	2645	2752	2885	3095	3094
E7-1	Temperature cycles (loaded) for 211 d **	No	0	2610	2938	2771	2748
E7-3	Temperature cycles (loaded) for 370 d **	No	0	2783	2565	2469	2512
E8-1	Outdoors for 184 d	No	2956	2963	3028	2898	3183
E8-3	Temperature cycles (loaded) for 370 d	Yes	2808	2928	3140	2989	2874
E9-1	Fire after outdoor exposure for 371 d ***	No	0	0	2129	2547	3028
			0	1370	205	250	878
			0	427	0	0	0
			0	0	0	3205	1201
*	Two specimens failed during the mechanical cycling						
**	One specimen failed during the environmental exposure						
***	Ten specimens failed in the fire						

Table L.3(a) Strength of the environmentally exposed coupon specimens with GPS pretreatment

No.	Description	Mechanically cycled prior to testing?	Ultimate load (kips)				
			1	2	3	4	5
E1-2	Air at 65°F for 180 d	No	9.56	9.21	9.09	9.58	8.27
E1-4	Air at 65°F for 447 d	No	10.45	10.13	10.01	9.71	8.97
E3-2	Immersion at 111°F for 92 d	No	8.93	8.46	8.28	8.89	8.50
E3-4	Immersion at 111°F for 210 d	No	8.62	9.07	8.43	8.18	7.83
E4-2	Air at -4°F for 196 d	No	10.18	9.77	9.84	10.57	10.08
E4-4	Air at -4°F for 382 d	No	10.20	10.37	10.24	9.58	10.84
E6-2	Temperature cycles (unloaded) for 197 d	No	10.07	10.55	10.39	10.40	10.16
E6-4	Temperature cycles (unloaded) for 380 d	No	10.06	9.53	9.35	9.76	9.64
E6-6	Temperature cycles (unloaded) for 207 d	Yes	10.25	9.85	10.03	10.26	10.22
E7-2	Temperature cycles (loaded) for 211 d	No	9.47	9.88	9.52	8.98	8.80
E7-4	Temperature cycles (loaded) for 370 d	No	9.71	8.05	2.59	8.21	8.48
E8-2	Outdoors for 184 d	No	8.74	8.84	9.47	9.42	9.59
E9-2	Fire after outdoor exposure for 374 d ***	No	7.46	3.14	3.82	4.20	0.00
			7.46	2.91	3.28	4.14	0.00
			2.95	7.14	1.15	3.64	0.17
***	Two specimens failed in the fire						

Table L.3(b) Stiffness of the environmentally exposed coupon specimens with GPS pretreatment

No.	Description	Mechanically cycled prior to testing?	Stiffness up to 50% of ultimate load (kips/in.)				
			1	2	3	4	5
E1-2	Air at 65°F for 180 d	No	3202	3119	3545	3961	3073
E1-4	Air at 65°F for 447 d	No	3836	3701	3526	3958	3549
E3-2	Immersion at 111°F for 92 d	No	2726	2618	2696	2794	2653
E3-4	Immersion at 111°F for 210 d	No	2545	3046	2841	2537	2667
E4-2	Air at -4°F for 196 d	No	2976	2894	2787	3098	3085
E4-4	Air at -4°F for 382 d	No	3751	3549	3036	3074	3737
E6-2	Temperature cycles (unloaded) for 197 d	No	2767	2960	2959	3109	2771
E6-4	Temperature cycles (unloaded) for 380 d	No	3306	2913	2316	2900	2655
E6-6	Temperature cycles (unloaded) for 207 d	Yes	3041	2860	2995	3617	2901
E7-2	Temperature cycles (loaded) for 211 d	No	2754	2773	2690	2772	2709
E7-4	Temperature cycles (loaded) for 370 d	No	2877	2795	771	2611	2544
E8-2	Outdoors for 184 d	No	3166	3307	2926	2982	3094
E9-2	Fire after outdoor exposure for 374 d ***	No	3594	2819	1953	3015	0
			2829	1152	515	972	0
			3813	3092	1811	3099	44
***	Two specimens failed in the fire						

## **Appendix M**

**The recommended procedure of applying the retrofitting angles in the field**

The following describes the recommended procedure of applying retrofit angles in the field:

36. Until a parametric study is completed, use of a  $\frac{3}{4}$  in. thick retrofit angle is recommended.
37. The angle should be cut into the correct size and the hole for the  $\frac{1}{4}$  in. diameter stainless steel bolt should be drilled.
38. [d7
39. The surfaces of the retrofitting angle, the top flange and the connection plate should be ground smooth.
40. The surfaces should then be wiped with acetone until no black oxide appeared when a new piece of white rag is used to wipe the surface. Since the black color of the oxide is most discernable in the white background, white rags are recommended.
41. A thick layer (thicker than 0.020 in.) of DP-460NS adhesive should be applied and spread over the surface of the retrofitting angle. A thin layer of adhesive should be applied and spread over the surface of the top flange and connection plate.
42. Twenty to forty 0.020 in. diameter glass beads should be sprayed onto each adhesive covered surface of the angle.
43. The retrofitting angle should then be pressed hard against the top flange while the bolt is tightened to snug tight, or until the glass beads begin breaking.

The temperature recommended for the use of this adhesive is around 70°F. Thus, best effect will be achieved if the retrofit is applied during the daytime of summer in the state of Minnesota.